SHUTTLE ENTRY AIR DATA SYSTEM (SEADS)

HARDWARE DEVELOPMENT
VOLUME II, HISTORY

JANUARY 1983

PREPARED BY

D. M. WHILE

VOUGHT CORPORATION

DALLAS, TEXAS

FOR

SHUTTLE ENTRY AIR DATA SYSTEM (SEADS)

HARDWARE DEVELOPMENT

VOLUME II, HISTORY

JANUARY 1983

PREPARED UNDER

CONTRACT NAS1-16000

PREPARED BY

D. M. WHILE

VOUGHT CORPORATION

DALLAS, TEXAS

FOR

PREFACE

This report, Volume II, is a historical summary of the Shuttle Entry Air Data System (SEADS) Program. It contains rationale for approaches taken, results of technical accomplishments, accounts of technical problems, and an assessment of lessons learned. The companion report, Volume I, presents a program summary by subject and covers only program highlights. The included information was obtained from Vought, Rockwell and NASA, but primarily covers the Vought activities.

The early development of the program was conducted by Vought to indicate feasibility. Rockwell and Vought jointly collaborated on final development to prove feasibility, and finalize production design. NASA/LaRC conceived the system and directed the development. NASA/JSC managed the Rockwell production design activity.

Development ultimately proved successful, leading to fabrication of SEADS for early incorporation on Shuttle OV-102 for flight test.

Acknowledgement is given to the following principals who had responsibility for managing their respective areas of activity:

- P. M. Siemers, III, NASA/LaRC, overall system development & Technical Manager of Vought activities

- R. L. Cox, NASA/JSC, Technical Manager of Rockwell activities

- R. M. Hamilton, Rockwell International

- D. M. While, Vought Corporation.

TABLE OF CONTENTS

LIST OF FIGURES

LIST OF TABLES

1.0 INTRODUCTION

Shuttle Entry Air Data System (SEADS), illustrated on Figure 1-1, is an innovative, flush mounted orifice, air data system, mounted in the Reinforced Carbon-Carbon (RCC) nose cap of the Shuttle Orbiter. Conceived by NASA/LaRC, it provides accurate data across the Orbiter speed range throughout the sensible atmospheric flight region. It is comprised of a cruciform array of fourteen total pressure ports located in the nose cap, that, when coupled with static pressure ports mounted on the fuselage, permits computation of angle of attack, angle of side slip, Mach number, and velocity. The large number of ports includes a degree of redundancy, such that the loss of data from some of the sensors produces only modest degradation of system accuracy.

The system is composed of the penetration assemblies, two tube arrays to transmit the pressure data through two manifolds to a series of transducers, mounted to the aft side of the nose cap support bulkhead, and a data recorder. The recorded data is analyzed after flight to provide the desired flight information. The system is capable of being expanded to provide real time data for flight profile management.

The production design penetration assembly is shown on Figure 1-2. A mockup of the system is shown by the photo on Figure 1-3 to better illustrate the two manifolds and the pressure tubes configurations. The production SEADS nose cap is shown on Figures 1-4 & 1-5 and shows the cruciform configuration of the pressure port array.

SEADS is currently a Shuttle OEX program, approved for early introduction on Orbiter OV-102. It's initial function will be to support the data analysis of other OEX programs by providing the necessary accurate flight data.

2.0 DEVELOPMENT SUMMARY

Development of the mechanical components of SEADS began in October, 1975 with the initial goal of conceiving approaches for incorporating pressure ports into the Orbiter nose cap and evaluating the local effect of the resultant holes. The design requirement was 2520F maximum surface temperature on the nose cap. A number of approaches were conceived and evaluated with promising candidates selected for test in a plasma arc. These were found to lack sufficient mission life, requiring both material and configuration changes. However, it was established in 15 hours of plasma arc exposure, that the presence of a countersunk hole to accept the pressure port assembly, was not locally detrimental to the nose cap RCC material. This, coupled with limited pressure port success in test, was sufficiently encouraging to proceed with development.

Utilizing the best features from the initially tested concepts, the pressure port assembly was redesigned to correct deficiencies. Three models were tested in the plasma arc of one geometric configuration, but with material variations. Two survived the planned 5-hour test, one with a coated columbium port and one with a silicon carbide coated graphite port.

A systems concept evaluation was also conducted, consisting of thermal analysis of the penetration assembly and dynamic analysis of both the small diameter pressure tubes and the support posts (manifolds) that collected seven each pressure tubes. Concept feasibility was established at the analytic level.

With this impetus more sophisticated analyses were conducted consisting of buckling analysis of the nose cap with SEADS holes, a detailed stress analysis for the region around a non-circular hole in the nose cap, a more refined thermal analysis of windward and leeward penetration assemblies, and a thermal analysis of the nose cap to assess heat blockage from the two support posts. Each of these analyses proved the SEADS design to be feasible.

An entry trajectory change was introduced that raised maximum design temperature to 2660F, prompting another modification to the selection of materials and produced the final configuration. This resulted in the use of all coated columbium components, including the pressure tubes, although coated graphite ports were retained as a backup in the event sufficient mission life could not be extracted from the coated columbium ports. Two additional models were tested in the plasma arc in an effort to establish satisfactory performance at the increased temperature. The models differed only in the above noted port material, and each survived the planned 5-hour exposure. However, it could not be proven that the desired test temperature was actually achieved. It was therefore necessary to build another plasma arc model for test in another plasma arc facility to conclusively demonstrate survivability at the design temperature. Only the columbium pressure port model was tested. Not only was it shown that the penetration assembly would meet the design temperature requirements, but an inadvertent overshoot to 2950F was experienced without detrimental effects. The penetration assembly was thus qualified.

Two other component tests were conducted to demonstrate, primarily, the acceptability of the pressure tubes to survive the design environments and to validate the dynamic analysis. The first of these was a vibration test of the

left hand set of pressure ports and consisted of seven pressure port assemblies, seven pressure tubes, and the associated manifold and its insulation system. This unique test involved two simultaneously operating, independently controlled shakers, one introducing the vibration environment from nose cap acoustic response, and one simulating the nose cap support bulkhead vibration environment, applied to the base of the manifold. The input levels for this test were derived from response data measured during the Orbiter nose cap assembly qualification test, conducted at NASA/JSC. A thorough pre and post test analysis of pressure tubes response was conducted by Rockwell to support this test. Test results and supporting analysis demonstrated the acceptable performance of the SEADS system in a vibro-acoustic environment.

The second major test was one conceived to evaluate the low cycle thermal fatigue life of selected pressure tubes in the presence of thermal cycling. The concern was the stresses induced from constrained thermal expansion, as well as possible creep at high temperature, leading to induced strain in the tubes, when returned to room temperature. Although it was intended to impose a low pressure oxidizing atmosphere, representing the entry environment, the bare graphite heating elements oxidized sufficiently to create a reducing, rather than an oxidizing atmosphere. Instead of producing a more benign environment, the reducing atmosphere actually caused embrittling of the coated columbium pressure tubes and resulted in premature failure. It was encouraging that the embrittled tubes survived for a minimum of 68 mission cycles, lending confidence that the tubes, operating in the correct environment, would produce a safe failure margin far in excess of the 25-30 mission life projected for the penetration assembly.

The successful accomplishment of the foregoing component tests resulted in acceptance of SEADS as a viable system, and a production assembly was fabricated for early incorporation on vehicle OV-102 for flight test.

The remainder of this report expands upon these highlights, providing rationale for approaches, results of analyses/tests, and identifies lessons learned. It is presented in an essentially chronological order, modified only for a more rational grouping of like activities.

3.0 EARLY CONCEPT DEFINITION DEVELOPMENT

The ini al objectives of the program were to devise a scheme for attaching fourteen pressure ports to the Orbiter nose cap and to demonstrate that the presence of a hole in the nose cap was not detrimental to the local thermal/oxidation/structural integrity of the silicon carbide coated Reinforced Carbon-Carbon (RCC) nose cap. The production nose cap dome, where the pressure ports would be attached is 19 plies (0.25 in.) thick, although localized beefup was considered desirable for countersinking and stiffening. Local nose cap thickness variations up to ±10% had to be accommodated.

The most significant environmental design environments, that actually influenced concept generation and evaluation, included a maximum surface temperature of 2520F for entry trajectory 14040, acoustic noise level during launch of 157 db O. A., and an induced deflection during launch of 0.10 in. in any direction. The latter is the result of the relative motion between the nose cap and its support bulkhead, and is caused primarily by bulkhead flexure.

Other design guidelines or objectives were (1) the penetration assembly mission life should at least equal that of the nose cap, (2) the penetration assembly should not compromise the life of the nose cap, and (3) replacement of a penetration assembly should be accomplished without damaging the nose cap.

Further, at the outset of the program it was estimated that pressure tubes roughly 1/16 - 1/8 inch diameter would be satisfactory near the nose cap, recognizing that a more definitive requirement would ultimately be established.

This early work is documented in reference 1.

3.1 Concepts

In developing concepts for attaching small diameter tubes to the nose cap it was judged that there would be no reliable method of directly anchoring a thin walled tube without some intermediary support structure. That is, bonding, or flaring and bonding, a small pressure tube to the nose cap was believed to be too risky in the presence of vibration and the push/pull associated with launch deflections and tube thermal expansion/contraction during entry. Hence, all concepts given serious consideration employed some plug (port) installed in the nose cap to which the pressure tube would be secured.

The material for the plug had to provide a high temperature capability, but also had to have a high emittance to avoid temperatures, possibly excessive to the adjacent nose cap coating. Some materials meeting these criteria included silicon carbide, silicon nitride, silicon carbide coated graphite, and silicide coated refractory alloys. These materials were given some consideration in concept generation.

Some fourteen candidate designs for the penetration assembly were conceived and evaluated in accordance with a set of evaluation criteria. Each of the concepts involved a plug or port inserted into a countersunk or counterbored hole in the nose cap, a retention nut, some locking feature to prevent plug/nut separation, a pressure tube and its retention feature, and a thermocouple installation. (Throughout much of the program, thermocouple(s) were included in the design of the penetration assembly to measure entry temperature. This requirement was subsequently eliminated in the final stage

of development because of complexity and the expected ability to obtain satisfactory nose cap temperatures with radiometers.) The concepts are included as Appendix A.

Each concept was examined to assess advantages and disadvantages and a simple point count system was used for ranking and selection. Evaluation criteria employed are shown on Table 3-1. Most of these are self explanatory, but it should be noted that weight, the first item listed, was actually the least important consideration, since the total weight of the penetration assemblies was expected to be small, regardless of the configuration or materials selection.

Many of the concepts employed a bonded system, such as Sermetel or Astroceram, for either retention or locking. This was deemed unreliable for retention in the presence of the extreme and multiple temperature excursions and the high level of acoustic noise. In addition, bonding to the RCC was considered undesirable because of possible damage to the RCC coating upon removal and replacement of the penetration assembly. For these reasons, bonded type systems for retention were downgraded, leading to their elimination.

The results of the evaluation produced three candidates for design and plasma arc test as shown on Figures 3-1, 3-2 and 3-3. These are discussed in detail later.

3.2 Materials Selection

As an aid to materials selection for the above noted concepts, several materials were considered for application to each component, and candidates were tested at the appropriate temperature for materials compatibility.

As noted previously, the port required a material with high emittance, which eliminated some materials like alumina, zirconia, and noble metals. Materials such as silicon carbide, siliconized graphite, or coated refractory metals have the potential for satisfying the port requirements. Silicon carbide was eliminated because it would require molding and grinding to achieve the desired shapes with attendant long lead time and high cost for the limited number of parts involved. Coated (silicide) refractory metals have thin coatings (a few mils thick), leading to concern of coating integrity in threaded regions and the danger imposed by the abrasiveness of the silicon carbide coating on the siliconide coating. (Both of these concerns were later found to be not restrictive for the life of the system.)

Because of our experience with machining and coating graphite, it was decided to select this material for the initial plasma test models, recognizing that this phase of the program was primarily exploratory.

The port retention nuts on two of the concepts permitted a wider selection of materials, since high emittance was not a concern for this internal component. However, it was decided to use siliconized graphite for one model and metal for the other.

Concept 6 (Figure 3-2) employed a union, which by virtue of its configuration, was more amenable to fabrication from metal. Noble metals, coated refractory metals, and possibly super alloys (depending on temperature)

6

TABLE 3-1

DESIGN CONSIDERATIONS
SELECTION CRITERIA

WEIGHT

COST

    INITIAL
    REPLACEMENT

COMPATIBILITY

    CHEMICAL
    TEMPERATURE (HOT SPOTS)
    STRESS (THERMAL EXPANSION, RCC)

ENVIRONMENTAL TOLERANCE

    NATURAL (MOISTURE, RAIN, FREEZE)
    APPLIED (LOAD, VIBRATION)
    INDUCED (NOSE CAP AND SUPPORT
        DEFLECTIONS)

AERODYNAMIC SMOOTHNESS (GAPS AND STEPS)

FABRICABILITY

    TOLERANCE CONTROL (AND WITH RCC)
    FACILITIES
    REJECTION RATE

SAFETY

    REDUNDANCY
    FAIL SAFE
    RUGGEDNESS

SEALING (FLOW AND SHINE THROUGH)

MISSION LIFE

    THERMAL/OXIDATION DEGRADATION
    WEAR DEGRADATION
    FATIGUE

INSPECTABLE

    AS-FABRICATED
    FLIGHT OPERATIONS

MAINTENANCE

    REPAIRABLE
    REPLACEABLE

MATERIALS AVAILABILITY

DEVELOPMENT STATUS

INTERCHANGEABILITY

7

were considered to be candidates. Coated refractories were dismissed in these early tests for the reasons previously cited, but they remained candidates for future exploration. Of the noble metals only platinum was considered potentially acceptable from cost and machinability standpoints. However, it was known that platinum is attacked by free silicon to form a low melting point eutectic. The question was, is there sufficient free silicon available in the siliconized coating on RCC or graphite to cause a problem? The chemical compatibility tests discussed below sought to answer this question. The oxide dispersed alloys were believed to be marginal on melt temperature for this application, but one material, TDNiCr, was nevertheless tested for chemical compatibility.

For pressure tube retention nuts remote from nose cap surface the metals noted above were the most likely candidates. The lowered temperature at this location enhanced the possibility of using super alloys.

Pressure tubes needed to be metallic to withstand dynamic environments, but the availability of high temperature ductile tube products limited the candidates. Inconel 702 is routinely used for thermocouple sheaths at temperatures in the 2300F - 2400F range, making it a likely candidate if the environment was not too hot. Platinum tubing is also readily available and if it did not suffer a reaction from the silicon environment, it was believed to be a safe choice from a temperature standpoint.

A very modest chemical compatibility test program was conducted to assess acceptance of the candidate materials in combination with siliconized RCC and several bonding materials. Bonding materials were at the time still under consideration as a locking feature, a means of attaching thermocouples, or even attaching components together, as a backup to mechanical attachment. The test was conducted as illustrated in Figure 3-4 and had a time varying temperature and pressure representative of the design entry trajectory. Six entry missions were imposed. Results are summarized on Table 3-2.

Several things are noteworthy from an examination of Table 3-2. Both platinum and iridium containing materials produced no reaction with the siliconized RCC, which was at the time encouraging, because of the high temperature capability of these materials. In addition, neither Huntington Alloy 953E, TDNiCr, or Inconel 702 melted, nor produced a reaction with RCC, giving some encouragement to their applicability. However, the cobalt alloy, Haynes 25, reacted with RCC causing the alloy to disintegrate. Since some of these tests later proved to be grossly misleading, it would be necessary to re-evaluate cobalt alloys in combination with siliconized RCC, should a combination of these two materials be proposed for some future application.

As indicated above and confirmed by the plasma arc test results, the chemical compatibility tests proved to be inadequate in judging the adequacy of certain of the materials. In particular, platinum was indeed found to react with the siliconized coating during plasma testing in as little as two hours. The reason for this disparity is not clear, although it is postulated that there was greater pressure at the contact surfaces of the plasma models than for the specimens used in the chemical compatibility tests. In fact, it may be possible that in fabricating the test specimens there was no intimate contact, and there was insufficient silicon vapor to produce a reaction. As a means of avoiding this, the specimens should be weighted to assure contact

8

TABLE 3-2 - CHEMICAL COMPATIBILITY TESTS RESULTS

| METAL | SERMETEL 487 | REACTION WITH | | |
		ASTROCERAM B	SILICONIZED RCC	AIR
PLATINUM	NONE	NO TEST	NONE	NONE
PLATINUM-RHODIUM	NONE	NO TEST	NONE	NONE
IRIDIUM	NONE	NO TEST	NONE	NONE
IRIDIUM-RHODIUM	NONE	NO TEST	NONE	NONE
HUNTINGTON ALLOY 953E(IRON-NICKEL)	NONE	NONE	NONE	NONE
UDIMET 700 (NICKEL)	REACTS	MINOR REACT.	SCALE	MELT
HAYNES 25 (COBALT)	REACTS	REACTS	REACTS	REACTS
NIMONIC 115 (NICKEL)	REACTS	NONE	SCALE	MELT
Td-Ni-Cr (NICKEL)	REACTS	SCALE	SCALE	NONE
INCONEL 702 (NICKEL)	SCALE	NO TEST	SCALE	SCALE

CAUTION: WHILE THIS TABLE SHOWS TEST RESULTS, SOME OF THESE RESULTS
WERE FOUND TO BE MISLEADING.

pressure and this was done in subsequent chemical compatibility tests. Further, the specimens should be somewhat larger, since in these tests, the test material was bonded to the RCC. It is feasible that bonding material got between the two test materials and voided the intimate contact. This would be less likely with larger and weighted specimens.

A self imposed criticism is, that with the known possibility of chemical reaction between coated RCC and platinum, we should have challenged the test results and retested in another fashion as a double check. Perhaps we were so elated over the possibility of being able to use a material that did not require coating for some of the more complicated components, that it clouded our judgement.

3.3 Plasma Arc Test Models

Three models were fabricated for test in a NASA/LaRC plasma arc, designated Facility B. These models were configured as shown by Figures 3-1, 3-2 and 3-3. Model 13 was also rebuilt after the first test sequence to replace the platinum nut with YDNiCrAl, an oxide dispersion strengthened (ODS) alloy, and to include a pressure tube of Inconel 702 to replace the platinum. Each of these models employed a 2.8 in. dia., 19-plies RCC disc to represent the nose cap. This material was not given the post coating impregnation of tetra-ethyl orthosilicate (TEOS). In addition a calibrator model was built in the same fashion as the test models, except that a plain RCC disc without penetration assembly was used. The calibrator served two purposes: (1) it was used to establish the plasma arc operating conditions, and (2) it was exposed in the plasma arc for 15 hours to compare subsurface attack of the RCC with one of the models, having a penetration assembly, and exposed for the same period of time.

Since part of the program involved an assessment of thermocouple response and life, each test model was instrumented at several locations with platinum/rhodium, chromel/alumel, and tungsten/rhenium thermocouples, the latter for diagnostic purposes, because it was realized that they would ultimately oxidize, embrittle, and fail. The calibrator employed only tungsten/rhenium thermocouples.

The approach that we take in plasma arc testing is to establish the test conditions, based on thermocouple temperature, and determine the correlation with optical pyrometers. When the thermocouples fail, the optical pyrometers continue to be used for surface temperature measurement. In effect this becomes an in situ calibration of the optical pyrometers. We believe this eliminates optical temperature measurement errors, that are sensitive to spectral emittance variations of the model surface; possible reflections from the arc; and window, mirror, and angle corrections in the optical path.

The target conditions for these tests were 2500F surface temperature, 0.05 atmosphere pressure, and 15 hours duration. Only one model survived for the full duration. Each exposure was for 15 minutes each, which provided multiple heating and cooling cycles.

Model Concept 1A, Figure 3-1, was tested for 15 hours. Upon disassembly, it was noted that significant subsurface oxidation occurred along the central hole of the graphite port, but there was no oxidation evident on the graphite nut. It was feared that the small diameter port hole may coat poorly, and the

test confirmed this. On the other hand, the larger diameter hole in the nut as well as both the internal and external threads on the two parts, coated quite well. The platinum pressure tube and washers had reacted with the graphite coating, melted, and welded the graphite components together.

The most significant finding from this test was that the RCC disc showed no evidence that subsurface oxidation was any greater than that experienced by the calibrator disc. This was determined from photomicrographic examination of the cross sectioned discs. Thus, one of the initial key concerns, regarding the introduction of holes in the nose cap, was eliminated. In addition, it was estimated that the 15 hours of exposure was in excess of the expected life of the nose cap and thus the presence of holes would not compromise its' life.

Model Concept 6, Figure 3-2, was exposed for only 1.97 hours, test termination being due to platinum melting because of reaction with the coated graphite. The melt essentially welded all components together.

The test of Model Concept 13A, Figure 3-3, with the platinum nut and pressure tube was terminated after 3.58 hours, again due to platinum reaction with the siliconized graphite. This model also demonstrated a degree of fragility, when the graphite port was broken during attempted disassembly of the nut.

Model 13 was reconfigured for another test by using a new graphite port, nickel nut, and Inconel 702 pressure tube. It was designated 13B. Total exposure was 3.96 hours, termination being due to loss of the pressure tube and fracture of the graphite port during attempted disassembly. Port breakage was believed to be due to torqueing the nut in the wrong direction, since these were left hand threads. Subsequent examination of the model revealed that the nut spun freely on the graphite port so that proper disassembly should have been conducted with ease. The problem is related to the test laboratory's unfamiliarity with the design configuration. The lesson to be learned is that proper instruction needs to be given to laboratory personnel, particularly when non-standard designs are employed.

The loss of the pressure tube was the result of melting, where it came in contact with the graphite. Up to this point there had been no thermal analysis of the plasma models, but it was expected that the Inconel 702 tube would be operating near its temperature limit. The test confirmed this. There was, however, no melting of the YDNiCrAl nut, suggesting that this material has a higher operating limit than the Inconel 702.

The chromel/alumel thermocouples on these models operated for a maximum of 1.97 hours, a time span unacceptably low for a flight system. Apparently, the internals of the models were too hot for their application. No data was obtained from the platinum/rhodium thermocouples, even during the initial exposure cycles. It was believed, and later confirmed, that the problem was due to lack of electrical grounding, which allowed signal interference from facility electrical noise. In subsequent tests grounding was provided and these type thermocouples responded adequately.

3.4 Summary of Findings

While this phase of the program did not produce the desired success, it

did produce some satisfactory results and provided impetus for continuing the development of SEADS. Some of the more significant satisfactory results were:

(1) The presence of a countersunk hole in the RCC was shown to have no local detrimental effect upon the material.

(2) Graphite parts, when configured to enhance coatability will indeed coat acceptably, including both internal and external threads; and some multiple mission life can be expected.

(3) The YDNiCrAl alloy performed acceptably at a temperature estimated to be in the 2400F range. It did not react with the silicon carbide coating and was readily disassembled. (It should be noted that this material was pre-oxidized before assembly to reduce the possibility of sticking during test.)

On the negative side, unsatisfactory results were as follows:

(1) None of the configurations tested demonstrated an acceptable mission life.

(2) Platinum cannot come in contact with the siliconized coating used on RCC and graphite components.

(3) Neither chromel/alumel nor platinum/rhodium thermocouples were demonstrated to provide acceptable life. (However, in subsequent tests with grounded platinum/rhodium thermocouples satisfactory performance resulted.)

(4) Inconel 702 melted during test, probably due to excessive temperature, since later chemical compatibility tests showed no reaction with the silicon carbide coating up to 2450F.

4.0 SECOND PHASE DESIGN AND TEST

While the initial phase of this program was disappointing in that none of the three originally tested concepts performed satisfactorily, valuable insight was gained, such that there was a high degree of confidence, that improvements could be introduced to gain success.

The second phase of the program consisted of the following major elements:

(1) Refine the best penetration assembly design to improve fabricability, mission life, and reliability.

(2) Conduct a materials study to select alternate materials for the penetration assembly.

(3) Conduct a study to investigate alternate thermocouples for improved performance.

(4) Develop a concept for routing pressure tubes and thermocouples from the nose cap through the nose cap support bulkhead and provide supporting analyses.

(5) Design, fabricate, and plasma test three improved penetration assembly designs and evaluate results.

This phase of the program is documented in reference 2.

Design requirements were modified somewhat for this phase and additional details were provided. The entry design trajectory was changed to 14414.1, which still produced a stagnation temperature of 2520F. The acoustic noise level remained at 157 db, but resultant calculated vibration respose power spectral densities for the nose cap and support bulkhead were obtained from Rockwell. Maximum integrated levels were 114 GRMS at the nose cap and 29.5 GRMS at the support bulkhead. Surface smoothness requirements included ± 0.017 in. step allowance between the port and the nose cap; and an allowable gap between the edge of the port and the nose cap of 0.065 in. was to be measured one edge radius deep or at a maximum depth of 0.065 in.

Additional guidelines were introduced and included:

(1) The mission life goal was to be equivalent to the nose cap (about 40 missions) and the penetration assembly should not compromise the life of the nose cap, either during flight operations or during replacement of a penetration assembly.

(2) The penetration assembly strength capability was to be such that it was not the weak link in the system. In effect this meant that failure of the pressure tube should occur at a load level substantially below that of the penetration assembly, or nose cap.

4.1 Penetration Assembly Concept Refinement

As a result of the initial plasma arc tests it was judged that Concept 6, Figure 3-2, would offer the best opportunity for success, once different materials and design refinements were incorporated. This conclusion was based upon the inherent ruggedness of the metallic components and the configuration

13

of the port, which allowed good coatability if graphite was selected as a backup material. However, Concept 6 required some refinement to provide a better method for mounting thermocouples, and, depending upon materials selection, a means of providing a chemical barrier in the event incompatible materials offered overriding benefits.

Optional concepts are pictured in Figure 4-1 for comparison with Concept 6. Rationale and salient features of these alternate configurations are described below.

To review Concept 6 the plug was conceived as possibly being coated graphite. Therefore, an internal thread was required to provide a sufficiently large bore to permit coating. Furthermore, internal threads on graphite coat much more reliably than external threads. And the flexural strength of internally threaded graphite is greater than for external threads because of the lower stress in the root of the thread and the inherently greater moment of inertia for a given assembly diameter.

A metalic union was employed for strength and to simplify installation in the nose cap. The plug, spacer, union and lockwasher were to be installed first. The pressure tube would then be installed without having a number of loose parts to juggle at this time.

The RCC spacer was used to simplify machining of the union, permit easier incorporation of the locking feature, and provide a modest standoff from the hotter nose cap. In addition, it provides for axial growth of the columbium relative to the RCC to offset radial columbium growth, thereby preventing RCC fracture.

The French lockwasher (bent in place) was a simple technique for keying the plug to the union. The nut was in turn lockwired to the French lockwasher. Positive locking is required, since assembly is essentially finger tight to avoid over-stressing the graphite, and to minimize any tendency to self-bond at high bearing pressure and high temperature.

The pressure tube used a welded-on washer or collar to anchor the tube between the nut and union. The extended end of the tube provided added stiffness and strength for tube bending moments.

Figure 4-1 (A) illustrates an alternative to the welded washer concept by using a flared tube. This is a workable approach, although there is less bending moment restraint. However, the main reason for not employing a flared tube in this phase of the program was the off-the-shelf unavailability of the desired 5/32 in. dia. tube material. This forced the test articles to 3/32 in. dia. tubing, which prevented flaring. Although the welded washer technique provided an adequate pressure seal in the plasma arc tests, the electron beam welding of the Inconel 702 tube/washer joint proved structurally inadequate, when the weld broke during test.

Concept 6 did not provide a good anchoring point for thermocouples, nor was it intended to, since the measurement of temperatures on that model was primarily exploratory to determine feasibility of measuring temperature somewhere on the model for extrapolation to and correlation with the RCC surface temperature. Response of the tungsten rhenium thermocouples in Phase I tests demonstrated the practicality of temperature measurement remote from

the surface of the nose cap by extrapolation to the surface temperature, so this design refinement sought to develop a practical approach for installation and anchoring of thermocouples.

Two thermocouple installation schemes are pictured in Figure 4-1 (B) and (C). Each employs a fundamentally desirable feature of bench assembling to an anchor plate or mount that does not have to be rotated as component parts are screwed together.

Depending on material temperature capability, the thermocouples could theoretically be located close to the RCC skin as shown in the alternate location in Figure 5(B) or located farther away in the cooler region between the union flange and spacer indicated by the primary location. The latter location was chosen for model tests in this program phase, because it allowed greater flexibility of material selection for the thermocouple mount.

The two thermocouple anchoring schemes, depicted in Figure 5, represent (1) a machined mount drilled for the thermocouple, which is then staked in place for securing, and (2) a sheet metal mount, which is bent and crimped over the thermocouple. In the latter design the thermocouple anchoring method is integrated into the lockwasher, but could be a separate part. The machined mount was selected for test because temperature measurement at the bottom of the hole was believed to be more precise than with an exposed thermocouple tip, as with the (C) approach. Also, staking was considered more positive than crimping sheet metal for anchoring.

In selecting the most desirable material for each part, it was determined that certain of the contacting materials may not be compatible with each other. Therefore, some chemical barrier would be required for mutual protection. Possible schemes for achieving the chemical barrier with iridium, which is compatible with all the materials of interest, are illustrated in Figure 4-1 (D) and (E).

In Figure 4-1 (D), as an example, an iridium washer and welded washer/tube assembly could provide the necessary standoff to permit a platinum pressure tube to be used in combination with a silicide coated refractory union and nut. Similar chemical insulators are shown in Figure 4-1 (E) as an example of protecting the thermocouple mount, which could be platinum, from a silicide coated union. Yet another application of a chemical barrier is the coiled wire illustrated in Figure 4-1 (E). This was envisioned as an iridium coil that would provide a standoff between possibly a platinum union and a silicon carbide coated graphite plug.

The various schemes, discussed above, provided sufficient alternatives to permit the selection of material combinations for evaluation in the plasma arc test program. The discussion of the candidate material combinations, selections for test, and final design details are covered in Sections 4.3 and 4.5.

4.2 Thermal Analysis

A 50-node axi-symmetric thermal math model was prepared for the Concept 6 plasma test article at the conclusion of the first phase of the program. The model was checked out against thermal response in plasma test, as measured by the thermocouples. The model is illustrated in Figure 4-2, while typical results are shown in Figure 4-3, where predictions are compared against

thermocouple data on an early test exposure. It was recognized that closer agreement would result from slightly lowering the recovery temperature, while slightly raising the time varying insulation temperature.

This thermal model was, thus, further refined to produce a temperature distribution and response rate with better correlation to experimental values. Model geometry was then adjusted to reflect installation in the nose cap, as opposed to the boundary conditions of the plasma models. Details of the analysis are provided in reference (3).

The thermal analysis was conducted in advance of and as a guide to, the selection of the final materials and design configuration for the plasma test models. As such, the analytic models do not exactly reflect the final test configurations, but the results were deemed adequate to describe anticipated temperatures.

Three models were analyzed, differing in the material of the plug: graphite, silic n carbide, and columbium. Analyses were conducted for a high emittance (0.85) and a low emittance (0.15) union, nut, and washer to bound the problem. The trajectory analyzed is that designated as 14414.1.

Maximum temperatures, which occur at about 600 sec., are shown on Figure 4-4 for the three plug materials, and with the low emittance union, nut, and washer. Note that there is little difference in temperature between the three.

Using the high emittance union, nut, and washer for the columbium plug configuration, the union maximum temperature decreased by 19F, the nut decreased by 55F, and the washer decreased by 26F. Similar analysis of the graphite plug yields reductions of 25F, 49F and 33F, respectively. The low emittance results would be applicable to platinum components, while the high emittance temperatures are applicable to columbium, molybdenum, or oxidized nickel alloy parts.

In summary, design temperatures for the various components covering the emittance range, were as follows:

Plug	2520F
Union	2455 - 2485F
Washer	2395 - 2430F
Nut	2370 - 2430F
Pressure Tube	2395 - 2440F

These temperatures reflect the maximums based upon higher temperature adjacent nodes, where applicable, rather than the average temperature of the node of interest.

The thermal analysis results were viewed as an aid in guiding the chemical compatibility tests and final selection of materials for plasma test articles.

4.3 Alternate Materials Evaluation

From the initial study phase, it was apparent that additional materials evaluations were necessary to eliminate the chemical attack experienced on the platinum components. It was also desired to examine other possible plug materials in the event coating deficiencies of the graphite plug could not be

resolved. Therefore, a study was undertaken to identify alternate materials and then perform more rigorous chemical compatibility testing than that conducted in Phase I.

The objectives of this task were to identify mature candidate materials that could be fabricated into the desired shapes, determine chemical compatibility between interfacing materials, and assess the inclination toward self-bonding at elevated temperature and modest pressure. Elimination of self-bonding is important for ease of disassembly to reduce possible damage to the nose cap during component inspection/replacement.

The penetration assembly is illustrated in Figure 4-5 to show the relationship between the various elements. Candidate material combinations, believed to be the most attractive for the assembly, are summarized in Table 4-1. Consideration was, also, given to ceramic plug materials that had high strength and high emittance, but because of their inability to be fabricated into the desired configuration with acceptable tolerances, they were eliminated. Examples of this were silicon carbide and silicon nitride.

A brief discussion of the rationale for the selection of these materials for evaluation is given below.

Vought coated Stackpole 2020 graphite - This material combination had shown good performance in previous tests on those areas readily coatable. It was believed that redesign to improve coatability in the internal threaded region would produce a viable candidate.

CVD SiC coated Stackpole 2020 graphite - This material system had produced excellent life on heater bars, used in temperature testing of Shuttle leading edge panels. Its' main draw back is that the coating is a buildup system, making design and dimensional control of threaded regions and center port hole difficult. It remained a backup approach in the event that the Vought diffusion coating could not be adequately applied in the internal threaded region. However, the Vought diffusion coating ultimately proved acceptable and the CVD coating was not used.

Silicide coated columbium or molybdenum - Either of these materials was advertised as having the potential for surviving the temperatures of interest. It was hoped that one of these would produce oxidation resistance sufficient to replace the coated graphite plug. Inherently, these refractory materials are less brittle than the graphites and therefore should provide greater reliability.

Nickel alloy YDNiCrAl - This ODS alloy does not require a coating and has one of the highest temperature capabilities of the super alloys. Although it would be pushed to it's temperature limit, it was hoped that it would be serviceable for some of the internal components.

Nickel alloy Inconel 702 - This alloy was considered to have potential for the pressure tube application, since it is used as a thermocouple sheath into the 2400F region. It requires no coating for oxidation protection.

Platinum or Platinum Rhodium alloys - These noble metals have a temperature capability far in excess of requirements and require no oxidation protection coating. They must, however, be protected against contact with

17

TABLE 4-1 - CANDIDATE MATERIALS

PLUG	SPACER	WASHER	UNION	CHEM BARRIER	NUT	PRESSURE TUBE	T/C MOUNT
COATED GRAPHITE	RCC	YDNiCrAl	YDNiCrAl	-	YDNiCrAl	INCO 702	YDNiCrAl
		IRIDIUM	PLATINUM	IRIDIUM	PLATINUM	PLATINUM	PLATINUM
					YDNiCrAl	INCO 702	PLATINUM
		REFRACTORY METAL	REFRACTORY METAL	-	YDNiCrAl	INCO 702	IRIDIUM
REFRACT. METAL (Cb OR Mb)	RCC	IRIDIUM	PLATINUM	IRIDIUM	PLATINUM	PLATINUM	PLATINUM
					YDNiCrAl	INCO 702	PLATINUM
		REFRACT. METAL	REFRACT. METAL	-	REFRACT. METAL	INCO 702	IRIDIUM
		YDNiCrAl	YDNiCrAl		YDNiCrAl	INCO 702	YDNiCrAl

(1) THESE CANDIDATES ASSUME 2520F MAXIMUM NOSE CAP TEMPERATURE.

silicon based coatings, since they react to produce low melting point eutectics.

Iridium - This noble metal also has a temperature capability in excess of requirements and requires no oxidation protection coating. Application of this material was confined to those areas requiring a chemical barrier between incompatible materials.

4.3.1   Test Technique - All of the materials except the noble metals and Inconel 702 were tested as 3/4" diameter x 1/4" thick buttons. The noble metals were tested as wire segments, while the Inconel 702 specimens were configured by slitting and flatening tube material. Materials were stacked in appropriate combinations and weighted with pieces of coated graphite blocks. This provided only modest pressure.

Testing was conducted in an electrically heated air furnace with no forced circulation. Exposure temperatures were 2500F, 2400F and 2450F, in that order for one-hour cycles, except for one three-hour cycle at 2500F. Total exposure time was 5-hour at 2500F, 2-hour at 2450F, and 2-hour at 2400F.

Specimens were visually examined after each exposure cycle for reactions, and hand tested for self-bonding tendency. Observations were recorded. In some cases the same specimens were exposed throughout the test program, while in others, new specimens were introduced periodically to test new combinations or variations, or to retest previously tested combinations.

4.3.2   Test Results - Summaries of test results are provided as Tables 4-2 and 4-3 for acceptable and unacceptable material combinations, respectively, based on the furnace tests. A photograph of a typical platen of specimens is shown in Figure 4-6. In addition to the summary results the following additional observations and conclusions are offered.

Other than the YDNiCrAl specimens, none of the materials used in the first test were pre-oxidized, and certain reactions occurred that were not evident in subsequent exposures. This led to the conclusion that the initial oxidation treatment was beneficial to chemical compatibility. Therefore it was decided that all test components, other than the RCC buttons, representing the nose cap, would receive a pre-oxidation treatment before assembly. All compatible materials listed in Table 4-2 are based upon having a pre-oxidation treatment, except the RCC with TEOS coating as noted. The pre-oxidation treatment selected was 1 hour exposure at 2100F in an air furnace. This proved adequate, and therefore, no other conditions were examined.

The coated columbium buttons discolored and formed a scale; and in some cases crazing was quite evident. The discoloration proceeded from a green tint to black as exposure time increased. The columbium also stuck to itself on the first exposure, but when pre-oxidized there was no further problem. Columbium buttons, exposed for the full 9 hours, showed no evidence of subsurface attack, as determined by picking at the surface in an attempt to uncover cavities beneath the coating.

TABLE 4-2 - SUMMARY OF FINDINGS
CHEMICALLY COMPATIBLE COMBINATIONS

Material	Chemically Compatible with	Up to "X" °F test temperature
RCC impregnated with TEOS (See Note 1)	Molybdenum	2500
	Columbium	2500
	CVD Coated Graphite	2500
RCC without TEOS	Iridium	2500
	Inconel 702	2450
	YDNiCrAl	2450
Molybdenum TZM Alloy With 518 Coating	Molybdenum	2500
	RCC with TEOS	2500
	Iridium	2500
	YDNiCrAl	2450
	Inconel 702	2450
Columbium C-103 Alloy With R512E Coating	Columbium	2500
	RCC with TEOS	2500
	Iridium	2500
	YDNiCrAl	2450
YDNiCrAl	YDNiCrAl	2450
	Molybdenum	2450
	Columbium	2450
	Inconel 702	2450
	Iridium	2450
	CVD Coated Graphite	2450
	RCC without TEOS	2450
	Platinum Rhodium	2400
Inconel 702	YDNiCrAl	2450
	Molybdenum	2450
	Platinum & Platinum Rhodium	2450
	Iridium	2450
	RCC without TEOS	2450
CVD Coated Stackpole 2020 Graphite	RCC with TEOS	2500
	Iridium	2500
	YDNiCrAl	2450
Iridium	Platinum	2500
	Molybdenum	2500
	Columbium	2500
	RCC with TEOS (Preoxidized)	2500
	CVD Coated Graphite	2500
	YDNiCrAl	2450
	Inconel 702	2450
Platinum	Iridium	2500
	Inconel 702	2450
	YDNiCrAl	2450

NOTES: (1)

Only the RCC in this test combination was not pre-oxidized so as to represent the
nose cap at first flight. All other combinations assume pre-oxidized components.

TABLE 4-3 - SUMMARY OF FINDINGS
CHEMICALLY INCOMPATIBLE COMBINATIONS

Material	Chemically Incompatible with:	
Platinum & Platinum Rhodium	Columbium Molybdenum RCC with or without TEOS CVD Coated Graphite	

The coated molydbenum performed better than the columbium in that there was no tendency to self-bond, even on the first cycle, and no scale developed. When a pit developed on a virgin molybdenum button in contact with YDNiCrAl, self healing apparently took place, since there was no subsurface attack as evidenced from picking at the coating. Specimens that were exposed for the full 9 hours had no indication of subsurface attack when tested by the picking technique.

Several tests were conducted using magnesium oxide slurry (Mg O) as a possible means of preventing self-bonding. This technique was recommended by one of the material suppliers. However, when specimens were stacked with a wet slurry, rather than preventing bonding, the slurry produced a rather tenacious bon^ which could not be broken, even with heavy rapping on a table. Later tests, using dry powder or dried thin slurry appeared to be helpful. As a later development, a SiC powder slurry using Methocel as a carrier was employed to prevent self bonding (Section 6.3).

Some of the tests involving platinum and platinum rhodium were expected to produce chemical incompatibility, but were tested anyway for completeness. In particular incompatibility with the silicide and silicon carbide coatings occurred, as expected.

As a result of these tests, which essentially confirmed predicted acceptable interfacing materials, possible combinations for the penetration assemblies were as defined in Table 4-1. Selections for plasma test are described in Section 4-5.

4.4 Alternate Thermocouples Evaluation

The initial plasma tests showed that chromel/alumel thermocouples had insufficient life at the temperatures involved and the platinum rhodium sheathed thermocouples produced no useful data at all. It was concluded that the problem with the platinum rhodium thermocouples was a lack of electrical grounding. However, Vought re-examined other possible thermocouples to determine if there were viable alternates. No testing was involved in this task.

Sheathed thermocouples are required for the application to provide structural support to the thermocouple wires. Standard sheaths available and their reported maximum temperature capability are listed below:

Inconel 702	2400F
Platinum	3050F
Columbium	3600F*
Molybdenum	4000F*
Tantalum	4500F*

The * temperatures assume operation in an inert environment. For an oxidizing environment a protective coating is required, which will limit the temperature capability of the sheath. Since there could be substantial flexing of the thermocouples during installation, it was Vought's position that coated sheaths should be avoided. The Inconel 702 sheath has a marginal temperature capability and represents too great a risk if thermocouples are installed close to the RCC skin. That leaves the platinum (or platinum rhodium) sheath as the most desirable.

For the thermocouple wires there is a choice of platinum/platinum rhodium alloys, tungsten/tungsten rhenium alloys, and iridium/iridium rhodium alloys. The platinum combinations have a temperature capability in the 2800F region, which is in excess of expected requirements, and remain ductile. The tungsten and iridium combinations, although having higher temperature capability, tend toward brittleness and possibly low reliability in a cyclic temperature and vibration environment. The most logical selection, therefore, was the platinum rhodium elements for the temperature range and environment in which the thermocouples must operate.

Consultation with Vought personnel also revealed that in cases where there is a strong electrical field present, such as in a plasma arc facility, thermocouples must be grounded to prevent electrical interference. It appeared then that there was no reason, other than lack of electrical grounding, for not obtaining good data from the platinum rhodium thermocouples in the Phase I plasma tests. Therefore, this thermocouple type was selected for this program phase with the requirement for grounding.

Platinum/platinum 13% rhodium elements were chosen for their high milivolt output and a platinum 20% rhodium sheath was selected for strength and ductility. Two sizes were used: 0.040 inch diameter sheath with 5 mil wire, and 0.0625 inch diameter sheath with 10 mil wire. The larger size was selected for better ruggedness, but because it wasn't clear if the temperature response would be adequate, the smaller diameter was also tested for comparison. In each case the element juncture was connected to the sheath, which was used as the ground. Magnesium oxide was the insulator.

During the plasma test program, discussed in Section 4.5.3, these thermocouples functioned well for times varying from 5 cycles to 34 cycles (end of test). However, it is not known whether the early failures occurred in the active region of the thermocouple or somewhere downstream.

4.5 Plasma Test Models

Three test models and one calibrator were designed, fabricated, and tested in a NASA/LaRC plasma arc facility. The objectives of the plasma arc tests were:

(1) Determine individual performance and mutual compatibility of the various components under temperature, temperature gradients, and pressure conditions more representative of maximum flight conditions, than achievable in furnace tests.

(2) Provide an indication of mission life capability of the various components.

(3) Establish feasibility of the temperature measurement scheme.

(4) Demonstrate the feasibility of measuring pressure with sufficient accuracy for the intended usage.

This section describes the design details, fabrication and test results. The basic model configuration is shown in Figure 4-7 and the typical thermocouple installation is shown in Figure 4-8.

23

4.5.1 _Design_ - As a result of the chemical compatibility tests and thermal analyses, candidate materials combinations were assembled from which three were selected for detail design and test. The candidates are summarized in Table 4-4.

Systems A and C are the least expensive but also offer the lowest temperature capability. These two differ only in the plug material. Systems B and D which also differ only in plug material, provide a higher temperature capability by replacing the nickel alloy parts in the higher temperature region with coated refractories. System E has the highest temperature capability, but is very expensive, and represents an "overkill" on the temperature requirements. As such, it was decided to not pursue System E, especially since Systems B and D would have a high probability of meeting the requirements.

Of the remaining systems, it was decided to test Systems A and B to obtain two tests of the coated refractory plug and obtain an evaluation of both super alloy and refractory metal internal components. Although in retrospect, System D might have been the better choice for the third model, it was decided to try System C, because it appeared that the super alloy would be satisfactory based upon furnace tests. Also, there was concern over the ability to coat the union satisfactorily if it were refractory metal. System B would provide this evaluation.

Therefore, Systems A, B and C were designed for plasma test. All components were of the same design configuration with only material selection producing the differences. Materials used are summarized in Table 4-5 with each model identification number. Design details of each component are included as Appendix B. The plug, union, nut, spacer and tube design are essentially the same as Concept 6, tested on the Phase I program. Minor dimensional changes were made to accommodate the thermocouple mount, which permitted the thermocouples to be inserted and staked in place before assembly to the penetration assembly. The lockwasher was changed from the French lock approach to a lockwire technique to avoid bending the coated refractory washer. The two platinum rhodium thermocouples, noted in Section 4.4, were included.

4.5.2 _Fabrication_ - The RCC parts were fabricated and coated by Vought, using the standard processes used in the fabrication of shuttle leading edge components.

The Stackpole 2020 plug was coated by Vought using a modified RCC coating process.

YDNiCrAl stock was obtained from Special Metals Corporation, Allegheny Ludlum. The initial material received had a higher hardness than desired (Rc 38 - 46 vs. Rc 31 - 34) and was subject to cracking and chipping (due to excessive porosity) during machining. When the material was replaced with another lot of material, no machining difficulties were experienced, and parts were acceptable.

The iridium thermocouple mount was purchased from Engelhard.

TABLE 4-4 - CANDIDATE MATERIAL COMBINATIONS

COMPONENT	SYSTEM				
	A	B	C	D	E
PLUG	Mb/Cb	Mb/Cb	2020 Gr	2020 Gr	2020 Gr
SPACER	RCC	RCC	RCC	RCC	RCC
UNION	YDNiCrAl	Mb/Cb	YDNiCrAl	Mb/Cb	PLATINUM
WASHER	YDNiCrAl	Mb/Cb	YDNiCrAl	Mb/Cb	IRIDIUM
T/C MOUNT	YDNiCrAl	IRIDIUM	YDNiCrAl	IRIDIUM	PLATINUM
NUT	YDNiCrAl	YDNiCrAl	YDNiCrAl	YDNiCrAl	YDNiCrAl
PRESS. TUBE	INCO 702	INCO 702	INCO 702	INCO 702	INCO 702
LOCKWIRE	PLATINUM	IRIDIUM	PLATINUM	IRIDIUM	PLATINUM
CHEM. BARRIER	-	-	-	-	IRIDIUM
THERMOCOUPLE SHEATH	PLATINUM	PLATINUM	PLATINUM	PLATINUM	PLATINUM

NOTES: A, B, C, & D ARE SAME DESIGN BUT E MUST USE IRIDIUM AS CHEMICAL BARRIER BETWEEN UNION AND PLUG.

CANDIDATES ASSUME 2520F MAXIMUM NOSE CAP SURFACE TEMPERATURE.

On the basis of the superior performance exhibited by the coated molybdenum in the chemical compatibility tests, it was decided to use molybdenum, rather than columbium, for the refractory components. These parts were procured from Hitemco, who supplied the buttons for the chemical compatibility tests. However, during the 2100F - 1 hour pre-oxidation conditioning cycle, it was discovered that the molybdenum parts oxidized severely. When informed of this, Hitemco stated that the button material, which performed admirably, was from a different source and manufacturing technique than that used for the component parts. They advised that coated molybdenum performance could not be guaranteed, but coated columbium could be guaranteed to survive 2500F for 10 hours in a 1 atm. air environment. Accordingly, the refractory parts were switched to C-103 columbium with the R512E coating system, that was tested in the chemical compatibility program.

When the coated columbium parts were subjected to the oxidation conditioning exposure, the only discrepancy found was a small pinhole oxidation site at the base of a thread on the union. This was not expected to compromise the plasma test and the part was used.

Assembly of the models provided a minor problem, when the threads on the nickel alloy unions had to be resized slightly to permit assembly. In addition, since the plugs and RCC discs were manufactured at separate facilities but at the same time, there was no opportunity to match fit the parts before coating the RCC. This resulted in the plugs not fitting flush with the RCC and a protruding plug step was obtained. This step varied somewhat but was a maximum of 0.024 inch. Improvement can be realized through closer tolerancing of the RCC countersink and possibly prefitting before coating. (Prefitting using a standard coated columbium part was employed when the production SEADS nose cap was machined.)

4.5.3   Plasma Test Data - The three plasma test models and one calibrator model, consisting of an instrumented RCC disc, were tested in the NASA/LaRC Plasma Arc Jet Facility "B". This is the same facility used for the Phase I program tests. The target test condition was 2500F plug temperature at 0.05 atm pressure. Target test duration was 5 hours. The test condition was established, using a calibrator model, which had three tungsten rhenium thermocouples attached to the aft side of the RCC disc. These were correlated with three optical pyrometers, sensitive at 2.3 μ wavelength. The test models are defined in Table 4-5 along with a summary of exposure cycles and exposure time.

4.5.3.1   Calibration Data - Two significant calibration runs were made: one to compare the three optical pyrometers and the other to compare the pyrometers against tungsten rhenium thermocouple output.

In the first test all three pyrometers were focused within 1/4 inch of the same spot on an RCC disc. The following readings were obtained:

	AT 0.05 ATM		AT 0.10 ATM	
PYROMETER	TEMP, F	ΔT, F	TEMP, F	ΔT, F
IRCON 174522	2540	Baseline	2685	Baseline
IRCON 174523	2585	45	2720	35
IRCON 144389	2625	85	2768	83

TABLE 4-5 - MODELS TESTED

COMPONENT	MODEL		
	-9	-10	-11
DISC	RCC (TEOS)	RCC(TEOS)	RCC (TEOS)
PLUG	C_B (c-103) R 512E COAT.	C_B (c-103) R 512E COAT.	STACKPOLE 2020 (VOUGHT COATING)
SPACER	RCC	RCC	RCC
LOCKWASHER	YDN, CRAL	C_B (c-103)	YDN, CRAL
THERMOCOUPLE MOUNT	YDN, CRAL	IRIDIUM	YDN, CRAL
UNION	YDN, CRAL	C_B (c-103)	YDN, CRAL
NUT	YDN, CRAL	YDN. CRAL	YDN, CRAL
PRESSURE TUBE	INCONEL 702	INCONEL 702	INCONEL 702
LOCKWIRE	PLATINUM	IRIDIUM	PLATINUM
THERMOCOUPLES (FLIGHT) (DIAGNOSTIC)	P_T/P_T13RH W5RE/W26RE	P_T/P_T13RH W5RE/W26RE	P_T/P_T13RH W5RE/W26RE
EXPOSURE CYCLES EXPOSURE HOURS	3 0.5	30 4.9	34 5.0

(1) FOR 2520F MAXIMUM NOSE CAP TEMPERATURE.

27

There was, therefore, at least an 85F variation between optical pyrometers.

The second calibration involved focusing the optical pyrometers at each thermocouple location. The thermocouples were mounted 90° apart at a radius of 0.85" on the aft side of the 25-ply (0.325") disc in depressions about 0.06" deep. Thus, the thermocouples were installed about 0.26" aft of the front face of the RCC disc. The following table lists results obtained at 0.05 atm and 690 sec. The pyrometer results, which are based on an emittance of 0.9, are consistently and significantly higher than the thermocouple data. Additional adjustment of pyrometer data to reflect spectral emittance correction at 2.3 μ (pyrometer sensitive wavelength) would produce even greater disparity between the two measurement techniques.

| PYROMETER | | | THERMOCOUPLE | | Δ TEMP, F | |
No.	Temp, F Uncorrected	Corrected*	No.	Temp, F	Uncorrected	Corrected*
174522	2460	2460	1	2306	154	154
174523	2540	2495	2	2265	275	230
144389	2530	2445	3	2299	228	143
	AVERAGE	2467		2290		176

*Correction based on 0.05 ATM calibration run of Pyrometers assuming 174522 as baseline.

Note that the maximum thermocouple scatter is only 41F and the maximum scatter of corrected pyrometer data is 50F. The average difference between pyrometer and thermocouple data is 176F, uncorrected for spectral emittance. The expected temperature gradient across the 25-ply RCC would be only about 74F if the analysis results of Figure 4-4 are used as a guide. Thus, if it is assumed that the thermocouples are reading the correct temperature, then the pyrometers read high by an average of 100F, using the IRCON 174522 as a baseline value for initial pyrometer correction. The high pyrometer readings are consistent with data reported in other tests of RCC material, where the high readings were attributed to arc or gas radiation.

4.5.3.2 Model Data - The tungsten rhenium thermocouples were for diagnostic purposes only and were expected to survive for no more than a few cycles. They were used to determine the temperature distribution through the model, as well as to provide backup instrumentation for assessing optical pyrometer accuracy. Data obtained for the first three cycles is provided in Table 4-6, while typical data is plotted in Figure 4-9 to indicate probable temperature gradients through the models.

Evaluation of the optical pyrometer data is subject to error, as noted above, since multiple corrections are required in an attempt to match the thermocouple data. For the plot of Figure 4-9 the pyrometer data was adjusted by reducing raw readings, as follows:

IRCON 174522, -100F
IRCON 174523, -145F
IRCON 144389, -185F

TABLE 4-6 - TEMPERATURE DISTRIBUTION DATA

MODEL	LOCATION	CYCLE		
		1	2	3
-9		(600 sec)	(600 sec)	(600 sec)
	Pyro 22	2679F	2635F	2662F
	Pyro 23	2725F	2749F	2785F
	Pyro 89**	2775F	2750F	2760F
	T/C Mount 20	2412F	2392F	2426F
	T/C Mount 21	2409F	2392F	2423F
	T/C RCC Disc	2440F	2450F	2405F
	T/C Spacer	2420F	2419F	2370F
	T/C Nut	2380F	2379F	BAD
-10		(497 sec)*	(597 sec)	(596 sec)
	Pyro 22	2345F	2625F	2640F
	Pyro 23	2653F	2662F	2695F
	Pyro 89 **	2756F	2805F	2790F
	T/C Mount 20	-	-	-
	T/C Mount 21	2475F	2470F	2510F
	T/C RCC Disc	2490F	2490F	2160F
	T/C Spacer	2470F	2476F	2510F
	T/C Nut	2440F	2419F	2460F
-11		(748 sec)	(718 sec)	(594 sec)
	Pyro 23	2535F	2530F	2570F
	Pyro 23	2580F	2480F	2610F
	Pyro 89 **	2780F	2780F	2660F
	T/C Mount 20	2325F	2340F	2300F
	T/C Mount 21	2370F	2380F	2350F
	T/C RCC Disc	2390F	2390F	-
	T/C Spacer	2360F	2360F	2275F
	T/C Nut	2300F	2300F	2275F

* Slight water leak probably affected pyrometer readings.

** Focused on plug. Other pyrometers focused on RCC disc.

The resultant indicated temperatures were then averaged for plotting on Figure 4-9. The agreement with the expected surface temperature is not particularly good. The distribution curves were drawn assuming the front face temperature of the RCC is 74F higher than the back face in accordance with calculations, Figure 4-4.

A typical temperature time history for the thermocouples is shown by Figure 4-10. Maximum temperature is reached in approximately 600 seconds. Each exposure cycle was targeted for 600 seconds, although in some instances this varied because of equipment problems.

The -9 Model, consisting of a columbium plug and nickel union, was tested first. This model was tested for only three cycles (30 minutes), since at the conclusion of the third cycle the plug fell out. This failure was attributed to melting of that portion of the YDNiCrAl union within the columbium plug. The corrected pyrometer data would suggest that the specimen was overheated, but the thermocouple data indicates that the union was heated to a maximum of about 2450F based on the RCC aft side temperature. If more reliance is placed on the thermocouples, then a YDNiCrAl union cannot be used at this temperature condition. Small pitting was also in evidence at the periphery of the columbium plug.

The -10 Model, which also used a columbium plug, but with columbium union, was exposed to temperatures above that for the -9 Model for the first few cycles, as indicated by Figure 4-9. The temperature was then lowered starting with the fourth cycle, which is shown on Figure 4-11. This was done to avoid overheating the columbium plug, which resulted in pitting on the -9 Model, and to bring the temperatures more in line with the requirements. Unfortunately, accurate temperature assessment of exposure conditions cannot be obtained, since no thermocouples were operable from the fourth cycle on. Therefore, reliance must be placed upon the pyrometer results shown in Figure 4-11. Using the estimated temperature corrections for pyrometer results, the IRCON 174522 indicates an RCC temperature of about 2570F - 100F = 2470F from cycle 5 through cycle 27. Pyrometer IRCON 144389, on the other hand, indicates a columbium plug temperature of 2700F - 185F = 2515F for cycle 5 through cycle 9, and then 2670F - 185F = 2485F through cycle 27. Pyrometer IRCON 174523 was inoperable for these cycles. Data from the -11 Model, however, provides more insight.

The -11 Model had operable platinum rhodium thermocouples for most of it's exposure cycles, the data from which is shown on Figures 4-12 and 4-13. On Figure 4-13 it is seen that the two platinum rhodium thermocouples consistently read 50F difference and the average value is used to represent the temperature of the thermocouple mount. Using cycles 5, 13, 16, 26, and 27 from the -11 Model indicates that the thermocouple mount of the -10 Model probably operated between 2325F and 2345F for cycles 5 through 27. This puts the temperature exposure near that plotted for the -11 Model on Figure 4-9.

Beyond the 27th cycle on the -10 Model, coating damage began to occur around the edge of the columbium plug. This exposed the lower emittance base material and may have caused the increase in surface temperature, as indicated by pyrometer output rise, Figure 4-11. It was also noted that the pressure and plasma arc power were increased for these three cycles and could have caused the coating failure and increased temperature. This is discussed later.

In summary, it is concluded that the -10 Model was exposed to an RCC surface temperature greater than 2550F for three cycles and greater than 2450F for an additional 24 cycles before the coating on the columbium plug began to fail. It is significant that, when coating failure began on the 28th cycle, the model survived an additional 20 minutes of testing before degradation of the columbium plug became serious enough to terminate testing. Total test time was 4.9 hours.

The -11 Model, which employed a graphite plug and YDNiCrAl union, was purposely targeted to lower temperature conditions than the -9 Model to avoid overheating the nickel alloy union. Temperature data is plotted in Figures 4-12 and 4-13. Although exposure conditions were variable, for the most part the thermocouple mount operated around 2350F, as determined by the platinum rhodium thermocouple data on Figure 4-13. The distribution of temperature was about like that shown in Figure 4-9. Of the 34 exposure cycles there were 6 that had sufficient water leaks in the plasma arc to cause low model temperatures. Apparently, the models are insensitive to this water "quench", as there was no evidence of thermal shock cracking on the specimens. This model was exposed for the targeted 5 hours in 34 cycles.

Unlike the -10 Model, where there was no output from the platinum rhodium thermocouples after 3 cycles, one of those on the -11 Model operated full term, while the other was intermittantly in and out through 27 cycles. The nature of failure of the thermocouples or the exact location is unknown.

4.5.3.3 Pressure Data - Target pressure conditions in the test was 0.05 atm, which is 38.0 mm Hg. For the three cycles on the -9 Model the measured pressure from the model pressure tube at the end of each exposure varied between 38.7 and 39.1 mm Hg.

For the -10 Model the first cycle pressure was 40.6 mm Hg. Cycles 2 through 27 resulted in a variation from 37.1 to 39.0 mm Hg. For cycles 28, 29 and 30, when the temperature climbed dramatically, the measured pressure rose to between 55.1 and 55.6 mm Hg or approximately 45% higher than target. For these last three cycles it was noticed that the plasma arc facility current was over 20% higher than for the immediately preceeding runs. It is possible then that the failure of the coating on the columbium plug could have been aggravated by higher heating and pressure environments applied to the model.

Exclusive of those tests, which experienced severe water leaks, the -11 Model measured a pressure variation between 38.0 and 39.6 mm Hg.

In general, then, it was concluded that the model pressure measurement system did indeed function satisfactorily throughout the tests on all three models.

Selected test runs were examined in detail in an effort to correlate pressure or temperature transients observed during the run. No real correlation was found between fluctuations observed in temperature, pressure, arc current or arc voltage, except for that cited above on the last three runs of the -10 Model.

Pressure response was also examined and it was found that the pressure rose to full steady state value within 10 seconds.

It is concluded that the pressure measurement capability and response, even with the lack of a perfect pressure seal at the tube connection, is adequate for the task.

4.5.4   Test Evaluation - This section describes the physical results of the plasma test and draws conclusions relative to the three model configurations tested. The materials makeup of each model is summarized in Table 4-5.

-9 Model - This model was tested for 30 minutes in three cycles. At the conclusion of test the columbium plug fell out, revealing that the nickel alloy union had melted. In addition, the plug suffered pitting on the exposed surface near the edge of the countersink. The pitting did not originate at the radiused edge but propagated to it. The same damage occurred on the -11 Model but right at the corner. All other components remained intact with no evidence of damage. The nickel nut was removed quite easily from the nickel union indicating no self bonding. In addition, there was no evidence of chemical reaction between the nickel, columbium, or coated RCC.

Photographs of the model, following test are included as Figures 4-14, 4-15 and 4-16.

It was concluded that the melting of the nickel alloy union was the result of overheating, perhaps due to higher temperatures than expected on the end of the union, rather than a chemical reaction. Therefore, a nickel alloy union cannot be used successfully in the maximum heating region of the nose cap, but, based upon results from the -11 Model, could find application in the cooler regions.

The pitting on the face of the columbium plug was experienced on both the -9 and -10 Models, and represents a marginal condition for this coating system. Since the pitting occurred at the same locale on both models, some improvement would result from increased corner radius of the countersink head. This would reduce local temperature and/or improve coatability.

-10 Model - This model, which had both a columbium plug and a columbium union, was expected to provide higher temperature capability than the -9 Model. However, in view of the surface pitting experienced by the -9 Model, the exposure temperature was reduced by about 100F after the first three cycles in order to avoid early pitting and provide data on longer term exposure. The RCC surface temperature for most of the run time is estimated at about 2470F, reference Figure 4-11 Pyrometer #22 with 100F correction. This is 30F lower than the target condition.

This model survived 30 test cycles for a cumulative exposure of 4.9 hours. It was disassembled completely without the aid of wrenches after both 2-hours and 3-hours exposure, but at 4-hours, the union could not be unscrewed from the plug with finger pressure. And at the conclusion of test, disassembly could not be accomplished, even by strenuous urging with wrenches. At this point, however, the nickel nut was still readily removed from the columbium union.

The inability to separate the plug and union after 4-hours exposure was not unexpected and was the reason for using a loose fit on the threads and assembling finger tight.

After 2-hours exposure no material degradation or chemical reaction was observed on any part.

The condition of the model after 3-hours of test is shown in Figures 4-17 through 4-19. Note that pitting has begun at the corner of the plug head, but, as noted below, propagation of the failure is rather slow, providing a degree of failsafe operation. None of the other parts showed any damage or chemical reaction with the exception of the welded washer to the pressure tube. In all models this electron beam welded joint failed, proving to be unsatisfactory. A standard flared tube end would correct this problem by eliminating the washer completely.

After 4-hours exposure, the model appearance was as shown in Figures 4-20 and 4-21. Note that the initial coating failure on the plug has not progressed greatly after the additional hour of exposure, but another pit has developed. At this point, only the nickel nut could be disassembled from the union. However, no other evidence of failure or chemical reaction could be observed on the assembly.

After the 27th cycle the columbium plug began to degrade rapidly as evidenced by Pyrometer 89 response, Figure 4-11. It is observed that as more bare columbium became exposed with it's low emittance, the temperature progressively rose higher until testing was terminated after the 30th cycle. The condition of the model at the conclusion of testing with 4.9 hours of exposure is shown in Figures 4-22 and 4-23. While the columbium plug is severely oxidized, the oxidation rate appears to be such that mission safety would not be an issue.

Only the nickel nut and pressure tube could be disassembled from the model. Visual inspection could reveal no areas on the nut, union, pressure tube, lockwasher, thermocouple mount, or thermocouples where melt, chemical reaction, or coating degradation were in evidence. However, the union and plug could not be disassembled even with hard wrenching. This eventually resulted in bending the washer and chipping the coating on both the washer and union.

This assembly had to be sectioned for examination. Photographs of sectioned pieces are shown in Figure 4-24. No evidence of coating failure or subsurface oxidation were found. Of particular significance is that the plug and union section, shown in the lower photo of Figure 4-24, were easily separated after sectioning. This indicates that there apparently was no diffusion bonding between the two parts. It was believed that the reason for being unable to disassemble the plug and union was not the result of self-bonding, but probably due to scale formation which tended to lock-up the threads. The scale formation was discovered in the chemical compatibility tests discussed previously. If this was indeed the case, then it was believed possible to extend the operational life of columbium parts by periodic disassembly and removal of loose scale. Actually, anti-seize tests did not bear this out, and an anti-seize coating was developed to enhance disassembly, Section 6.3.

-11 Model - This model utilized a coated graphite plug and a nickel alloy union. It was exposed to temperature conditions approximately 50F lower than targeted to avoid premature failure of the nickel alloy union. This permitted testing for the full 5-hours desired.

There was no periodic disassembly of this model and at the conclusion of test only the nut and pressure tube could be removed. The union and plug were bound together tightly, such that the plug had to be fractured to separate the two. Post test photographs of this model are provided as Figures 4-25 through 4-27.

In Figures 4-25 and 4-26 the assembly looks as good as the pretest condition. However, upon disassembly it is seen in Figure 4-27 that the nickel alloy union suffered some melt damage. The "blob" of material projecting from the end of the union was analyzed and found to be the same as the union material. In addition this material and the union itself on the plug end were highly porous. It is not known when this "blob" formed, nor whether it was purely an over-temperature condition or a result of a chemical reaction promoted by the graphite coating. Interestingly, the protuberance did not take the shape of the cavity in the graphite plug, and pressure from the model pressure measurement system during the last cycle was consistent with values measured throughout the test program. The formation of this protuberance thus remains a mystery.

The graphite plug was examined visually for evidence of subsurface attack; that is, graphite oxidation at the coating/graphite interface. There was no evidence of any significant subsurface oxidation, although there probably was a modest amount, since some of the fractured surfaces tended to undercut the coating slightly. However, there were no pockets of oxidation, and the coating was firmly attached to the graphite.

The coating thickness on the plug was evaluated by the burnout technique, wherein the sectioned material is exposed in an air furnace to oxidize the graphite away from the coating. This leaves the coating, as a shell, that can be readily measured. This operation revealed a dense outer "skin" roughly 5 - 10 mils thick and a total coating thickness that varied between 25 mils in the internal cavity and threaded region, to 35 mils on the outer surface of the shank, and 45 mils on the surface exposed to the plasma environment. These thicknesses are in accordance with the desired 20 mil minimum.

Note in Figure 4-25 that the pressure port hole and cavity have remained intact, indicating that the design modifications made to this graphite part has resulted in good coatings. This is in contrast to the Phase I design, where the pressure port hole did not coat sufficiently thick, resulting in oxidation in the hole.

4.6   Pressure Tubes Routing Concept

4.6.1   Design Concepts - There were fourteen pressure ports distributed in the nose cap in initial locations shown by Figure 4-28. Each location had a 5/32 inch diameter pressure tube, which was to ultimately increase in diameter to 3/8 inch and pass through the nose cap support bulkhead to pressure transducers located on the aft side of the bulkhead. Tube runs were to be maintained as short as possible for best pressure response at the higher altitudes, and the transition to the larger diameter tube was to be made as quickly as possible, but preferably the small tubes were not to be over one and a half feet in length.

The primary considerations involved in developing and evaluating concepts for tube routing included:

(1) The dynamic vibration loads imposed from the nose cap and bulkhead during launch and transonic flight, as well as the acoustic noise environment imposed on and within the nose cap cavity during this period.

(2) The high temperature inside the nose cap cavity during entry which was in the 2300 - 2500F range, and the need to limit the aluminum support bulkhead temperature to an acceptable level as the tubes pass through the bulkhead.

(3) The relative deflection between nose cap and the nose cap support bulkhead under the action of the boost pressures.

(4) Acceptable locations on the support bulkhead to provide tube pass through and tube support.

(5) Ability to install the system initially and permit periodic replacement of components in the event that the SEADS would not have a mission life capability equivalent to the nose cap.

(6) Minimizing loads introduced into the nose cap from SEADS.

Three basic approaches were examined qualitatively and are illustrated in Figures 4-29, 4-30 and 4-31. They are:

(1) Route each tube individually from the nose cap to the bulkhead.

(2) Gang groups of tubes together for mutual support and route to the bulkhead.

(3) Provide a stiff support structure mounted off the bulkhead to which groups of tubes are routed for support.

Individual tube routing as illustrated in Figure 4-29 with or without conduits leads to a flexible tube system, not likely to be compatible with vibration and acoustic noise requirements unless the conduit is overly large. Moreover, each tube requires individual insulation and individual mounting provisions at the bulkhead. The expected flexibility and complications with fourteen insulation blankets and mounting brackets make this approach unattractive.

Ganging tubes together, as shown in Figure 4-30, provides for mutual support to more efficiently stiffen the system, as compared to individual tube routing. Only one insulation blanket for each group of ganged tubes is required. However, unless each tube diameter is increased significantly above the 3/8 inch required, the system was still expected to be too flexible for the long tube runs to meet vibration requirements. In addition, methods of tieing the tubes together to produce effective mutual support could become overly complicated. These considerations led to the support tube concept, which was considered to be the best approach.

The support tube concept, pictured in Figure 4-31, gives the opportunity to provide the stiffness required to meet vibration requirements. Two support tubes are employed, each collecting seven pressure tubes. Fortunately, there are locations on the bulkhead that allow the passage of seven tubes in a

localized area as well as to permit the large footprint of the fitting that ties the support tube to the bulkhead. One insulation blanket is required for each support tube. The length of the support tubes and the location of their nose cap ends can be adjusted to optimize the unsupported lengths of the 5/32 inch diameter tubes. Further, the system offers the flexibility of transitioning from the 5/32 inch diameter to the 3/8 inch diameter tubes at any location between the nose cap and support tubes to balance the design of the small diameter tubes between the vibration and static deflection requirements. For these reasons this concept was selected for further analysis, which, as described later indicated feasibility of the support tube concept.

4.6.1.1 <u>Support Tube Concept Options</u> - The support tube approach (Figure 4-32) has several options that were qualitatively evaluated as discussed below.

The 3/8 inch diameter tubes may be routed either internally or externally to the support tube. External routing would produce lower stiffness for a given external diameter than for the internally routed tubes and it was felt that mounting the pressure tubes external to the support tube may lead to a more complicated overall design. Although the external approach would probably permit easier replacement of individual tubes in service, it was felt that damage to the 3/8 inch diameter tubes was highly unlikely based on the design envisioned. The weak spot of this system should be the 5/32 inch diameter tubes. Therefore, easy replacement of the larger tubes was no real advantage. Because of the greater stiffness offered by internal routing, the internal approach was selected. The concept is shown on Figure 4-32.

The support tube and the pressure tubes will operate at different temperatures and experience different heating rates. Therefore, the pressure tubes should be anchored at one end and allowed to expand at the other end of the support tube. Since the tubes at the bulkhead end are mounted in an insulator block to protect the bulkhead against overheating, it was considered better to permit the tubes to expand freely at the nose cap end to avoid possible cocking and subsequent jamming of the insulator block on the support tube if it was designed to slide.

Because of possible excitation of the 3/8 inch diameter tube inside the support tube, bulkheads were added to provide periodic support to the pressure tubes. The bulkheads also add structural and geometric stability to the support tube skin, which was envisioned as a rolled configuration, perhaps 0.010 inch thick.

As noted previously, the internal temperature environment of the nose cap was in the 2300 - 2500F range, yet the support bulkhead must not exceed 350F. Therefore, an insulation blanket covers the tube. Insulation is also added at the end of the tube that views the nose cap. This produces a substantial temperature drop at the hot end of the tube. However, both the insulation blanket and hot end insulation were not expected to be sufficient for limiting the bulkhead temperature rise. Therefore, an additional tubular insulator, made of polyimide fiberglass, was added at the bulkhead end of the support tube. Similarly, a polyimide block is added at the bulkhead end to provide thermal insulation from the 3/8 inch diameter pressure tubes. The thermal adequacy of this design is covered in Section 4.6.2.

4.6.1.2 <u>Support Tube Locations</u> - The nose cap support bulkhead was examined for possible locations acceptable for mounting the support tube and

permit pass-through of the seven pressure tubes for each support tube. This examination revealed that the region between nose cap support fittings numbers 2 and 3 and 9 and 10 would be the most optimum acceptable location for the penetration array. This required canting the support tubes to minimize and balance the tube runs of the 5/32 inch diameter tubes. This is shown in Figure 4-33. For this particular pressure port array the support tube arrangement is symmetrical about the vertical centerline, but for another array pattern the cant angle of each tube can be optimized for the pressure tubes each collects.

4.6.2   Thermal Analysis - The support tube was thermally analyzed to show feasibility of the insulation design to protect the support bulkhead; however, no attempt was made to optimize the design. Preliminary estimates established the insulation blanket thickness at 2.5 inches and the length of the polyimide fiberglass tube. Finite element analyses were then conducted to evaluate the effectiveness of the design, reference 4.

Entry trajectory 14414.1C was used in this analysis, which is slightly hotter than trajectory 14414.1. Insulation surface temperatures were specified with time and were determined from the baseline nose cap thermal analysis. Boundary temperatures are shown in Figure 4-34. The bulkhead temperature limit was set at 350F and the polyimide fiberglass temperature was limited to 650F. Two different insulation materials were analyzed - 12 lb/ft Dynaflex, and 9 lb/ft^3 HRSI.

Analysis was conducted using the Southwest Research Institute thermal analyzer routine with the model pictured in Figure 4-35. For simplicity the tube was assumed normal to the bulkhead plane with a length equal to the shortest dimension of the true canted tube. Heating was applied axi-symmetrically. The seven pressure tubes were combined into one, but, because of radiation view factors of the true individual tubes, only 75% of their surface area was allowed to participate in radiation heat transfer.

Temperature time histories of selected nodes are given in Figures 4-36 and 4-37 to illustrate the differences in results for the two insulation materials. HRSI shows better efficiency, but for either material the bulkhead temperature peaked below the 350F limit. Polyimide fiberglass maximum temperature is examined further in Figure 4-38 to show the value at the hot end of the tube. Note that with HRSI the temperature is within the 650F limit, but with Dynaflex the limit is exceeded by only 30F, indicating a small adjustment to the design would be required if Dynaflex was to be used. The effectiveness of the polyimide fiberglass in reducing heat conduction to the bulkhead is also indicated on Figure 4-38 by the temperature gradient along the polyimide fiberglass tube.

Temperatures at the nose cap end of the support tube are shown in Figure 4-39 at time cuts representative of maximum values achieved for the nodes of interest. Because of the modeling technique used, the temperature of node 3 may be understated, but the effectiveness of the insulation within the support tube is indicated by the temperature drop between nodes 2 and 5. This insulation primarily acts as a radiation barrier, but has some heat sink effect, as well. Note that the temperature gradient along the pressure tube is rather small, as indicated by a comparison of nodes 4, 5 and 6. This small gradient also exists in the support tube and indicates that heat transfer to the polyimide fiberglass and the bulkhead is primarily due to radial heat conduction rather than conduction down the length of the tube. This is

attributed to the radiation heat blockage afforded by the insulation in the nose cap end of the support tube.

In summary, the following results and conclusions were obtained from the thermal analysis:

(1) The support tube concept is thermally feasible.

(2) Blockage of radiation heating by insulation at the nose cap end of the support tube is very effective in producing a thermally efficient design.

(3) Heat conduction is primarily radial once the blockage noted in (2) is employed.

(4) It may be feasible to eliminate the polyimide fiberglass tube by increasing the thickness of the insulatio·· blanket.

4.7 Dynamic Analysis

One of the most critical aspects of the SEADS design is the ability of the small diameter pressure tubes to withstand the dynamic environment, yet be flexible enough to meet static and thermal deflections. It was clear from static analysis that each of the tubes would require bends or a coil or loop to maintain tube stresses to reasonable levels, and to avoid introducing significant loading into the penetration assembly or the nose cap. A dynamic analysis, references 2 and 5, was conducted to determine the feasibility of the support tube concept and to establish guidelines for tube configurations that would meet the vibration requirements.

One of the support tubes and all seven of it's pressure tubes were modeled and analyzed using Vought Dynamics' PAS System. A 922 degree-of-freedom finite element model was used to describe the support tube and pressure tubes numbers 2, 4, 5, 9, 10, 12 and 14 (Figure 4-28). This was reduced to 168 degrees-of-freedom by static condensation and imposition of constraints at the nose cap and support bulkhead. Twenty-four elastic modes were used in the frequency response analysis.

The support tube analyzed was 2 3/4 inch diameter, 0.012 inch thick Inconel skin stepped up to 0.025 inch effective thickness at the base to represent the region with the polyimide fiberglass. The 5/32 inch diameter pressure tubes were assumed to have 0.015 inch wall thickness, while the 3/8 inch diameter tubes were 0.020 inch wall thickness. Modal damping was assumed to be 2% of critical. Twelve pressure tube configurations were evaluated.

For this feasibility analysis, a maximum of $2G^2/Hz$ vibration level, was simultaneously applied and correlated in all three axes at both the bulkhead and at the nose cap end of the system. Realistically, the environment at the bulkhead should have lower levels inplane than those normal to the bulkhead web. Therefore, the application of this environment in all three axes at the base of the support tube produces larger responses at the nose cap end of the tube and tends to offset the reduced level at the nose cap skin, which was $30G^2/Hz$ at the time the study was conducted (reference 2). Significantly reduced design and test levels were ultimately used for final design as shown by the test spectrum on Table 9-1.

While all tubes were analyzed together, evaluation to determine acceptable configurations was conducted by changing only one tube at a time. These individual changes were found to effect the response of the other tubes of the array and further adjustments were sometimes required. Acceptable tube configurations are pictured in Figure 4-40. Tube number identifications are referenced to Figure 4-28.

A summary of the maximum RMS loads obtained on the support tube and pressure tubes is listed in Table 4-7. Maximum bending stresses, resulting from these loads, are as follows:

<div style="margin-left: 2em;">

Support Tube	= 18380 psi
Pressure Tube at Nose Cap (5/32 in. dia.)	= 19070 psi
Pressure Tube at Bulkhead (3/8 in. dia.)	= 2770 psi

</div>

In the process of optimizing and evaluating preliminary design configurations, trend or sensitivity analyses were conducted. Results are summarized in Tables 4-8 and 4-9.

The influence of support tube variations upon support tube stress and upon the average of stresses of the seven 5/32 inch diameter tubes at both the nose cap end and the coupler end (connection to the 3/8 inch diameter tube) are shown in Table 4-8. Note that the inclusion of a "vibration isolator" between the support tube and bulkhead produces a reduction of support tube stress, but it has a significant adverse effect on pressure tube stresses. Therefore, the vibration isolator was eliminated from further consideration.

Results also show that stiffening the support tube produces modest stress change to the support tube, but, again, can have an adverse effect upon the stresses of the pressure tubes, producing as much as a 60% increase for the case examined, where the diameter is increased. If the thickness of the support tube is decreased, support tube stress increases almost inversely proportional to the thickness decrease, but the pressure tubes stress increases only modestly. If the thickness of the base of the support tube is increased, while the basic thickness is decreased, support tube stresses decrease, but pressure tube stresses go up.

The conclusion reached from this study is that the operating stresses for both the support tube and the pressure tubes are sensitive to support tube geometry variations and the system must be tuned for optimum performance. If changes are made the system must be retuned. Of course the low operating stresses of the system (less than 20000 psi) indicates that moderate increases in stress can be tolerated without becoming critical.

Sensitivity analyses for selected pressure tubes are summarized in Table 4-9. It is apparent that a change in an individual pressure tube has a finite, but small, influence on support tube stress, unless the change is extreme. The results show that in general, once a pressure tube is optimized, adding or deleting loops produces adverse stress changes. In particular, overly long or extremely short, stiff tubes result in high stresses. However, there are changes that can be made without seriously degrading the system. Typical is the 3 inch length increase to tube #10 with a resultant decrease of stress or the addition of a loop to tube #14 with only 22% stress increase. Thus, while there is a requirement to design tune each tube, there remains a degree of flexibility for deviations that might occur during mock-up of the tubes or during production installation.

TABLE 4-7

DYNAMIC ANALYSIS RESULTS RMS LOADS

Member	Location	Shear lb.	Moment in.-lb.	Axial lb.	Torque in.-lb.
Support Tube	Base at Bulkhead	167	2748	16.0	5.3
Pressure Tubes 3/8" dia.	Bulkhead	0.1	5.2	1.7	0.9
	End of Support Tube	0.8	5.4	1.8	0.9
5/32" dia.	3/8" to 5/32" Coupler	1.3	3.7	0.6	0.9
	Nose Cap	1.8	4.1	0.9	1.3

TABLE 4-8

RESULTS OF PARAMETRIC INVESTIGATIONS OF SUPPORT TUBE

PARAMETER	PARAMETER RATIO	STRESS RATIO (1)		
		SUPPORT TUBE	PRESSURE TUBE	
			AT COUPLER	AT NOSE CAP
BASELINE	1.0	1.0	1.0	1.0
VIBRATION ISOLATOR AT BASE OF SUPPORT TUBE	10^{-3}	0.74	2.31	1.67
DIAMETER OF SUPPORT TUBE	1.19	0.92	1.61	1.40
THICKNESS OF SUPPORT TUBE	2.08	1.11	1.10	1.17
THICKNESS OF SUPPORT TUBE	0.48	1.93	1.09	1.20
THICKNESS OF SUPPORT TUBE				
BASIC TUBE	0.48	0.52	1.18	1.19
FIBERGLASS REGION	2.00			

(1) The stress ratio represents the average effect of all tubes.

TABLE 4-9

RESULTS OF PARAMETRIC INVESTIGATIONS OF PRESSURE TUBES

TUBE NO. (1)	PARAMETER	PARAMETER RATIO	STRESS RATIO		
			SUPPORT TUBE	PRESSURE TUBE	
				AT COUPLER	AT NOSE CAP
#14	ADDED 3" DIA. LOOP AT NOSE CAP END LENGTH ≈ 23"	1.64	1.0	1.22	1.02
	ADDED 3" DIA. LOOP AT BOTH ENDS OF TUBE LENGTH ≈ 32"	2.29	0.82	7.75	2.04
#10	INCREASED TUBE LENGTH TO ≈ 17"	1.23	1.0	0.59	0.97
	ADDED 3" DIA. LOOP AT NOSE CAP END LENGTH ≈ 24"	1.71	0.97	0.85	2.12
#4	REMOVED LOOP LENGTH ≈ 8.5"	0.49	1.06	3.98	1.20

(1) Refer to Figure 18 for baseline configuration.

42

A preliminary assessment of the expected fatigue life of the pressure tubes was made using a technique that expresses the RMS stress from random vibration into an equivalent sinusoidal stress. Then, using the highest of the range of significant response frequencies, the time to failure was computed from Inconel 718 fatigue data, since Inconel 702 data was not available. Time to failure for the 19.07 KSI RMS stress level was 67 minutes, 4.8 times the requirement for the maximum environment. The indication is that the tubes would survive 100 missions.

As a result of the dynamic analyses to evaluate feasibility, the following conclusions and guidelines are offered:

(1) The support tube concept is feasible.

(2) The system must be tuned to obtain frequency separation between the support tube and pressure tubes, and to optimize the design.

(3) A vibration isolator at the mounting base of the support tube should not be used.

(4) The small diameter pressure tube length should generally fall in the range 14 - 18 inches.

(5) A stiff support tube base in the region of the fiberglass should enhance an optimized system.

(6) Simple bends in the pressure tubes are best, but if loops are required to meet length/stiffness requirements they should be located at the nose cap end of the tube. This guideline presumes the response at the end of the support tube is greater than the environment at nose cap. If this condition doesn't exist then the loops in the pressure tubes should be near the support tube.

4.8 Structural Analysis

Preliminary structural analyses were conducted on system components and are summarized in this section.

4.8.1   Support Tube - The support tube was statically analyzed for an arbitrary 200 pound ultimate load applied at the free end. This loading was intended to cover the possibility of a man supporting his weight on the support tube, while leaning into the nose cap cavity, installing or replacing pressure tubes. This analysis was conducted primarily to establish rough sizing for the dynamics analysis and to obtain consistent strength/stiffness of the support tube and its' mounting provisions.

The Inconel support tube was analyzed for buckling where it attaches to the polyimide fiberglass tubes. Results for two assumed tube thicknesses are as follows:

Wall Thickness t, in.	Applied Stress f_c, psi	Allowable Stress F_c , psi	Margin of Safety
0.010	47200	53400	0.13
0.012	39330	60000*	0.53

*Buckling allowable limited to yield stress.

A similar analysis to evaluate stability of the polyimide fiberglass section yielded a thickness requirement of only 0.02 inch. However, in order to maintain uniform stiffness or prevent a "soft" region at the base of the support tube, the polyimide fiberglass was sized to produce equivalent axial stiffness to the Inconel section. Thus, for 0.010 inch thick Inconel the fiberglass thickness should be 0.12 inch and would increase to 0.14 inch for a 0.012 inch thick Inconel tube.

Attachment of the Inconel and fiberglass is by Monel rivets to survive the 600F temperature during entry, when loads are very small. Two rows of rivets are required for strength continuity.

Because of the insulative capability of the polyimide fiberglass, the bulkhead attach fitting and the rivets, connecting to the fiberglass, are aluminum. The fitting collar is 0.050 inch thick, sized to develop rivet strength in bearing in the 6061-T6 material. The flange of the fitting was sized for simple bending and resulted in a 0.20 inch thickness requirement. The bolts tieing the fitting to the bulkhead have a non-uniform pattern to permit the bolts to either go through the thickened portion of bulkhead web intersections, or to miss the webs entirely. Analysis of bolt tension with some prying on the bolt heads, resulted in a requirement for 3/16 inch diameter bolts.

It should be reiterated that the structural sizing conducted was to assure realistic and uniform design of the support tube and no attempt was made to optimize or perform rigorous analysis. The resultant design was released as Vought drawing 221GT4069.

4.8.2   Pressure Tubes - A static analysis was conducted on the longest and shortest tube in the array to determine the magnitude of tube stresses and loads imposed on the penetration assemblies. Both forced deflection and thermal deflections were evaluated. Forced deflections are imposed from applied airloads to the nose cap, which in turn loads and deflects the support bulkhead. As the bulkhead deflects the surface on which the support tube is mounted rotates, causing the end of the support tube to swing. This produces a net movement between the support tube end and nose cap end of each pressure tube. Maximum forced deflections occurred during a descent phase, when the tubes were essentially at room temperature. Maximum thermal deflections occurred during entry when air loads were small. This analysis proved highly conservative when deflections were reduced to insignificant values, but is included here for completeness.

Maximum forced deflections at the time period analyzed (February 1977) occurred for a condition designated AT369, which was a descent condition at 2000 ft. altitude. Bulkhead deflections at the nose cap attach fittings and nose cap deflections were obtained from the baseline nose cap analysis. Vertical and side deflections were insignificant but the aft limit load deflections were:

$$
\begin{array}{ll}
\text{Nose Cap} & = 0.183 \text{ in.} \\
\text{Fittings 2 and 10} = 0.177 \text{ in.} \left.\rule{0pt}{1.5em}\right\} \quad \text{Avg. 0.162 in.} \\
\text{Fittings 3 and 9} = 0.148 \text{ in.}
\end{array}
$$

Since the support tubes attach between fittings 2 and 3, and 9 and 10, the average of these deflections was used to calculate tube rotation. The motions used in the deflection analysis are shown as follows:
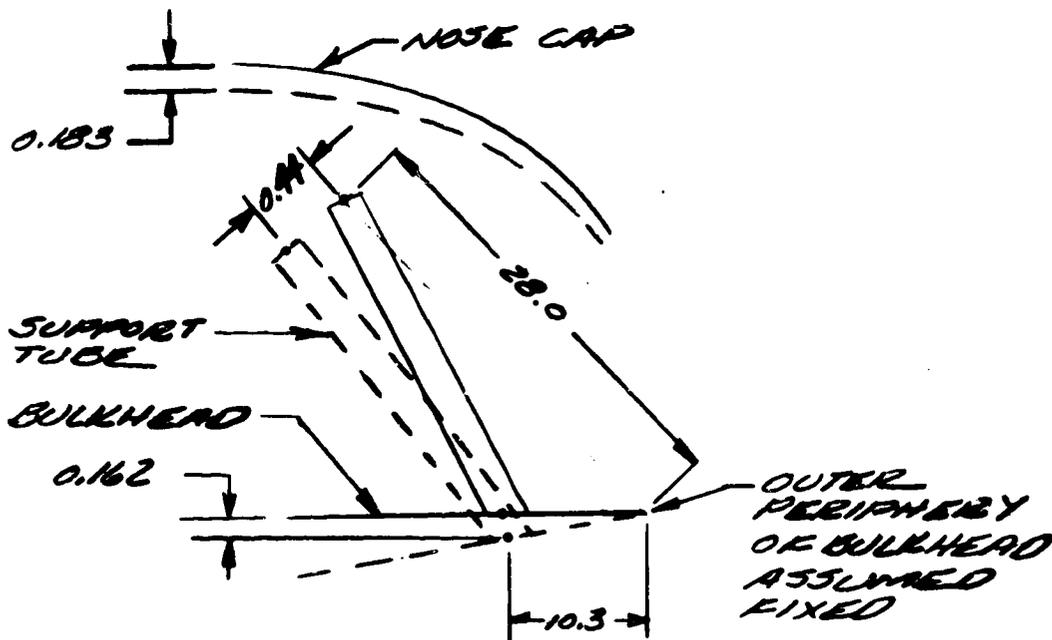
Using a full scale layout, it was found that the forced deflection for the longest tube was 0.28 inch, while that for the shortest would be 0.25 inch, the difference being due to their location on the nose cap. For this preliminary evaluation the long tube was actually analyzed for 0.3 inch deflection. As noted in the picture above, the outer periphery of the bulkhead was assumed fixed. A deflecting bulkhead boundary was also examined based upon spring rates supplied by Rockwell. This resulted in a 15% reduction in the rotation of the support tube, but the deflections noted above were used because they were documented.

The configurations of the tubes analyzed and the resultant end loads and maximum moments obtained are shown in Figure 4-41. It was found that the long tube produced the highest loads on the penetration and experienced the highest tube bending moments.

For a 5/32 inch diameter Inconel 702 tube with wall thickness of 0.010 inch and a modulus of elasticity, E, of 31.5×10^6 psi, the following loads and stresses are obtained for the long and short tubes:

	LONG TUBE	SHORT TUBE
Shear Load, H, lb.	9.3	4.8
Axial Load, V, lb.	2.4	0.6
End Moment, M, in.-lb.	19.0	8.6
Max. Moment, in.-lb.	19.0	11.3
Bending Stress, psi	120,700	71,765

These computed stresses are rather high and exceed the yield strength of precipitation heat treated material, which is 60,000 psi (MIL-HDBK-5C). However, there are some offsetting factors as enumerated below.

(1) The elongation of the material is in excess of 30% (MIL-HDBK-5C), and will permit the tubes to be repeatedly flexed beyond yield.

(2) As the material is flexed beyond yield, the stiffness reduces and the actual stresses obtained will be somewhat lower then those computed.

(3) Later design loads, and hence bulkhead deflections, are only 56% of those used in this analysis. Therefore, calculated stresses will be reduced accordingly. (Final design studies produced an insignificant forced deflection on the tubes, making coated columbium tubes feasible.)

(4) Work hardening due to flexing at ambient temperature should be offset to a degree by the intermediate high temperature conditioning during entry.

(5) The analysis assumed complete fixity at the tube ends. This is most likely not the true condition.

(6) The long tube stresses could be made to approach those of the short tube by extending the length of the 3/8 inch diameter tube and adding a loop in the 5/32 inch diameter tube. That is, design optimization can be conducted.

The thermal expansion condition was examined for the long tube assuming a temperature rise of 2400F for the 5/32 inch diameter tubes and an average 600F rise for the 3/8 inch diameter tubes. Referring to Figure 4-41, this results in an effective deflection in the V direction of 0.21 inch and an effective deflection in the H direction of 0.12 inch. Computed end loads are:

$$H = 0.0140 \text{ EI}$$
$$V = 0.00404 \text{ EI}$$
$$M = 0.0264 \text{ EI}$$

At 2400F the modulus of elasticity, E, is probably only 10 - 20% of the room temperature value (data not available at this temperature), so that induced loads are roughly only one-tenth of those computed for the room temperature condition. The number of missions that the tubes can survive under these conditions can only be determined by test.

4.8.3   Penetration Assembly - The tube end loads applied to the penetration assembly are very low, being a maximum of 19 in.-lb. bending, 9.3 lb. shear and 2.4 lb. axial compression, assuming no load reduction for the tube stress exceeding yield. An analysis of the strength capability of the penetration assembly was conducted for these loads. It was found that shear strength of the threads in the graphite plug produced the minimum strength margin. For a shear allowable of 1000 psi the factor of safety was calculated to be greater than 5. Thus, it appears that there is adequate strength capability in the penetration assembly.

46

4.9 Summary and Conclusions

4.9.1   Overall Design Concept - By structural, dynamic and thermal analysis it was shown that the basic design concept, involving the support tubes, small pressure tubes and the pressure port assembly, is feasible. Design refinements can improve the concept, particularly with respect to small pressure tubes configurations.

4.9.2   Pressure Port Assembly - Both coated graphite and coated columbium may be used for the plug with an unknown mission life. Improved life of the columbium plug would be possible by using a larger edge radius on the countersink head. The oxidation rate on columbium appears sufficiently low as to provide a measure of flight safety in the event of localized coating failure.

The nickel alloy, YDNiCrAl, cannot be used safely for the union regions where the nose cap surface temperature will operate in excess of about 2400F. However, a coated columbium union will successfully operate at the design temperature.

It appeared that nickel alloys can be used for the pressure tubes, the attaching nut, and the lockwasher for lower design temperature regions. The use of coated columbium for these parts provide a temperature margin of safety, and a platinum rhodium alloy should be a viable alternate for the small pressure tubes, when an iridium chemical barrier is used to provide protection from silicide coatings.

Platinum rhodium thermocouples produced varying degrees of success, but appear to remain the best candidate. Electrical grounding of the thermocouple sheath solved initial problems, when no usable data was obtained from these thermocouples. The 10 mil wire size thermocouple produced response as good as the 5 mil wire configuration, and due to increased ruggedness, is the preferred configuration.

Thermocouple mounts of either iridium or nickel alloy may be used and depends in part on thermal margin desired. Iridium is roughly an order of magnitude more expensive than the nickel alloy. It is probably feasible to design a coated columbium thermocouple mount, but thermocouples would have to be bonded in place, since staking with the coating would be unacceptable.

In summary, the ingredients for producing a sound system were demonstrated by analysis or test. It remained to select the best materials combinations, upgrade the design and analyses, and conduct additional tests to verify the analyses and establish the expected mission life of the system.

5.0 NOSE CAP RELATED ANALYSES

Having demonstrated the fundamental feasibility of the SEADS thermo/ structural design by analysis and/or test, it became timely to perform more detailed analyses to assure that each facet of the system was adequately addressed and quantitized, where practical.

The nose cap became the target for detailed analyses to answer concerns expressed by NASA and Rockwell. In particular the questions posed, and associated analyses, summarized in this section, are as follows:

(1) With the introduction of fourteen penetration holes in the nose cap, how do they, or any local stiffening required, affect nose cap strength and buckling?

(2) What effect does a non-circular penetration hole in the nose cap have upon local stresses? (This item is taken out of chronological sequence, since it logically should be combined with nose cap analyses.)

(3) Would a more sophisticated thermal analysis of the penetration assemblies to account for cross-radiation and unsymmetrical heating produce possible thermal stress concerns for either the nose cap or the penetration assemblies?

(4) Does the presence of the two insulated support posts in the nose cap block cross-radiation to the extent that thermal stress in the nose cap is significantly affected?

Each of these items are covered in this section of the report.

5.1 Structural Analysis of the Nose Cap

For the Phase II program, discussed in Section 4.0. the test program and thermal analyses were based upon thickening the nose cap around each penetration assembly, such that the local thickness was 25 plies as opposed to the basic nose cap 19-ply dome construction. The reasons for this were (1) to restore local strength and stiffening, where the material was cut out for the penetration assembly, and (2) to provide sufficient thickness to permit countersinking for the relatively large diameter ports. The local stiffening was to be accomplished by tapered circular ply doublers, and was established by engineering judgement.

The finite element analyses conducted, reference 6, and described herein were intended to examine the effect of the penetration holes upon nose cap buckling stability, as well as local stress around the holes. Alternate configurations were analyzed in an effort to select the best design for the SEADS nose cap. These were compared against the baseline nose cap to ensure that the selected SEADS approach would not reduce the buckling allowable.

The configurations analyzed were as follows:

(1) Unstiffened, i.e., basic 19-ply dome with penetration holes.

(2) Local ring stiffening with a nominal 2.5 inch diameter, 6-ply doubler pack to produce a 25-ply thickness around each penetration hole.

(3) Local ring stiffening with a nominal 2.5 inch diameter, 13-ply doubler pack to produce a 32-ply thickness around each penetration hole.

(4) Uniform stiffening of the entire dome region by adding 2 plies for a total thickness of 21 plies.

The fourteen pressure port penetrations of the original configuration, shown in Figure 4-28, were re-arranged, based upon systems analysis by NASA, to the more optimum cruciform arrangement shown on Figure 5-1. Port spacing is approximately 4.8 inches. The nose cap was analyzed for the cruciform configuration.

5.1.1   Modeling Approach - In order to provide the desired direct comparison with the baseline nose cap, while obtaining the local stress distribution around the holes, the basic finite element grid system of the baseline nose cap was retained, but a finer grid was desired around each of the holes. Analysis of the number of terms, bandwith, and density of matrix data for the SEADS analysis resulted in a forecast of impractical computer costs, computer resource needs, and data storage constraints. Several alternatives were examined, but the most desirable option found was to model only half the nose cap. The practicality of this was based on the fact that both the nose cap and the applied loads were symmetrical about the vertical centerline. The feasibility of this approach was demonstrated on the baseline nose cap by analyzing both the full nose cap and a half model. Identical results were obtained.

The SEADS configurations were then analyzed as half models using the grid pattern illustrated on Figure 5-2. Each hole was modeled as an octagon with inside diameter of 1.0 inch, the average of the 0.75 inch x 1.25 inches countersink dimensions for the port. The grid is shown on Figure 5-3.

The nose cap was supported on springs, representing the support fittings with spring rates identical to those used in the baseline analysis. T-seals and expansion seals were excluded as being inconsequential to the analysis results.

Material properties for the RCC were based on the then current mass loss predictions. The minimum secant modulus band was used for the dome region, while average secant modulus was used for the 38-ply flange.

A NASTRAN differential stiffness analysis approach was used, which is an iterative solution, that accounts for the deflected shape in arriving at a solution. It is, in effect, a large deflection analysis. With this technique either deflection or change in slope of individual elements are tracked as load is increased to determine the buckling limit. For this nose cap thickness the change in slope technique was determined to be appropriate and was based upon analysis of tests of two development nose caps, one of which was 7 plies thick, while the other was 15 plies thick. Two modes of determining the buckling limit are employed and are represented on Figure 5-4. The first is termed "snap through" and is characterized by a reversal of the slope of an element. The limiting buckling load (insipient buckling) is taken where the change in slope is zero. The second mode, termed "collapse", is one in which the slope of an element goes divergent and the limiting buckling load is that determined by the asymptote to the slope change.

5.1.2 **Loading Conditions** - The primary intent of the analyses was to investigate the buckling resistance of the dome region of the nose cap. Examination of vehicle 5.3 design load conditions revealed that boost condition BP432 dominated for the dome region, and was the condition analyzed.

In addition, the individual pressure tubes can induce local moments at each of the penetrations. It was conservatively estimated that the maximum induced limit load moment would be 25 in.-lb. This value was applied at each of the holes simultaneously on the unstiffened nose cap and in directions most adverse to the stability of the dome. However, due to the symmetry of the model, the moments also had to be applied in a symmetrical fashion. This is illustrated on Figure 5-5.

5.1.3 **Results** - Summaries of predicted failing load levels for various areas of the nose cap configurations analyzed are shown on Table 5-1. Note that the critical areas between the various nose cap configurations remain essentially unchanged, although in some cases the critical element may have moved slightly. The regions of interest are shown on Figure 5-6. It is also important to note that flange strength in the region of transition between the 19-ply dome and the 38-ply flange is by far more strength critical than the dome. (It will be shown later that the 38-ply lug region at one of the attachments is the most critical region of the nose cap.) Even when stability in the dome region is considered, Table 5-2, the flange transition region is more critical by a factor of three. The buckling concern, therefore, became a rather academic issue.

In both the dome and flange regions there is little difference between predicted failing or buckling loads for the production and SEADS configurations. The 21-ply SEADS concept showed the lowest strength, even lower than for the unstiffened 19-ply dome. This was not expected and was examined in depth. It was concluded that by stiffening the entire dome region, the relative stiffness between the flange and dome changed sufficiently to cause some load redistribution. This resulted in more load being carried in the critical regions, which, even in the dome, was not completely offset by the additional stiffness/strength afforded by the two extra plies.

The stability results are shown on Table 5-2, while the locations of instability are pictured on Figures 5-7 and 5-8 for the production and SEADS configurations, respectively. It is observed that the unstiffened SEADS is slightly less stable than the production nose cap, due to the loss in stiffness created by the holes. With 6-ply ring stiffening, stability improves and becomes greater than the production design. But when stiffening is increased further, the behavior is like that of the 21-ply nose cap in that load redistribution actually results in lowered stability. From these results it is concluded that the 6-ply ring stiffened design is nearly optimum for the SEADS nose cap.

The influence of tube moments on the stability of the nose cap was examined only for the unstiffened SEADS configuration. It was found that in

TABLE 5-1

PREDICTED FAILING STRENGTH LOAD LEVELS

PLY	PRODUCTION		UNSTIFFENED		6-PLY RING STIFFENED		13-PLY RING STIFFENED		2-PLY DOME STIFFENED	
	ELEM. I.D.	β_{FAIL}	ELEM. I.D.	β_{FAIL}	ELEM. I.D.	β_{FAIL}	ELEM. I.D.	β_{FAIL}	ELEM. I.D.	β_{FAIL}
19	609	28.49	609	28.61	609	28.61	609	28.61	609	27.32
	1111	24.10	1111	24.21	1111	24.04	1111	24.15	1111	22.88
22	1210	8.94	1210	9.02	1211	9.09	1211	9.09	1211	8.58
	1217	14.41	1216	14.06	1216	14.04	1216	14.04	1216	13.81
	1224	10.87	1224	12.25	1224	12.31	1224	12.31	1224	11.32
32	1312	4.24	1312	4.29	1312	4.28	1312	4.28	1312	4.06
	1305	5.19	1305	5.40	1316	5.21	1316	5.21	1305	4.94
38	1624	5.83	1624	5.98	1624	6.03	1624	6.03	1624	5.95
	1412	7.15	1412	7.28	1412	7.25	1413	7.19	1412	7.25

$$\beta_{FAIL.} = \frac{\text{FAILING LOAD}}{\text{LIMIT LOAD}}$$

TABLE 5-2

SEADS NOSE CAP FAILURE SUMMARY

Failing Load Level (Margin of Safety at Ultimate)

$$M. S. = \frac{Failing\ Load\ Level}{1.4} - 1$$

NOSE CAP CONFIGURATION	STRENGTH FAILURE				STABILITY FAILURE
	DOUBLER FLANGE	FLANGE LUG	ORIFICE HOLE WITHOUT TUBE BENDING	ORIFICE HOLE WITH TUBE BENDING	
LESS PRODUCTION	4.24(2.03)	1.91(0.37)	N.A.	N.A.	12.74(8.10)
SEADS, UNSTIFFENED	4.29(2.06)	1.96(0.40)	14.11(9.08)	7.45(4.32)	11.70(7.36)
SEADS, 6-PLY RING STIFFENED	4.28(2.06)	1.96(0.40)	15.79(10.28)	11.35(7.11)	13.25(8.46)
SEADS, 13-PLY RING STIFFENED	4.28(2.06)	1.96(0.40)	18.41(12.15)	13.82(8.87)	11.60(7.29)
SEADS, 2-PLY DOME STIFFENED	4.06(1.90)	1.96(0.40)	15.19(9.85)	8.03(5.31)	8.28(4.91)

Failing Load = (Failing Load Level) x (Applied Limit Load)

the critical buckling region, at a load level ten times limit, that the rotational effect on the critical grid point was a mere 0.27% change. Since this is insignificant, no other of the candidate configurations were analyzed for this condition.

The tube moments do, however, influence the local stresses at the holes, being most pronounced for the unstiffened SEADS configuration. The influence of local moments is summarized on Table 5-2, where the failing load levels and resultant margins of safety are shown with and without tube moments. These values were computed for Hole No. 1, Figure 5-1, because this was found to be the most critical of the fourteen. Note that the effect of tube moment is most pronounced with the unstiffened SEADS and least with the 13-ply ring stiffening, as expected. It was judged that the 6-ply ring stiffened configuration would be more than adequate.

The lug flange failing load levels and margins of safety are listed in Table 5-2 for comparison with the other sections of the nose cap. The lug analysis includes consideration of stress concentration factors around the lug hole and is, therefore, more critical than flange element 1624, shown in Figure 5-6 and Table 5-1. The difference in margins of safety between the production design and the SEADS configurations is due to the fact that the production model included T-seals and expansion seals, while the SEADS models did not. But only a modest difference is observed. It is clear that the lug region is by far the limiting element, governing load capability for the nose cap.

5.1.4   Non-Circular Hole Analysis - As a result of an evaluation of concepts to prevent possible rotational oscillations of the penetration ports, a non-circular hole configuration was selected. (This is discussed in Section 6.4.) This hole configuration was then stress analyzed in greater depth, reference 7, than the circular hole configuration, discussed in the previous section.

The non-circular hole configuration is depicted in Figure 5-9. This geometry was used for all fourteen ports but, since the previous analysis showed Hole No. 1 to be critical, this hole was analyzed. The static BP482 boost loading condition was applied, and in fact, boundary conditions (loads and enforced displacements) from the previous model were used for the detail analysis. The analytical approach was verified by analyzing the octagonally modeled hole from the previous model. Stresses and deflections matched the original model's results.

The technique employed was to determine the maximum tube moment that could be applied in combination with the collapse pressure aerodynamic loads. Unit 20 in.-lb. tube bending solutions were obtained in two mutually perpendicular directions. These were then coupled to the pressure loads to determine the maximum tube moment to cause failure. The tube moments were introduced as running bearing loads on the RCC.

The overall math model is shown on Figure 5-10, while a more detailed view of the solid elements, describing the local region around the hole, is provided as Figure 5-11.

The results showed that a moment vector parallel to the flat sides of the hole produced maximum stresses. The maximum stresses occurred in the small radius between flat sides and the 0.720 inch diameter section. The allowable moment was computed to be 109.5 in.-lb. at ultimate load, which is three times

the estimated 35 in.-lb. required to fail 0.25 inch diameter coated columbium tubes. Recognizing that the ultimate margin of safety for the critical lug attachment hole on the nose cap is 0.40, the non-circular hole is far from producing the limiting stress condition for the SEADS nose cap.

5.2 Thermal Analysis of the Penetration Assembly

In order to obtain updated temperatures for entry trajectory 14414.1C, provide more refined analysis, and assess thermal gradients around a penetration assembly, the thermal analysis was re-done, reference 8. The model was also upgraded to reflect the latest configuration at the time of analysis. (Additional configuration refinements were made after this analysis to eliminate the thermocouple mount, change to coated columbium, increase the diameter of the pressure tube to 0.25 inch diameter, and incorporate the tube flared end. These changes are not considered significant to the thermal analysis results reported here.)

The thermal model, shown on Figure 5-12, consists of 48 nodes and was divided into quadrants to enable circumferential thermal gradients to be predicted. (Note that the model includes a 3/32 inch diameter platinum rhodium pressure tube. It was intended that this material would be chemically isolated from the columbium components by pure iridium foil.) Two penetration assemblies were analyzed: port No. 7, which experiences the highest temperature; and port No. 1, which is subjected to the largest circumferential gradients, since it "sees" the cooler leeward side of the nose cap on the upper quadrant and the hotter windward side of the nose cap on the lower quadrant.

Cross-radiation between the penetration assemblies and the nose cap and the bulkhead insulation were input as time-varying temperatures. These were obtained from the production nose cap analysis. Additionally, a factor of 1.61 was applied to the edge of the plug (node 15) to account for local step and gap heating effects between the plug and the nose cap. This factor, which is the same as that used at the junction of the nose cap and T-seals, is believed to be conservative for the SEADS application.

Maximum temperatures at port location No. 7 are reached at about 700 sec., and are summarized on Figure 5-13. Temperatures for the RCC nose cap reach 2700F, which is 40F higher than computed for the production nose cap for the same trajectory and is attributed to the differences in modeling. The RCC in this model was limited to an 11.0 inch diameter segment, which limited conduction paths and participation in cross-radiation. It was found that the nut and spacer temperatures were higher by 156F and 187F, respectively, for the 14414.1C trajectory than the previously analyzed 14414.1 trajectory. The columbium port exhibits lower temperature than the RCC, due primarily to the higher emittance of columbium at these temperatures. In summary, the columbium port will operate to 2650F, and the pressure tube will reach 2573F along most of its' length, but must connect to the union and nut, which experience a temperature of 2580F.

Maximum circumferential gradients at the No. 1 port location were found to remain consis'ant over a broad temperature range. The computed temperatures and maximum gradients between leeward and windward sides are noted on Figure 5-14. The worst cases are only 29F in metal components and only 36F in the RCC spacer. These were judged to be insignificant in terms of creating meaningful thermal stresses in components.

5.3 Cross-Radiation Blockage Analysis

During entry a portion of the heat input to the lower surface of the nose cap is transferred by radiation to the relatively cooler upper surface. The net heat exchange determines the nose cap local temperatures. The SEADS nose cap assembly incorporates two insulated support posts or manifolds, each collecting seven of the pressure tubes. These produce two 8-inch diameter proturberances into the nose cap cavity, which interfere (or block) to a degree with cross-radiation. There was a concern about the magnitude of this blockage and the attendent effect upon nose cap temperature distribution and resultant thermal stresses. Therefore, this was analyzed, reference 9.

The support posts arrangement is shown on Figure 5-15. Since the port side post extends downward and inward, while the starboard post extends inward and slightly upward, a full nose cap model was required for analysis. Production nose cap analyses were conducted using a half model, because of symmetry and view factors were calculated by the SwRI thermal analyzer routine. However, the SwRI program cannot calculate view factors with blockage, and necessitated the use of another routine to compute view factors.

Because of these analytical differences, temperatures were computed with and without blockage to ensure more accuracy in assessing blockage effects. Without blockage, nose cap temperatures compared favorably with production nose cap analysis results. Only 2F difference was found at the maximum heating location, while the maximum difference anywhere between two corresponding nodes was only 18F, thus confirming the approach.

The thermal model employed nose cap shell and bulkhead insulation nodes identical to those used in the production nose cap analysis. Each support post was divided into four lengthwise sections around the perimeter plus an "end cap". For each division an external surface node and an insulation node were used. The small diameter pressure tubes were not modeled, since their contribution to heat blockage was considered insignificant in comparison to that produced by the two 8-inch diameter posts. The entry trajectory 14414.1C was analyzed.

Changes in peak nose cap temperatures caused by cross-radiation blockage are shown on Figure 5-16. The largest increase is near the forward end of the port side tube on the inner surface and is 56F. The corresponding external surface increase is 34F. This raises peak nose cap temperature to 2693F, as compared to 2684F without the blockage. The largest decreases of temperature are on the lee side above the starboard post and amount to 42F for the inside surface and 31F on the external surface. The maximum temperature gradient due to blockage was found to be only 1F per inch.

The hottest support post is on the port side, where the end cap surface temperature reaches 2585F, Figure 5-17. By contrast the starboard post surface temperature peaks at 2476F on the cylindrical surface, Figure 5-18.

The nose cap temperatures were examined for their effect upon thermal stress. The 56F increase in temperature represents a 2% change in local temperature which could result in no more than a corresponding increase in thermal stresses in the dome, reference 10. Thermal stresses in the nose cap are considerably lower than those produced by airloads. Moreover, dome stress and stability margins of safety are significantly higher than the airloads

critical lug attachment region. Therefore, these temperature changes in the dome are considered insignificant. Thermal growth of the dome and its effect upon flange stresses was, also, considered and was estimated to be no more than a 3% increase. Here again, high margins of safety exist in the flange area for thermoelastic stress so the effect is considered insignificant.

6.0 UPDATED DESIGN

Previous development work supported the viability of the SEADS concept, particularly with respect to the lack of criticality to the nose cap, when fourteen holes are introduced. The optimism, derived from the development activities, brought about the involvement of Rockwell as systems managers and, as a consequence, a re-alignment of responsibilities. It was agreed that Vought would retain responsibility of the nose cap, the penetration assembly and certain testing, while Rockwell, in addition to the systems management role, would be responsible for the pressure tubes, support posts, bulkhead modification, insulation, data acquisition, and overall systems integration with the Orbiter.

The entry trajectory was updated to 14414.1C, which produced a 2660F maximum nose cap temperature. This eliminated nickel alloys from any location on the penetration assembly, including the pressure tubes. Thus, a redesign was necessary to replace the nickel with columbium components and to refine the port design to reduce the tendency for coating damage near the edge radius. A task was also undertaken to develop a scheme for minimizing self bonding of columbium parts during long term temperature exposure. Rockwell elected to use flared coated columbium pressure tubes, which necessitated coordination with, and reconfiguration of, the union and retention nut. These changes, coupled with the higher temperature entry condition, promoted the requirement for additional plasma arc testing to confirm the design changes.

Vought had recommended that Rockwell strongly consider platinum-rhodium pressure tubes, rather than coated columbium, due to concern about the integrity of the coated columbium, particularly in the induced thermal strain (creep) environment. Platinum-rhodium would have required the application of localized iridium foil chemical barriers at the union connection to protect the platinum from chemical attack by the columbium silicide coating, but would have, potentially, provided greater reliability. Rockwell, however, was concerned in part by the possibility of a silicon rich atmosphere, produced by the siliconized nose cap, and resultant chemical attack. Therefore, Rockwell elected to pursue the coated columbium, where they, together with VacHyd, developed a technique for coating the inside of the tubes. The approach used was to suck the coating slurry through the tube like in a soda straw. This proved highly effective, as determined by oxidation tests, and subsequent inspection, using fiber optics. The coated columbium tubes integrity was demonstrated in thermal strain (Section 8.0) and vibration tests (Section 9.0). However, the end of the flare proved fragile, as determined by plasma tests of penetration assembly models and vibration tests (Sections 7.0 and 9.0).

Two other investigations were conducted. First, concern was expressed that the penetration assembly could oscillate in the nose cap and perhaps cause excessive wear from the dynamic environment on either the RCC or the columbium coatings. Concepts to preclude this were examined. Second, it was considered desirable that the strength of the penetration assembly should exceed that of the pressure tubes so that in the event of over-load, the tubes would be exposing only a small hole into the nose cap cavity to admit the hot plasma. The strength was evaluated by both analysis and test.

Each of these activities are discussed in this section.

6.1 Penetration Assembly Redesign

The coated columbium port was modified to incorporate a 0.06 inch radius (previously 0.03 inch radius) at the edge of the head that encounters the convective heating. This radius still permitted meeting the local gap requirements between the port and the nose cap countersink. In addition the internal thread form was changed from a 3/8 - 16 to a 3/8 - 14 configuration to enhance coatability.

The union was configured to accept the flared tube design furnished by Rockwell, and the nut end threads were changed from 3/8 - 16 to 7/16 - 14. The Rockwell tube design incorporated split coated columbium ferrules to permit assembly of the nuts to the coated columbium tube, which was initially to be flared on both ends. Flaring couldn't be accomplished on assembly, because of the strain limits of the coating. Assembly required insertion of the flared tube through the nut, locating the ferrules on either side of the tube, and then trapping the ferrules by moving the nut to the end of the tube. Rockwell demonstrated this approach using machined aluminum components on a flared aluminum tube, where it worked well. However, when it was employed on the coated columbium parts, used on the plasma arc test models, it was discovered that the ferrules invariably opened slightly aft of the nut. The problem was identified with tolerance variations, including surface roughness, inherent with coated parts. While the approach was considered functional, it was considered less than desirable and was ultimately abandoned in favor of a different approach. The revised design for tube installation, employed a coated flare on the penetration end only. A short section of the cool, manifold end of the tube was left uncoated so that it could be flared on assembly. This ultimately proved successful and eliminated the need for the split ferrules.

The nut was reconfigured to conform to the new tube design and the wire locking feature was revised to provide a flange with multiple lockwire holes.

The washer thickness was increased from 0.02 inch to 0.06 inch to improve coatability and ruggedness in the event it was necessary to use spanners for disassembly.

At this stage of the program, the requirement for measuring temperature at the penetration assembly still existed, and therefore, the thermocouple mount was retained. However, because of the coated columbium parts, an iridium mount was used. Coated columbium was considered, but the concern of reliably coating the small 0.04 or 0.06 inch diameter holes for thermocouple insertion and the possibility of using staking for thermocouple retention, caused this to be dismissed. In the final design thermocouples were eliminated from the penetration assembly, because of the complexity of installation and routing. Radiometers, focused on the nose cap inner surface like those used for the baseline nose cap temperature measurement, were substituted.

Component designs are included in Appendix C.

Previous tests of columbium components employed the HiTemco R512E silicide coating, which, except for the local region of the sharp corner of the head of the port, performed acceptably in the 2500F test environment. With the increased temperature of 2660F Rockwell suggested that the more refractory VH109 silicide coating by VacHyd be used. Since Rockwell selected that coating for the pressure tubes, we also selected it for the penetration assembly components. However, there was concern about the ability of either coating to survive at these temperatures for a sufficient length of time. The

literature also indicated that the emittance of coated columbium would degrade with exposure time, causing temperature increases. These concerns were investigated in a limited plasma arc test program using 0.75 inch diameter x 0.25 inch thick buttons. Initial plasma arc conditions were set up, using silicon carbide coated RCC to achieve the 2660F temperature target, and were to be held constant through 10-hours of testing. However, due to misunderstanding, the first 5-hours resulted in some lower temperatures than desired. Temperatures achieved are provided on Figure 6-1 and show temperature excursions to 2700F. At the conclusion of the 10-hours exposure, neither coating system exhibited any evidence of oxidation damage and no obvious subsurface oxidation, as determined by probing the surface with a pointed tool. It would appear that either coating system would function satisfactorily.

Nevertheless, a backup to the coated columbium port was retained in the form of silicon carbide coated Stackpole 2020 graphite. It was known that this combination would meet and exceed the temperature requirements, although the life of the port would eventually be degraded through subsurface oxidation. Therefore, one of the plasma arc models tested in this phase incorporated a coated graphite port. All other components remained the same as for the coated columbium port model. It should be mentioned that the design of the penetration assembly was always predicated on the possible eventual use of a graphite port as an alternative. As such, the columbium port became somewhat massive and far over-strength. However, since weight was not an issue, this was not a concern.

6.2 Penetration Assembly Strength Determination

As noted above, a graphite port was retained as a backup to the columbium port. Graphite is substantially weaker than columbium so strength analysis and test were conducted using the graphite port.

6.2.1 Bending Test - Testing, reference 11, was conducted in two sequences. The first test employed coated columbium, 5/32 inch diameter, pressure tubes with the split ferrules, using the configuration shown on Figure 6-2. This test resulted in excessive deflection and yielding of the two tubes at maximum bending moments of 13.3 in.-lb. and 14.2 in.-lb., where the tube enters the nut. A 5/32 inch diameter steel rod was employed in a third test, where the maximum moment achieved was 109.6 in.-lb. before excessive yielding of the rod forced termination of the test. There was no apparent damage inflicted on the penetration assembly components.

Since the 5/32 inch diameter tubes and rods could not fail the graphite, a second test series was conducted using 0.25 inch diameter, 120 KSI heat treat steel rods. For this series three of the four graphite ports were pre-oxidized at 2500F to produce weight losses up to 18.4% (7-hours exposure). (It should be noted that no post coating treatment was applied to these ports. The Type A treatment, as used on leading edge components, would significantly reduce weight loss and enhance strength retention.) The results of these tests are shown on Figure 6-3, where it is seen that the maximum moment achieved was 122 in.-lb. where the rod enters the nut. Failure was produced in the graphite ports, where two failure modes were evident. The first was complete fracture across the port in the hollowed out region for thread termination. The second mode occurred on one port, and resulted in thread shear and fracture of the aft edge of the port. In this case the union could not be extracted without disassembly.

At this point of the program the pressure tube size was increased to 0.25 inch diameter x 0.015 inch wall primarily because of lightning strike consider- ations. The estimated failing strength of this size tube is shown on Figure 6-3 for comparison with test results. It is concluded that the graphite port possesses bending strength in excess of that required to fail the pressure tube up to a certain weight loss. If a graphite port were to be used, additional testing would be required to characterize the strength/weight loss behavior and to correlate weight loss with mission cycles. A post coating seal treatment would be employed to increase mission life.

6.2.2   Axial Strength Analysis - A strength analysis was conducted to determine the weakest link of the penetration assembly and pressure tube and to estimate the maximum axial load capability of the system, reference 12. Here again, the graphite port was considered, since it is only one-tenth as strong as the columbium. Stackpole 2020 tension stress allowable was estimated to be 2730 psi, while the shear stress was taken at half that value.

It was calculated that a 5/32 inch diameter columbium pressure tube would fail at 170 lb. but this would increase to 313 lb. for the 1/4 inch diameter tube. The port was calculated to fail at 400 lb. in tension. When thread shear was considered, it wasn't clear how the SiC coating would contribute to strength so a range between 132 lb. and 484 lb. was computed, the lower value representing graphite strength and the higher value being for SiC threads. It is expected that the true strength for unoxidized material is closer to the higher value, based upon the bending tests, where thread shear didn't occur until the weight loss became appreciable. However, even if the lower strength value is used, it is far in excess of that which could reasonably be expected to be applied by bent or coiled tubes.

6.3 Evaluation of Sticking Threads

It was discovered during plasma testing of columbium components that the union and port could not be disassembled after 4-hours exposure. It wasn't certain whether this was due to diffusion bonding or simply the result of scale from the coatings, causing binding in the threads. In either event it was deemed necessary to devise some scheme to prevent this binding action. Accordingly, a program was undertaken, reference 13, to evaluate the feasibility of using some anti-seize compound to enhance disassembly of components and minimize potential damage to the nose cap.

Testing was conducted using both 0.75 inch diameter buttons and union/nut combinations. Test exposure was 2500F at 1 atm in one-hour increments for times ranging to 7-hours. Because of the limitation on the number of coated columbium parts available, many had to be reused to examine alternate anti-seize compounds and in some cases even when parts were severely oxidized. No precautions were taken to minimize wrench damage on either the unions or nuts.

In the first series of tests, lasting 5-hours, a comparison was made between union/nut combinations where (1) no anti-seize precautions were taken, (2) threads were brushed clean after each hour to remove scale, and (3) a dry MgO powder was brushed onto the threads. Initial assemblies were finger tight. Breakaway torques ranging to 15 ft.-lb. for the non-powdered assemblies, dropped to 10-12 ft.-lb. when the threads were squirted with isopropyl alcohol (IPA). There was essentially no change in breakaway torque when the threads were brushed off after each hour, leading to the belief that loose scale was

not the only contributer to high disassembly torque. The application of MgO powder was beneficial in that disassembly torques were roughly 80% of that for the unpowdered assemblies. However, improvement was desired.

In other tests, slurries, combining powders and carriers of IPA or Methocel were tried, along with commercial brazing anti-seize compounds. Those powders found to have merit included SiC, Mo_5Si_3, and HfO_2 with ZrO_2 and MgO showing less favorable performance. Of the commercial products only the green Stop-Off material indicated potential. Red Stop-Off and white Stop-It proved ineffective in this application.

Since the most promising combination appeared to be SiC, 1200 grit powder in a Methocel carrier, and SiC powder was readily available and compatible with the silicide coating on columbium, confirmation tests were conducted with this combination. In one trial involving VH109 coated parts, exposed for 4-hours, disassembly torque varied between 5 and 8 ft.-lb. In another test, using R512E coated columbium, breakaway torques remained in the 2 - 3 ft.- lb. range through 6-hours and was only 3 - 4 ft.-lb. after the 7th hour of exposure. In all cases IPA was squirted into the threads to enhance release. One interesting note is that on one attempt the IPA was ignited and then re-applied. In this case breakaway torque was estimated at a mere 1 in.-lb. This approach may have merit in stubborn cases, since the heat generated from burning IPA should not be detrimental to the refractory materials involved.

In the course of these tests damage was readily inflicted on the wrenching surfaces of the unions and nuts, pointing out the need for carefully designed, plastic faced wrenches for use on the columbium parts. In addition, oxidation of threads was evidenced, some of which can be attributed to mechanical damage from high torque requirements and others to improper radiusing of threads, particularly on the lead-in threads.

In summary, the study resulted in the successful demonstration of a SiC powder/Methocel slurry baked onto the parts, as being an effective improvement against part seizure with elevated temperature exposure. When IPA is squirted into the threaded connection, disassembly is eased. Igniting the mixture appears advantageous to reducing torque.

6.4 Anti-Rotation Concepts

A concern was expressed by NASA/JSC that oscillatory motion of the SEADS penetration assembly could cause loosening of the assembly in the countersunk nose cap hole. The loosening would aggravate the situation, producing more undamped oscillation, with a result of producing coating wear and, ultimately, loss of oxidation protection. In this scenario the initial loosening would be caused by excitation in the acoustic noise dynamic environment due to imperfect seating of the port in the nose cap because of high points or powdery residue from either the nose cap or columbium coating.

Therefore, a study was undertaken to devise concepts to prevent rotation of the support assembly, evaluate the concepts, and select one or two for vibration test evaluation. Eight concepts were defined and ranked in two separate studies, references 14 and 15. These concepts are shown in Figure 6-4. It should be noted that any of the concepts will allow a degree of oscillation due to tolerancing and gaps between mating parts. Initially, only the first seven concepts were ranked by a team consisting of Engineering disciplines, Tooling and Manufacturing. The apparent simplicity of Concept 7

resulted in its' emergence as a clear winner. The falacy of this was that the penetration assembly relies upon the pressure tube to provide the restraint, whereas in fact the tube dynamics is the biggest driver to produce oscillation of the penetration assembly. Concepts 4, 6 and 1 were closely grouped behind 7 and would have required quantitative cost analysis to determine the best.

In a re-look at these ideas, reference 15, Concept 8 was introduced, and an analysis of angular movement was made, based on tolerance buildup. The results of this evaluation and final ranking are shown in Table 6-1. This shows the ball lock (#8) and flat sided hole in the nose cap (#1) to be the favored schemes.

The ball lock was conceived as being 3/16 inch diameter, high density alumina, ruby, or sapphire. Synthetic rubys were procured for test because they have high hardness, are made to close tolerance, are readily available and are inexpensive. Concern was expressed by NASA/JSC that the rubys may suffer thermal shock, even though they were relatively small in diameter. A test ball, supplied to NASA for thermal shock test, passed with no problem.

Both the ruby ball lock and non-circular hole anti-rotation concepts were incorporated in a vibration test, Section 9.0, and each performed acceptably (as did the penetration assemblies without anti-rotation). In addition the ruby ball lock was employed on the thermal expansion tests of the pressure tubes, Section 8.0, where no problems with the concept were experienced. It was concluded that either technique would prove satisfactory, but by concensus the non-circular hole scheme was selected for the production SEADS. It was shown, Section 5.1.4, that the non-circular hole design was structurally adequate.

CONCEPT	ADVANTAGES	DISADVANTAGES	COMPUTED ROTATION	RANKING
1 - Rout Nose Cap Hole	• Positive Lock • Simple • Minimal Change	• Tooling for Hole Routing	$\pm 1.2^{\circ}$	2
2 - Key Lock	• Positive Lock	• Extra Part • N'tch in Nose Cap • Port Notch Machining	$\pm 3.5^{\circ}$	4
3 - Eccentric Counterbore	• Positive Lock	• Port Head Vulnerable to Overheating • Larger Hole in Nose Cap • Creates Possible Nose Cap Delamination Site • Complicated Machining	$\pm 2.9^{\circ}$	6
4 - Eccentric Through Hole	• Positive Lock • Eliminates Main Disadvantages of #3	• Moderately Complicated Machining	$\pm 2.9^{\circ}$	3
5 - Cylindrical Groove	• Positive Lock	• Very Expensive Nose Cap Tooling • Added Complexity of Spacer Machining • Local Decrease of Nose Cap Thickness	$\pm 1.2^{\circ}$	7
6 - Wire Bracing	• Positive Lock • Minimal Change	• Difficult Installation • Coating Damage Risk on Lockwasher	$\pm 2.2^{\circ}$ - 4.6°	5
7 - Tube Wired To Penetration	• None	• Not an Effective Lock	N/A	N/A
8 - Ball Lock	• Positive Lock • Simple	• Tooling for Nose Cap Dimple • Extra Part • Added Cost of Spacer Machining	$\pm 2.4^{\circ}$	1

7.0 FINAL PLASMA ARC TESTS

The change of design requirement to the 14414.1C entry trajectory resulted in a maximum design temperature of 2660F, a redesign of components as noted in Section 6.0, and a need for retest in a plasma arc facility to confirm that the design would survive the higher temperature. Two new models (and a calibrator) were fabricated for re-test in the NASA/LaRC Facility B plasma arc. These models differed only in the port material, one being VH109 coated C-103 columbium, while the other was silicon carbide coated Stackpole 2020 graphite. The latter was retained as a backup design in the event the test conditions proved too demanding for the silicide coated columbium. In each model the union, nut, lockwasher, and pressure tube were fabricated from silicide coated columbium.

Unfortunately, the desired temperature, as determined by model mounted thermocouples, could not be achieved in this facility, forcing another test to be conducted in the NASA/ARC Aerodynamic Heating Tunnel. The two test programs are discussed in this section. A more detailed treatment is found in reference 16.

7.1 NASA/LaRC Plasma Tests

The test models, the calibrator and the associated thermocouple locations are illustrated by Figures 7-1 and 7-2, respectively. Note that on these tests the 5/32 inch diameter pressure tube and ferrules design were used, since the increased tube diameter and elimination of ferrules were not yet introduced. In addition, the thermocouple mount was retained because the decision to delete temperature measurement for the production design was not yet made. All thermocouples were 10-mil diameter tungsten 5 rhenium/tungsten 26 rhenium in alumina insulators with a ground wire. Astroceram "A" was used to bond thermocouples to RCC parts. Three Ircon 300 pyrometers were also used to monitor test conditions, two focused on the RCC disc and one on the port. The intent was to use these for temperature monitoring, when the thermocouples burned out.

The calibrator was used to set the test conditions, but a disparity between temperature measured by the thermocouples and that determined by the pyrometers was immediately apparent. Pyrometers indicated the desired temperature was met, while the thermocouples, corrected for the temperature gradient across the disc, showed that the temperature was 100F - 150F lower than the target 2660F. Higher temperature could not be achieved in this test facility, while still maintaining 10-minutes exposure times. This led to a controversy over which temperature measurement technique was the more correct. NASA/LaRC test personnel and Rockwell sided with the pyrometers, while Vought took the position that the thermocouples were the more accurate. Attempts to resolve this discrepancy are discussed in Section 7.3.

Since there was no other facility available at the time in which to conduct the tests, it was decided to test in Facility B and gain valuable information on long term columbium behavior with the modified parts, VH109 coating, and anti-seize compound on the threads. This limited the exposure temperature to about 2525F at 0.05 atm. Each model was tested for 5-hours in 10-minute increments with disassembly at 1-hour intervals. The SiC anti-seize compound was re-applied after each disassembly.

7.1.1   Columbium Port Model - Throughout the test of the -2 model with columbium port, the various columbium parts evidenced areas of breached coating. These were identified by yellow oxide formations. The flared end of the pressure tube suffered the most damage, but still, after 5-hours of exposure, it remained anchored in place and was not in immediate danger of coming loose. All parts, even with the local oxidation sites, were considered as not posing a threat to structural integrity. Photographs of the individual parts, following test, are shown on Figures 7-3 through 7-7. Most of the variegated appearance is due to normal discoloration or the SiC anti-seize powder. Oxidation sites were found on the corners of the hex part of the union and two locations on the threads; one of the lockwire holes on the nut (but not a lockwire location) oxidized; one of the ferrules showed an oxidation site; and the port was damaged locally, where a buildup of scale between the port and RCC ruptured during disassembly to expose bare columbium. No damage was in evidence on either the lockwasher or the RCC components.

An anomaly was found after the fifth hour of test when it was discovered that the thermocouple mount was displaced from its' intended position. No logical explanation could be postulated for this, other than improper assembly following the fourth hour inspection.

After each hour of test, the parts were readily disassembled, being enhanced by the application of IPA to the threads. This pointed up the effectiveness of the SiC powder as an anti-seize agent.

Temperature data was obtained using three Ircon 300 pyrometers and five tungsten rhenium thermocouples. One of the pyrometers was calibrated by viewing through a window and mirror at the 55° angle used in the test facility. The other two pyrometers were in turn calibrated from the first by viewing at a common spot on the calibrator disc at various plasma arc operating conditions. Pyrometer correction was arbitrarily taken at an emittance of 0.85. However, at the pyrometers sensitive wave length of 2.3 , the emittance of coated RCC is somewhat lower as indictated by the temperature correction chart of Figure 7-8. This chart was constructed using RCC spectral emittance data generated on the LESS Program.

Typical temperature response, during a 10-minute exposure, is shown on Figure 7-9. Note that the pyrometer data is uncorrected for spectral emittance. End-of-run temperature distribution, through the model, is provided by Figure 7-10 for four exposures, illustrating repeatability of the thermocouple response. The difference in front face temperature measurement, as predicted by thermocouple data and calculated gradient across the RCC disc, compared against uncorrected and spectral emittance corrected pyrometer measurements, is indicated. Thermocouple data projects 2525F maximum temperature, while corrected pyrometer data indicates 2820F surface temperature, a difference of nearly 300F. This disparity is discussed in Section 7.3. To illustrate temperature variations experienced during the 30 exposures, uncorrected pyrometer data is provided on Figure 7-11. The data is not always consistent between the three pyrometers. Of particular interest is the apparent stability of the emittance of the silicide coating when the questionable data from pyrometer number 89 is discounted. Pyrometer data from the thirtieth run is not higher than from previous runs. Therefore, there is no apparent decrease of emittance of the VH109 for at least 5-hours and based upon button tests, Section 6.1, this observation could be extended to 10-hours.

68

Pressure measurements were made on this model for the entire test sequence and were compared with the arc jet pressure probe. Good agreement was obtained indicating that the finger tight joint at the tube/union interface is adequate. Sample data from test are shown below, which compares facility pressure measured before each run with model pressure obtained at 60 sec. and 600 sec. into a test run. Pressure fluctuations preclude precise comparisons.

PRESSURE COMPARISON

	PRESSURE IN MM Hg		
RUN SEQUENCE	TUNNEL PRESS.	MODEL 60 Sec.	PRESS. 600 Sec.
1	38.8	38.4	42.2
2	39.5	37.8	38.5
3	38.7	37.9	38.6
4	39.6	37.6	38.3
5	35.6	37.8	38.4
6	39.1	37.7	38.4

7.1.2 Graphite Port Model - This model, designated -1, was exposed for 33 cycles to accumulate 5-hours exposure, the extra cycles being necessary to make up for aborted runs, caused primarily by facility water leaks. Oxidation resistance of the columbium parts proved somewhat better on this model, although several oxidation sites were evident. The nut experienced oxidation on the flanged end, as before, initiating at an unused lockwire hole. The last thread on the nut end of the union also had a coating breach. The flared end of the pressure tube again suffered oxidation, which scalloped the end, but the damage was significantly less than on the -2 model tube. Although there was discoloration in varying degrees, and flaking of scale on the lockwasher, none of the other metallic components suffered any oxidation.

The graphite port developed an unusual buildup of material in the port hole beginning in the first hour of test and continued through the fourth hour, but never approached complete blockage of the hole. After the fifth hour the material buildup had disappeared so its makeup and origin are unknown. At the conclusion of test, it was noted that the first three threads on the port were chipped, probably as a result of subsurface oxidation. Subsurface oxidation can be dramatically decreased with the most recent post coating treatment, but this graphite port did not employ this.

Disassembly at one-hour intervals was judged to be easier than with the -2 model. Port to union separation required only finger pressure, but the nut to union connection required wrenches. Photos of the -1 model components following test are shown on Figures 7-12 through 7-19.

As with the -2 model, this -1 model was judged to be structurally functional after the 5-hour exposure, even though oxidation was present. Once the coating is breached and oxidation commences, the rate is so slow as to pose no immediate threat to the safety of the system. For example, those oxidation sites, evident after the first hour of exposure, did not progress sufficiently far through the fifth hour, as to be considered hazardous.

Temperature data for the -1 model are shown on Figures 7-20 through 7-22. Typical temperature time histories during a run are provided on Figure 7-20. The pyrometer data are uncorrected for spectral emittance. The data shown are for Run #1 but Run #2 data fell almost on top of these plots, indicating reproducibility of the thermocouples. The heatup rate was somewhat greater than for the columbium model, Figure 7-9, possibly due to the difference of mass between the columbium and graphite ports.

End of run temperature gradients through the model for the first four runs are shown on Figure 7-21. Data from Runs #1 and #2 are consistent, Run #3 had a facility water leak to lower the temperature and Run #4 was simply a lower temperature run, due to facility operation variations. The gradients through the model are consistent, but are slightly lower than those for the columbium port model. This was not investigated, so the reason for this difference is unknown.

The uncorrected pyrometer temperature data for each run is plotted on Figure 7-22. These provide an indication of exposure conditions.

7.1.3 - <u>Conclusions</u> - Even though some design changes were made to the columbium components to improve coating life, localized oxidation did occur in these tests. It was apparent that additional changes were required to enhance coatability and reduce damage potential from the use of wrenches for disassembly. This was done for components used in vibration and tube thermal tests.

The effectiveness of the anti-seize compound was demonstrated.

The chipping of the threads on the graphite port due to subsurface oxidation demonstrated the need for a post coating treatment seal or the mission life would probably be less than for the columbium port.

Even though oxidation pits developed on several columbium parts, the oxidation rates were low, and structural integrity was not in jeopardy.

7.2 <u>NASA/ARC Plasma Test</u>

Since it was not confirmed that the target temperature was reached in the NASA/LaRC tests, because of the thermocouple/pyrometer disparity, an additional test was conducted in the NASA/ARC Aerodynamic Heating Tunnel, reference 16. A test model was built identical to the columbium port model, used at NASA/LaRC, but with thermocouple changes and with flared holder to interface with the NASA/ARC plasma arc facility. The NASA/LaRC calibrator model was also re-instrumented for this test. Instrumentation differences were in the placement of tungsten/rhenium thermocouples adjacent to the front face coating in order to obtain the temperature gradient across the RCC disc. The model and calibrator are illustrated by Figures 7-23 and 7-24, respectively, while the flared holder is shown on Figure 7-25.

The objectives of this test were to demonstrate survivability of the penetration assembly at the 2660F design temperature, as measured by thermocouples, and for a reasonable period of time, which was limited to two hours.

As in previous tests, the facility conditions were set using the calibrator. In fact confirmation of the established operating condition was made just prior to insertion of the test model.

However, the first model run produced an anomaly, when the temperature soared to 2950F, before power was reduced, but remained at 2920F at the conclusion of the run, which was aborted at 6 1/2 minutes. It was discovered that the coating on the front face of the model holder had burned off, exposing bare graphite. This occurrance was attributed to an excessively thin coating. It was thought at the time that the loss of the low catalytic coating to expose catalytic graphite with resultant higher temperature was responsible for the excessive temperature. Later analysis revealed that the columbium port was probably also catalytic and contributed to the high temperature. This is discussed in Section 7.4.

Inspection of the model, after removal from the holder, disclosed no apparent damage to any of the penetration components. Only normal discoloration was present, and a faint line around the periphery of the port head near the radius tangent was observed. It was speculated that the silicide coating began to "flow" at the high exposure temperature, which would have been greatest in this region. The glassrock insulation in the holder was found to be cracked confirming the over-temperature exposure. The condition of the assembly is shown on Figures 7-26 and 7-27.

At this point the model was transferred to the calibrator holder for continuance of test. All of the thermocouples were preserved, which was remarkable, since tungsten/rhenium embrittles badly after high temperature exposure.

The second exposure was conducted at slightly reduced power setting compared to that at the end of the first run. Still the temperature exceeded the desired value, reaching 2830F before power and pressure were reduced further to produce an end-of-run temperature of 2710F. Subsequent runs were made at 0.03 atm and power level about half of that setup with the calibrator. This resulted in highly repeatable conditions and surface temperatures about 50F higher than the target.

The model was exposed for a total of 11 cycles, accumulating 1 hour and 57 minutes. Front and backface disc temperature, obtained during the first hour of test, are shown on Figure 7-28. A typical temperature-time history is illustrated on Figure 7-29, while temperature gradients through the model are provided as Figure 7-30. Note that the gradient is less than that obtained in the NASA/LaRC test, possibly the result of higher heating and the relatively higher temperature of the port due to catalycity effects, Section 7.4. In the NASA/ARC test there was no pyrometer focused on the port so that the speculation that the port operated at a higher temperature than the RCC disc was not confirmed experimentally.

All of the thermocouples were destroyed at the end of one hour, when model disassembly was attempted. Pyrometer data was relied upon thereafter to monitor surface temperature. On the basis of the early exposures, when the thermocouples were active, an in situ "calibration" between the front surface thermocouple and each pyrometer was obtained. Using this, the true estimated surface temperature for each run, based upon pyrometer output, was made and shown on Figure 7-31. After the first run, surface temperature was maintained between 2640F and 2740F, and generally exceeded the 2660F target temperature.

As indicated above, an attempt was made to disassemble the penetration assembly after the first hour of test for inspection. Inspection after removal from the holder revealed no oxidation and all parts appeared normal. However, the parts would not separate within the torque limits of the plastic coated wrenches, and the desire to avoid significant damage to the coatings. Even light tapping and chilling in dry ice in an attempt to break any bonds, proved unfruitful. However, in the effort to disassemble, it was suspected that some coating damage was inflicted. No further attempts at disassembly were made and the model was re-installed in the graphite holder for test continuance.

At the conclusion of, test it was observed that a corner of the union hex was oxidized slightly, promoted, undoubtedly, from the earlier attempt to disassemble. No other damage was observed.

It was feared that the threaded connections were diffusion bonded together, but disassembly was nevertheless attempted. WD-40 penetrating oil was squirted into the nut to union connection - not into the union to port threads. The lockwasher was protected by plastic strips, while the nut was protected only with masking tape. Gripping the lockwasher in a vise and using a standard six-inch open end wrench to apply torque to the nut, the union unscrewed from the port at an estimated 10-15 ft. lb. of torque. Gripping the union in the vise with protective plastic strips, permitted the nut to be unscrewed from the union, again at an estimated 10-15 ft. lb. of torque. No observable damage was inflicted to the coatings from this disassembly operation.

The significance of this is two-fold: first, the parts can be disassembled, even after excessive temperature exposure, without inflicting damage to the columbium or risking damage to the RCC; second, it is concluded that better designed plastic wrenches should improve the ability to disassemble the parts.

Upon disassembly there was no observed internal damage to the union, port nut, or ferrules. Although a shiney spot did appear on a union thread it was not accompanied by oxidation "flowering". One corner of the hex section of the union exhibited oxidation, as noted previously, but this is attributed to damage while attempting to disassemble after the first hour of exposure. There was slight damage and scalloping of the flared end of the tube, but this was significantly less than that observed on the -2 model tested at NASA/LaRC. The RCC hole exhibited slight scale buildup from the columbium, similar to that observed in previous tests.

It was discovered that the iridium thermocouple mount was securely attached to the columbium lockwasher. When pried apart, some of the columbium coating adhered to the iridium, thus exposing bare columbium. There appeared to be an iridium/silicide coating reaction. This had not been experienced in previous, lower temperature tests. This condition is of academic interest, since the iridium mount is not employed on the production SEADS design. Further, while iridium lockwire is used between the lockwasher and nut, no reaction or sticking was observed at the lockwire holes, indicating the application of iridium lockwire is acceptable.

The last item to note is that the cavity between the union and port contained flakes presumed to be scale from the coated columbium parts. Scale has been observed in previous tests.

Photographs of the components following tests are included as Figures 7-32 through 7-43.

This test proved highly successful in that it demonstrated over temperature capability of the columbium components, and the ability to survive multi-mission exposure to the design temperature condition. Further, even with the temperature overshoot, the components could be disassembled without risking damage to the nose cap, assuming appropriately designed wrenches.

7.3 Thermocouple/Pyrometer Disparity

The discrepancy between the surface temperature, as determined by the thermocouples and that measured by pyrometers during the NASA/LaRC plasma arc tests, was examined. Attempts to determine if the apparent high pyrometer readings were due to arc reflection by continuing data collection, after the arc was extinguished, proved unfruitful. The inability to correlate arc decay with pyrometer measured temperature decay, presumably due to data system time lag, prevented a conclusive investigation.

Two other approaches were, therefore, taken in an effort to obtain some indication of which measurement technique appeared the more plausible:

(1) The plasma arc test model was thermally analyzed by a finite element differencing technique to establish the temperature gradient through the RCC disc, and to assess measured thermal gradients in the model with analytical predictions, reference 17.

(2) Thermocouple mounting and routing variations were tested in a small furnace and compared against the furnace platinum/rhodium thermocouples and pyrometers, reference 18.

Each of these are discussed in the following sections.

7.3.1 Test Model Thermal Analysis - Only the -2 model, employing the columbium port, was analyzed for this investigation. This model employed five tungsten-5% rhenium/tungsten-26% rhenium thermocouples positioned as shown in Figure 7-1. In addition, three Ircon 300 pyrometers, sensitive in the 2.3 wave length, were focused on the front face of the model, two on the RCC and one on the port. The second exposure, Run #2 (Figure 7-9) was analyzed. This was very repeatable for Runs #2 through #5 as indicated by end-of-run temperatures, plotted on Figure 7-10. Run #1 was the only exposure for which pyrometer measurements were taken during cooldown but this run suffered from a facility water leak and temperature was affected.

The thermal math model used, Figure 7-44, was a modified and updated version of that used in previous analysis, Section 4.2. The internal cavity was allowed to cross radiate. External heating rates were defined according to two schemes:

(1) A uniform front face heat flux adjusted such that the response of node 23, Figure 7-44, approximated the temperature indicated by T/C #5, Figure 7-1.

(2) A uniform front face heat flux adjusted such that the response of node 32, Figure 7-44, closely matched the temperature indicated by pyrometer #82 as corrected for spectral emittance, Figure 7-8.

The side walls of the graphite holder received a uniform heat flux of one tenth that of the front face values in both cases. Analysis included the 600 sec. heating phase, as well as 15 sec. of cool-down.

7.3.1.1 <u>Controlling to thermocouple #5</u> - The results of the heating portion of the analysis are shown on Figures 7-45, 7-46 and 7-47. The maximum computed gradient across the RCC disc is 119F. The difference in temperature between thermocouple #4 and pyrometer #82 is 400F. An error of this magnitude (400F vs. 119F) in predicting the gradient across the disc is highly unlikely.

The agreement between calculated temperature response and thermocouple data on Figures 7-46 and 7-47, while not perfect, are reasonably good, recognizing that we were searching for a disparity of several hundred degrees fahrenheit. Better agreement could be achieved by reshaping the imposed heat flux, but the problem did not warrant the expenditure of additional effort.

Results for the cool-down phase are shown on Figures 7-48, 7-49, and 7-50. On Figure 7-48 the calculated and measured response of node 23 agree well. The corresponding calculated temperature drop for the surface node is 275F in 15 sec. By contrast the pyrometer data indicates a 900F reduction in 15 sec. Although the convective environment is not known, this drop seems unusually large. Calculations show that this represents a heat loss greater than if both the front and back face surface nodes were allowed to radiate to absolute zero.

However, if the pyrometer was reading high due to arc reflections, it would be expected that the true value would be indicated shortly after plasma arc shut-down. Such is not the case, since the pyrometer indicates a temperature value 350F lower than calculated 15 sec. after arc shut-down and continues to fall at a much steeper rate. This anomaly is not understood.

Calculated versus measured temperature comparison for the RCC spacer, Figure 7-49, are in good agreement, including the cool-off rate. Neither the nut, Figure 7-49, nor the thermocouple mount, Figure 7-50, temperature comparisons are as good in that the computed temperature drop-off does not match the measured change. It is believed that this difference is due to an accumulation of modeling weaknesses, since the disparity becomes greater as distance increases from the controlling surface nodes.

7.3.1.2 <u>Controlling to Pyrometer #82</u> - When the imposed heat flux is adjusted to match pyrometer data, the computed end-of-run temperature gradient across the RCC disc increases to 161F as shown on Figure 7-51. For this case the computed Node 23 temperature is 280F higher than that indicated by the thermocouple. Similar disparities between calculated temperature and thermocouple temperature are shown by Figures 7-52 and 7-53.

Results for the cool-down phase of analysis are provided as Figures 7-54, 7-55 and 7-56. Differences between calculated and measured temperatures remain large.

7.3.1.3 Conclusions

(1) The thermal math model provided a reasonable representation of the temperature response of the test model. While additional refinement could have been introduced, it was judged to be an unnecessary expenditure.

(2) The maximum steady state computed temperature across the disc is probably about 119F, but even assuming pyrometer accuracy, the gradient would not exceed 161F.

(3) If the pyrometer data is assumed to be correct, all five of the thermocouples would have to be in error on the low side by a magnitude in excess of 200F. This is not supported by the thermocouple evaluation reported in Section 7.3.2.

(4) Although arc reflections are generally suspected for pyrometer discrepancies, this is not fully supported by the test data, since pyrometer temperatures failed to level off to the predicted temperatures during cool-down. The reason for this remains unknown.

7.3.2   Thermocouple Evaluation - The tungsten rhenium thermocouples, used in the plasma test model, were assessed for measurement accuracy, reference 18. At the same time, alternate mounting schemes were examined for comparison with that used in the arc jet and for possible improved installation if it proved necessary.

When the pyrometer/thermocouple accuracy question was first raised, concerns were expressed by the NASA test agency regarding possible poisoning of the thermocouples with the Astroceram A cement, possible heat conduction down the wires leading to a low temperature reading at the wires juncture, or possible electrical leakage through the alumina insulators.

Accordingly, a test program was conducted wherein different mounting schemes for the tungsten rhenium thermocouples would be evaluated and compared against platinum-rhodium and chromel-alumel thermocouples. In addition these thermocouples were compared with pyrometer indicated temperature. Tempilac temperature indicating paint was also used as a rough guide to temperature level. All testing was conducted at 2300F in a small, resistance heated, tube furnace, that is routinely used for RCC acceptance testing on the LESS program. The thermocouple mounting techniques employed are illustrated on Figure 7-57, while a schematic of the test is provided as Figure 7-58. Photographs of the test set-up and specimens are shown on Figures 7-59 through 7-62. Note that the thermocouple leads were covered with thermal insulation to maximize the thermal gradient along the leads from the junction aft.

The tungsten-rhenium thermocouples were mounted to RCC segments and either routed straight aft (perpendicular installation) or run along the surface of the RCC a short distance before being run aft (parallel installation). Both Astroceram A and Sermetel 487 bonding materials were tested. The platinum rhodium thermocouples, which were used as the prime source for comparison are the standard temperature measuring devices for tube furnace operation; they are installed in wells and were not attached to the RCC.

The specimens were exposed for at least 10 minutes (with temperatures recorded at one minute intervals) to assure reaching steady state

temperatures. Representative data are summarized in Table 7-1. Note that three different pyrometers were employed. Examination of the data reveals rather good consistency for the tungsten rhenium thermocouples with no significant difference in results between perpendicular or parallel installation, or between Astroceram or Sermetel bonding. More significantly, the data is comparable to that obtained with the platinum-rhodium thermocouples, being only an average 15F lower, considering all the data. Note also that the Ircon 300 pyrometer was in relatively good agreement with the thermocouples, certainly not producing the 300 - 350F disparity found in the plasma test. Where Run #6 produced high pyrometer data, the recheck with refocusing confirmed consistency with the thermocouples. The Tempilaq also confirmed that a large temperature measurement discrepancy does not exist.

The chromel-alumel thermocouples read consistently low for some unknown reason and shed no light on the prime question.

In conclusion, these tests demonstrated that the use of tungsten rhenium thermocouples and the mounting and routing scheme used in the plasma models did not result in low thermocouple readings. Further, the Ircon 300 data suggests that the disparity encountered in the plasma test is facility related. The prepondrance of data from this test and analysis leads to the conclusion that the thermocouples were indeed predicting the more correct temperature results in the plasma arc test. The only unknown in these investigations is whether there is some problem in the data system in the plasma arc facility that would produce a consistent bias in all thermocouple readings.

7.3.3   Conclusions - Temperature data from the thermocouples were consistent and repeatable in the plasma arc tests at NASA/LaRC. Experimental results showed that these data were not effected by the method of attachment to the model, the routing scheme, or electrical loss through the insulators. Thermal analysis also confirms the reasonableness of the thermocouple data, and by contrast cannot support the pyrometer data. It is concluded by the prepondrance of data that the thermocouple data is correct and the pyrometer results must be high. The only factor that could change this conclusion would be a bias error in the plasma arc facility data systems, and this has not been indicated.

7.4 NASA/ARC Plasma Arc Test Anomaly

Experiencing 2950F during the first exposure of the test model in the NASA/ARC plasma test, when the calibrator model indicated that the target temperature of 2660F should have been reached, prompted a study to investigate possible sources of the anomaly. Several possibilities were postulated as follows:

(1) The presence of the penetration assembly could have altered internal cross-radiation relief, causing the disc to run hotter.

(2) Loss of coating from the holder changes the non-catalytic surface to catalytic with resultant higher holder temperature, which pumps more heat into the disc.

(3) The coated columbium port could be catalytic, thereby operating at a higher temperature than encountered in previous tests, and drive

76

TABLE 7-1

TEST RESULTS

(Temp. °F)

| INSTRUMENT | CALIBRATION | SPECIMEN NO. | | | PYROM. CHECK |
		1 (10 Min.)[1]	2 (6 Min.)[1]	3 (7 Min.)[1]	2
MANUAL	-	-	-	-	2057
	-	-	-	-	(1990)
PHOTO II ϵ_λ [2]	2393	2380	2170	2393	2045
$\epsilon = 1.0$ [2]	(2280)	(2270)	(2090)[3]	(2280)	(1980)
IRCON 300 ϵ_λ [2]	2382	2288	2522	2315	2057
$\epsilon = 1.0$ [2]	(2248)	(2177)	(2348)[3]	(2198)	(1990)
P_t/P_t 10 Rh #1	2295	2230	2275	2290	1990
P_t/P_t 10 Rh #2	2300	2290	2300	2290	2010
W/Re ⊥ ASTRO		2260	2260	2270	2000
		2260	2260		
		2255		2270	
W/Re ‖ ASTRO				2280	
				Failed	
W/Re ⊥ SERM.			2260		
			Failed		
CHROMEL ALUMEL ⊥ ASTRO		2191	2235		1975
TEMPILAQ 2200F	-	Melt	Melt	Melt	
2300F	-	Melt	Melt	Melt	
2400F	-	No Melt[4]	No Melt	No Melt[4]	
2500F	-	No Melt	No Melt	No Melt	

NOTES:

(1) Time into run when data was taken.

(2) Bracketed values are raw data for an emittance of 1.0. Unbracketed temperatures reflect spectral emittance corrections for the wavelength sensitivity of the specific pyrometer used.

(3) Pyrometers probably misfocussed leading to pyrometer check run data in last column.

(4) No melt but dark spots present.

more heat into the disc. The NASA/ARC plasma arc operates at an enthalpy level about three times as great as the NASA/LaRC facility, thus producing conditions, where catalycity effects become pronounced.

(4) Local gap heating around the edge of the port could provide increased heating to the disc.

(5) A combination of the above could exist.

As a point of clarity a portion of the plasma in an arc jet facility is dissociated; the higher the enthalpy the greater the dissociation. A catalytic surface is one that promotes the recombination of atoms into molecules; the heat of recombination is then given up to the surface, and maximum temperature at a given heat flux exists. A non-catalytic surface prevents this recombination of atoms and therefore operates cooler. Materials can exhibit characteristics between these extremes, where partial recombination occurs.

The study, reference 19, was conducted by developing a thermal math model of both the plasma test specimen and the calibrator. The test specimen math model was geometrically a duplicate of one used previously. The imposed heat flux and distribution across the front face and along the sides of the model holder were iterated to produce a reasonable correlation with measured temperatures at the front and aft face of the calibrator disc. This heat flux was then imposed upon the test model to assess the impact of the penetration port. Adjustment factors were applied to both the heat flux and heat flux distribution to assess the effect of catalycity of the holder and/or port, and to determine the influence of local gap heating. Since the precise enthalpy of the test facility was unknown, both 7000 Btu/lb and 12000 Btu/lb were analyzed to bracket the estimated 9000 Btu/lb operating enthalpy.

The two math models are pictured on Figures 7-63 and 7-64, while the basic imposed heat flux and distribution are shown in Figures 7-65 and 7-66. The initial heating ramp on Figure 7-65 attempts to account for the model moving into the plasma stream. Predicted versus measured temperature response for the calibrator, using this shaped heat flux, is shown on Figure 7-67. Good agreement was reached for the outer surface, and the 240 sec. time at the inner surface. Analysis produced higher heating rates on the inner surface earlier in the exposure than measured, but further refinement was deemed unwarranted, since we were searching for a nearly 300F surface temperature discrepancy.

Using the calibrator model derived heating rates and applying gap heating factors of 1.63 at node 31 and 1.23 at node 32, produced the results shown on Figure 7-68 for the penetration model Predicted temperatures are substantially below measured values, thus eliminating gap heating as a dominant factor in the high exposure temperatures experienced. Note that the calculated outer surface is 60F higher and the inner surface is 40F lower at 240 sec. than computed for the calibrator. This was verified as being due to the gap heating effect. When the test model was analyzed without gap heating, surface temperatures lower than for the calibrator resulted, because of the added heat sink of the penetration assembly.

78

The effect of holder front face catalycity influence was examined by increasing heat flux to the bare graphite by a factor of 2.67 for 7000 Btu/lb and 3.70 for 12000 Btu/lb enthalpy. The results are illustrated on Figure 7-69. Predicted temperatures approach measured outside values at 240 sec. and bracket inner wall measurements. The extreme heating rate on the outer surface is not approached.

When only the penetration port was assumed fully catalytic, Figure 7-70, a higher heating rate was obtained than that on Figure 7-69, but end temperatures were roughly equivalent.

The two above analyses were conducted to show individual effects. Because the holder face was eroded and definitely catalytic, yet did not totally account for the high temperature phenomenon, it became apparent that a combination of partially catalytic port and catalytic holder would produce the best correlation with test data. This produced the final results shown on Figure 7-71, where the enthalpy bands bracket the measured temperatures at 240 sec. The results were based upon a recombination rate for the columbium port of 2212 cm/sec. (A recombination rate of zero is for a non-catalytic surface, while a fully catalytic surface has a recombination rate of infinity. For comparison coated RCC has a calculated recombination rate of 410 cm/sec., which is in the low catalytic range.) Note that the temperature response rate on Figure 7-71 does not track the extreme heating rates from test. It is believed that much better correlation could be achieved by reshaping the initial incident heat rate on Figure 7-65. However, it was felt that this additional expenditure would not effect the end conclusions.

The end surface temperatures achieved in the final computation are as follows:

COMPONENT	Enthalpy, Btu/lb.	
	7000	12000
Columbium Port	2729F	2821F
RCC Disc	2883F	2993F
Holder Surface	3195F	3517F

It is significant to note that the temperature of the columbium port is reasonable and does not exceed the temperature limit of the VH109 silicide coating, which is in excess of 3000F.

7.4.1   Conclusions

(1) These analyses indicate that the over-temperature condition, experienced in the NASA/ARC test, was probably the result of a combination of catalytic heating on the front face of the holder, once the coating was lost, and a partially catalytic columbium port. These conditions were promoted by the high operating enthalpy (approximately 9000 Btu/lb.) in this test facility. This phenomenon was not encountered in the NASA/LaRC tests, because that facility operates at a relatively low 3000 - 4000 Btu/lb., which is not conducive to significant catalytic effects.

(2) Gap heating around the port was found to have a modest influence on the surface temperature.

(3) The presence of the penetration assembly and its effect upon cross-radiation and, therefore, surface temperature was found to be a non contributing factor in the high temperature experienced in test. In fact, this factor alone would result in a lower temperature than that of the calibrator, due to the added heat sink.

(4) Improved shaping of the imposed heat flux would result in a better time history correlation of computed versus measured temperature response.

7.4.2   Ramification of Catalytic Effects - One of the thermal analysis runs assumed a fully catalytic port and a non-catalytic RCC disc and holder. This produced a port temperature 400F higher than the RCC for an enthalpy of 12000 Btu/lb. This differential is conservative because the port is not fully catalytic. However, this temperature differential was analyzed to determine its impact upon, (1) the interface clearances between the penetration assembly and the RCC, and (2) locally higher radial thermal gradients in the RCC.

The radial stress situation was examined by assuming the full temperature gradient acts on fully restrained RCC, but the magnitude of the gradient was proportioned according to the temperature at which the maximum gradient occurs without catalytic effects. Without considering catalycity the maximum radial gradient is 234F at 1100 sec. during heatup and produces a stress of 384 psi. Assuming catalytic effects, the gradient at this time increases to 398F and the stress rises to 653 psi which is not significant. These stresses are computed assuming the simplistic relation $F = E \alpha \Delta T$ where:

E   =   elastic modulus
α =   coefficient of thermal expansion
ΔT =   temperature differential

The change in diametral clearance between the port and RCC at maximum temperature, assuming the port is 400F hotter, is computed to be only 0.00057 inch. The axial growth was similarly examined and an additional gap between the conical port head and countersunk hole in the RCC of 0.00010 inch was computed. Both of these values, which are conservative, are considered insignificant.

Therefore, it is concluded that a partially catalytic port in combination with the catalytic RCC will pose no problem.

80

3.0 THERMAL EXPANSION TEST OF COLUMBIUM PRESSURE TUBES

The coated columbium pressure tubes are subjected to forced deflections during launch arising from nose cap support bulkhead bending. This in turn causes the support posts to rotate slightly, pulling the pressure tubes with them. Additionally, during entry, the pressure tubes heat to about 2580F average and expand along their length, but they are constrained at the ends by the nose cap and the support post. This expansion requires that the tubes be bent to relieve potentially high thermal stresses imposed by restraint. However, even with tube relief bends, some tube bending stress is still induced. If this stress is sufficiently high during the imposed time/temperature profile, creep strain can occur. Then, during cooldown, reversed stresses are induced, becoming maximum at the cooled condition. This possible creep, then cooldown cycling with its attendent stress reversals, could ultimately cause a breach in the coating and produce oxidation failure, or low cycle fatigue. Hence, the need for a thermal cycling test to evaluate, experimentally, the survivability of selected pressure tubes in this temperature cycling environment.

Initial boost phase calculations by Vought indicated forced tube deflections from bulkhead bending could be as high as 0.25 - 0.30 inch (Section 4.8.2). Subsequent analyses by Rockwell for a reduced load launch condition and shorter support tubes, resulted in forced deflection conditions an order of magnitude less. The associated tube stresses thus became inconsequential. However, the Rockwell predictions were made after the tube test rig was designed to accommodate a forced deflection feature, which was not used.

Rockwell analysis showed that tubes #5 and #8 would be the most critical for the thermal stress environment. Each of these tubes were tested, #8 in tripilicate and a single #5 tube. These VH109 coated columbium tubes were supplied by Rockwell to Vought for testing. They were of the final configuration; i.e., 0.25 inch diameter with 0.015 inch wall.

A schematic of the test arrangement is illustrated in Figure 8-1. A bare Stackpole 2020 graphite fixture was employed to support the nose cap end penetration assembly and the post supported end of the tube. The nose cap end consisted of a 2.8 inch diameter RCC disc, complete with penetration assembly and ball lock anti-rotation device) to simulate the installation in the nose cap. The other end of the tube passed through alumina and glass rock insulators and was clamped by a split graphite conical retainer.

Tube length at the "support post" end was increased by 2.5 inches to account for thermal expansion deflection that would be imposed by a 100F support post, and to offset the thermal expansion relief from the graphite fixture, which was allowed to reach 500F during test. The 100F support post temperature was obtained from a Rockwell thermal analysis and occurs at the time of peak pressure tube temperature. The 500F graphite temperature was a self imposed limit, guided by a thermal analysis of an insulated graphite fixture, and later verified as being a reasonable limit, based upon calibration runs.

Initially it was planned to heat the tube assembly in air in the Vought Mission Cycling Facility which employs resistance heated SiC rods. Pressure during the period of maximum tube temperature ranges up to about 1 mm Hg, but in order to prevent arcing between SiC rods, this was increased to 50-60 mm Hg

with Rockwell concurrence. However, even at this pressure it was found that the 2580F temperature could not be achieved without breakage of heater bars. The potential damage to test tubes from falling debris forced the test to be moved to another facility, one in which bare graphite heater bar elements could be used.

The test was finally conducted in the Vought Nerva vacuum chamber in the arrangement depicted in Figures 8-2, 8-3 and 8-4. Two tubes were cycled simultaneously. They were rolled under the heater elements for the heat pulse and then rolled back under a water cooled cover for cooldown. Temperature was monitored and controlled by two tungsten rhenium thermocouples attached to each tube and three on each graphite holder as shown on Figure 8-5. Testing was conducted in air at 0.4 mm Hg, which was representative of the flight pressure at peak temperature. A calibrator tube of the No. 8 configuration was used to establish the test procedure and was instrumented with five thermocouples, four of which were not covered by insulation. Results showed that the desired conditions could be met and that temperature distribution along the pressure tube was satisfactory, varying by a maximum of 31F for the four exposed thermocouples.

Although no attempt was made to exactly duplicate the flight time/ temperature profile, it was a goal to roughly produce the flight temperature pulse to assure that if creep were to occur there would be sufficient time for its' development. But, over-test, that could yield unrealistic creep, was to be avoided. The fidelity of the test profile is shown on Figure 8-6 where a typical cycle is shown against the computed flight temperature history. If the flight profile is slid to the left to eliminate the initial slow heatup portion of the curve, it can be envisioned that the peak temperature region of the curves will superimpose satisfactorily.

The results of this test, reference 20, were both disconcerting and gratifying: disconcerting, in that tube fractures occurred, ranging between 68 and 136 cycles with one going 140 cycles without failure; gratifying, because the test environment produced severe embrittling of the tubes and yet they withstood the thermal stress conditions for at least 68 cycles. This is at least a factor of two longer than the coated columbium penetration assemblies are expected to survive. A typical fracture is shown on Figure 8-7. The embrittlement was investigated by Rockwell, where they concluded that the problem resulted from incomplete oxidation of the heater bars in the presence of low pressure air. The production of CO, rather than CO_2, resulted in a smaller molecule being generated than O_2 for which the coating was designed. The CO was able to penetrate the microcracks in the silicide coating and combine with the underlaying columbium. Micrographic analysis, conducted by Vought on one failed tube, revealed a nearly single crystal state in the high temperature, embrittled region, while at the cooler tube ends normal granular structure was observed.

As a qualitative check of the local atmosphere, a shiney, steel bar was inserted in the facility during seven test cycles. At the conclusion of exposure the bar was dull gray with a mottled appearance indicating neither a completely reducing atmosphere nor a highly oxidizing one.

It was concluded that the thermal exposure of the pressure tubes, resulted in a gross overtest, due to the nature of the local atmosphere, and that more ductile tubes would have survived without fracture.

Two other observations from the test are noteworthy. Typically, flaking of the coating was observed. This was discovered in chemical compatibility tests conducted in a 1 atm furnace and has been observed on components exposed in a plasma arc. This is apparently normal for the VH109 coating system and, while it may reult in reduced life, the life of the system is deemed satisfactory.

The second observation was that a deposit of material tended to form in the tube just down stream of the flare. No deposits were found in the unions or ports. (The other end of the tube was stuffed with insulation and no deposits accumulated there.) The deposited material was analyzed by Rockwell and found to be silica, believed to come from outgassing of the silicide coating at low pressure and high temperature. The gaseous product traversed toward the open end of the tube and then condensed at a cool region of the tube creating a degree of blockage. This is not expected to be a flight problem since (1) the port end of the tube remains hot, when the center section is hot, preventing condensation, and (2) localized pressure and flow at the port hole from leakage or turbulence should discourage buildup.

The cycling history for the four tubes tested is as follows:

SPECIMEN	TUBE CONFIGURATION	CYCLES COMPLETED	FAILURE
1	8	74-87	Yes
2	5	140	No
3	8	68	Yes
4	8	136	Yes

The specific cycle of failure for specimen number 1 is unknown, since initially the tubes were to be inspected after each block of cycles. Subsequent to the first tube failure, visual inspection was made through a sight port in the side of the chamber. Note that all of the failed tubes are of the No. 8 configuration.

Measurement was also made periodically of the dimensional location change of the manifold end of the tube. The purpose of this was to obtain a "feel" for accumulated creep set during exposure. Upon initial assembly of the tubes into the graphite fixtures, the manifold end of the tube was allowed to seek its own location along the tube axial direction before clamping it in place. The location of the end of the clamped tube was determined relative to the fixture surface. After "x" thermal cycles, the clamp was released and the movement of tube relative to its' initially installed location (set) was determined. The tube was then repositioned to its' initial location for continuance of the test. "Set" measurements (overall shortening of the tube) are as follows:

SPECIMEN	TUBE CONFIG.	MEASUREMENT CYCLE	"SET", IN.
1	8	50	0.19
2	5	50	0.25
3	8	36	0.10
4	8	49	0.15
4	8	100	0.14

Certainly, the set measurements are not extremely accurate, but it is believed that they do indicate that some creep strain takes place during the heat pulse when the tube ends are constrained.

In conclusion, the test demonstrated that the pressure tubes would sustain the accumulated thermal cycling in a constrained condition to levels in excess of the expected life of the penetration assembly. This was even with embrittled tubes which should be much more susceptible to fatigue cracking than ductile material. Creep strain, judging from the set data obtained, does exist but should not be detrimental for the life of the system with ductile tubes.

The test atmosphere was unexpectedly severe for the coated columbium due to the incomplete oxidation of the bare graphite bars to form CO rather than CO_2. Unfortunately, Vought was unaware of this potential problem, and Rockwell did not identify this problem until the test was concluded.

9.0 VIBRATION TEST OF THE LEFT SIDE SEADS ASSEMBLY

9.1 Introduction

Probably the most complex test performed on SEADS was the random vibration test of the left hand system. It was comprised of the manifold, seven pressure tubes and the seven associated penetration assemblies. In an effort to compromise between the high cost of an "all up" acoustic test of an assembly (complete with a nose cap) and the desire for a comprehensive test program, an approach was devised wherein two vibration shakers were employed simultaneously. One shaker introduced the vibration spectrum representing the nose cap, while the second shaker imposed a spectrum simulating the support bulkhead response. Input environments were derived from responses measured during the acoustic test of the baseline nose cap assembly at NASA/JSC. The nose cap was simulated by a multifaceted aluminum casting to which the seven penetration assemblies were attached. Two test setups were employed to produce inputs in two separate pairs of axes, which were determined to be the most critical by analysis. The test scheme is illustrated on Figure 9-1, while the overall test setup is shown on Figure 9-2.

The primary reasons for conducting this test were to:

(1) Validate the Rockwell dynamic analysis for both the left hand and right hand tube arrays, since analysis was the means by which the SEADS was certified for flight.

(2) Demonstrate the structural dynamic integrity of the system.

9.2 Test Environment

Rockwell had responsibility for establishing the test environments and did a very thorough analysis in a logical manner. Details of the analysis are not reported here but the approach is covered to indicate the soundness of the test and results. The Rockwell pre and post test analyses are documented by references 21 and 22.

Input levels at both the nose cap and nose cap support bulkhead were derived from accelerometer response, measured during an acoustic test of the baseline qualification nose cap assembly at NASA/JSC. The outputs were enveloped to produce the random vibration test levels and exposure times like those shown on Table 9-1. Note that the levels shown are the adjusted levels for the designated test axes that were ultimately determined by analyses discussed below.

The enveloped response spectra were imposed on each tube assembly using finite element modeling techniques. A tube assembly consisted of the manifold and the seven pressure tubes. Each tube was modeled as 26 nodes and 24 elements. Input vibration levels were simultaneously applied. In addition, the model was used to generate static stresses for launch accelerations and entry thermally induced loads. The output of the analyses included modes, frequencies, vibration responses, deflections, stresses, and bending moments. Dynamic and static stresses were combined to determine maximum stress in each tube. Results showed that the tubes would not be over stressed and fatigue life was adequate.

<div align="center">

TABLE 9-1
SEADS RANDOM VIBRATION TEST CRITERIA

BULKHEAD

</div>

X-Axis

20-25 Hz:	+15dB/OCT
25-30 Hz:	$0.117g^2$/Hz
30-40 Hz:	-15dB/OCT
40-120 Hz:	$0.025g^2$/Hz
120-300 Hz:	-3dB/OCT
300-2000 Hz:	$0.010g^2$/Hz

Y-Axis

20-50 Hz:	+6dB/OCT
50-100 Hz:	$0.018g^2$/Hz
100-2000 Hz:	-6dB/OCT

<div align="center">

NOSE CAP

</div>

Y-Axis

20-30 Hz:	+6dB/OCT
30-50 Hz:	$0.55g^2$/Hz
50-120 Hz:	-10dB/OCT
120-600 Hz:	$0.028g^2$/Hz
600-700 Hz:	+24dB/OCT
700-900 Hz:	$0.11g^2$/Hz
900-2000 Hz:	-10dB/OCT

Z-Axis

20-30 Hz:	+6dB/OCT
30-50 Hz:	$0.44g^2$/Hz
50-120 Hz:	-10dB/OCT
120-600 Hz:	$0.022g^2$/Hz
600-700 Hz:	+24dB/OCT
700-900 Hz:	$0.088g^2$/Hz
900-2000 Hz:	-10dB/OCT

<div align="center">

DURATION

42 seconds/mission/axis in each axis of vibration
(70 minutes/axis/100 missions)

</div>

Next, the optimum test setups were determined by analyzing the tube tresses for nine combinations of input vibration - 3 axes at the nose cap end nd 3 axes at the bulkhead end. Examination of results showed that two shaker etups would produce maximum stress levels in all tubes without significantly verstressing any one tube. The selected axes were:

(1) Bulkhead Y-axis with Nose Cap Y-axis
(2) Bulkhead X-axis with Nose Cap Z-axis

Because the test inputs are in one axis, rather than three simultaneously, esultant stresses would necessarily be lower than flight if the analyzed nput single axis spectra were applied during test. This was resolved by djusting the test spectra upward to produce flight computed stress levels. he adjusted levels are those listed on Table 9-1.

9.3 Test Configuration

As previously noted, the left hand system was selected for test because it lad the longest manifold with the greatest tilt angle relative to the support bulkhead. This tends to produce larger manifold response to bulkhead X-axis ibration. Pressure tube dynamic analysis confirmed that this was true for lost of the tubes.

The test hardware consisted of the flight design manifold assembly, seven coated columbium pressure tubes and seven penetration assemblies mounted in 2.8 inch diameter RCC discs to duplicate the nose cap mounting. The RCC discs were clamped to a cast aluminum test fixture, which was machined to provide facets for acceptance of the RCC discs. Thus, each penetration assembly was nounted in the same position as it would be in the nose cap. The assembly is shown on drawing 221GT4098, Figure 9-3. Note that this drawing is actually a nirror image of the desired test article and is discussed in Section 9.5.

The penetration assemblies varied in configuration and port material. Two of the ports, Nos. 7 & 11 were coated graphite, while the other five were coated columbium. Two anti-rotation features were employed as well as no locking feature. Port Nos. 6 & 9 employed a flat sided hole in the disc to restrain port rotation and port Nos. 7 & 10 used the synthetic ruby ball lock concept to prevent rotation. (See Section 6.4 for descriptions.) The remaining ports employed no anti-rotation device.

The reason for testing graphite was that it had not yet been demonstrated that the coated columbium would survive the flight temperature and the vibration test provided an opportunity to evaluate coated graphite in the dynamic environment as a backup material. Plasma testing of graphite had already been conducted to show that it did have some mission life.

Similarly, alternate lock features were tested, since none had been firmly selected, and it wasn't even clear that an anti-rotation device was needed. As it turned out, no observable oscillations of the ports in the discs occurred, even with no lock. However, the flat sided hole approach was ultimately incorporated into the SEADS nose cap as a safeguard.

The test support bulkhead was simulated by a block of aluminum to which the manifold was bolted. The support bulkhead stiffness did not have to be represented, since bulkhead response was an input loading for the test.

Although this vibration test would not adequately test the manifold insulation, it was included in the test configuration to provide a representative mass and to evaluate the installation of the insulation system.

The insulation, manifold and columbium pressure tubes were designed by and provided by Rockwell. All other components and designs were Vought responsibility.

The shakers had to be elevated to place them in proper position for test. Support structures were fabricated from welded 6 inch square steel tubing. One of these is shown on Figure 9-2. The support structures and fixtures were evaluated to assure no adverse response.

9.4 Instrumentation

Four triaxial accelerometers and four axial accelerometers were installed on the "nose cap" fixture, one triaxial accelerometer was mounted to the "bulkhead" fixture, and two triaxial accelerometers were attached to the manifold, one at the base and one at the free end. The four axial accelerometers were located adjacent to selected penetration assemblies to detect any loosening, should it occur.

In addition, each pressure tube was instrumented with three axial strain gages at each end of the tube with each gage spaced 120° apart. These were mounted as close to the fixed ends as possible. The base of the cylindrical section of the manifold was also instrumented with three rosette gages mounted 120° apart. The manifold strain gages were calibrated by bending about two axes and by applying compression along the axes, reference 23. This was done to provide backup data in the event there was an anomally in the accelerometer data. The pressure tube strain gages were not calibrated since there did not appear to be a satisfactory way to accomplish it.

The number of desired data channels (21 accelerometers and 51 strain gages) far exceeded the recording capability so it was necessary to selectively sample the data for one minute intervals through the first three minutes in each test axis to gather data on all of the channels. The data was then reviewed and the most critical channels were selected for recording for the duration of the test.

9.5 Installation and Setup

Accurate positioning of the shakers was extremely important to assure the proper geometric relationship between the "nose cap" and "bulkhead" to avoid having to forcibly bend the pressure tubes into place. This was accomplished by fabricating a tubular fixture that spanned the distance between shakers. This permitted fine adjustment of shaker location, and it worked well.

A serious problem surfaced during the trial setup. It was discovered that the entire Vought test system was designed and built around the mirror image of the left hand assembly, while the Rockwell tubes and manifold were designed correctly. With all the checkers, reviewers, and signers of the controlling drawing (Figure 9-3) no one noted the drawing error. It was a case of "not seeing the forest for the trees."

The solution was relatively simple, however. The manifold could be salvaged by rotating it about its mounting base until it was oriented into a mirror image position. All of the pressure tubes on the other hand had to be refabricated to produce mirror image components. With this approach we were able to test a system dynamically identical to the left hand system. This required new pressure tube check fixtures, but it was the least costly and least schedule consuming approach.

A new problem was encountered by Rockwell during refabrication of the pressure tubes. In the process of adjusting the last tube to the proper geometry the end of the tube broke at the juncture of the uncoated to coated portion of the tube, indicating a brittle condition. This was traced to the oxidation test of the tubes, which is routinely conducted to assure soundness of the coating. The uncoated portion of the tube was "protected" by wrapping and stuffing with Fiberfrax insulation. However, the end of the tube exceeded 300F and was embrittled by oxidation. Rockwell corrected this by employing a water cooled collar on the uncoated end when the tubes were remade. No further problem was encountered.

A set of aluminum tubes were also fabricated to use in fit check of the setup, and to establish the procedure for cutting and flaring on assembly. This was a good idea and added experience and confidence before committing the columbium tubes to the cut and flare operation.

It was discovered during the trial assembly that three of the seven elbows, that install in the end of the manifold and tie to the pressure tubes, were out of angular tolerance. These were standard procured parts. Rockwell supplied replacement units so we could pick and choose acceptable units. When this was corrected the pressure tubes mated up well between the "nose cap" and manifold.

Installation of the columbium tubes worked equally as well. The flaring operation was conducted by a Rockwell representative. Small cracks in the end of the flare were observed on two tubes but these were dressed up and found acceptable. Installed tubes are shown on Figure 9-4 after trial installation.

Installation of the insulation system on the manifold proved to be somewhat difficult. This was a five segment configuration with two of the segments, that sandwiched the manifold, split in two. The insulation system components are shown on Figure 9-5. The two collars had to be slipped onto the manifold before the tubes were assembled, then the manifold end cap insulation segment was installed. This is shown on Figure 9-6. The collars were then slipped into place, using mylar to facilitate this operation. The installed collars and the mylar can be seen on Figure 9-7. The fit was so tight between the inner collar and the end cap and pressure tube elbows, that a great amount of force was required. As a result severe damage to the inner layer of fabric occurred, as illustrated on Figure 9-8. It was concluded that this would be a very difficult task if it had to be accomplished inside the nose cap. The remaining segments are shown installed in Figure 9-9. Note that the segment toward the base of the manifold was modified from the original flight configuration to match test geometry and the segments were taped rather than strapped in place because of this. It was observed that significant corner gapping was present, where segment halves came together, and it was feared that this would admit radiation heating. In addition, the platinum wire wound around both collar segments was judged to be too loose and

fragile to be effective. As a result of the installation experience and observations made, Rockwell undertook to redesign the insulation system for flight. The fact that the insulation was installed for the vibration test proved highly beneficial in ferreting out problems.

After the insulation was in place, the unions and nuts at the penetration assembly were torqued to 20 in.-lb. using a torque wrench. This torque was judged to be sufficiently low to prevent self bonding of flight hardware, yet provided a finite, measurable value to be used for inspection. Previously, we were using the qualitative "finger tight" specification. The amount of torque to unscrew the nuts from the union were measured after test and are covered in the next section.

9.6 Test

Some months prior to the test, a meeting was held with NASA and Rockwell to cover all details including alignment of shakers, installation of test hardware, movement of shaker heads between the 'at rest' and 'power on' condition, method for reconfiguring the assembly for the second set of axes, instrumentation, method of control, equalization, control tolerance, automatic abort limiters, startup and shutdown transients, and responsibility for early termination of a run should it be necessary. In short, all details of the whole operation were discussed to assure that all parties involved understood and agreed to the method of conducting the program. This meeting was considered both necessary and worthwhile to assure technical excellence and to avoid post test disagreements.

The Y-Y axis configuration was tested first. Three one-minute tests were conducted first to allow acquisition of all data, since a maximum of 18 accelerometers and 22 strain gages could be recorded at one time, due to limited recording capability. For the completion of the test only the most prominant of the data, as determined by the three initial runs, was recorded. Two nine-minute runs were made to conclude the planned 21-minute test duration, which is equivalent to 30 missions including a scatter factor of four.

The X-Z axis configuration was tested in a like manner for a total of 21-minutes.

All data was recorded on magnetic tape and is available for review. Typical control accelerometer data for the nose cap and bulkhead ends are shown on Figures 9-10 and 9-11, respectively, for the Y-Y axis test. Specified upper and lower pre-test limits are shown for comparison. Typical X-Z configuration data for the control accelerometers is shown on Figures 9-12 and 9-13.

Maximum deflection of the shaker heads when power is applied was measured and shown on Figure 9-14. These produce forced deflections of the pressure tubes, but are considered rather modest.

Predicted versus measured stresses for each of the tubes are summarized on Table 9-2. These were developed by Rockwell. In general predicted stresses were higher than measured, due to the purposely conservative analysis. Only Tube No. 8 displayed a significant reversal in the trend, which is discussed below. A comparison of predicted and test natural frequencies is shown on Table 9-3. The correlation is quite good.

90

TABLE 9-2

COMPARISON OF PRESSURE TUBE STRESSES

| TUBE NO. | TUBE END | PEAK TUBE STRESS, PSI | | | |
| | | Y-Y AXES* | | X-Z AXES* | |
		TEST	ANALYSIS	TEST	ANALYSIS
5	Blkhd.	5640	7548	5264	8312
	Nose Cap	3399	11179	2578	6737
6	Blkhd.	4984	7311	4480	6970
	Nose Cap	2669	9412	2298	7430
7	Blkhd.	5144	8706	4429	6813
	Nose Cap	3441	7837	3246	6679
8	Blkhd.	14836	12730	10872	8458
	Nose Cap	4801	7344	1665	3459
9	Blkhd.	3172	8478	7416	10712
	Nose Cap	2048	4427	3770	3877
10	Blkhd.	3600	7858	8244	9380
	Nose Cap	2519	3957	3708	6650
11	Blkhd.	4638	7099	6552	8338
	Nose Cap	5838	5618	4086	5550

*Y-Y Axes = Shaker Y-Axis Bulkhead and Y-Axis Nose Cap.
 X-Z Axes = Shaker X-Axis Bulkhead and Z-Axis Nose Cap.

TABLE 9-3

COMPARISON OF NATURAL FREQUENCIES

TUBE NO.	FREQUENCY, HERTZ		
	ANALYSIS	Y-Y TEST	X-Z TEST
5	62	62	60
6	64	64	60
7	68	60	60
8	105	110	-
9	68	60	70
10	79	80	80
11	63	60	60

Tube No. 8 displayed the highest strain levels for both test onfigurations, and typical of all tubes, was greater at the manifold end than he penetration end. This tube was the straightest of all, having two 90° ends, but no 180° bends, so it perhaps, is not surprising that the strain as highest. Typical PSD strain plots of Tube No. 8 response are shown on igures 9-15 through 9-18 for both tests and at each end. The "M" designation efers to the manifold end, while the "P" denotes the penetration end. Both ages are at the 0° circumferential location on the tube.

The low frequency response was typical of all of the tubes, and was elieved to be due to forced deflection, rather than resonant frequency. This as confirmed, when the control accelerometers were analyzed for isplacement. A typical PSD of displacement is shown on Figure 9-19. It eveals a shape similar to the strain gage data, providing evidence that the igh strains are not resonance induced.

Rockwell re-analyzed this low frequency region for Tubes 5 and 8, eference 22. These tubes represented both a typical and stiffest tube espectively. Strain spectral density (SSD) plots were generated which ompared very favorably (though conservatively) with the test results. ypical results for Tube 8 are shown on Figures 9-20 and 9-21.

The test hardware withstood the vibration test with no problem. No ailures were encountered and no loosening or rotation of penetration ssemblies was evident by either visual observation or accelerometer data. 'his was true with or without an anti-rotation feature.

Nut to union removal torques varied between 5 and 30 in.-lb., with the low nd typical of tubes 5, 6 and 8 and the higher torque for tubes 7 and 11. In he course of removing the No. 9 penetration assembly, the graphite port was roken. It isn't clear if the graphite was damaged during test or whether ailure was the result of improper disassembly technique. It does point out, owever, that if graphite was to be used, much more data on the performance of he material would have to be gathered, and greater handling care would have o be exercised.

The ends of the flares on the pressure tubes appeared to have coating amage, which is typical of findings in the plasma test programs. The best nd worst of the tube ends are shown on Figure 9-22. This region is fragile nd vulnerable to chipping, when sandwiched between the union and nut. ockwell exposed the tubes to 2000F for 15 minutes at 1 atm to determine xidation resistance. It was found that there was no evidence of oxidation long the tube length, but the suspect area at the flare end, produced xidation products. This is typical of the plasma arc test experience. They roposed that this vulnerability could be reduced by dressing the local oating buildup to avoid the localized crushing of the coating.

In conclusion, once the test program overcame the early diappointments of irror image hardware and brittle tubes, it was well conducted and emonstrated the integrity of the SEADS design in the dynamic environment. urther, the use of two simultaneous, independently controlled shakers, is elieved to be unique.

Analytical predictions were deemed adequate to certify the tubes for light and all stresses were within the allowables.

10.0 FINDINGS

The most significant findings from this program may be summarized as follows:

(1) Holes can be introduced into the nose cap shell without impairing its structural integrity, as determined by analysis.

(2) The introduction of SEADS penetration holes does not reduce the mission life of the nose cap as demonstrated by long term plasma arc test exposure.

(3) Silicide coated columbium will survive the design temperature for multiple missions and will tolerate significant temperature overshoot.

(4) Small diameter, unsupported pressure tubes can be designed to withstand the Shuttle dynamic environment and yet be flexible enough to avoid damaging thermal stress.

(5) With the application of silicon carbide powder, as an anti-seize compound, self bonding of silicide coated columbium, exposed to high temperature, can be prevented for an acceptable operational period.

(6) Silicide coating of the inside of small diameter columbium tubes can be accomplished.

(7) Siliconized graphite can serve as a viable backup to coated columbium port components, although with a reduced mission life.

(8) Iridium wire provides an effective lockwire approach.

(9) The oxidation rate of unprotected columbium is sufficiently slow, at least in the 2500F region, as to pose no safety of flight concern, when the silicide coating is breached.

(10) Coated columbium is partially catalytic and must be accounted for in high enthalpy environments.

(11) Optical pyrometer and thermocouple temperature measuring techniques can provide widely differing data in plasma arc testing. Controversy persists on which device is the more accurate.

(12) Vibration testing, using two independently controlled shakers, is feasible.

(13) Pressure measurement for this system is practical, even with high temperature, finger tight joints, although response may suffer.

(14) A ball lock device, employing a synthetic sapphire sphere, will provide a satisfactory, high temperature, anti-rotation scheme.

(15) Platinum and cobalt based alloys are chemically incompatible with siliconized RCC when in direct contact.

(16) This development program, involving four entities (NASA/LaRC, NASA/JSC, Rockwell and Vought), with the industrial companies operating under separate contracts was accomplished without conflict only because the personnel assigned worked well together, and were dedicated to producing a satisfactory SEADS system.

11.0 CONCLUSIONS

The SEADS system was developed over a period of years. The design is supported by detailed thermal, static and dynamic analysis, as well as, comprehensive thermal, static and dynamic tests. It is estimated that mission life will be approximately 25-30 missions. At this writing, only the insulation subsystem has not been certified for flight; but, a forthcoming system thermo/acoustic test is scheduled to accomplish this task.

As a result of the extensive and satisfactory development activities, the system was judged acceptable to proceed into production design.

2.0 POSTSCRIPT

The SEADS system, which includes the nose cap and support bulkhead, together with the pressure measurement and recording system have been fabricated. It is currently planned for installation on the OV-102 Orbiter for operations at a convenient refurbishment period.

Photographs of the assembly are provided as Figures 1-4 and 1-5. On Figure 1-5 some of the tubes can be seen, as well as, the insulation on the two manifolds and the pressure transducers mounted on the nose cap support bulkhead.

REFERENCES

1. 2-52400/7ACP-2, dated 1/13/77, Final Summary Report, Materials Evaluation For Modification of the RCC Nose Cap for Pressure Analysis Temperature Measurement.

2. 221RP00767, dated 5/1/79, Final Summary Report, Shuttle Entry Air Data System (SEADS) Feasibility Demonstration.

3. 2-53230/7ADP-7, dated 2/9/77, Design Information Release (DIR), Air Data Probe - Phase II Thermal Analysis.

4. 2-53200/7ADP-15, dated 10/17/77, Design Information Release (DIR), Shuttle Orbiter Air Data Probe Support Tube Thermal Analysis.

5. 2-58020/7ADP-11, dated 6/1/77, Design Information Release (DIR), Air Data Probe Dynamic Analysis.

6. 2-30400/8ADP-0037, Rev. "A", dated 9/21/78, Design Information Release (DIR), Structural Analysis of The Shuttle Nose Cap Incorporating Shuttle Air Data System.

7. 2-51210/0DIR-12, dated 12/15/80, Design Information Release (DIR), Stress Analysis of the Presure Ports on Production SEADS Shuttle Nose Cap.

8. 2-30320/8ADP-0035, dated 6/22/78, Design Information Release (DIR), Air Data Probe Predicted Temperatures - Trajectory 14414.1C.

9. 2-30320/9ADP-0013, dated 7/5/79, Design Information Release (DIR), SEADS Cross-Radiation Blockage Thermal Analysis.

10. 2-30400/9ADP-0015, dated 7/20/79, Design Information Release (DIR), SEADS Thermoelastic Stress Analysis, Trajectory 14414.1C.

11. 2-30400/9ADP-0019, dated 9/24/79, Design Information Release (DIR), Strength Determination SEADS Penetration Assembly.

12. 2-30400/9ADP-0014, dated 7/20/79, Design Information Release (DIR), Axial Load Analysis SEADS Penetration Assembly.

13. 221TQ00762, dated 9/10/79, Evaluation of Sticking of Threaded Parts.

14. 2-51600/RCC/8-0045, dated 10/13/78, Design Information Release (DIR), Anti-Rotation Concepts - SEADS System Penetration Assemblies.

15. 2-30400/9ADP-0019, dated 8/28/79, Design Information Release (DIR), Re-Evalution of Anti-Rotation Concepts for SEADS Penetrations.

16. 2-51210/ADP/1-0009, dated 5/20/81, Design Information Release (DIR), Plasma Arc Models Test Summary.

17. 2-30320/RCC/0-0004, dated 1/16/80, Design Information Release (DIR), Thermal Analysis of SEADS Penetration Port Plasma Arc Jet Test.

PRECEDING PAGE BLANK NOT FILMED

18. 2-30400/RCC/0-0011, dated 3/12/80, Design Information Release (DIR), Thermocouple Measurement Accuracy Evaluation.

19. 2-53200/ADP/2-001, dated 1/14/82, Design Information Release (DIR), Investigation of SEADS Temperature Anomaly NASA/ARC Plasma Arc Test - DSI 357.

20. TR 80-59940-416, dated 10/30/80, Test Information Report, Thermal Deflection, SEADS Pressure Tube Assemblies.

21. STS-81-0131, dated 1/81, Shuttle Entry Air Data System (SEADS) Static & Dynamic Analysis of Manifold & Pressure Tube Assembly - Final Report (Rockwell).

22. Review Item Disposition (RID) No. 19 Closeout, dated 3/3/81, Frequency Distributions in SEADS Analysis STS-81-0131 (Rockwell).

23. TR-80-59940-415, dated 5/6/80, Test Information Report, Static Load Calibration, Manifold, SEADS Vibration Test.

24. ETL-181, dated 12/17/80, Test Report, Engineering Development Vibration Test of the Shuttle Entry Air Data System (SEADS).
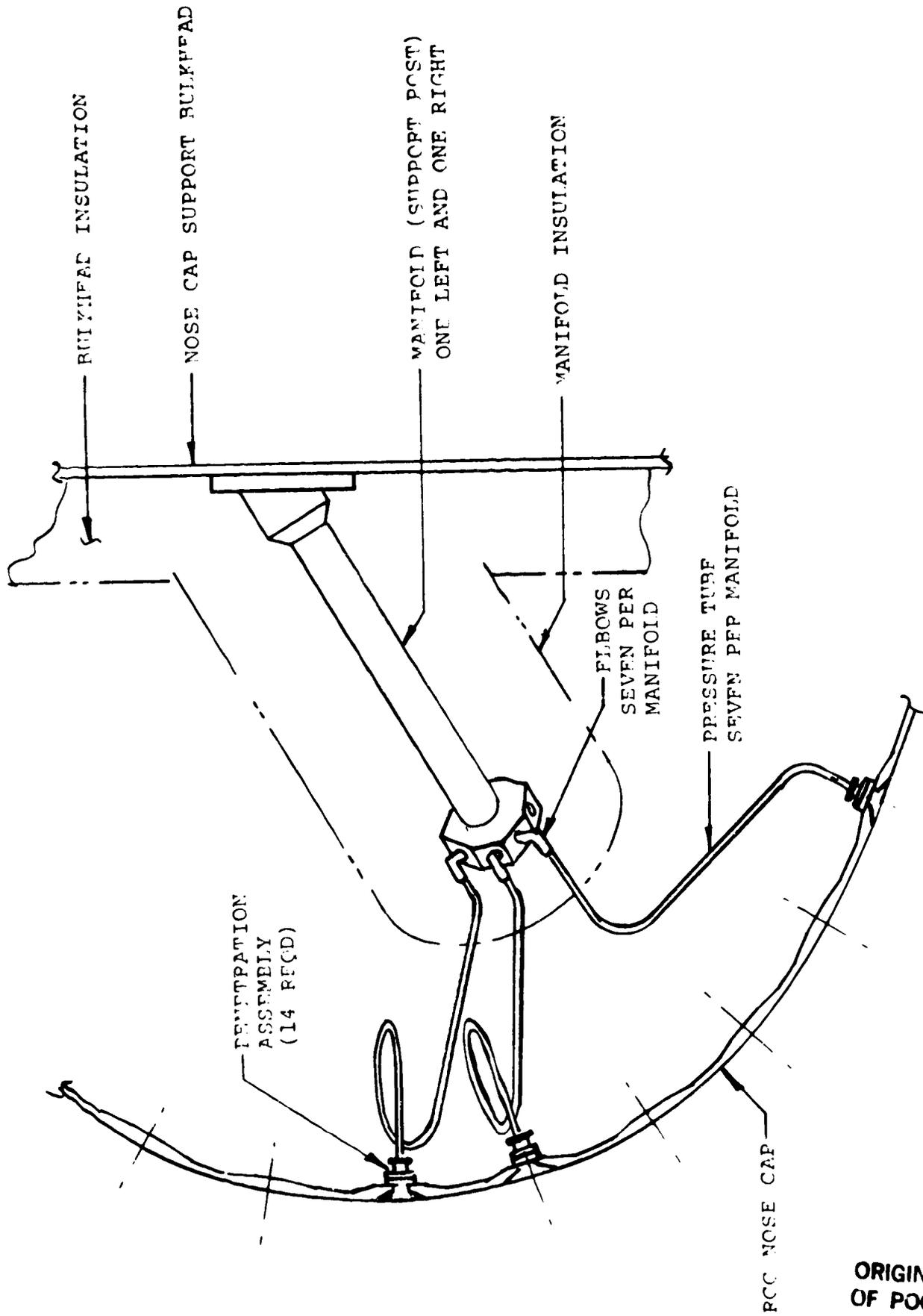
FIGURE 1-1 - SEADS HARDWARE

BULKHEAD INSULATION

NOSE CAP SUPPORT BULKHEAD

MANIFOLD (SUPPORT POST)
ONE LEFT AND ONE RIGHT

MANIFOLD INSULATION

ELBOWS
SEVEN PER
MANIFOLD

PRESSURE TUBE
SEVEN PER MANIFOLD

PENETRATION
ASSEMBLY
(14 REQ'D)

RCC NOSE CAP

221-10025 Port (Plug) (Columbium)

221-10026 Spacer (RCC)

221-10027 Lock Washer (Columbium)

221-10028 Union (Columbium)

Lockwire (Iridium)

221-10024 Nut (Columbiu

Pressure Tube (Colur
(Ref.)

221-10022 Nose Cap (RCC) Ref.
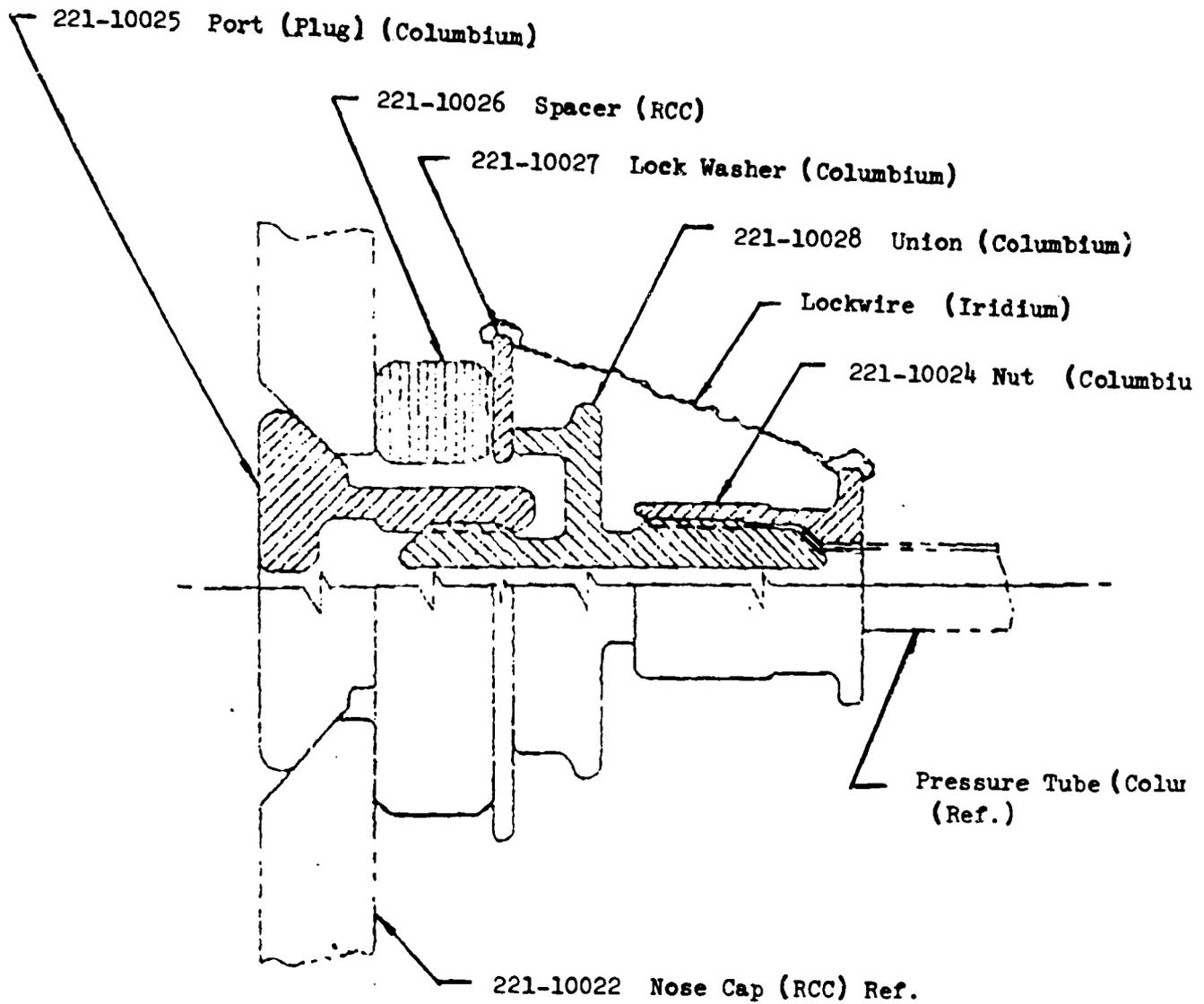
FIGURE 1-2 - PENETRATION ASSEMBLY PRODUCTION DESIGN

104
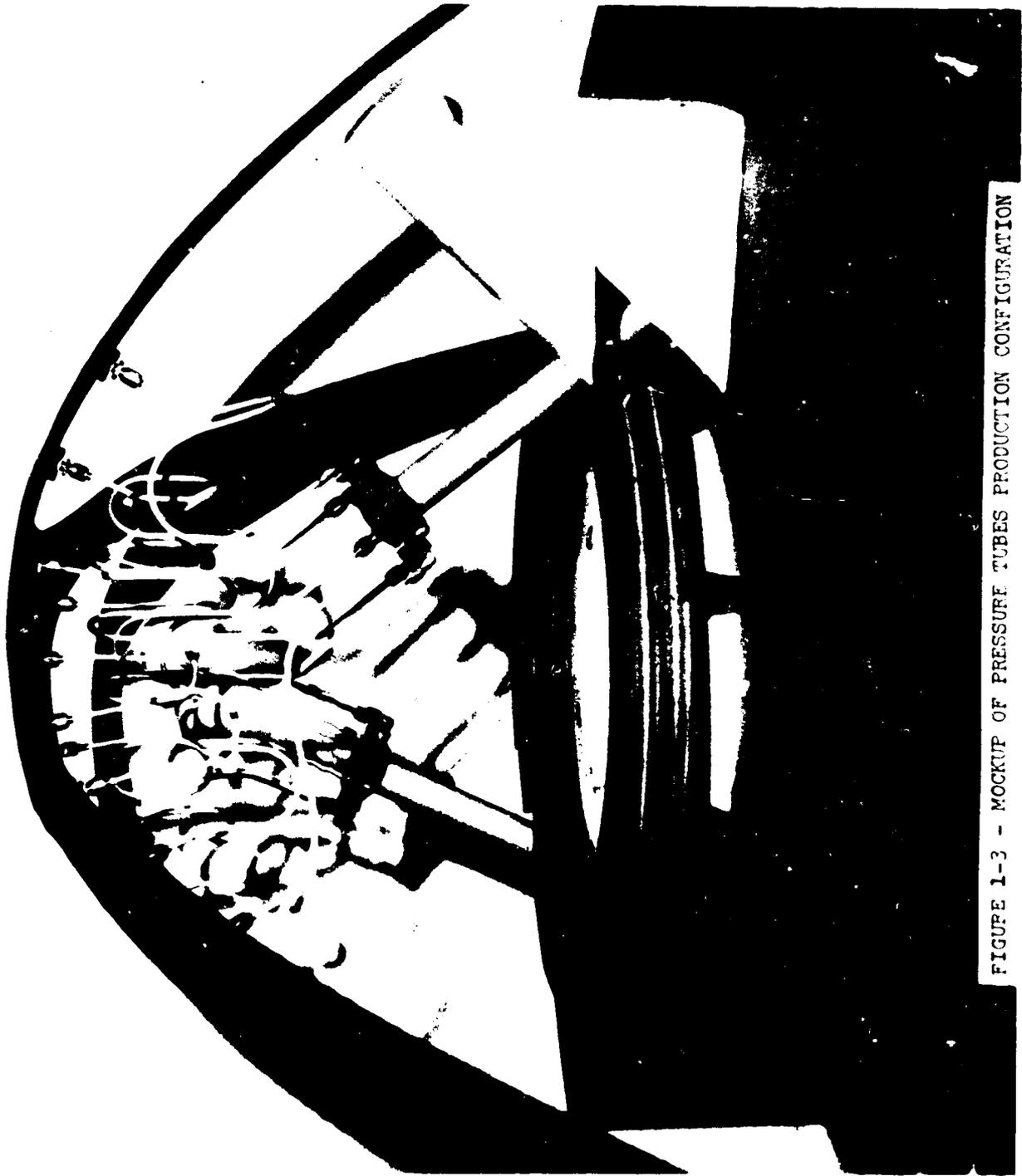
FIGURE 1-3 - MOCKUP OF PRESSURE TUBES PRODUCTION CONFIGURATION
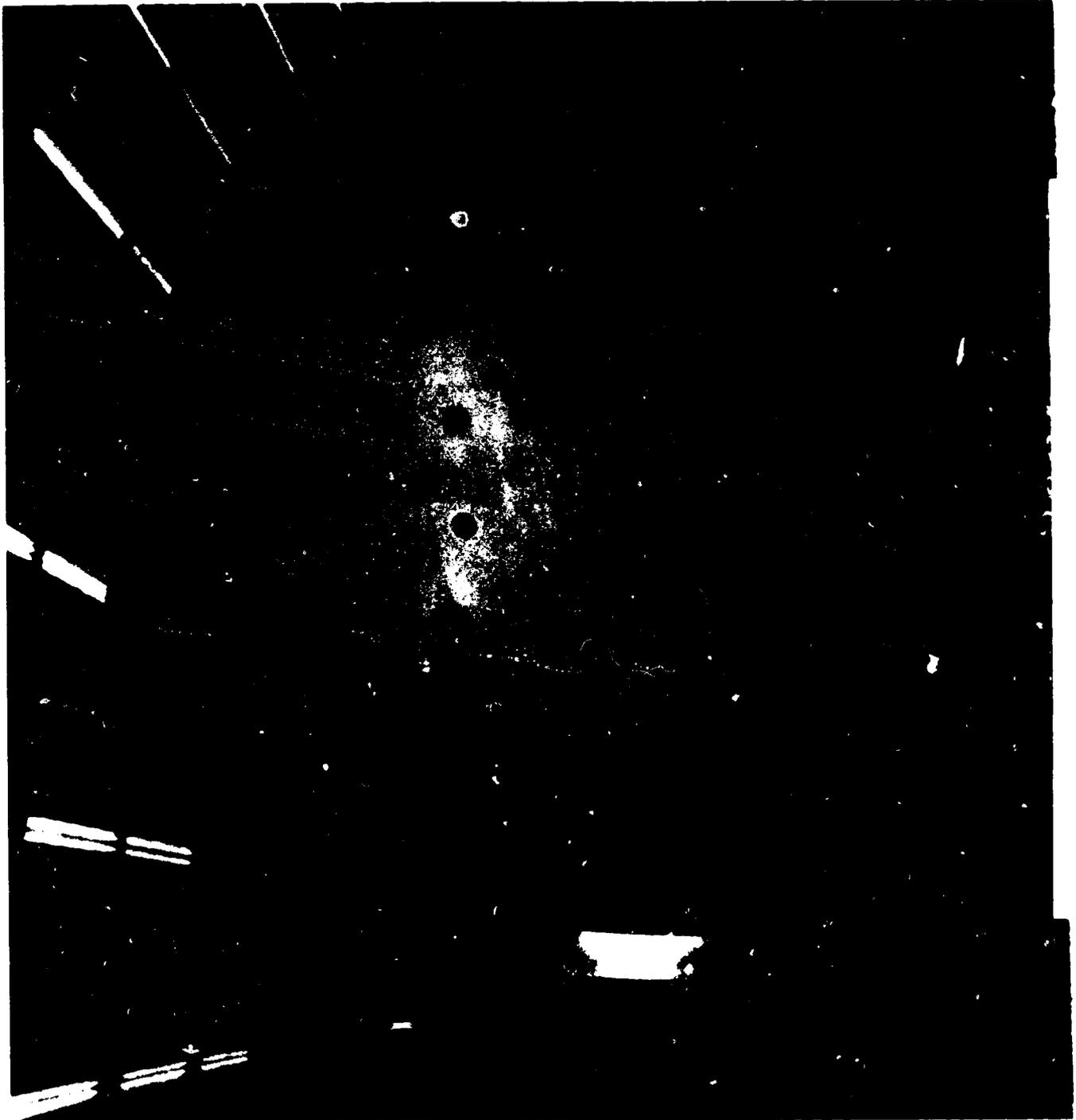
ORIGINAL PAGE
BLACK AND WHITE PHOTOGRAPH
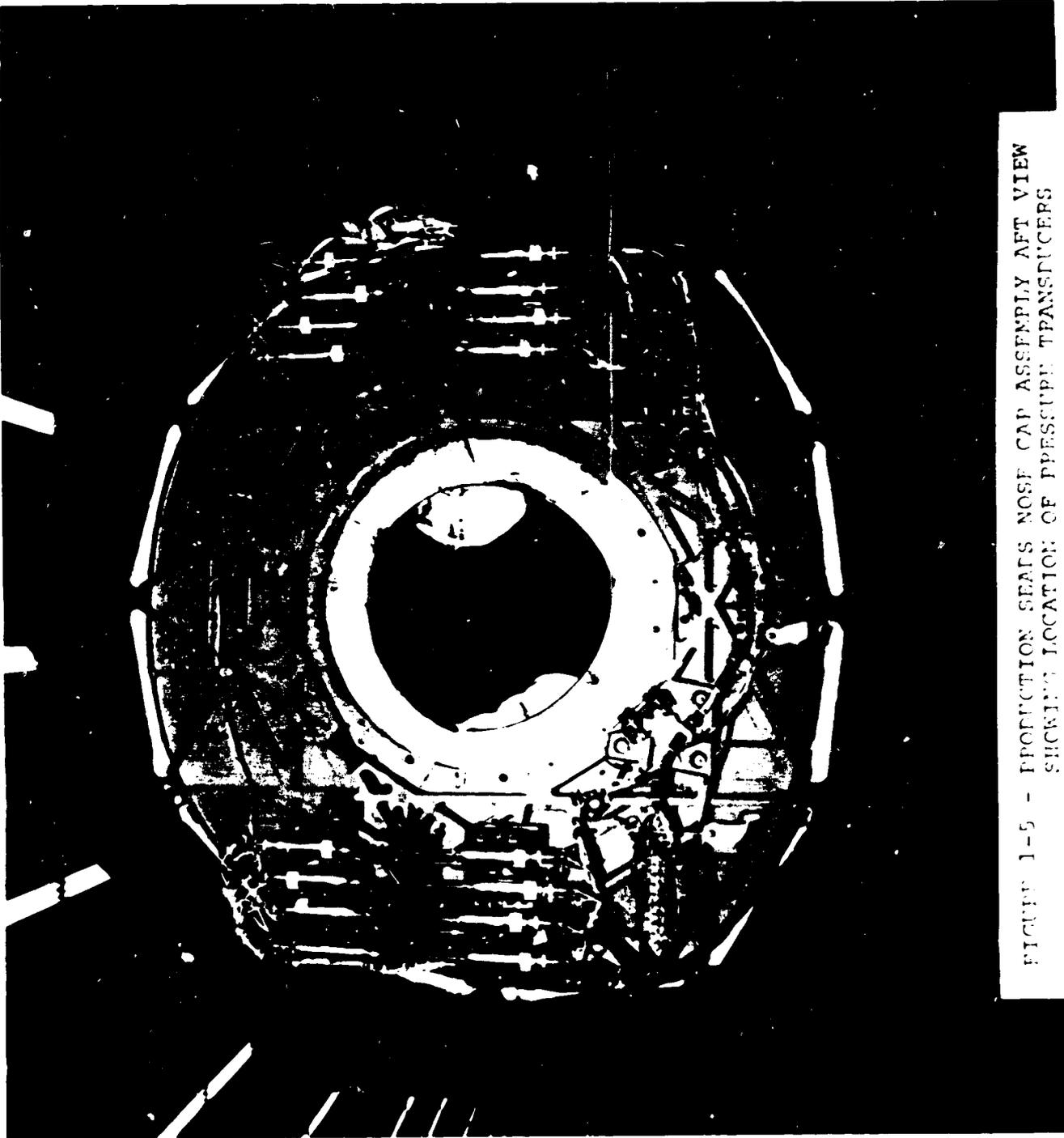
FIGURE 1-5 - PRODUCTION SRB/S NOSE CAP ASSEMBLY AFT VIEW SHOWING LOCATION OF PRESSURE TRANSDUCERS

FIGURE 3-1 - CONCEPT 1A ASSEMBLY
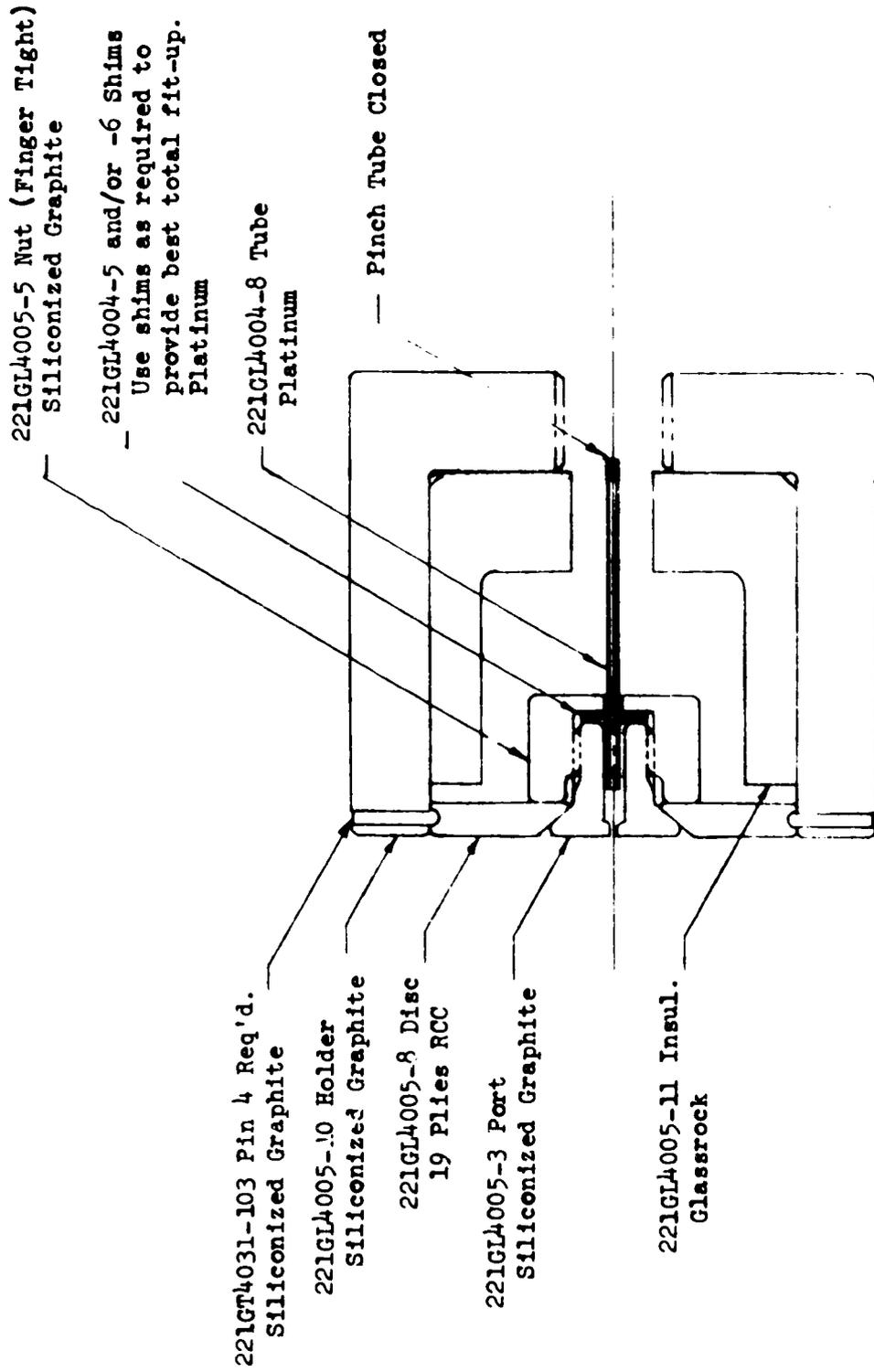
221GL4005-5 Nut (Finger Tight)
Siliconized Graphite

221GL4004-5 and/or -6 Shims
Use shims as required to
provide best total fit-up.
Platinum

221GL4004-8 Tube
Platinum

Pinch Tube Closed

221GT4031-103 Pin 4 Req'd.
Siliconized Graphite

221GL4005-10 Holder
Siliconized Graphite

221GL4005-8 Disc
19 Plies RCC

221GL4005-3 Port
Siliconized Graphite

221GL4005-11 Insul.
Glassrock

FIGURE 3-2 - CONCEPT 6 ASSEMBLY

Single Hole Edge to RCC
Siliconized Graphite

221GL4004-3 Lock
Platinum

Lock Wire with Platinum
Thermocouple Wire

221GL4004-7 Tube
Platinum

Pinch Tube Closed

221GL4004-2 Nut
Platinum

221GL4004-1 Union
Platinum

Siliconized Graphite

221GT4031 P'n 4 Req'd.
Siliconized Graphite

221GL4005-7 Disc
19 Plies RCC

221GL4005-1 Port
Siliconized Graphite

221GL4005-11 Insul.
Glassrock

221GL4005-10 Holder
Siliconized Graphite

221GT4031-103 Pin 4 Req'd.
Siliconized Graphite

221GL4005-7 Disc
19 Plies RCC

221GL4005-2 Port
Siliconized Graphite

221GL4005-11 Insul.
Glassrock

221GL4005-4 Nut
Siliconized Graphite

Lockwire with Platinum
Thermocouple Wire

221GL4004-4 Nut
Platinum (YDNiCrAl for 13B)

221GL4004-7 Tube
Platinum (Inconel 702 for 13B)

Pinch Tube Closed

FIGURE 3-3 - CONCEPT 13 ASSEMBLY

110

SPECIMEN
CONFIGURATION

Coated RCC

Various Metals

Sermetel or Astroceram
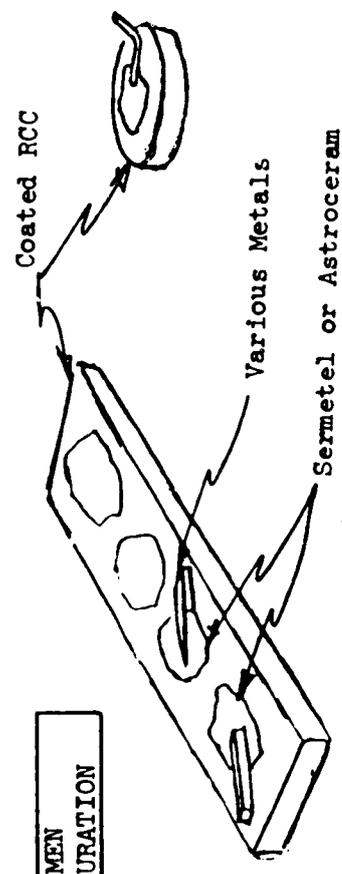
MISSION PROFILE

6 Cycles Applied
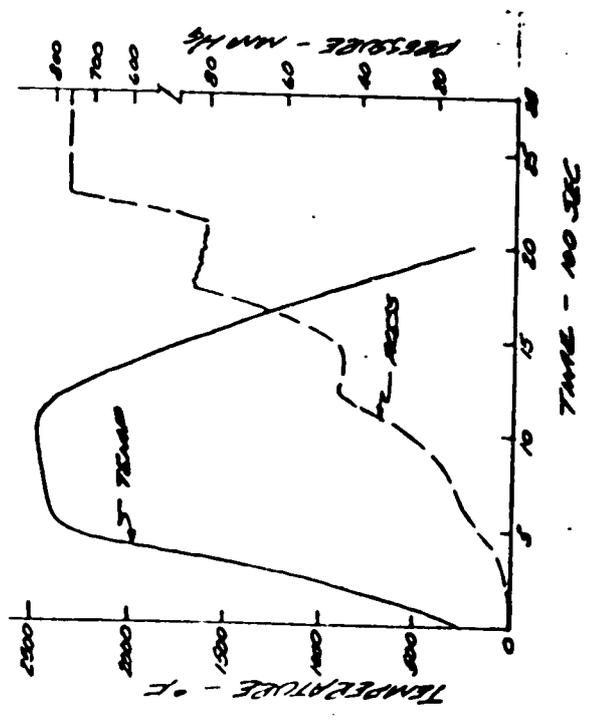
FIGURE 3-4   CHEMICAL COMPATIBILITY TEST

111

CONCEPT 6
PHASE I CONFIGURATION

Pressure Tube
Washer Welded to Tube
Nut
Union
French Lockwasher
Spacer
Nose Cap
Plug

Ⓐ

Flared Pressure Tube

Chemical Barriers:
Washer
Washer/Tube Assy.

Ⓓ

Chemical Barrier
For The T/C Mount
Lockwasher/Chem Barrier
Wire Coil As A
Chemical Barrier

Ⓔ

Thermocouple Mount
Thermocouple
Lockwasher
Alternate Location

Ⓑ

Thermocouple
Lockwasher
(Crimped to
Secure T/C)

Ⓒ
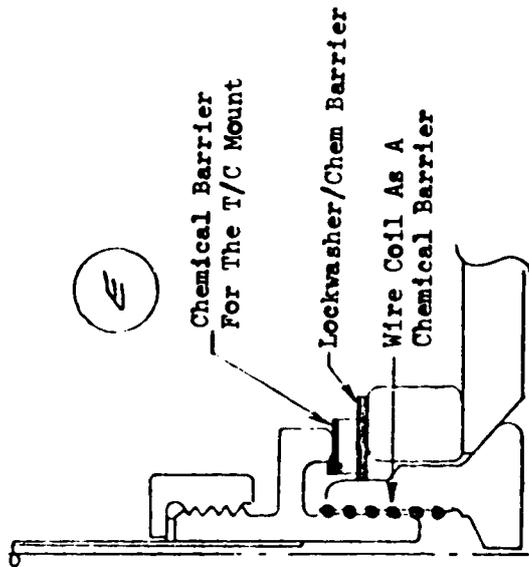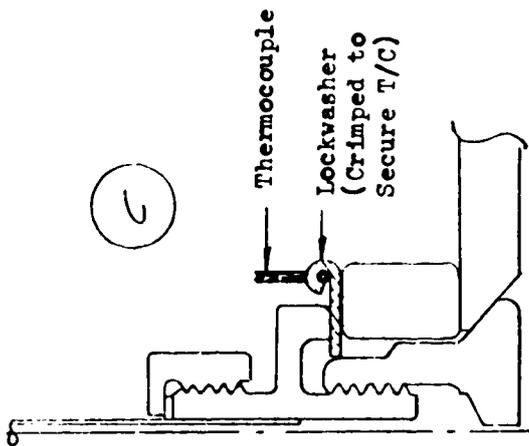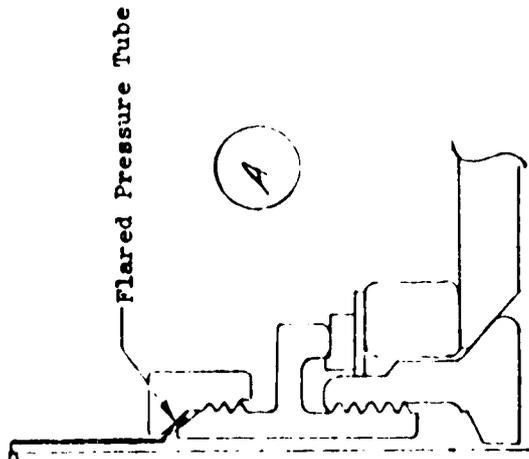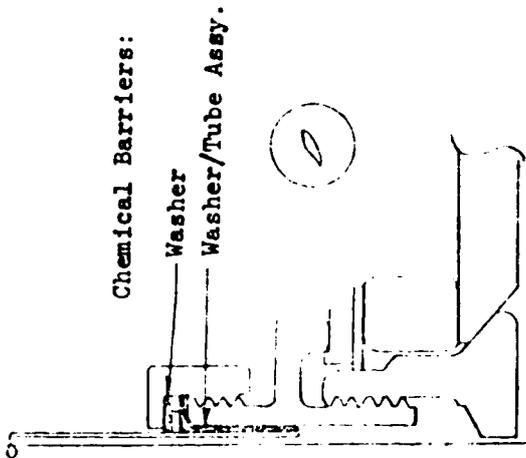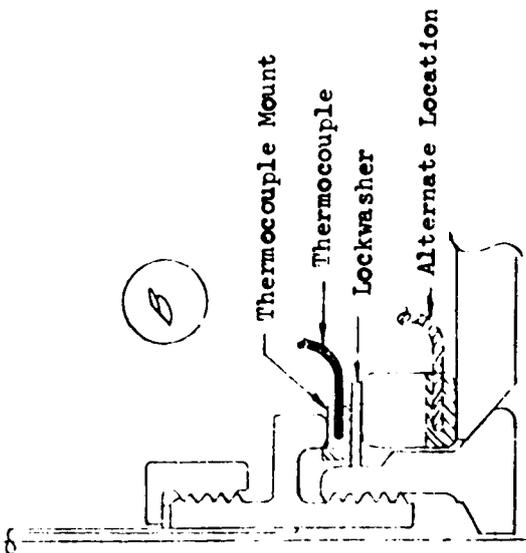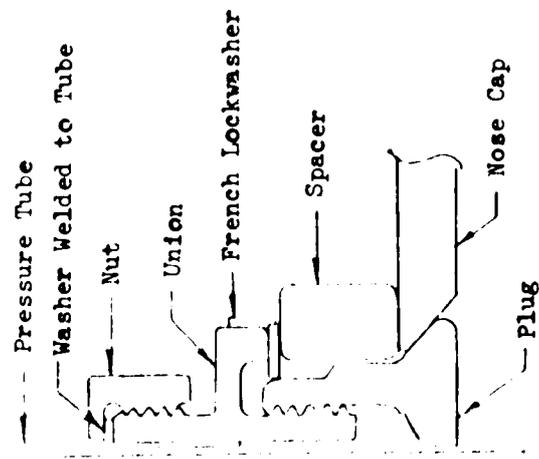
FIGURE 4-1 - DESIGN CONCEPT VARIATIONS
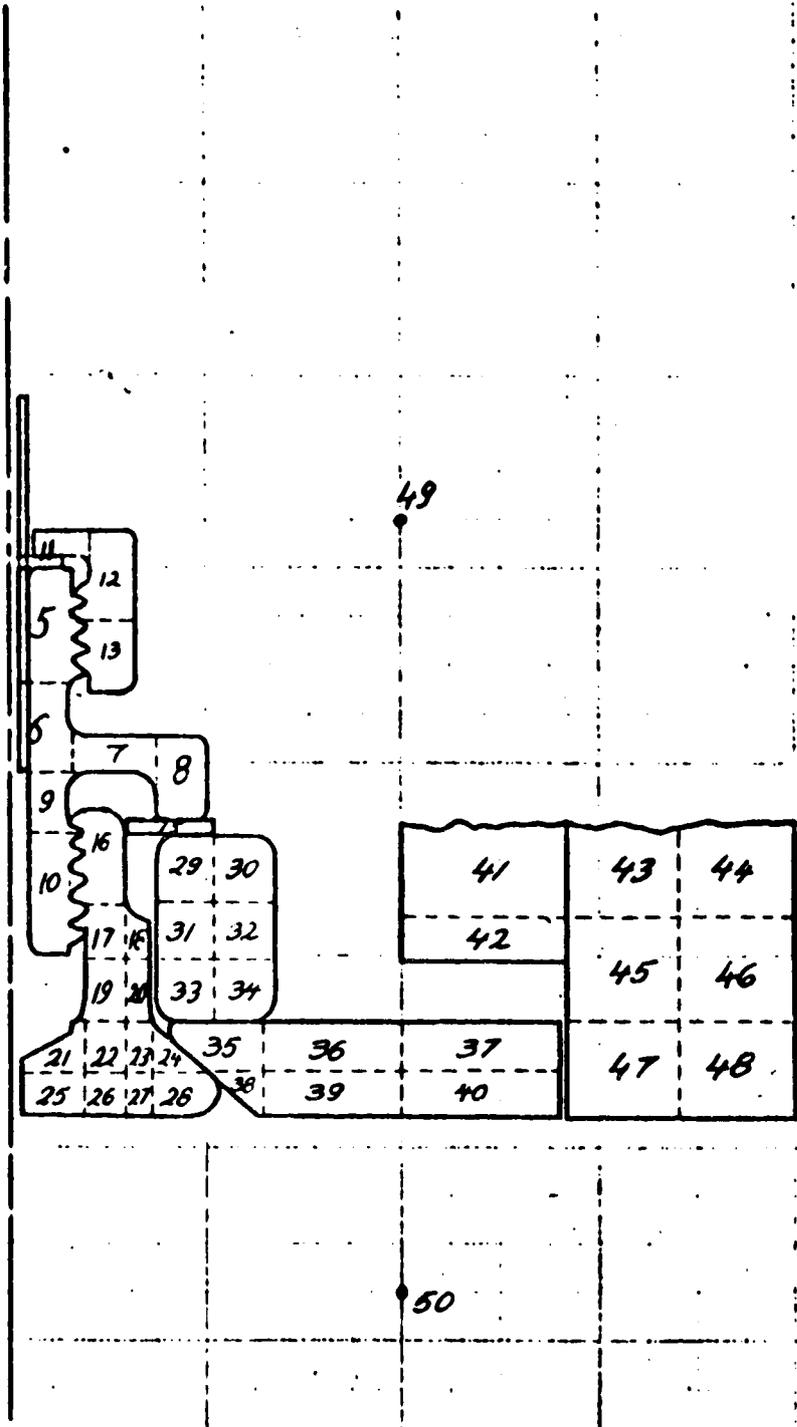
FIGURE 4-2 - THERMAL MODEL OF CONCEPT 6 TEST MODEL
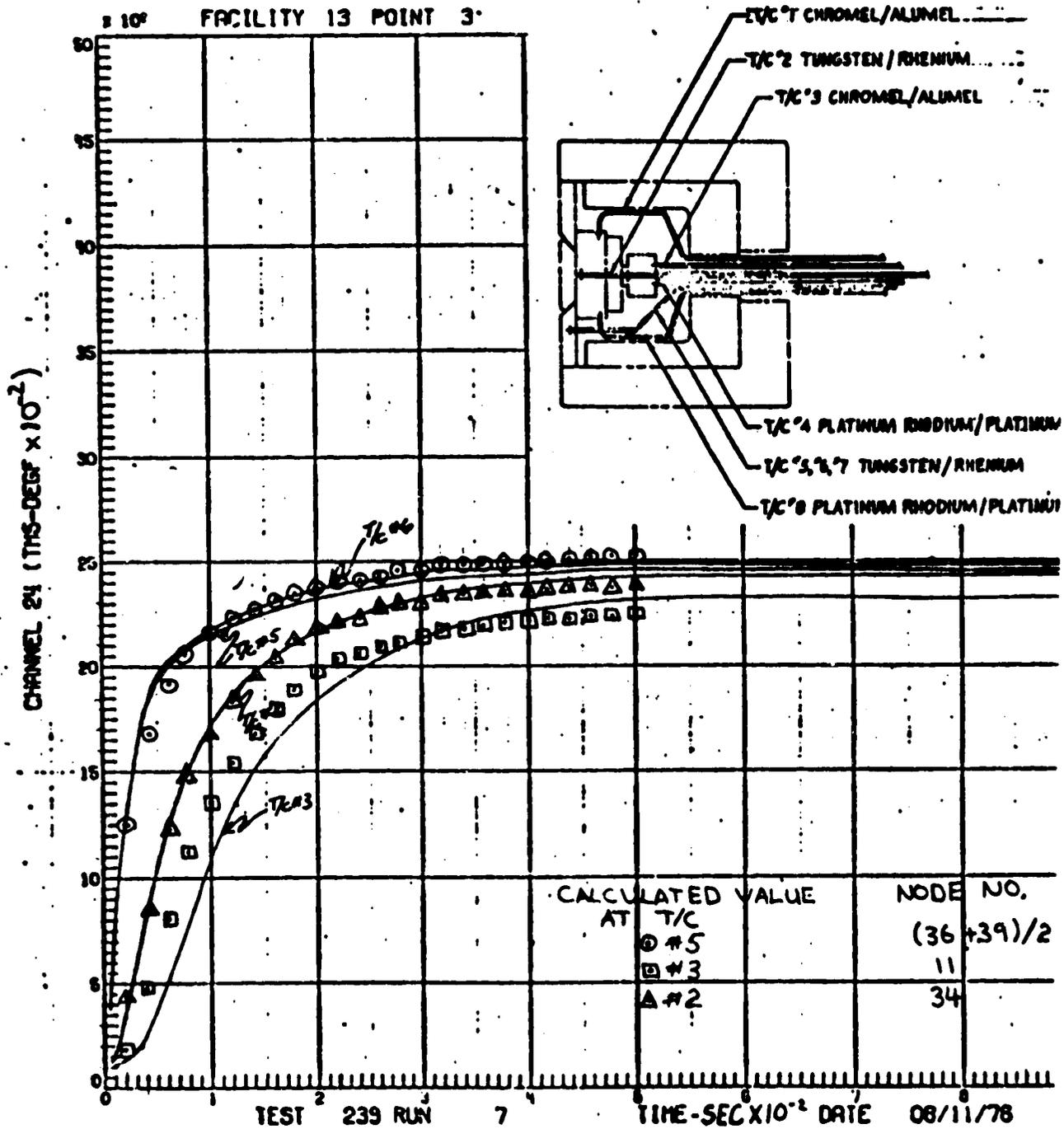
FIGURE 4-3 - THERMAL ANALYSIS TEMPERATURE DISTRIBUTION - MODEL 6

2348

2330°F *(INSULATION)*

NOTE: RCC temperatures are surface
temperatures rather than
average element values.

2427
2424
2420 2417
2423 2422
2428 2428

RCC

| 2456 | 2437 | 2434 | 2433 | 2433 | 2433 |
| 2513 | 2506 | 2508 | 2504 | 2500 | 2500 |

GRAPHITE

2330°F *(INSULATION)*

2349

2427
2427
2434
2427 2424
2428 2427
2431 2431

RCC

| 2458 | 2438 | 2434 | 2433 | 2433 | 2433 |
| 2516 | 2507 | 2508 | 2505 | 2500 | 2500 |

COLUMBIUM

2330°F *(INSULATION)*

2342

2403
2404

2411 2410

2402
2410
2470

RCC

| 2441 | 2429 | 2425 | 2424 | 2424 | 2424 |
| 2502 | 2504 | 2500 | 2496 | 2496 |

SILICON
CARBIDE
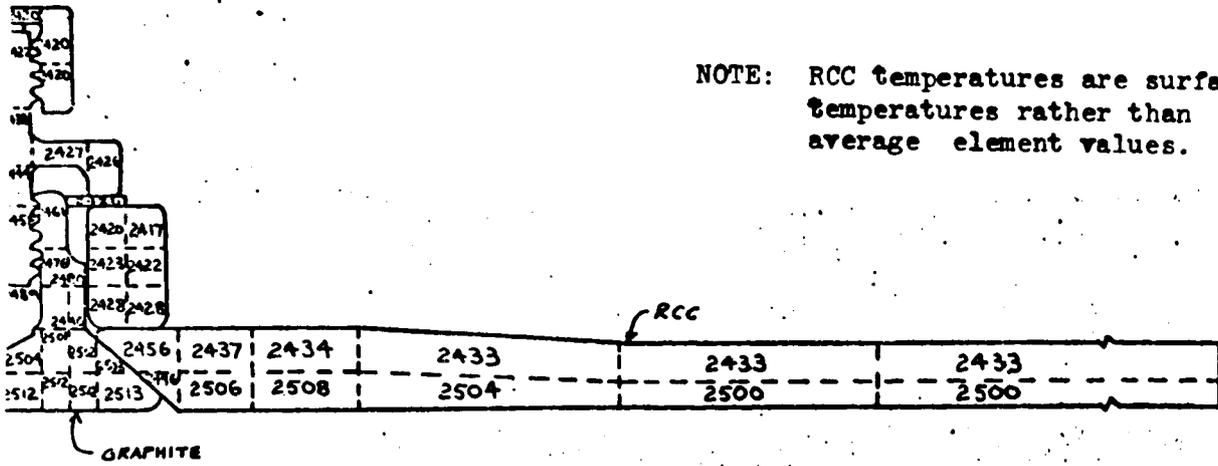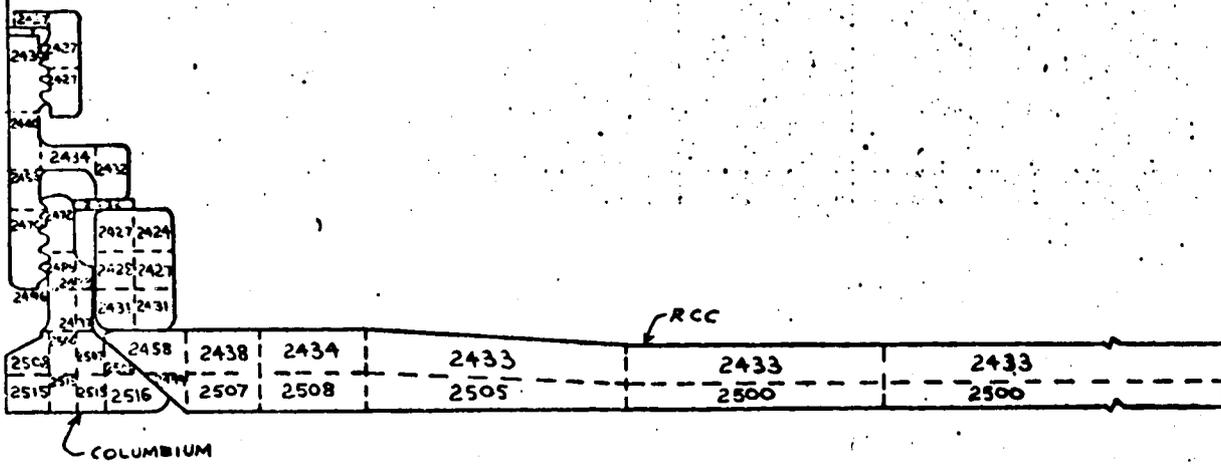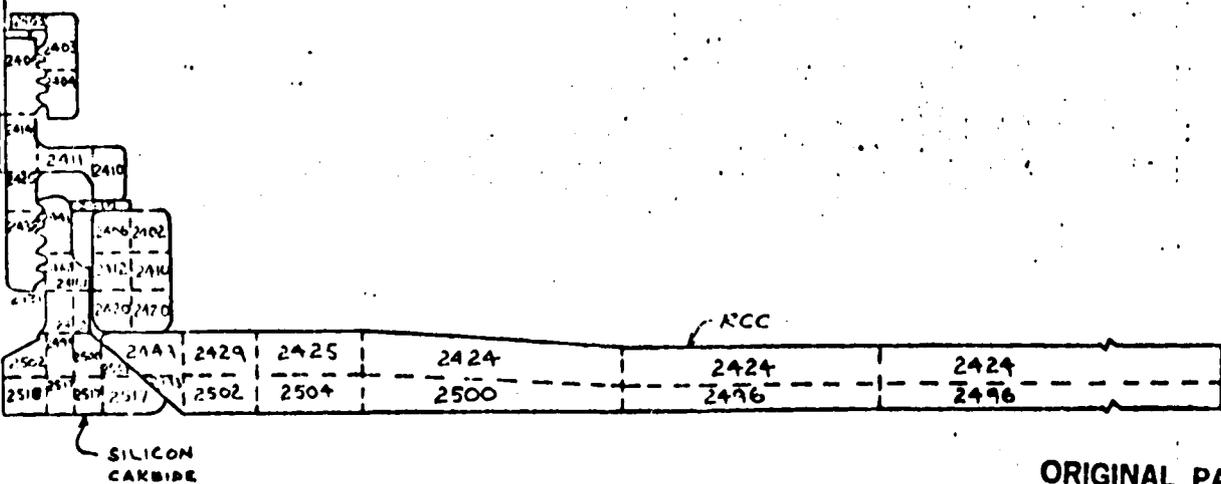
FIGURE 4-4 - THERMAL ANALYSIS RESULTS
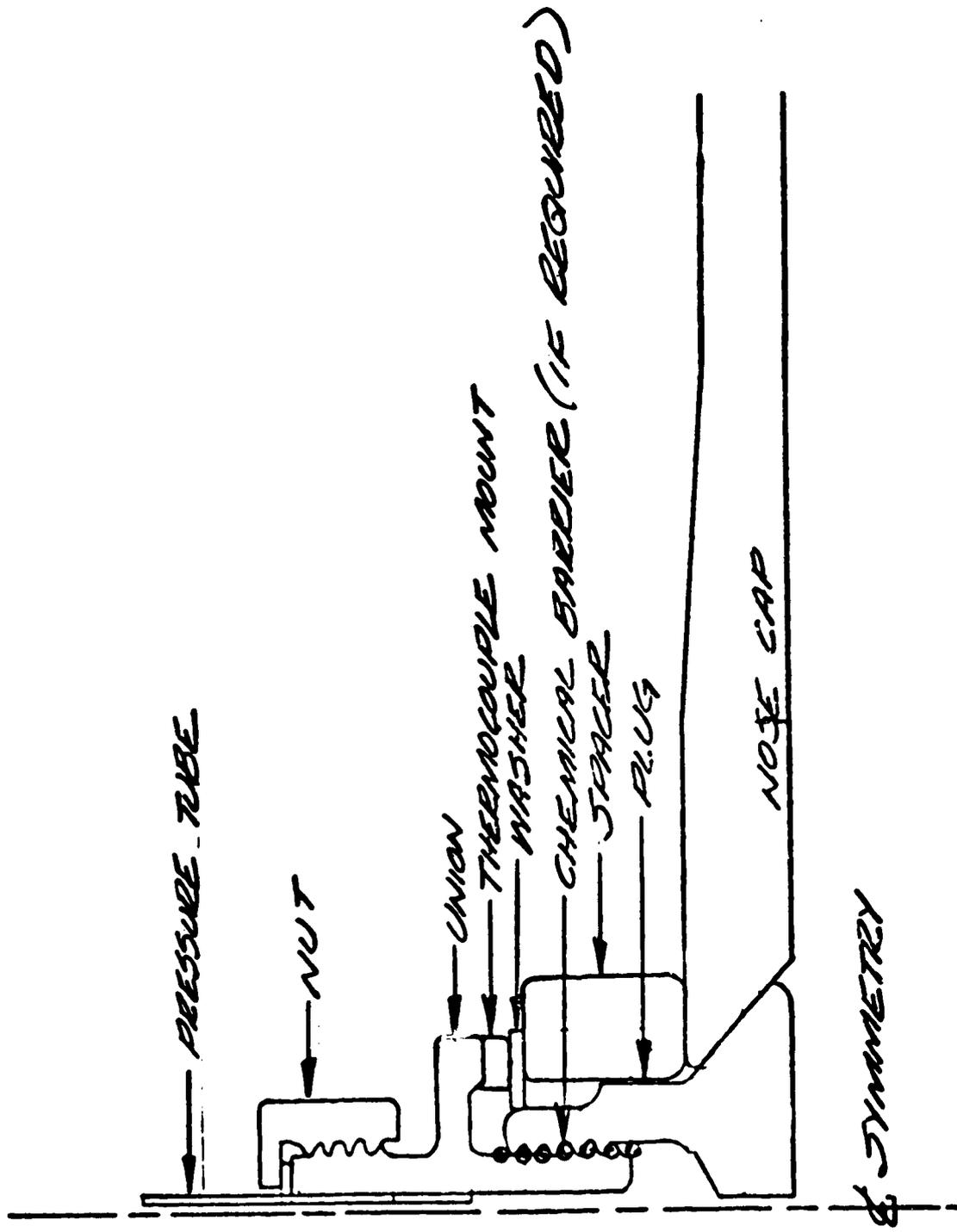
FIGURE 4-5 – SEADS PENETRATION ASSEMBLY

VERTICAL/Al/Pt_b/Pt_b/RCC

PL/INCO721/Inco 722/RCC /
Inco 722/Pt_t/Pt_h

Inco 722/Pt_t & Pt_t/Pt_h
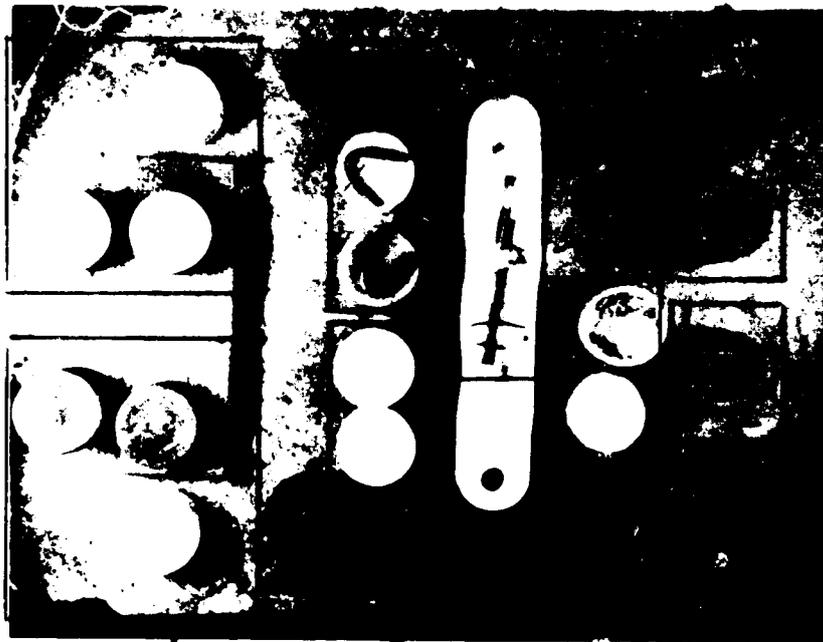
RCC/CL/CL/RCC

STACKING ORDER (TYP)

RCC/Ir/CL/RCC

PHOTO SHOWS ELEMENT AFTER UNSTACKING FOR EXAMINATION

FIGURE 4-6 - TYPICAL CHEMICAL COMPATIBILITY TEST ARRANGEMENT

HOLDER

INSULATION

LOCKWIRE

PRESSURE TUBE

NUT

UNION

PIN (4 REQD)

SPACER

PLUG

DISC

WASHER

T/C MOUNT
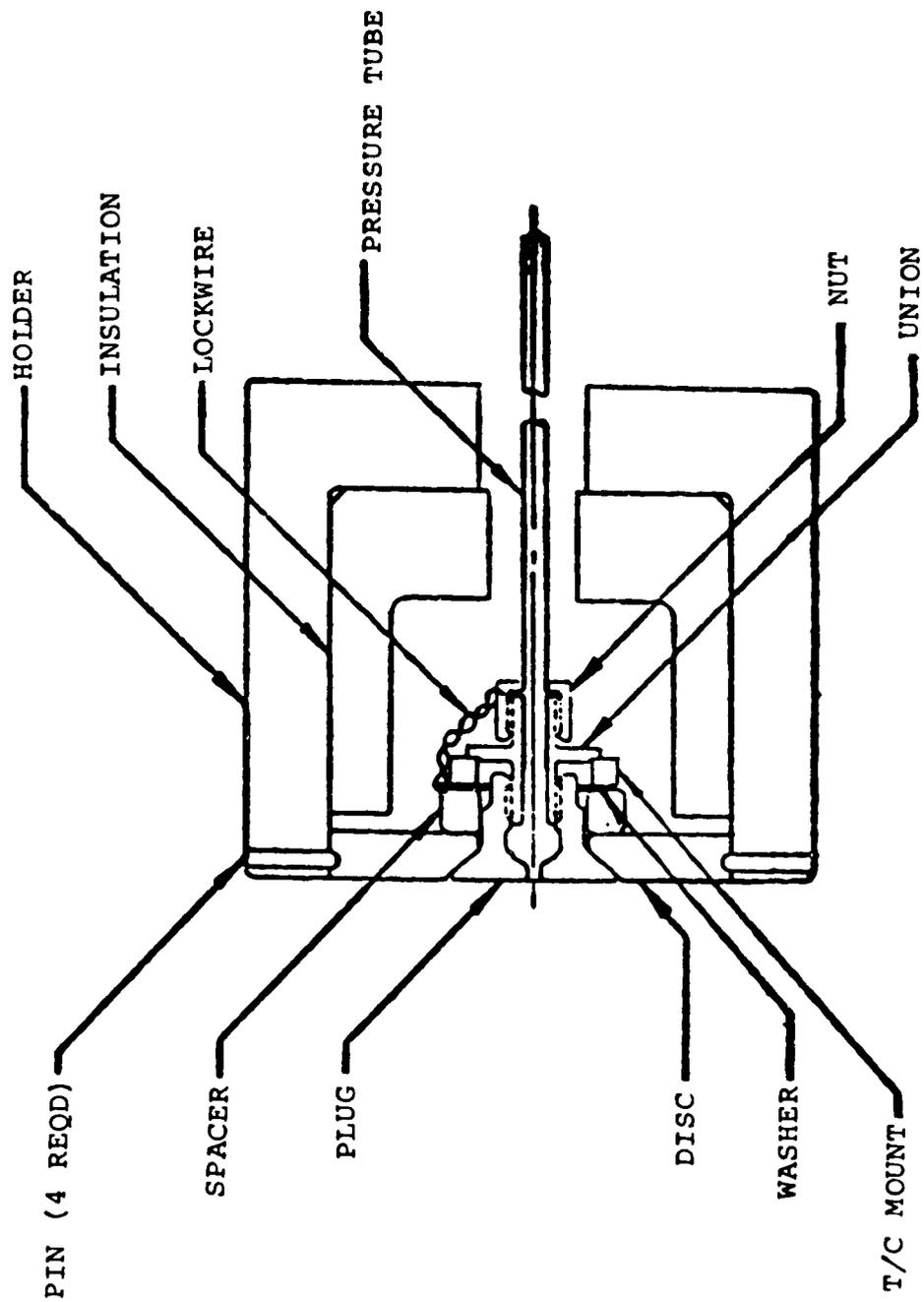
FIGURE 4-7 - PLASMA TEST MODEL CONFIGURATION

FIGURE 4-8 - PLASMA TEST MODEL THERMOCOUPLE INSTALLATION

T/C #3 TUNGSTEN 5% RHENIUM /
TUNGSTEN 26% RHENIUM

T/C #1 .040 PLATINUM 13% RHODIUM/
PLATINUM - PLATINUM 20% RHODIUM SHEATH

T/C #4 TUNGSTEN 5% RHENIUM /
TUNGSTEN 26% RHENIUM

T/C #2 .0625 PLATINUM 13% RHODIUM/
PLATINUM - PLATINUM 20% RHODIUM SHEATH

T/C #5 TUNGSTEN 5% RHENIUM /
TUNGSTEN 26% RHENIUM
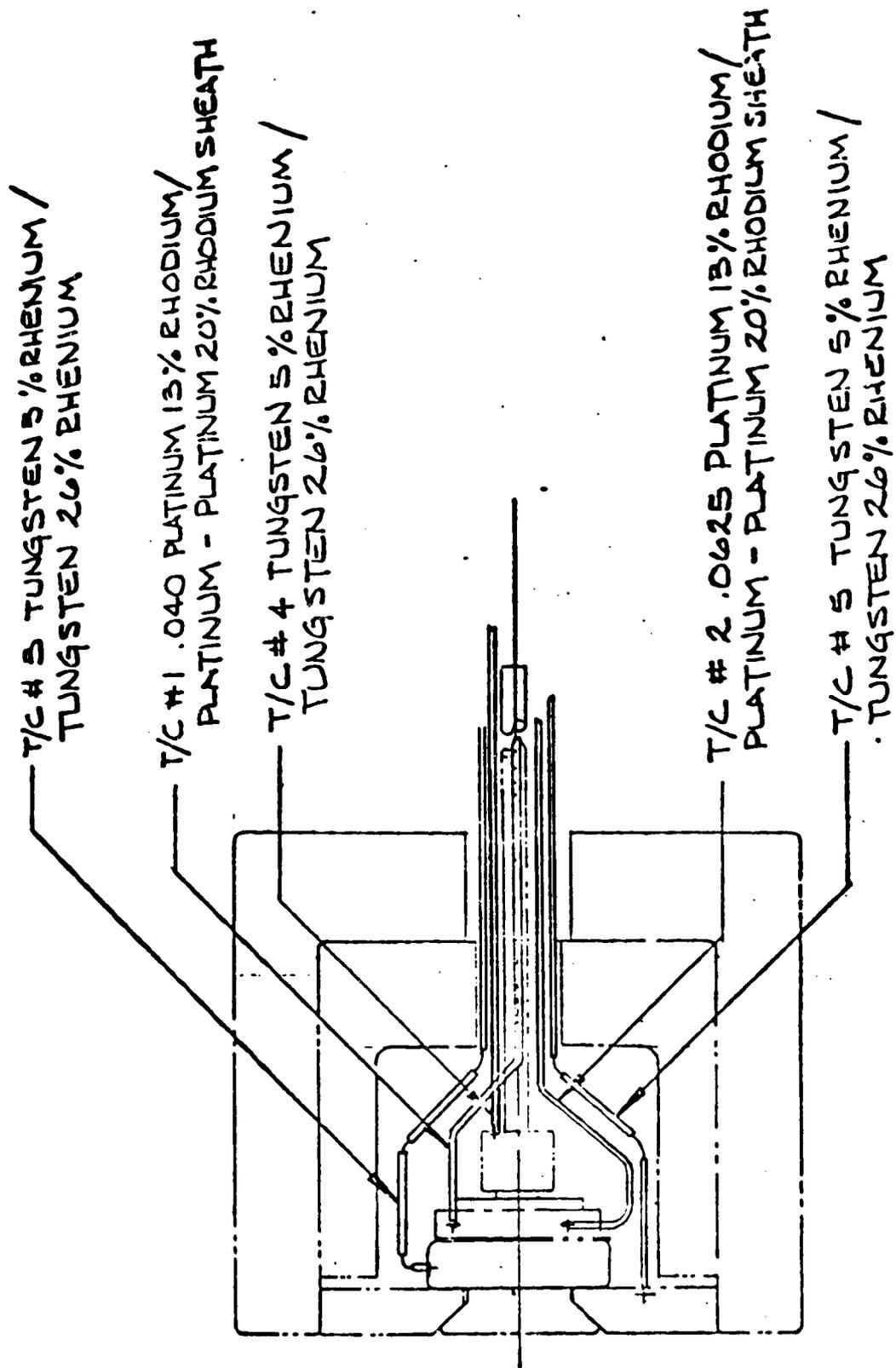
FIGURE 4-9 - TEMPERATURE DISTRIBUTION THROUGH MODEL
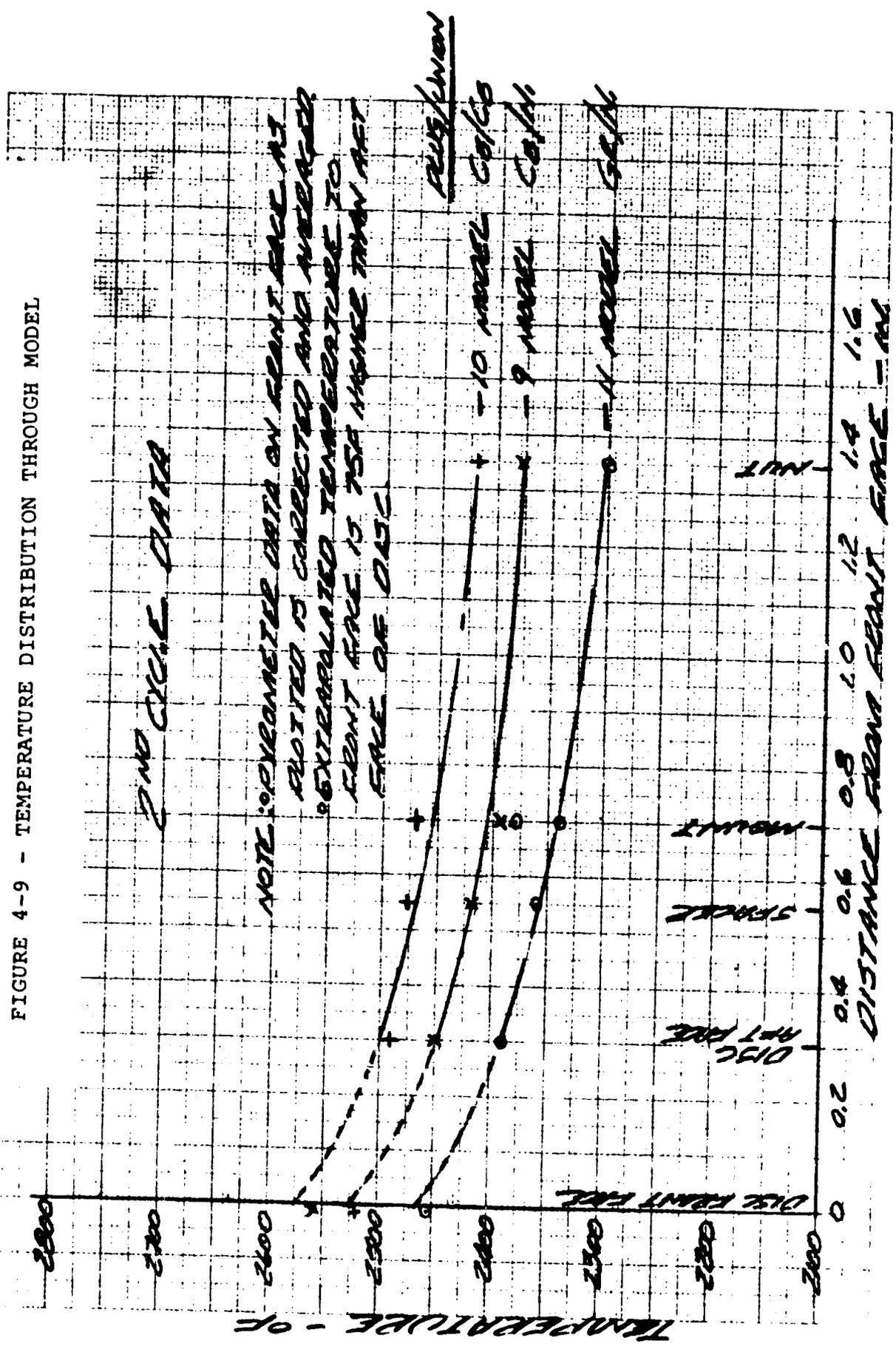
FIGURE 4-10 - TYPICAL TEMPERATURE TIME HISTORY
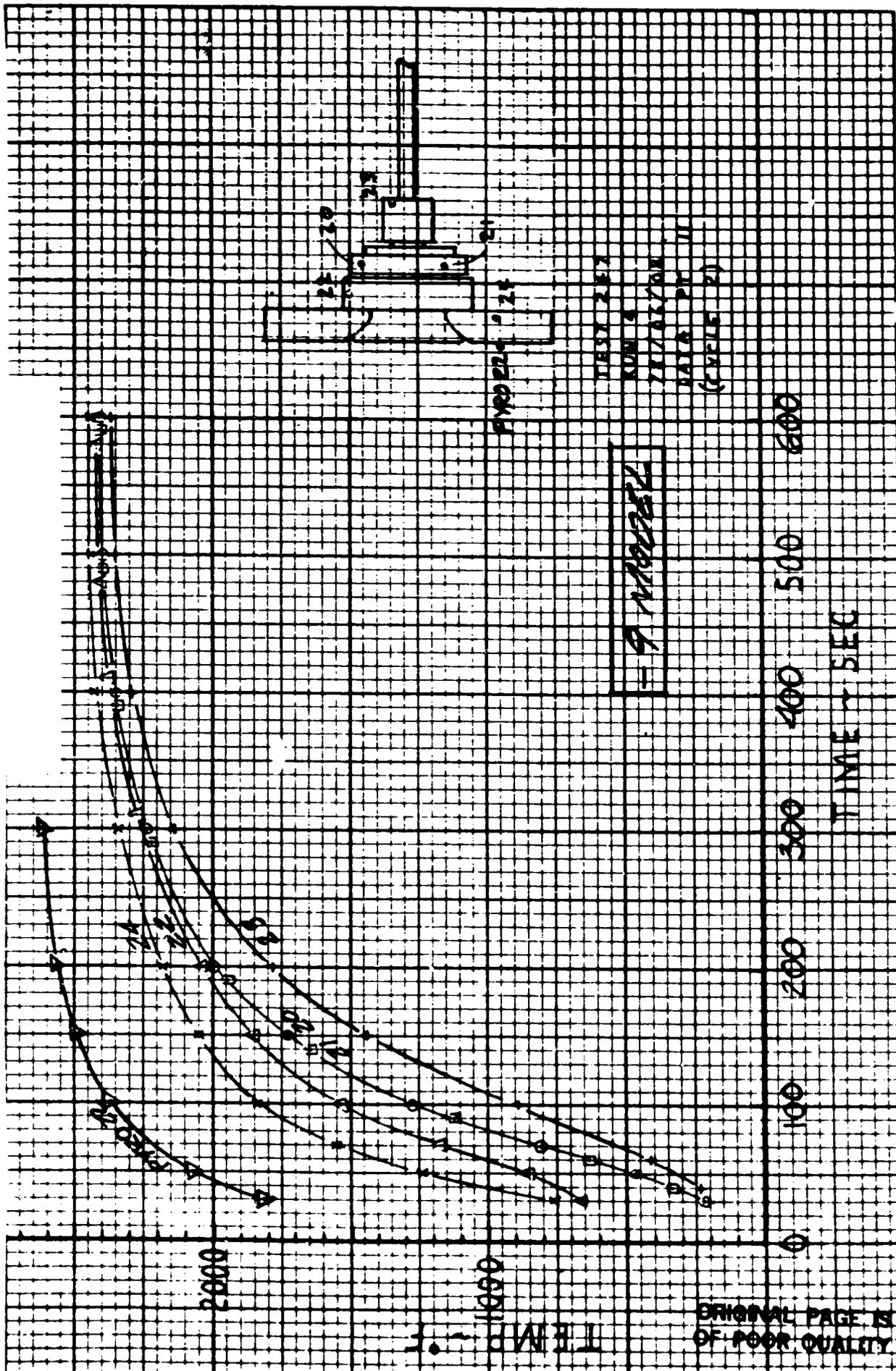
FIGURE 4-11 - PYROMETER OUTPUT HISTORY
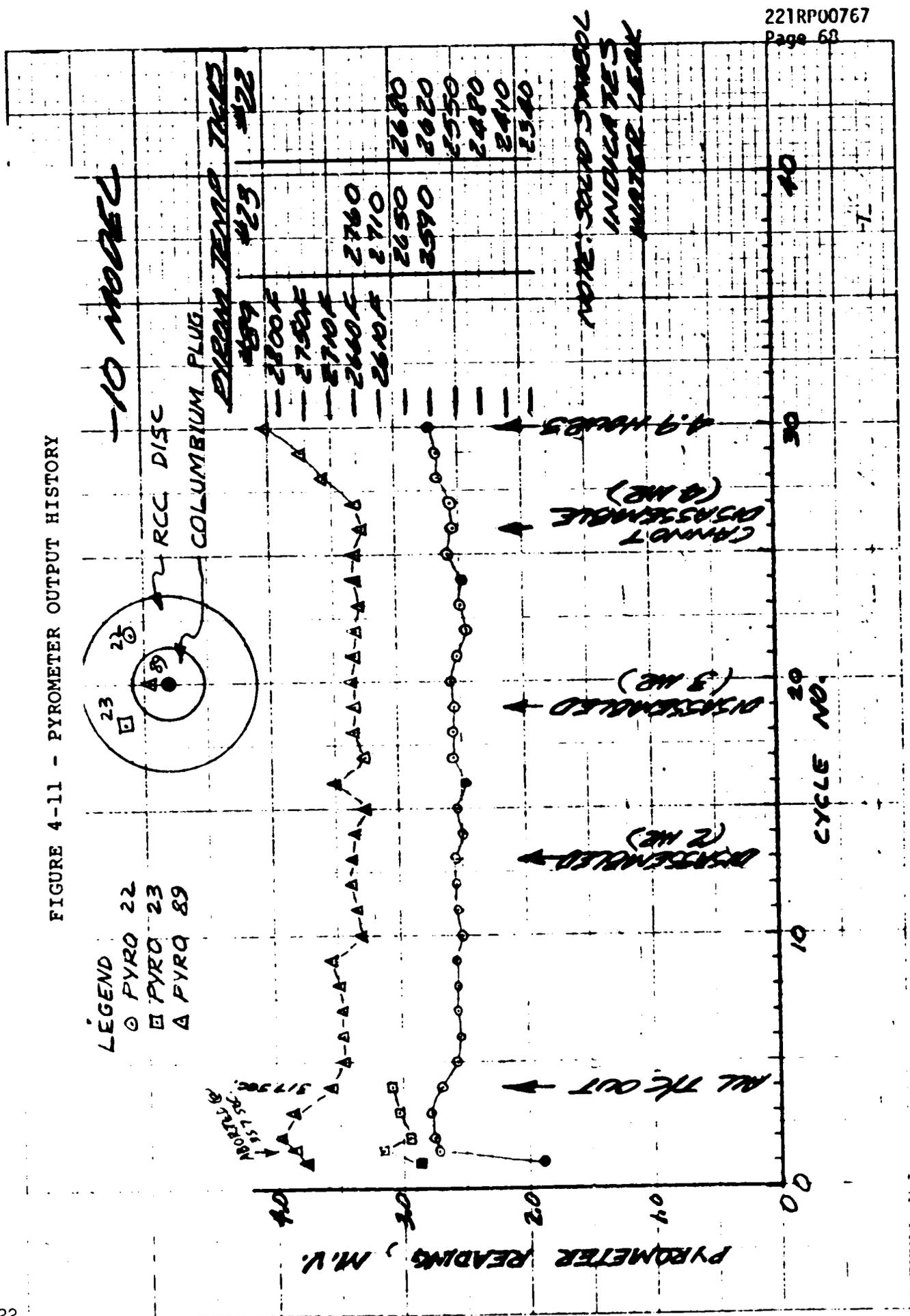
FIGURE 4-12 - PYROMETER OUTPUT HISTORY

- N MODEL

RCC DISC

GRAPHITE PLUG

LEGEND
⊙ PYRO 22
▣ PYRO 23
△ PYRO 89

PYRON. TEMP TRIS		
#59	#73	#22
—2770F		
—2710F		
—2660F		
—2605		
2560F	2650	2680
2500F	2570	2620
2450F	2530	2550
2380F	2460	2490
2320F	2390	2410
2250F	2520	2340

NOTE: SOLID SYMBOL
INDICATES
WATER LEAK

(APPROX. 5 HOURS EXPOSURE)

CYCLE NO.

PYROMETER READING, M.V.

127
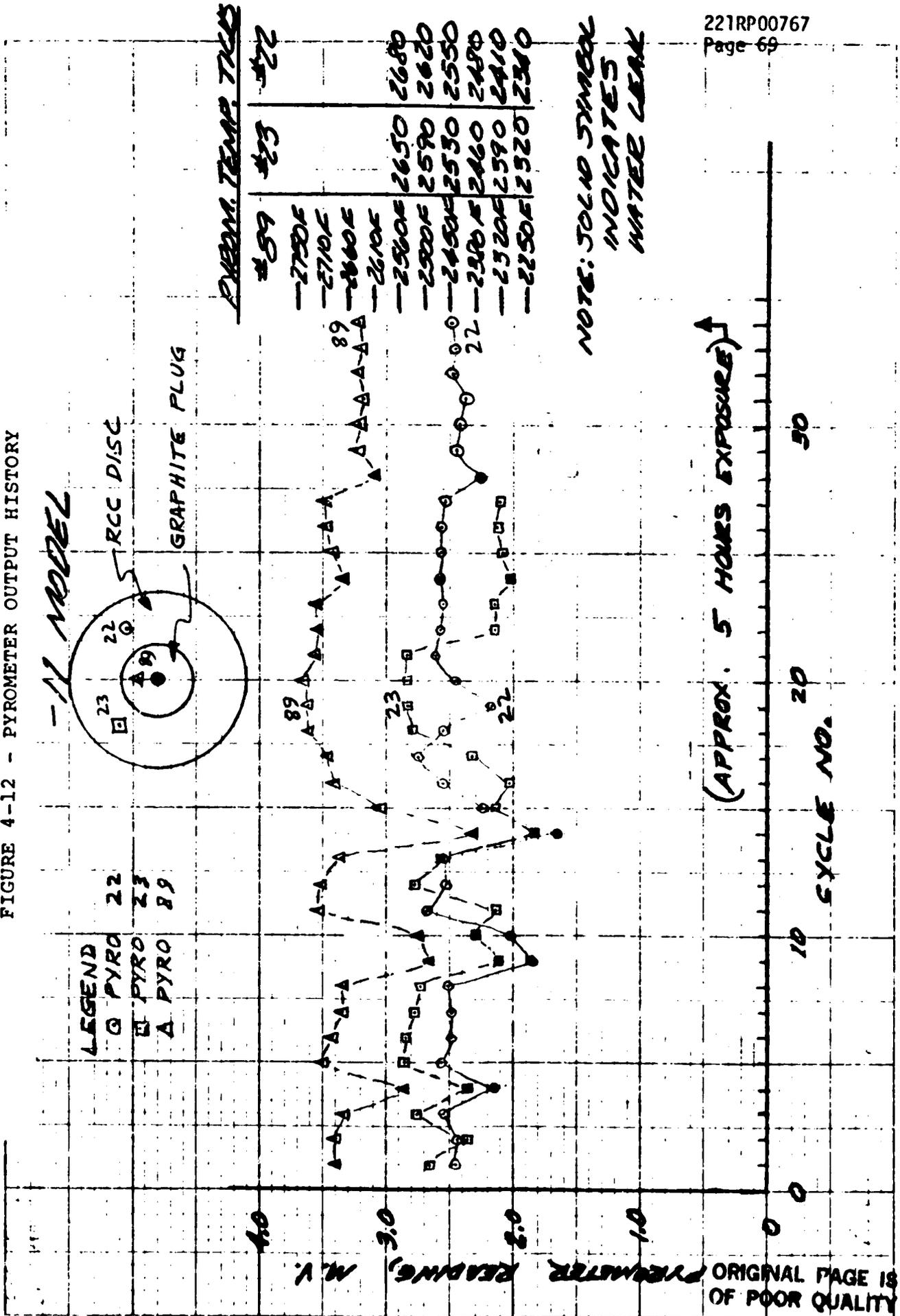
FIGURE 4-13 - TEMPERATURE HISTORY THERMOCOUPLES
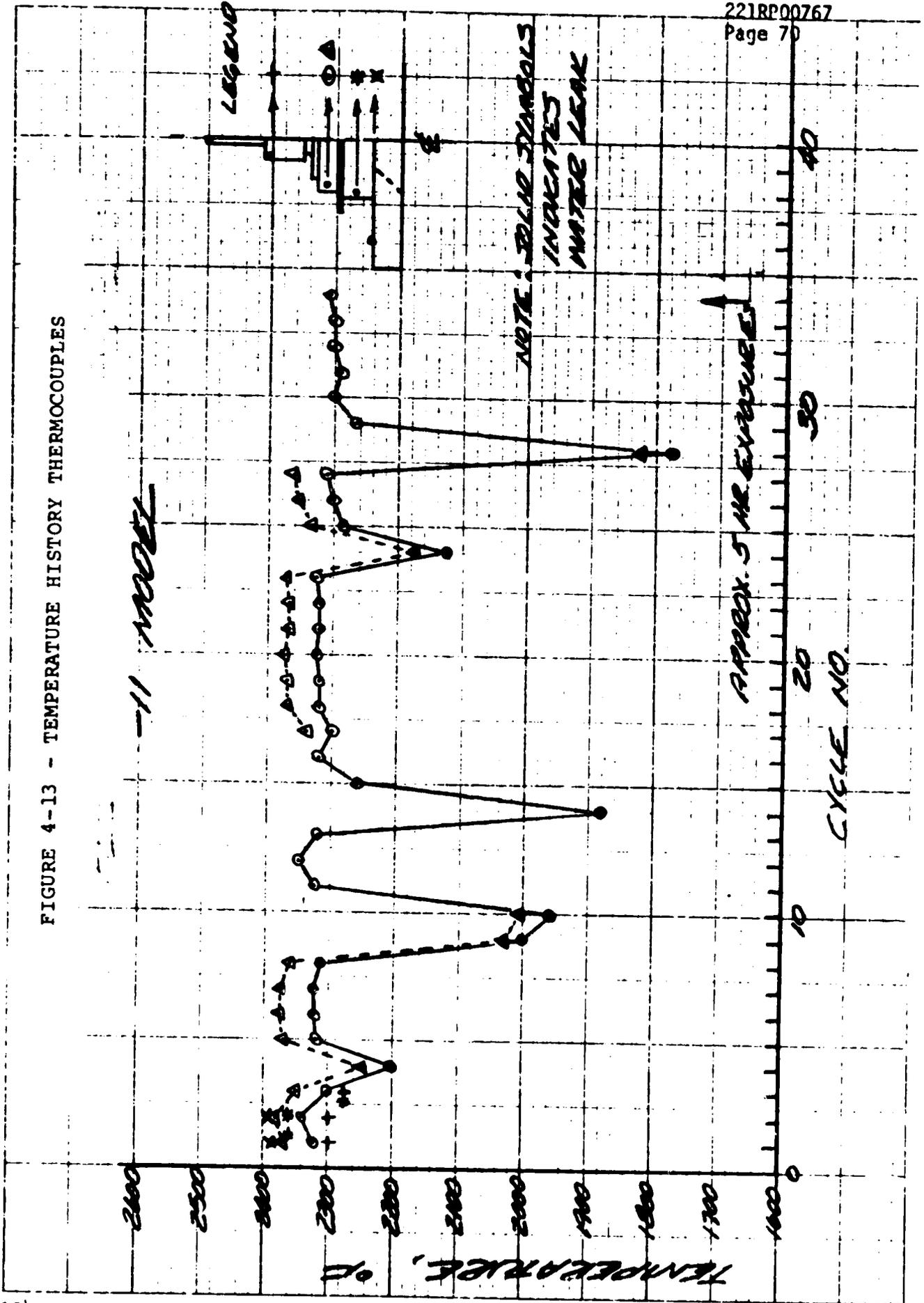
FIGURE 4-14 - POST TEST PHOTO OF -9 MODEL PLUG

FIGURE 4-15 - POST TEST PHOTO OF -9 MODEL

ORIGINAL PAGE
BLACK AND WHITE PHOTOGRAPH

FIGURE 4-16 - POST TEST PHOTO OF -9 MODEL

FIGURE 4-17 - -10 MODEL AFTER 3-HOURS OF TEST

FIGURE 4-18 - -10 MODEL AFTER 3-HOURS OF TEST

129

FIGURE 4-19 - -10 MODEL AFTER 3-HOURS OF TEST
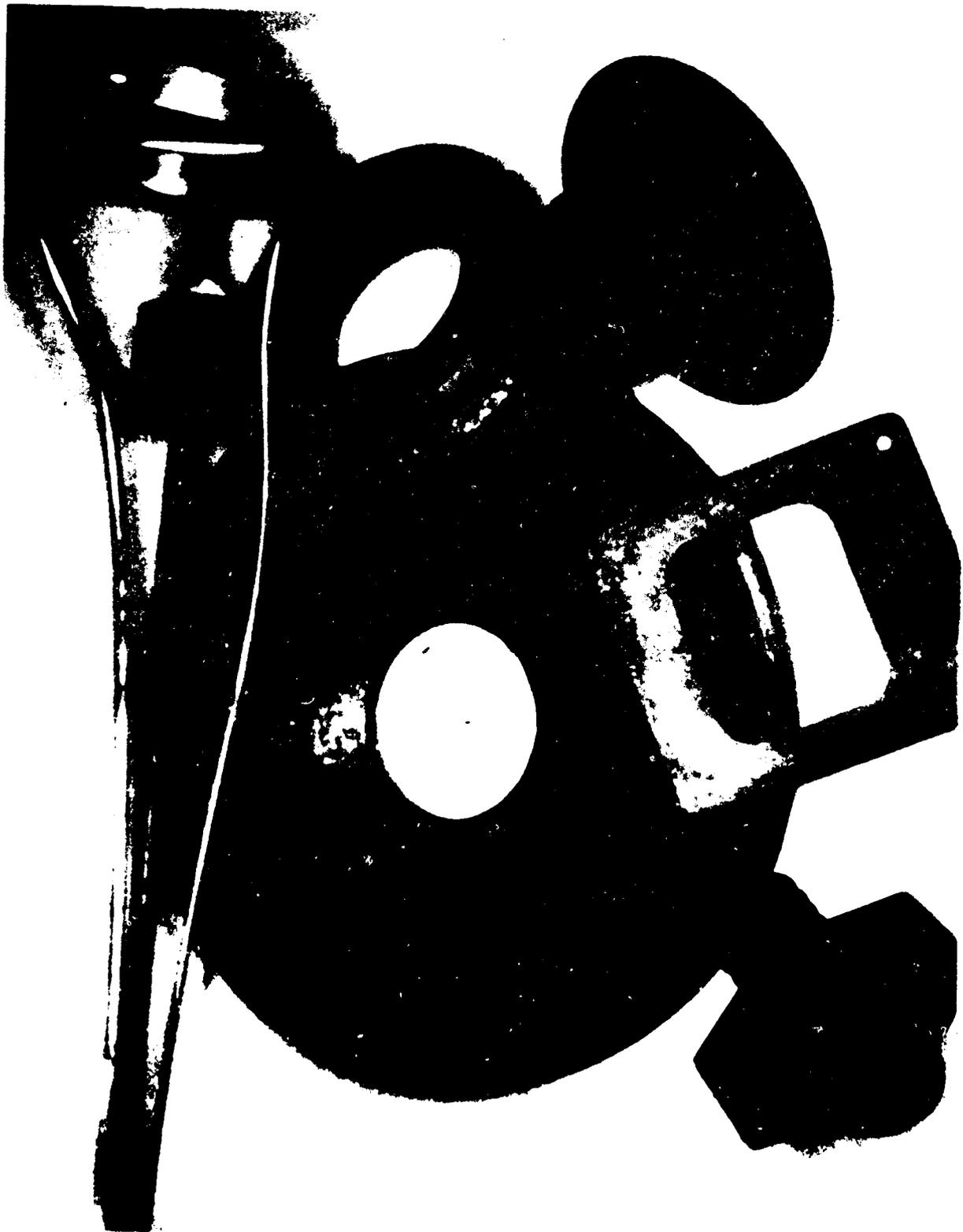
FIGURE 4-20 - -10 MODEL AFTER 4-HOURS OF TEST
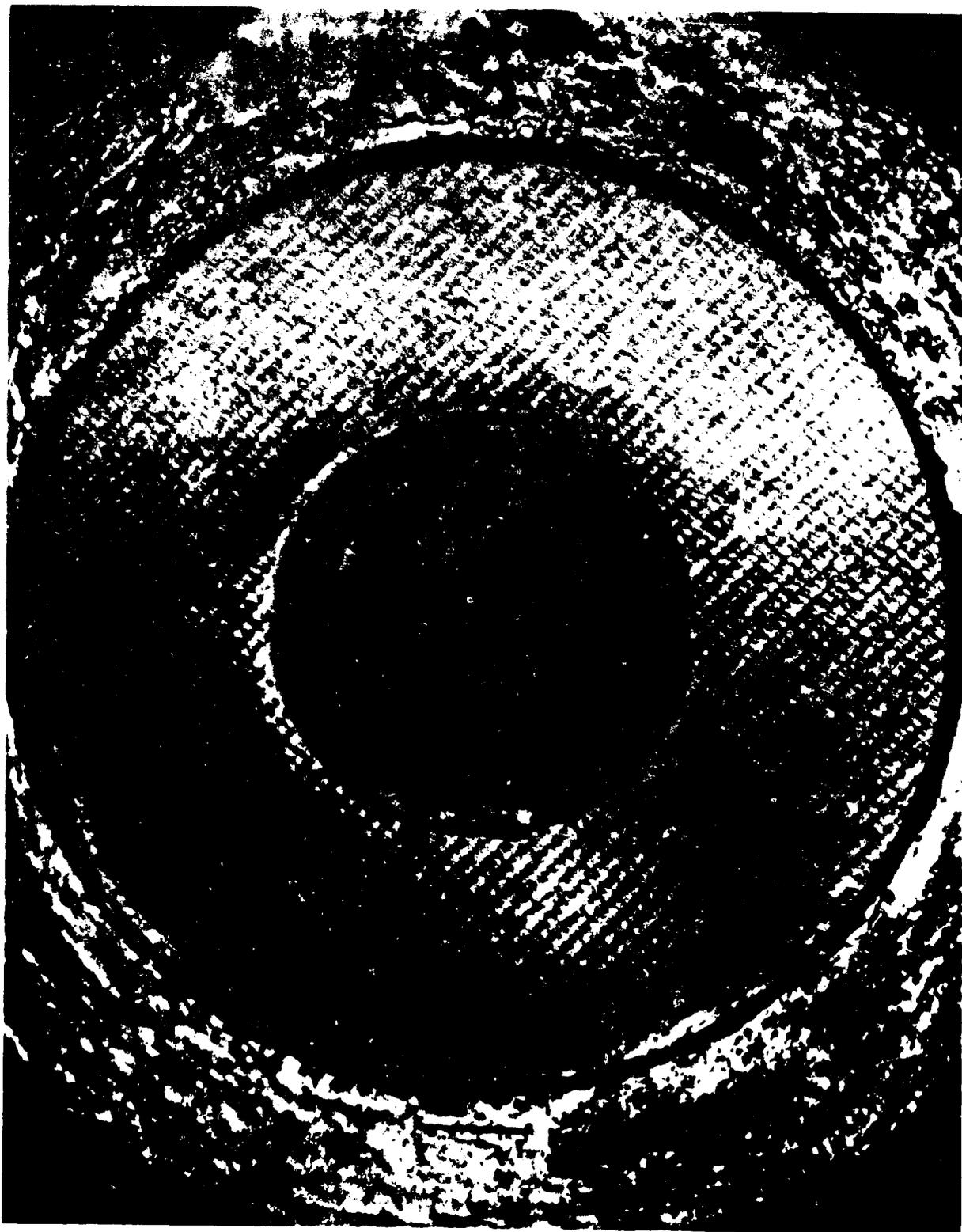
FIGURE 4-21 - -10 MODEL AFTER 4-HOURS OF TEST

ORIGINAL PAGE
BLACK AND WHITE PHOTOGRAPH
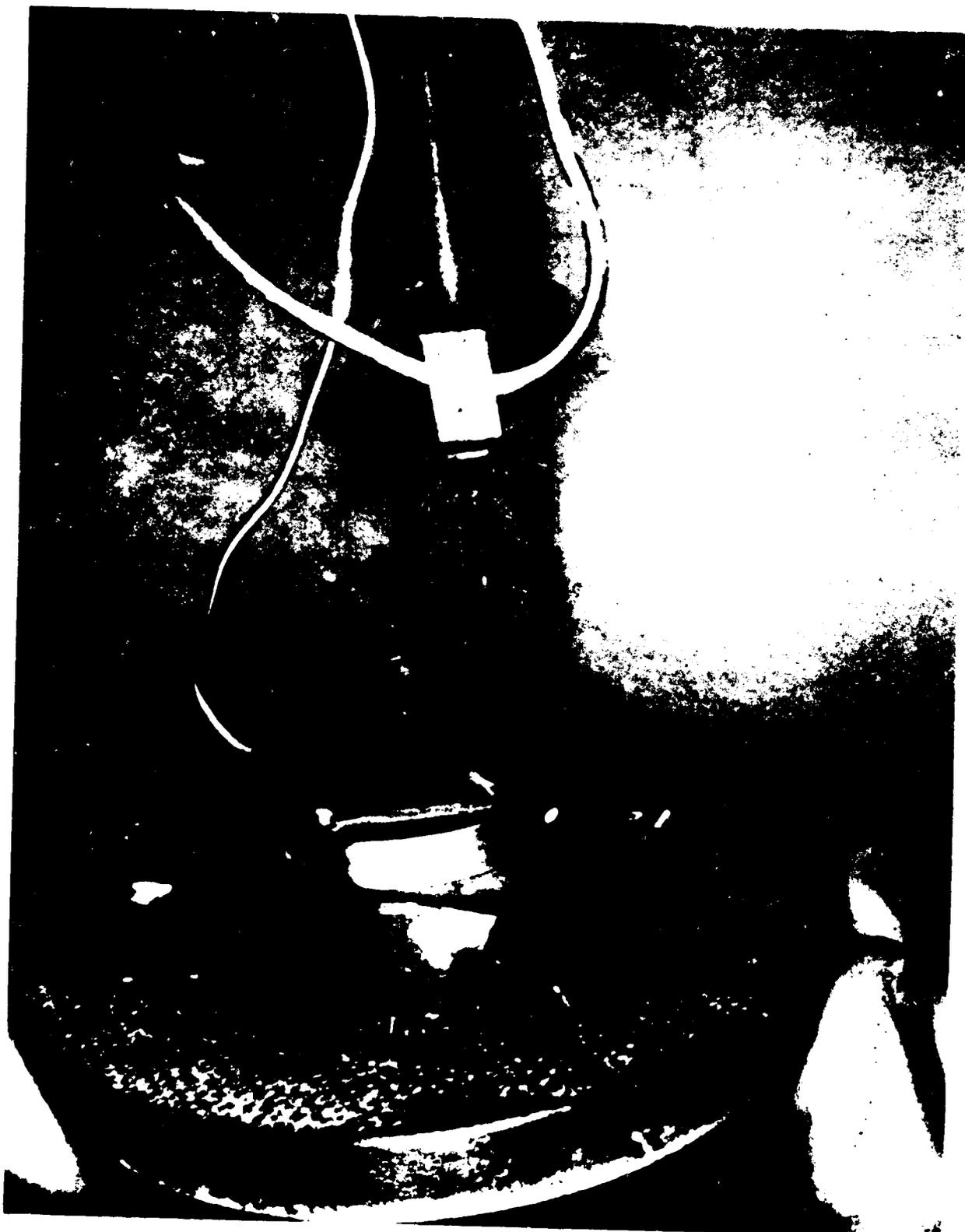
FIGURE 4-22 - -10 MODEL AT CONCLUSION OF TEST
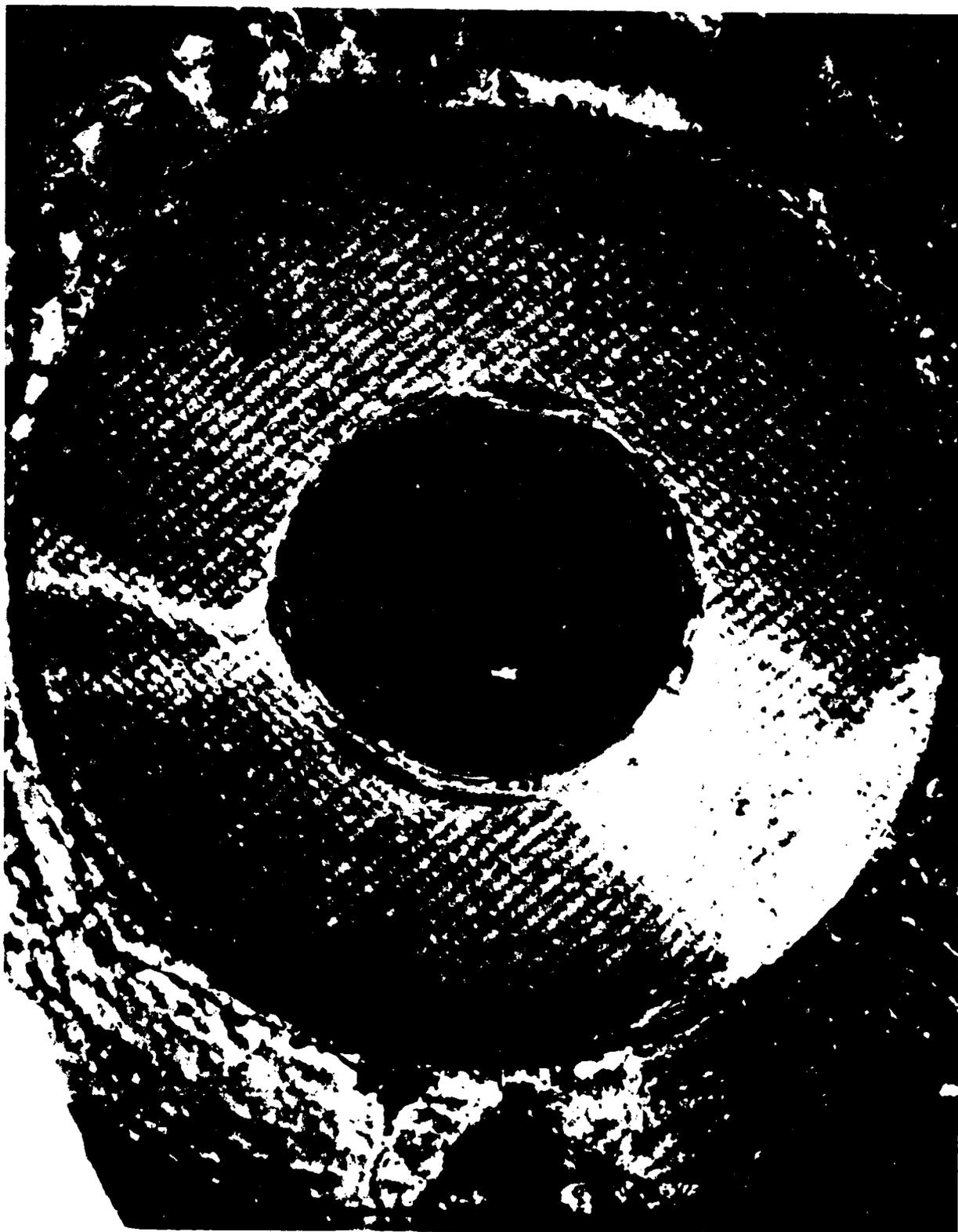
FIGURE 4-23 - -10 MODEL AT CONCLUSION OF TEST

UNION
NUT END

PLUG & UNION

PLUG
&
UNION
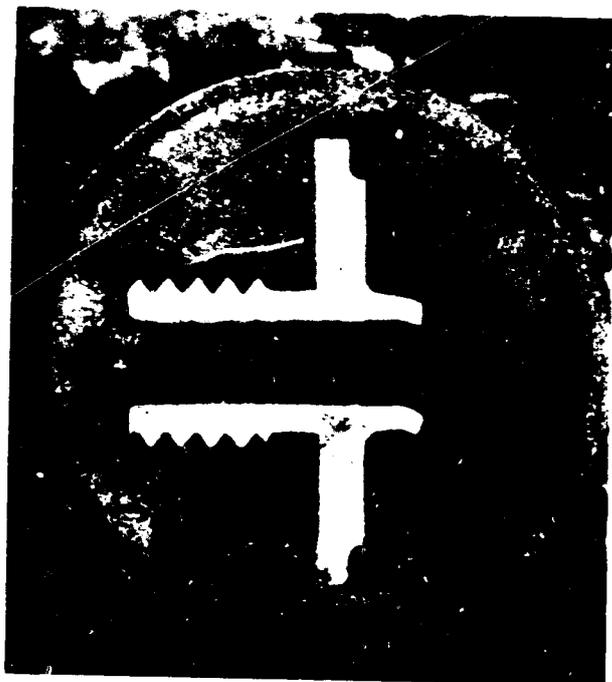
FIGURE 4-25 - POST TEST PHOTO OF -11 MODEL
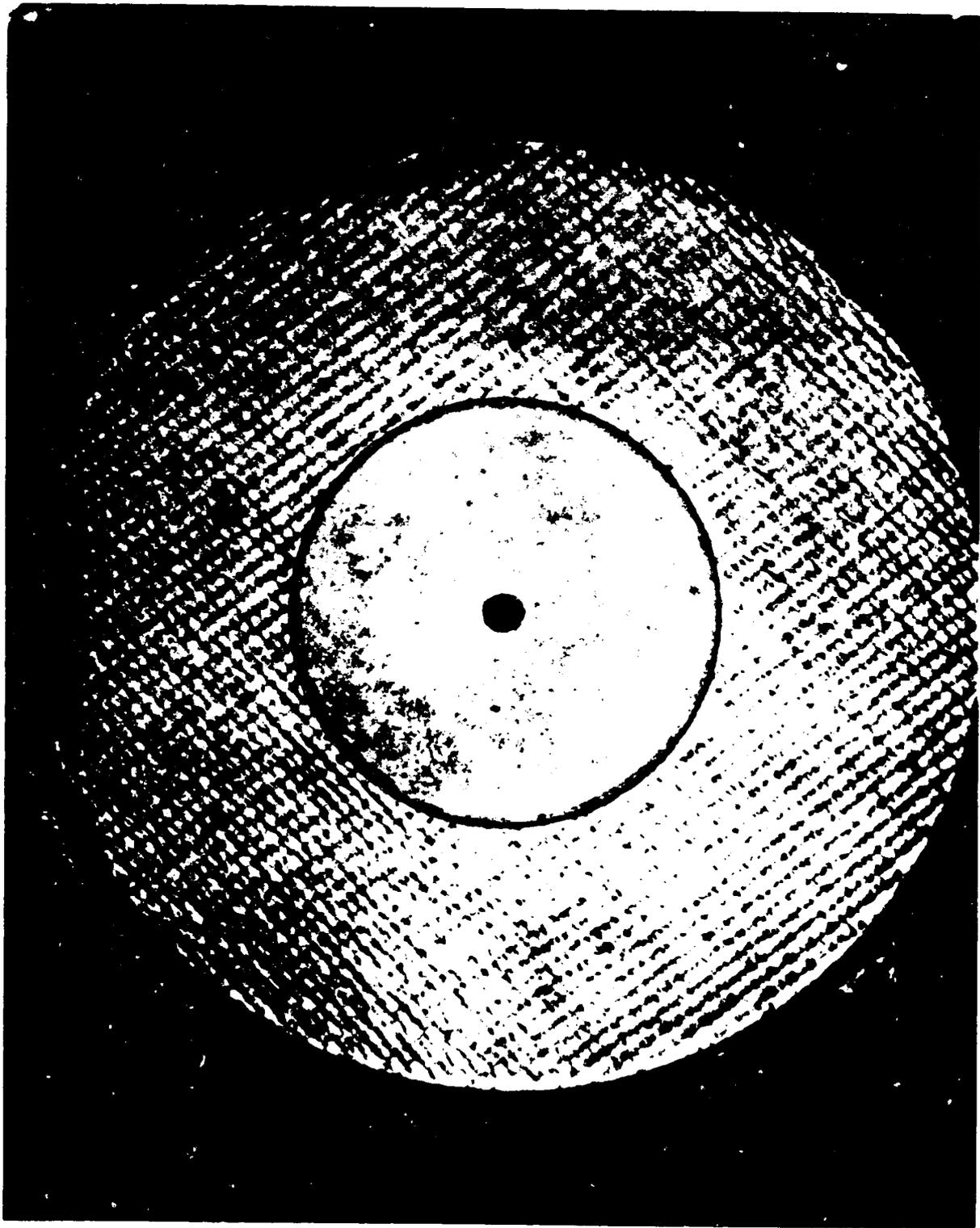
FIGURE 4-26 - POST TEST PHOTO OF -11 MODEL
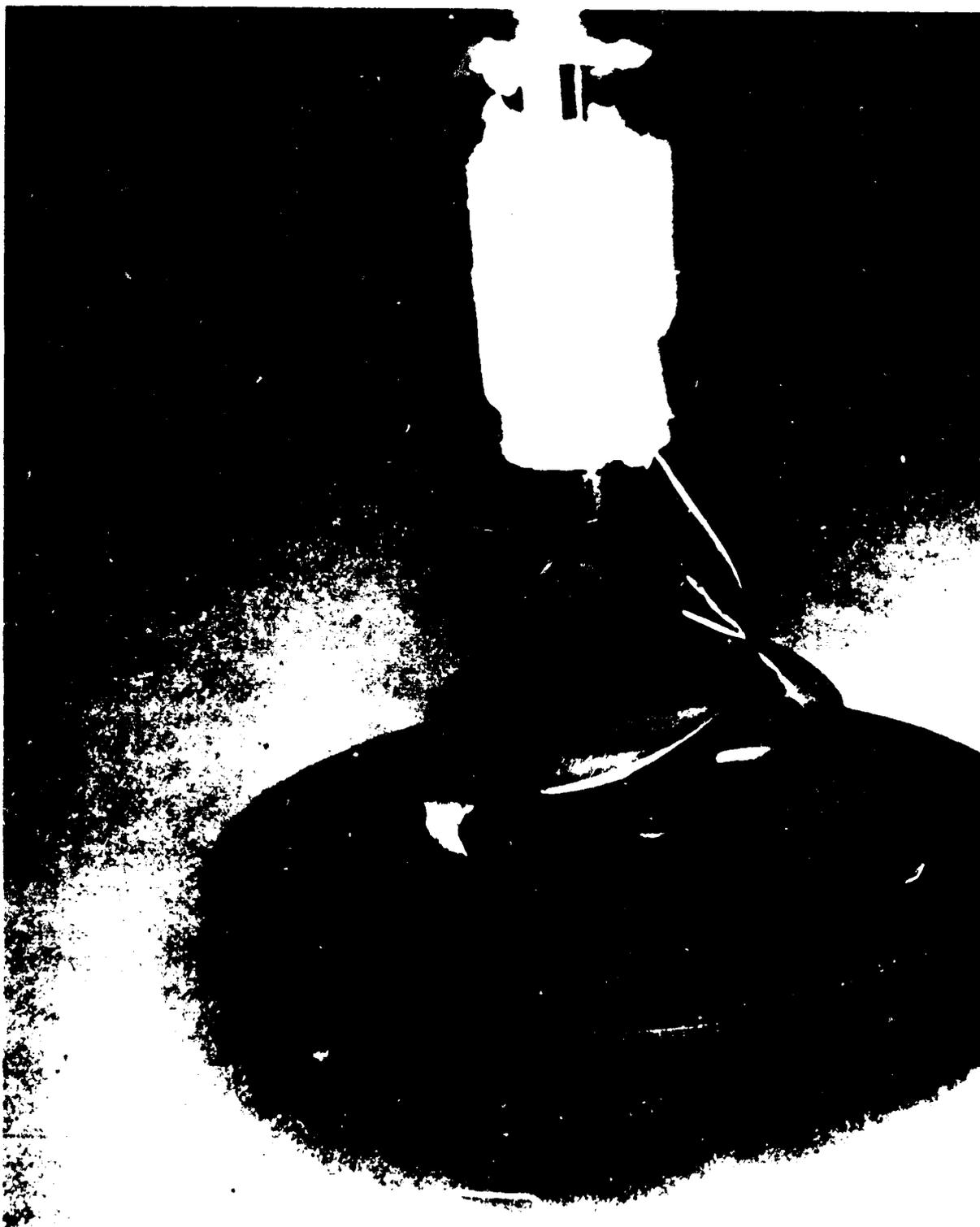
FIGURE 4-27 - DISASSEMBLED -11 MODEL, POST TEST
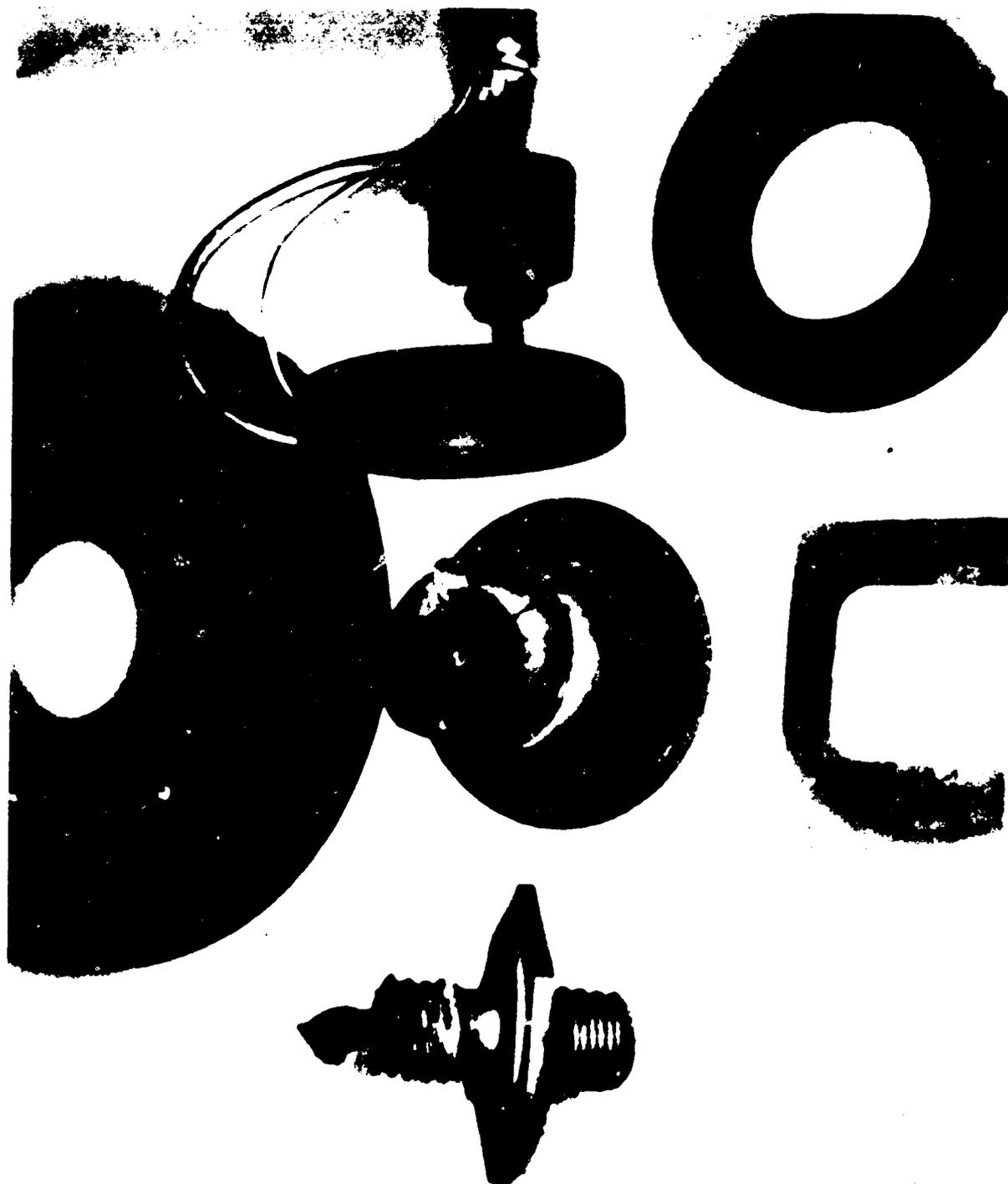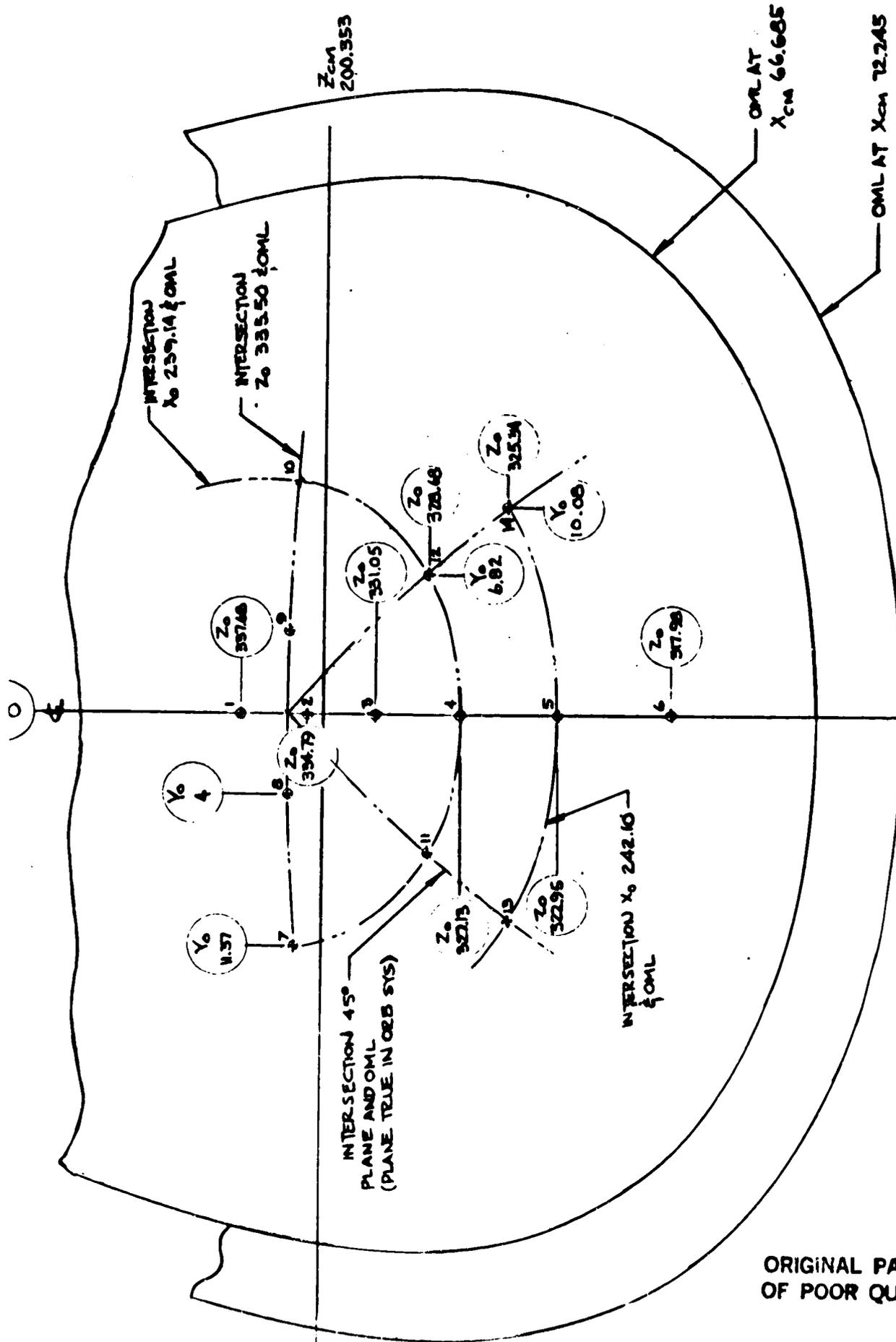
FIGURE 4-28 - PRESSURE PORT LOCATIONS - INITIAL

INSULATION
CONDUIT
3/8 DIA. TUBE

NOSE CAP SUPPORT
BULKHEAD

INSULATION

NOSE CAP
SUPPORT

3/32 TUBES

PORT-ASSY

RCC BASELINE
NOSE CAP
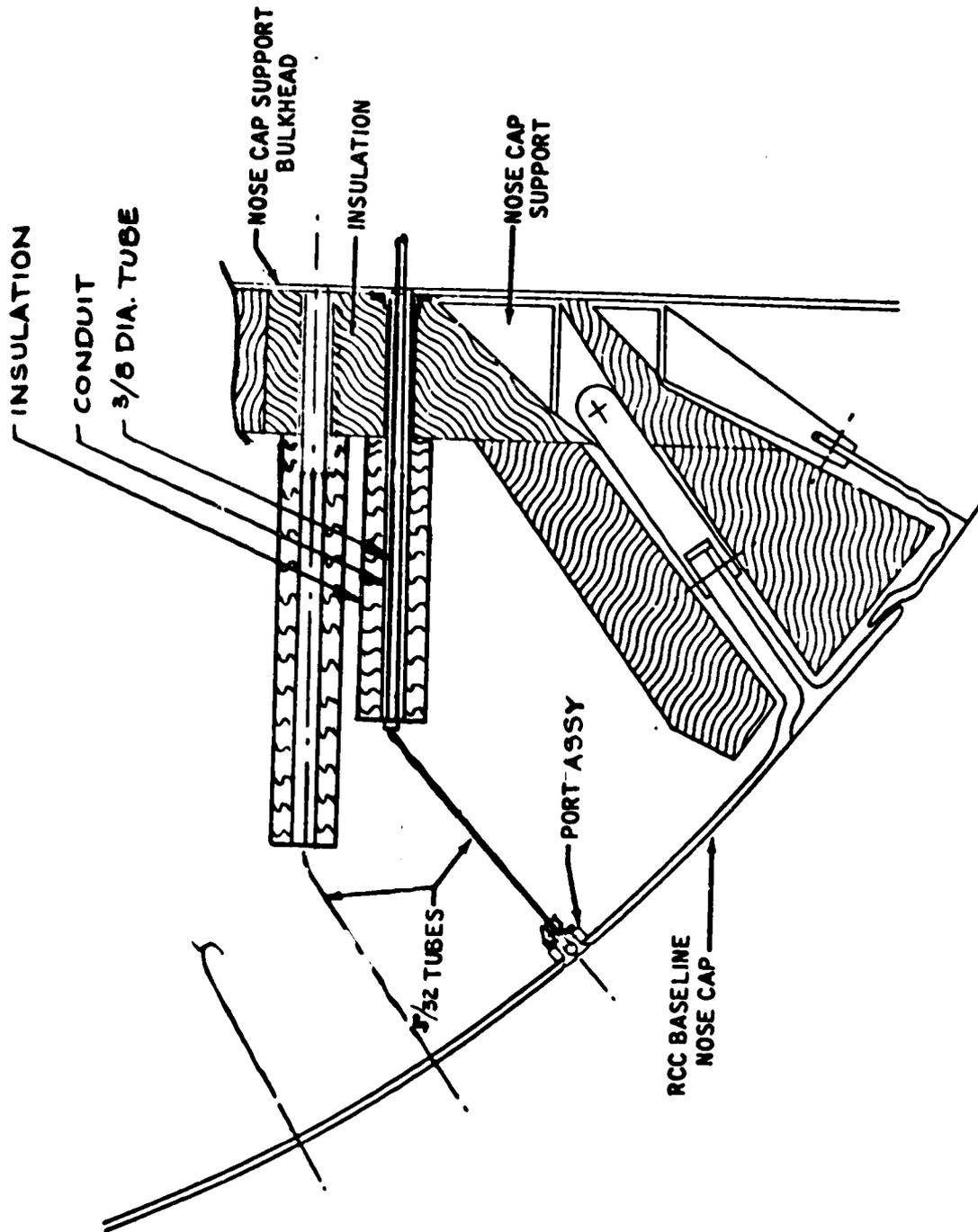
FIGURE 4-29 - INDIVIDUAL TUBE ROUTING CONCEPT

140
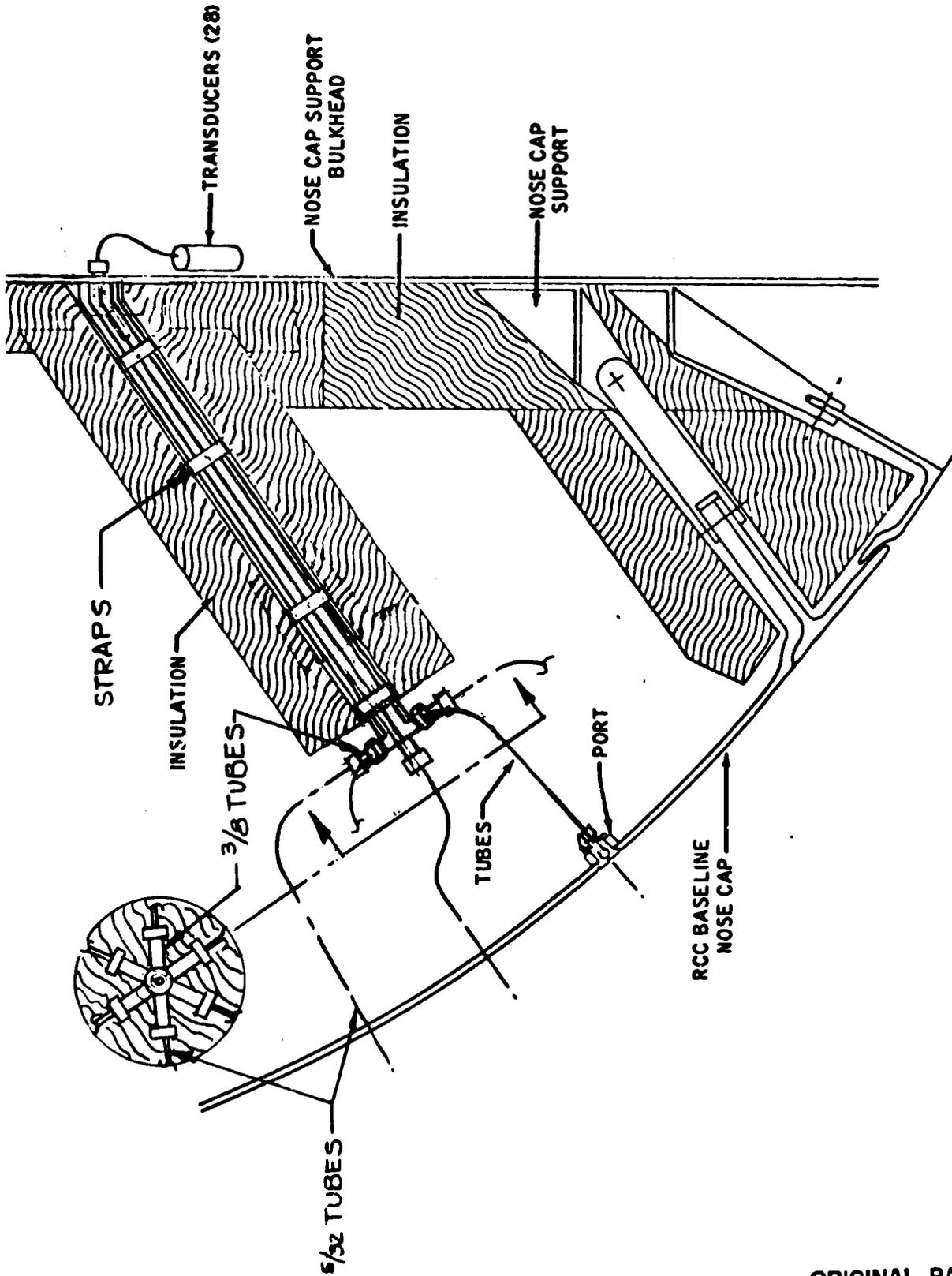
FIGURE 4-30 - GANGED TUBES CONCEPT

TRANSDUCERS (28)

NOSE CAP SUPPORT BULKHEAD

INSULATION

NOSE CAP SUPPORT

STRAPS

INSULATION

3/8 TUBES

5/32 TUBES

TUBES

PORT

RCC BASELINE NOSE CAP

POLYMIDE BLOCK

TRANSDUCERS (28)

NOSE CAP SUPPORT BULKHEAD

INSULATION

NOSE CAP SUPPORT

SUPPORT TUBE

INSULATION

TUBES

PORT

RCC BASELINE NOSE CAP
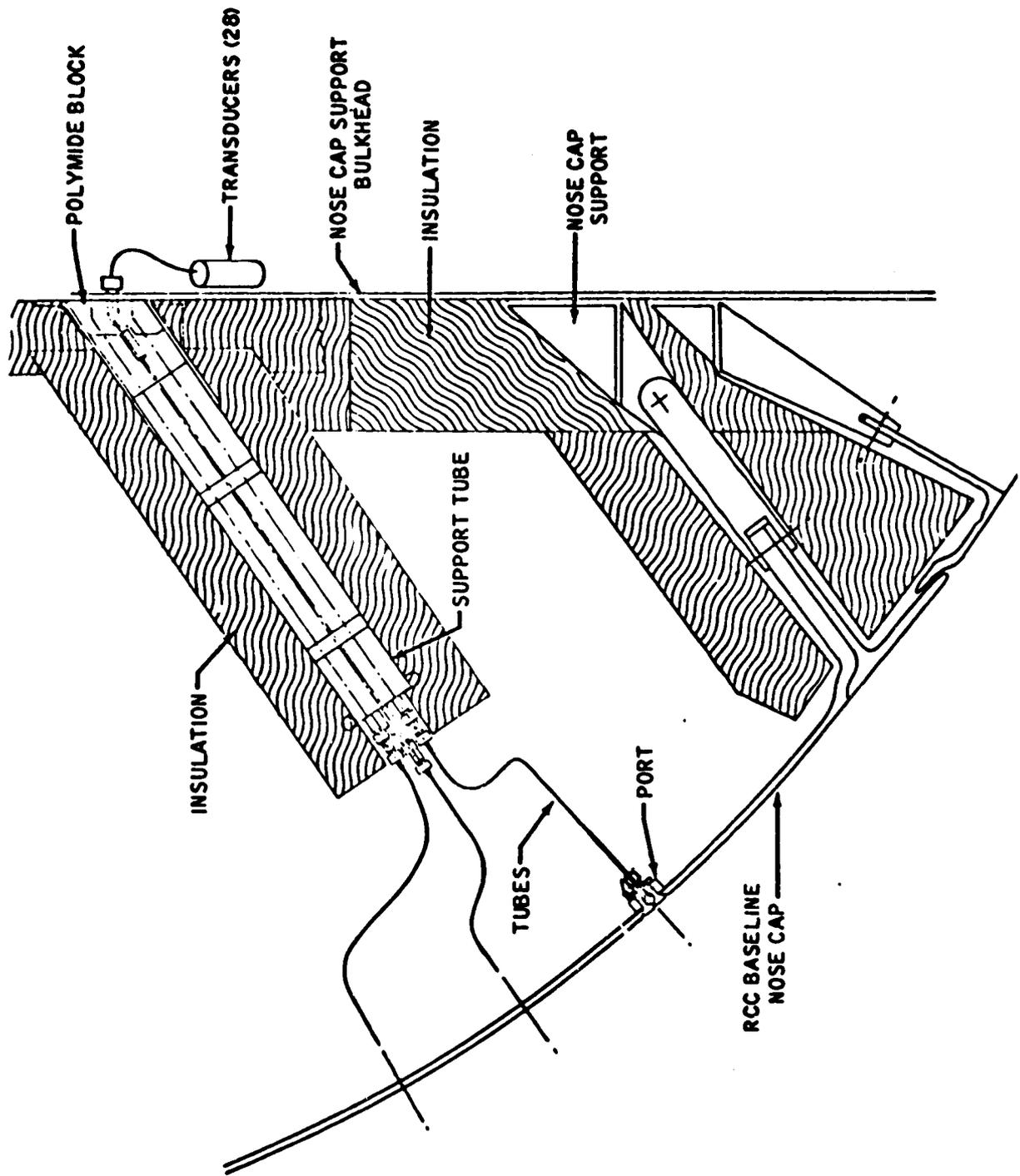
FIGURE 4-31 - SUPPORT TUBE CONCEPT
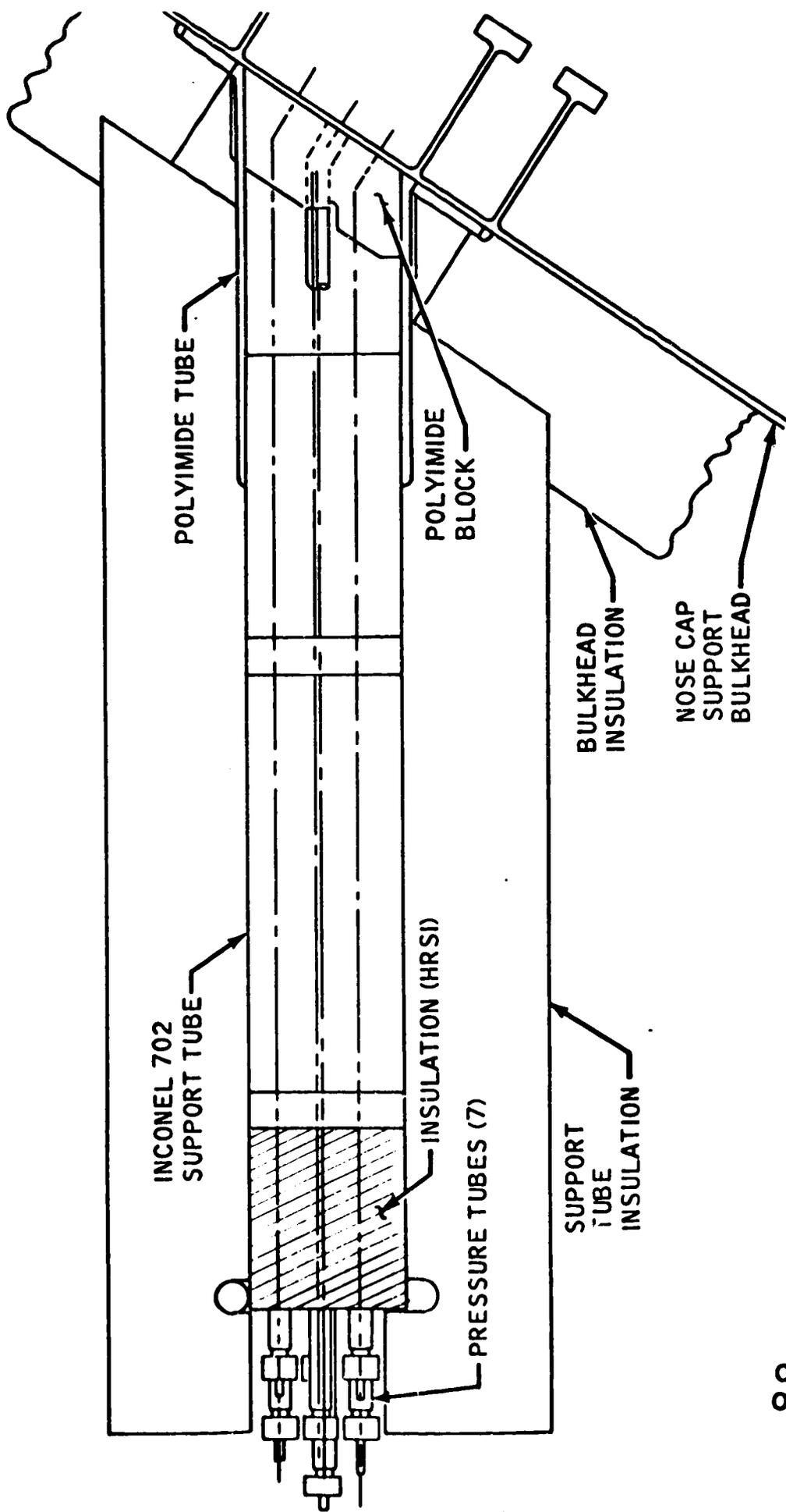
FIGURE 4-32 - SUPPORT TUBE DESIGN

POLYIMIDE TUBE

POLYIMIDE BLOCK

BULKHEAD INSULATION

NOSE CAP SUPPORT BULKHEAD

INCONEL 702 SUPPORT TUBE

INSULATION (HRSI)

PRESSURE TUBES (7)

SUPPORT TUBE INSULATION

VIEW LOOKING AFT

PRESSURE PORT
14 PLACES

FIG. 10

STIFFENER &
NOSE CAP SUPPORT
BULKHEAD (TYP.)
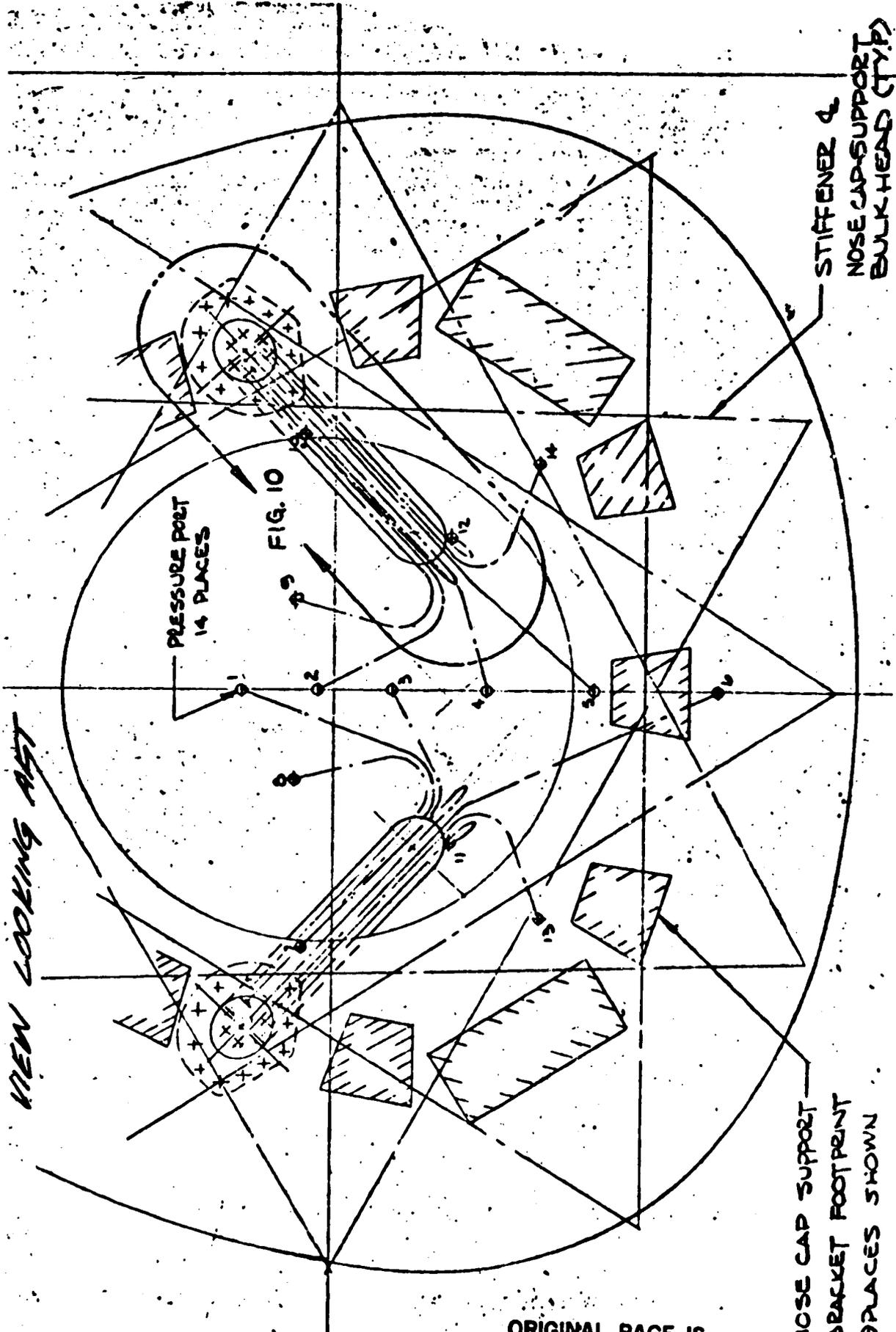
NOSE CAP SUPPORT
BRACKET FOOTPRINT
9 PLACES SHOWN

144
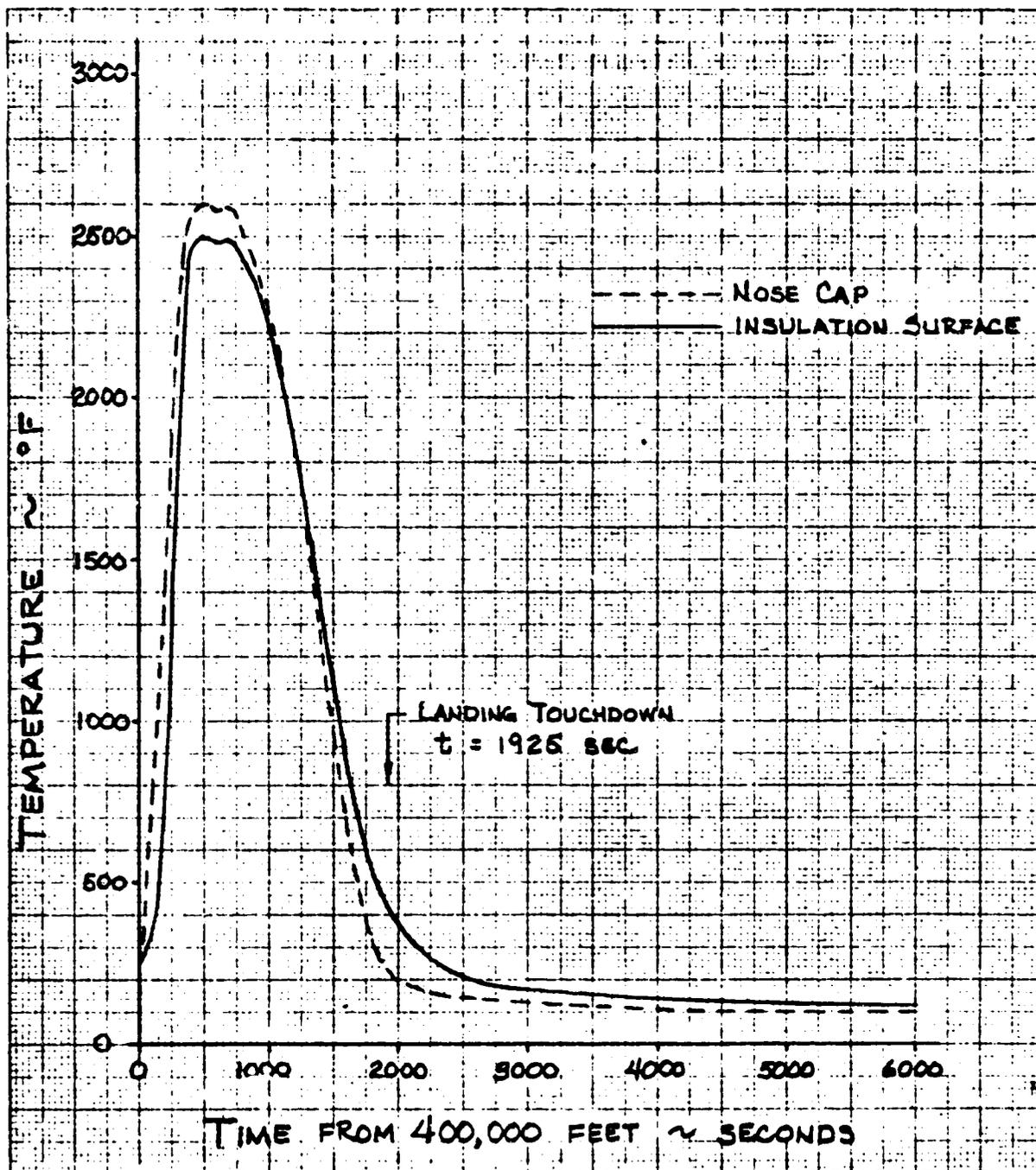
FIGURE 4-34 - BOUNDARY TEMPERATURES FOR SUPPORT TUBE ANALYSIS
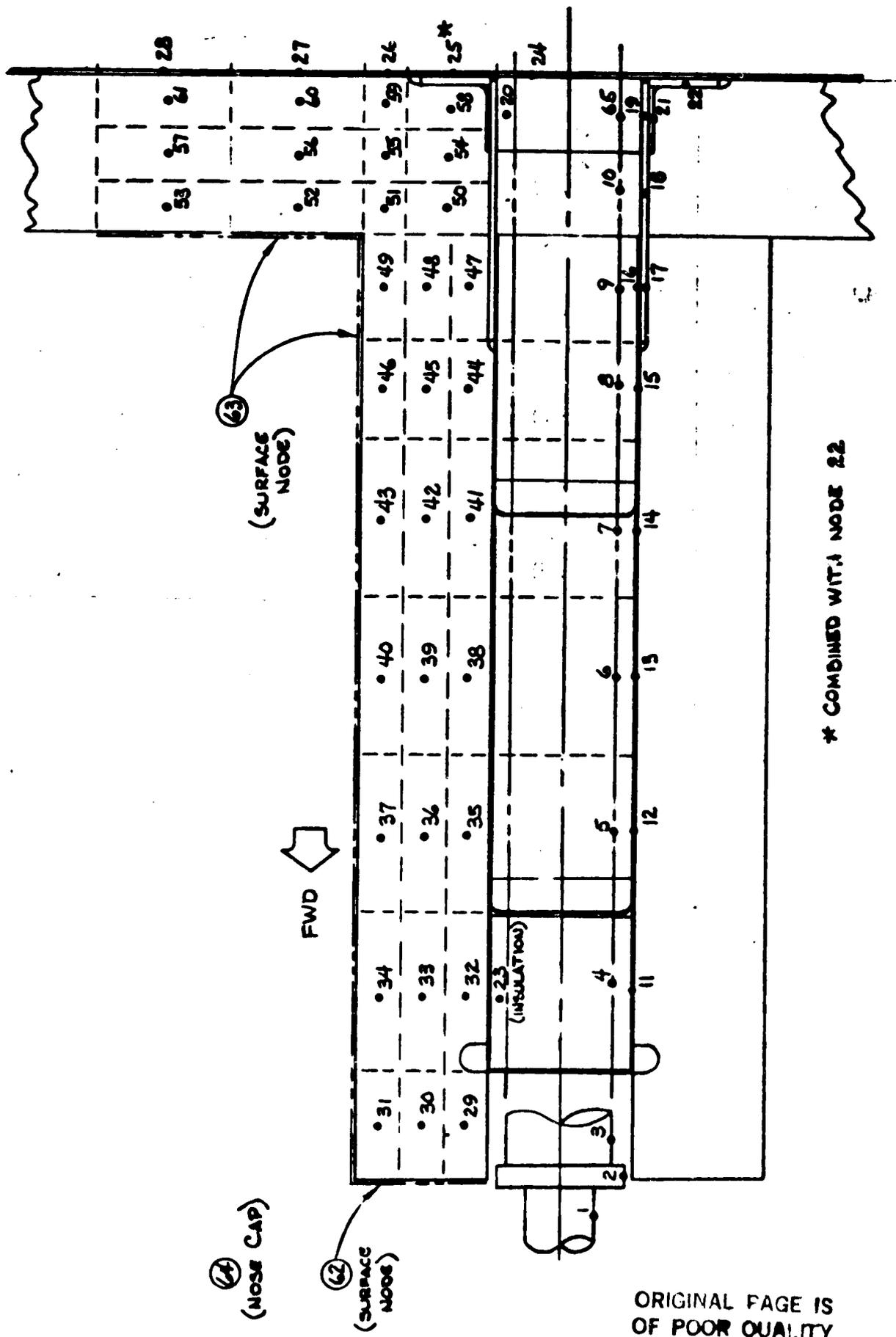
FIGURE 4-35 - SUPPORT TUBE THERMAL MODEL

* COMBINED WITH NODE 22

146
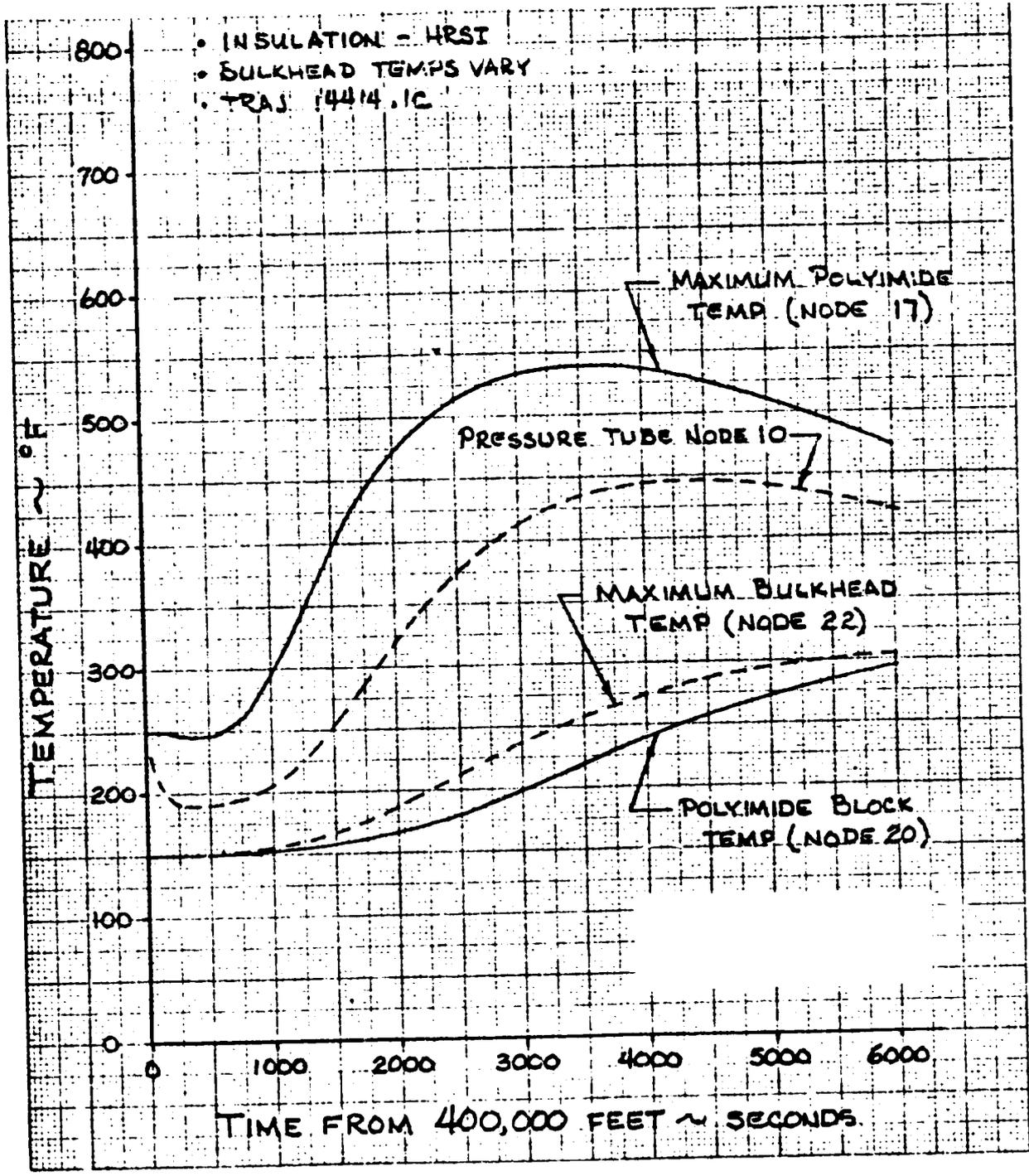
FIGURE 4-36 - SUPPORT TUBE THERMAL ANALYSIS POLYIMIDE TEMPERATURES
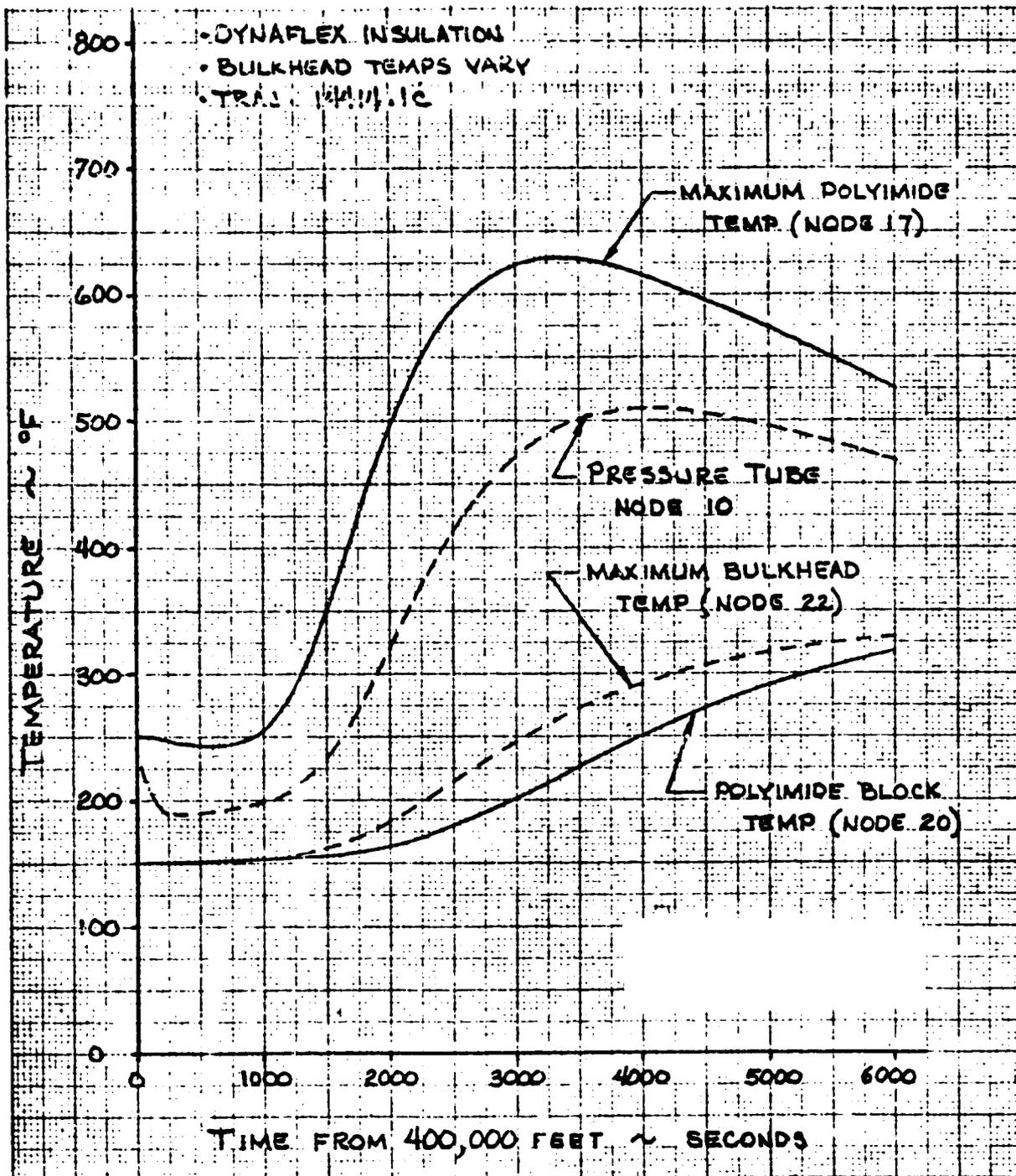
FIGURE 4-37 - SUPPORT TUBE THERMAL ANALYSIS POLYIMIDE TEMPERATURES
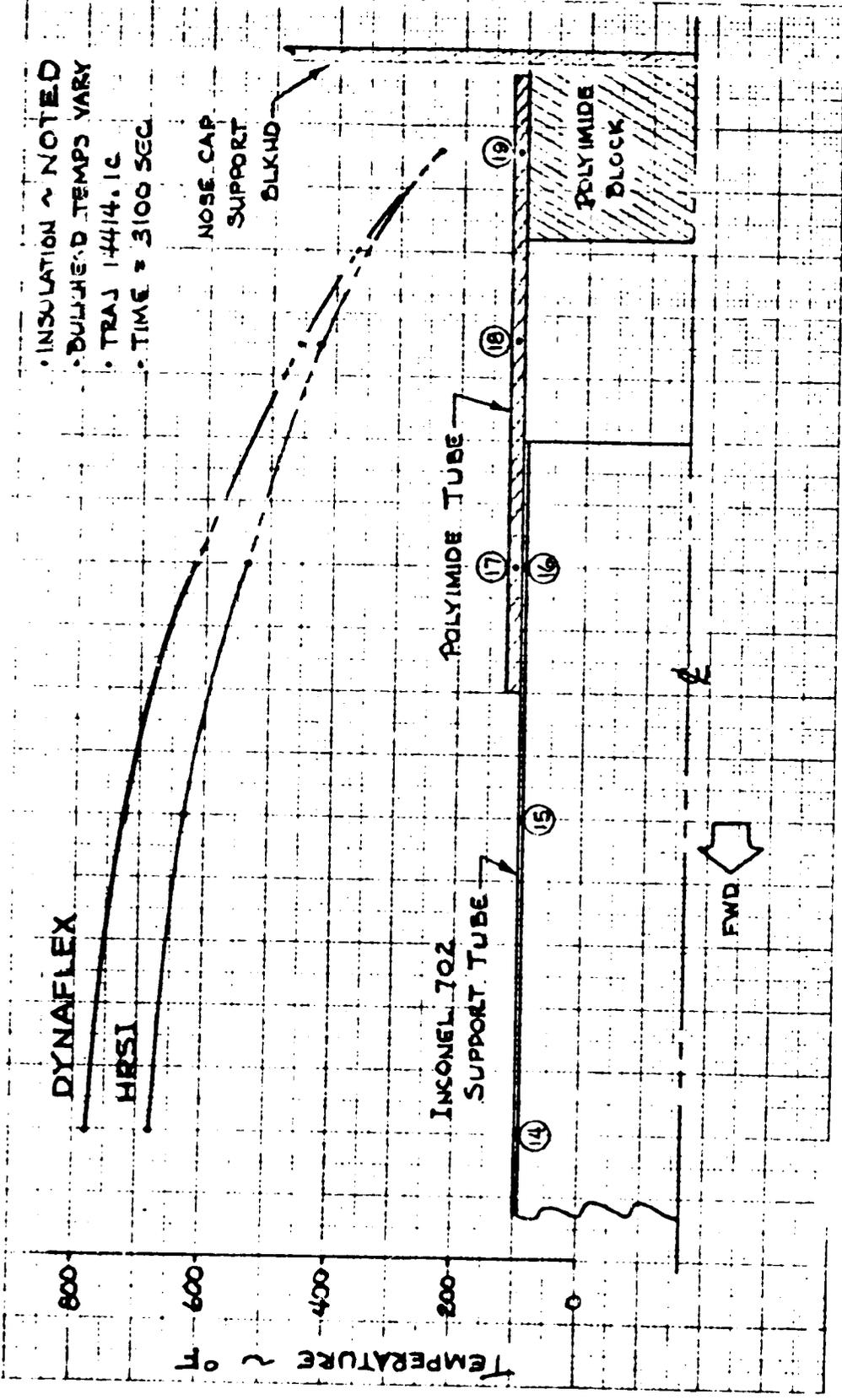
FIGURE 4-38 - SUPPORT TUBE THERMAL ANALYSIS TEMPERATURE DISTRIBUTION
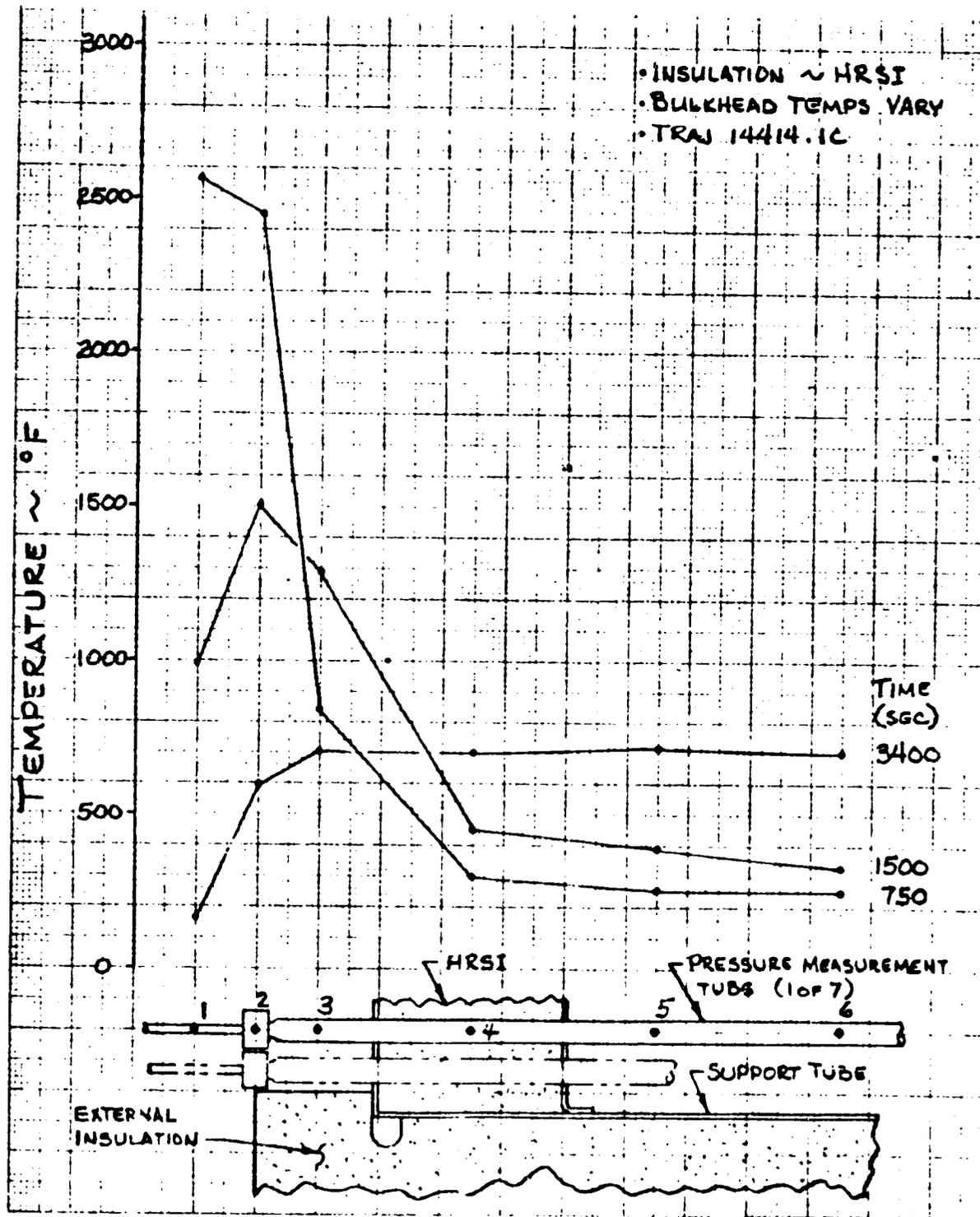
FIGURE 4-39 - PRESSURE TUBE TEMPERATURE DISTRIBUTIONS

FIGURE 4-40 - ACCEPTABLE PRESSURE TUBE CONFIGURATIONS
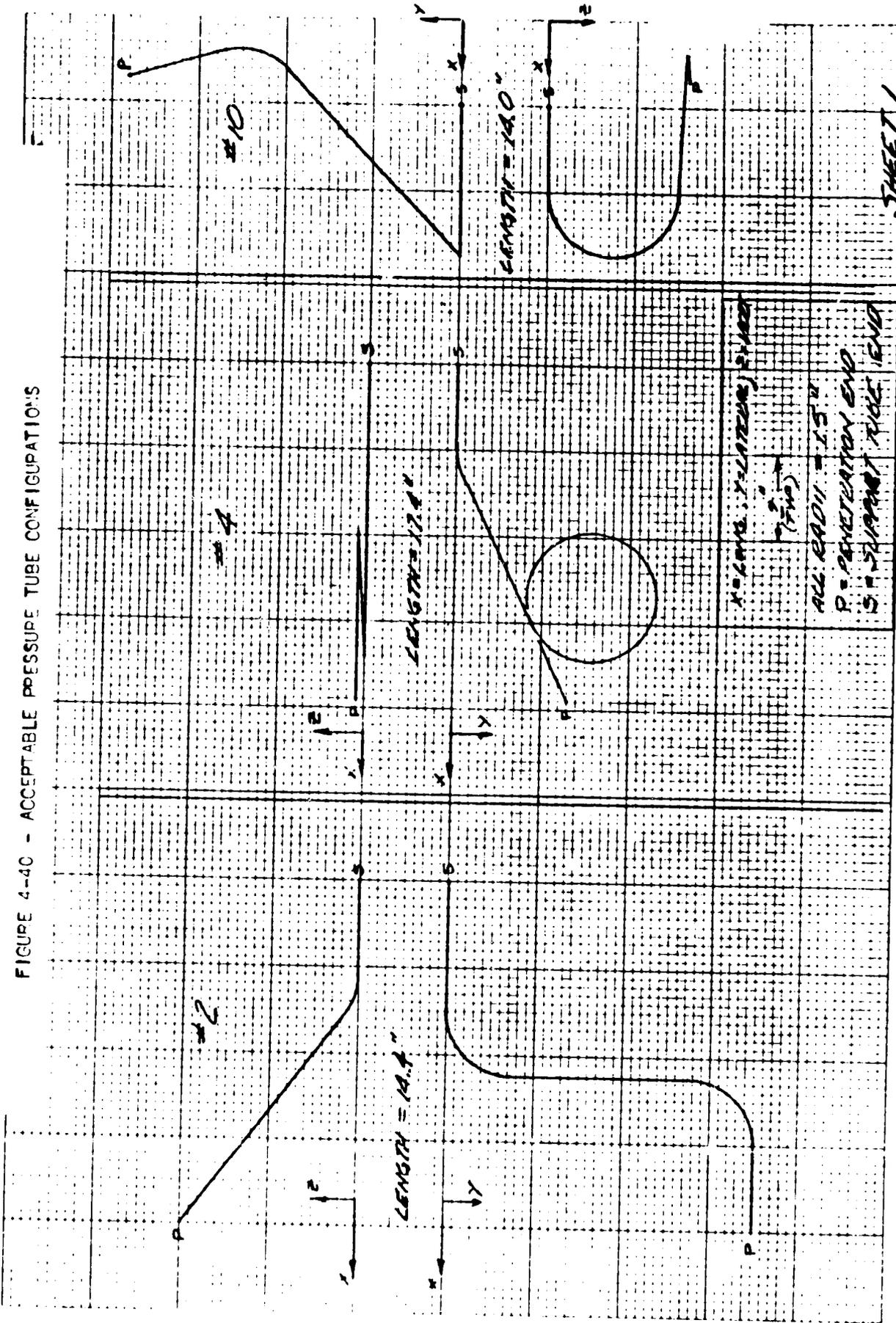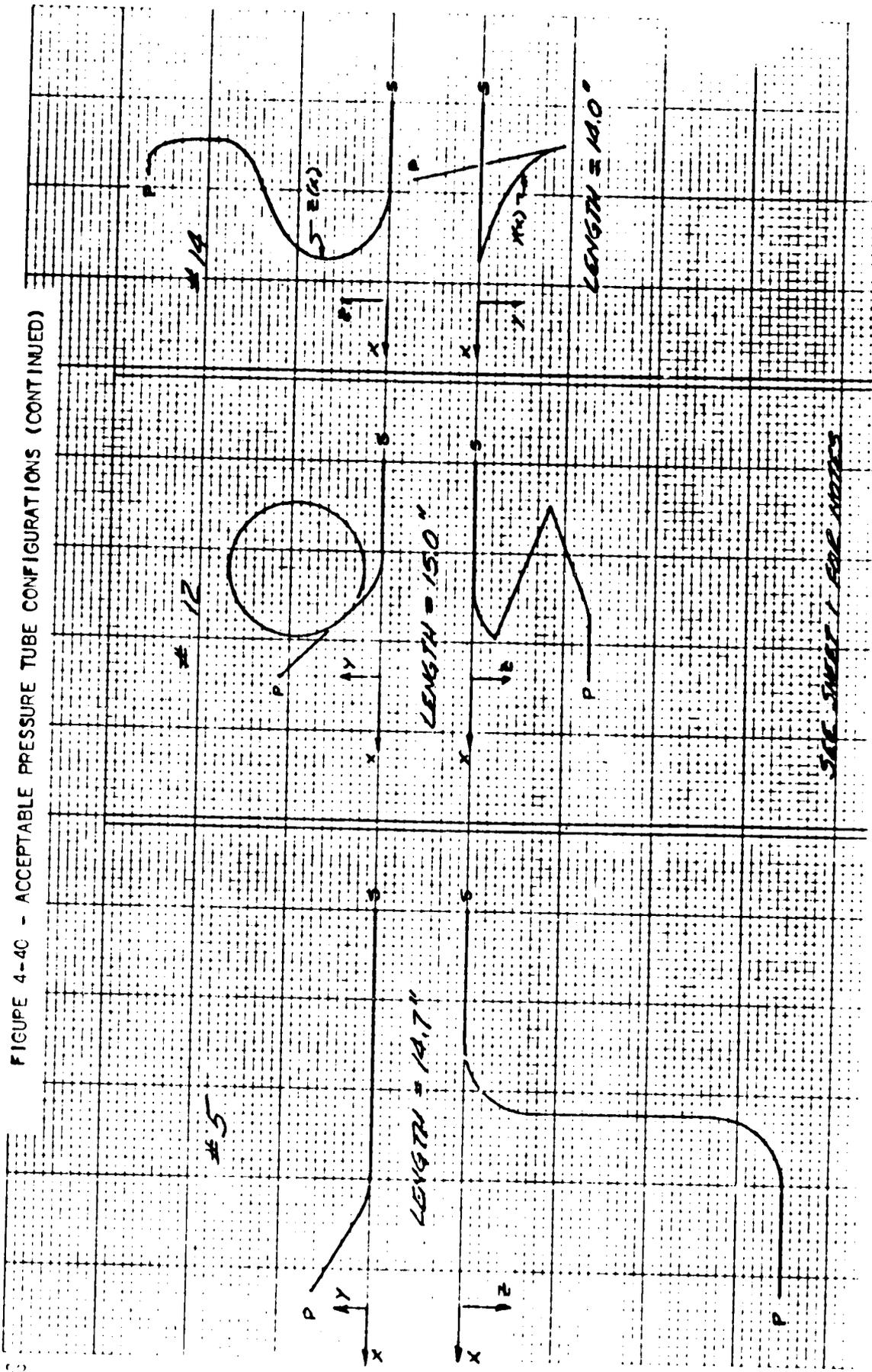
FIGURE 4-40 - ACCEPTABLE PRESSURE TUBE CONFIGURATIONS (CONTINUED)

FIGURE 4.40 - ACCEPTABLE PRESSURE TUBE CONFIGURATIONS (CONTINUED)

LENGTH = 15.0"

SEE SHEET 1 FOR NOTES

153

LONGEST TUBE RUN

$H = .02400 \, EI$

$V = .006114 \, EI$

$M = M_{max} = .04986 \, EI$

$\Delta = 0.3"$ (SHORTENED)

3.5'

3.3"

9.8"

SHORTEST TUBE RUN

$V = .00448$

$N = .01235$

$M_C = .0225.$

$\Delta = 0.25"$ (SHORTENED)

2.5"

2.0"

.5"

$M_A = .01035 \, EI$

$M_B = M_{max} = .0_L$

4.5"
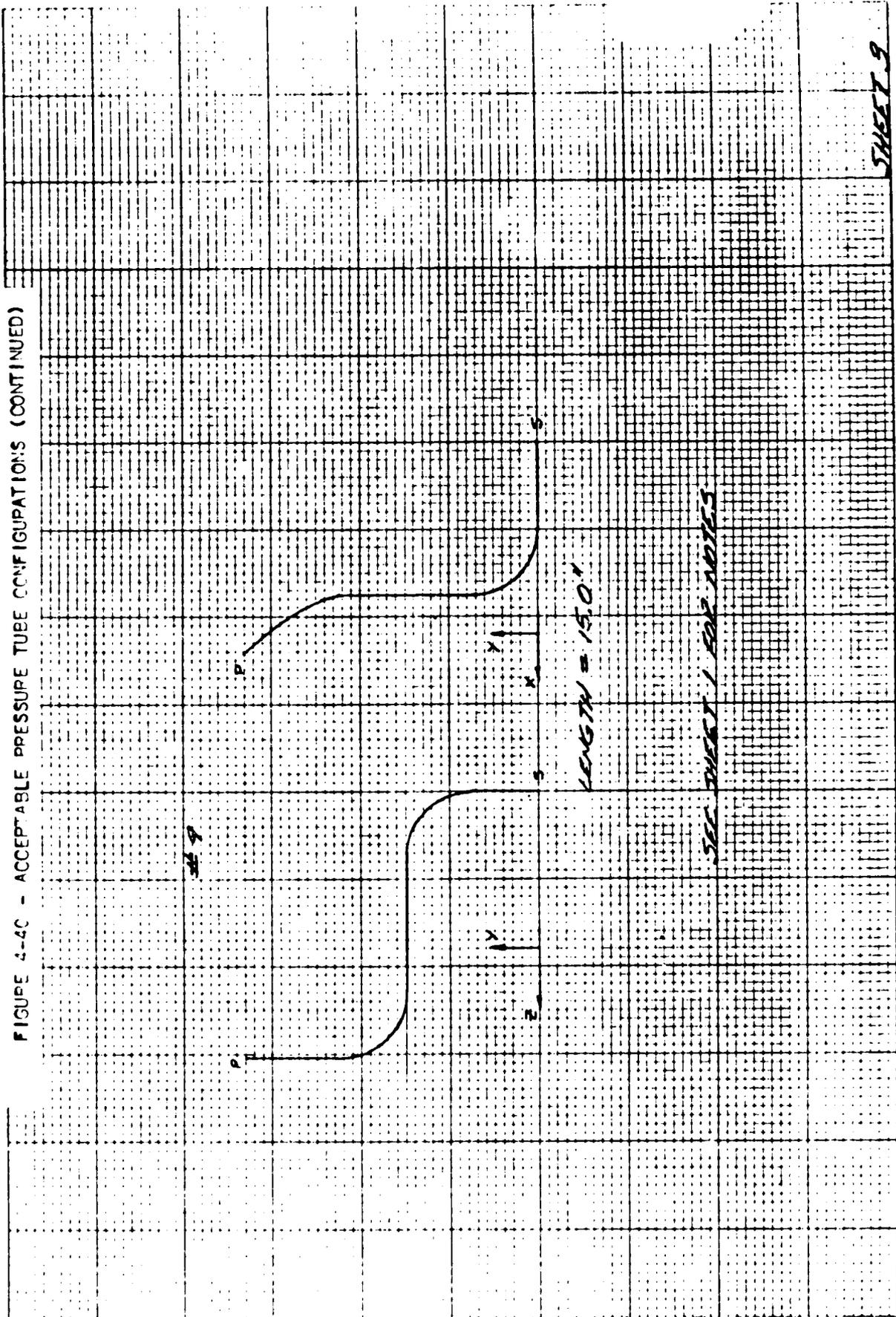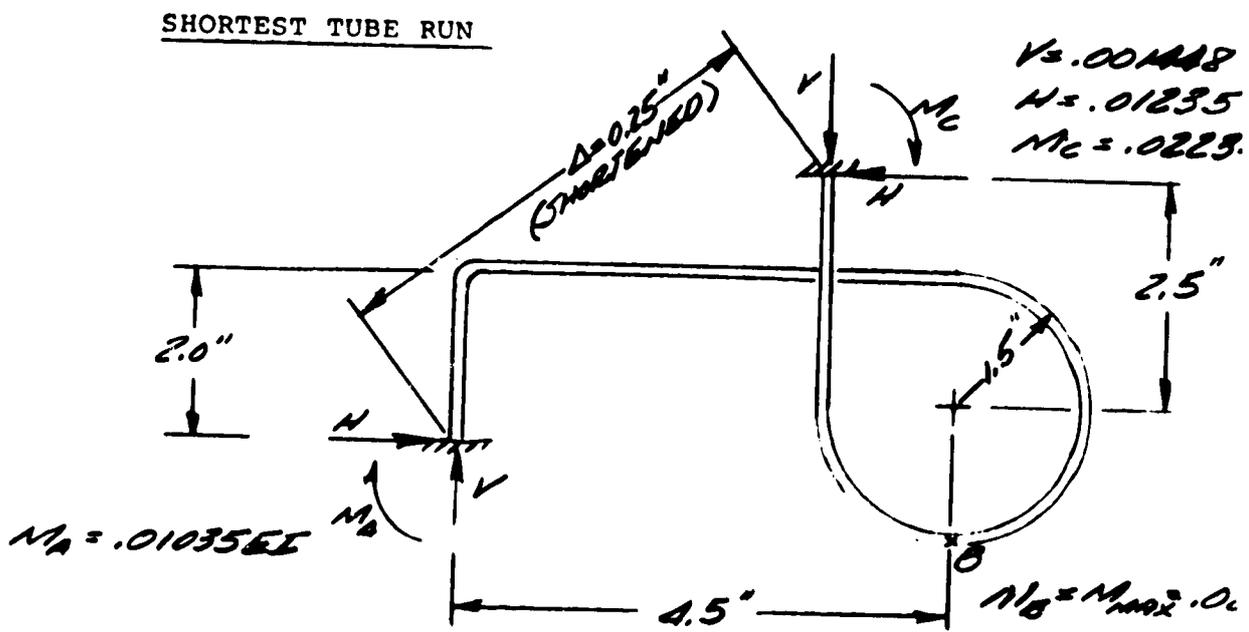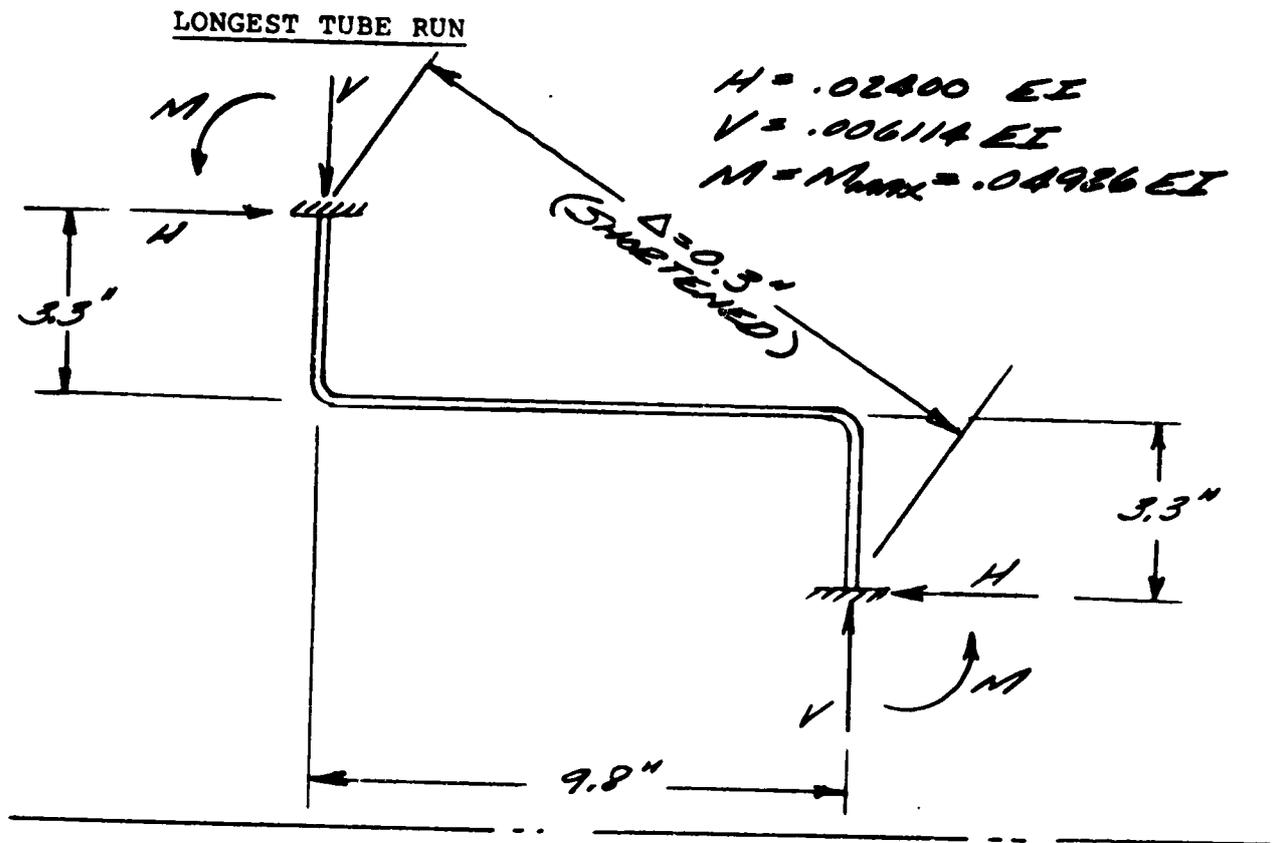
FIGURE 4-41 - TUBE CONFIGURATIONS STATIC ANALYSIS

154
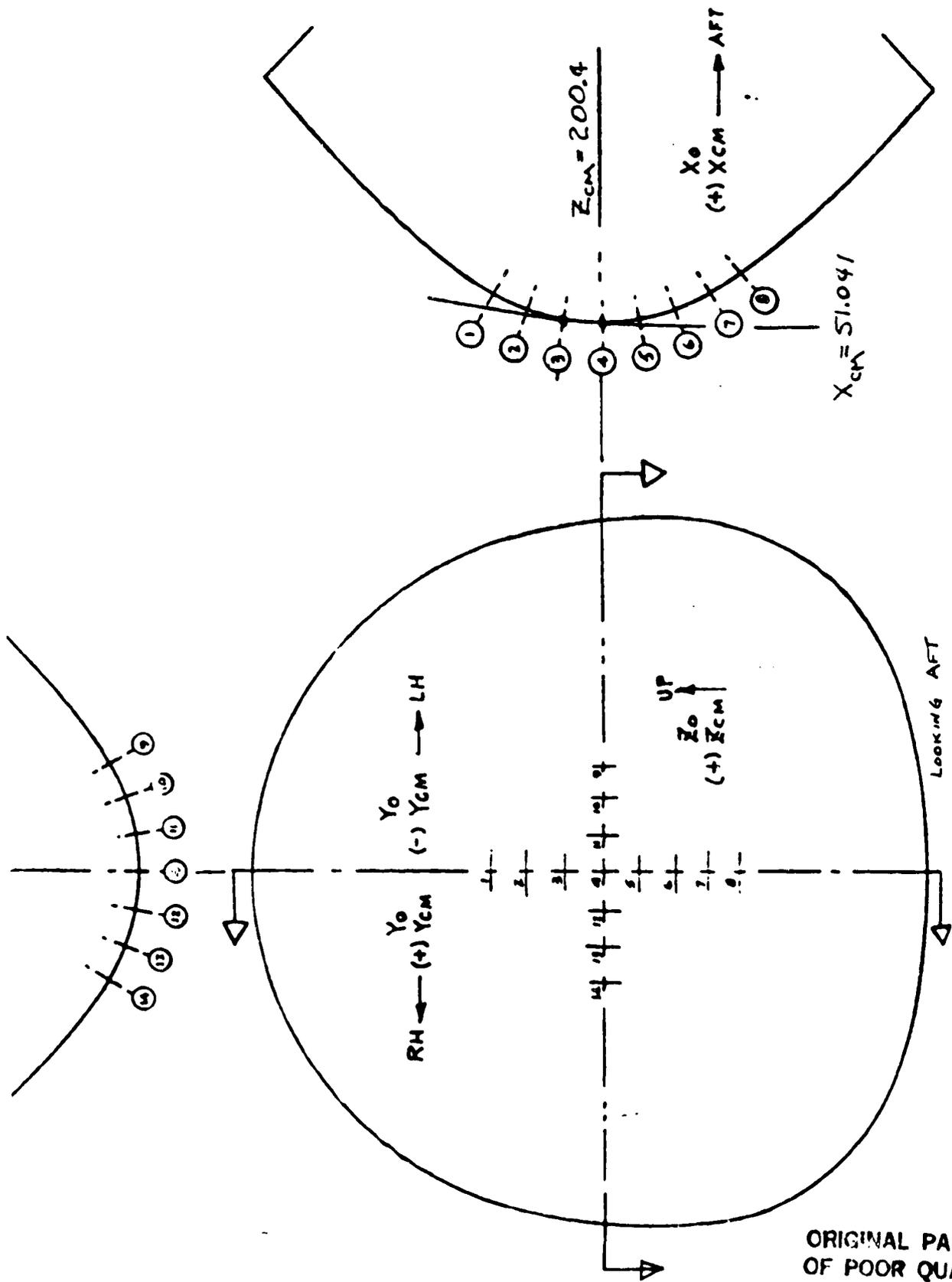
FIGURE 5-1 — SEADS ORIFICE GENERAL ARRANGEMENT

$Z_{cm} = 200.4$

X_o
(+) X_{cm} → AFT

$X_{cm} = 51.041$

Y_o
(-) Y_{cm} → LH

Y_o
RH ← (+) Y_{cm}

Z_o
(+) Z_{cm}
UP

LOOKING AFT
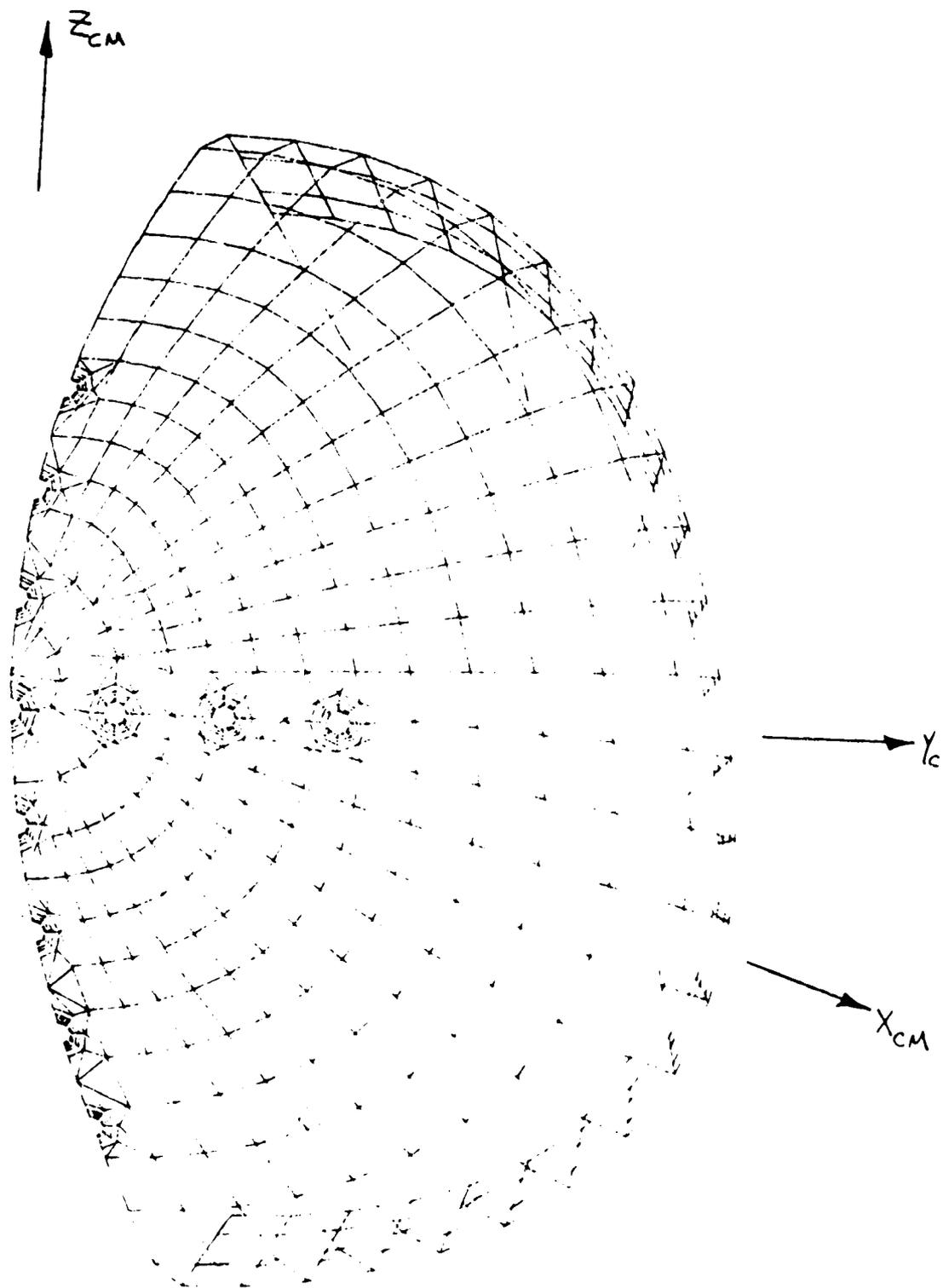
FIGURE 5-2 - FINE GRID SEADS HOLES, HALF MODEL
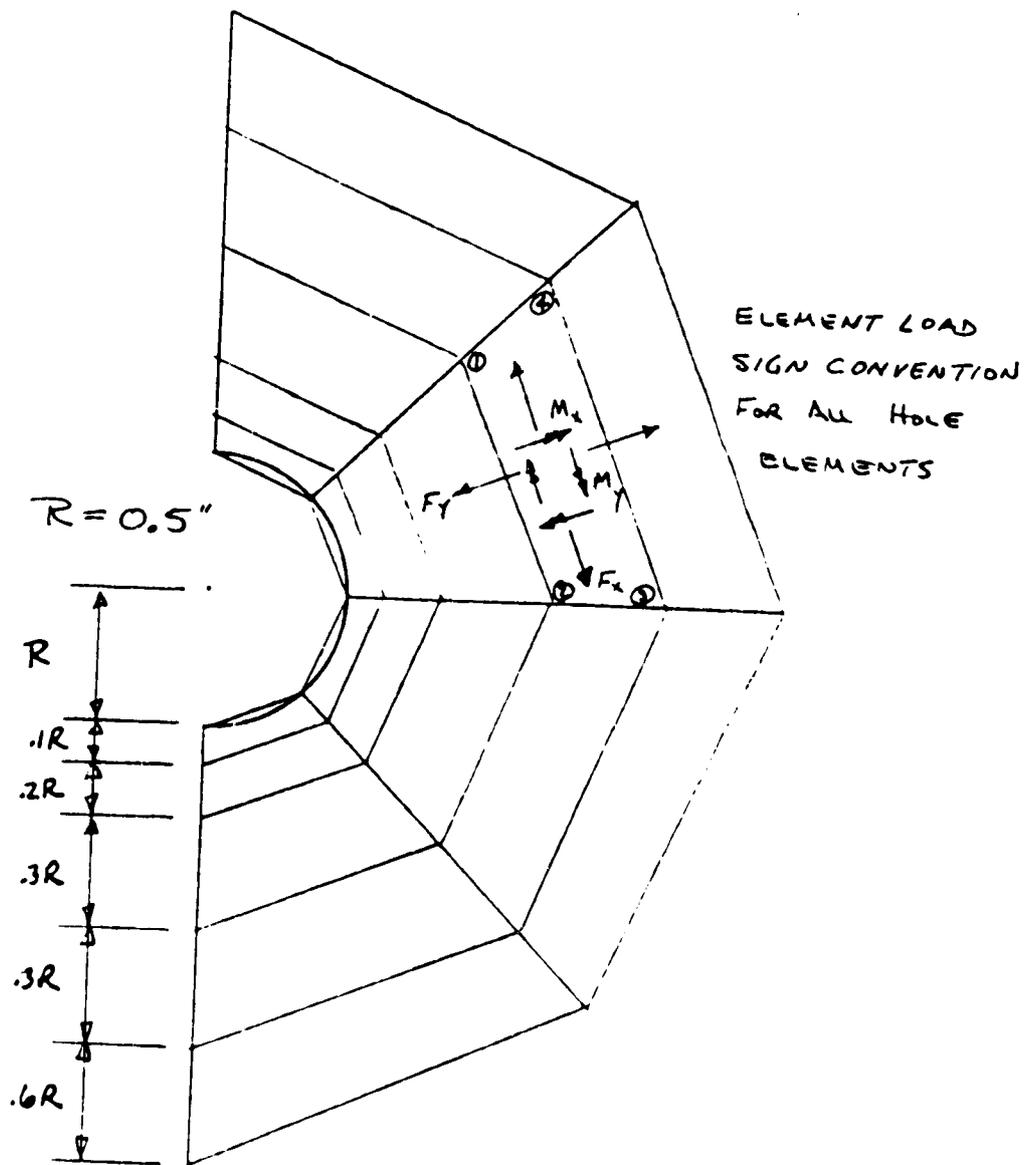
FIGURE 5-3 - SEADS HOLE MODEL GRID MESH

The figure shows two plots illustrating types of stability tracking.

Upper plot (A): δ_i versus β, with vertical lines at $\beta = 1.0$, β_{CRIT_i}, and $\beta = \lambda_{CRIT_i}$. At the peak: $\dfrac{d\delta_i}{d\beta} = 0$. Labeled **GRID POINT i** and **(A) SNAP THRU**.

Lower plot (B): δ_j versus β, with vertical lines at $\beta = 1.0$ and $\beta = \lambda_{CRIT_j}$. Annotation: $\beta_{CRIT_j} = \dfrac{d\delta_j}{d\beta} \equiv UNDEFINED$. Labeled **GRID POINT j** and **(B) COLLAPSE**.
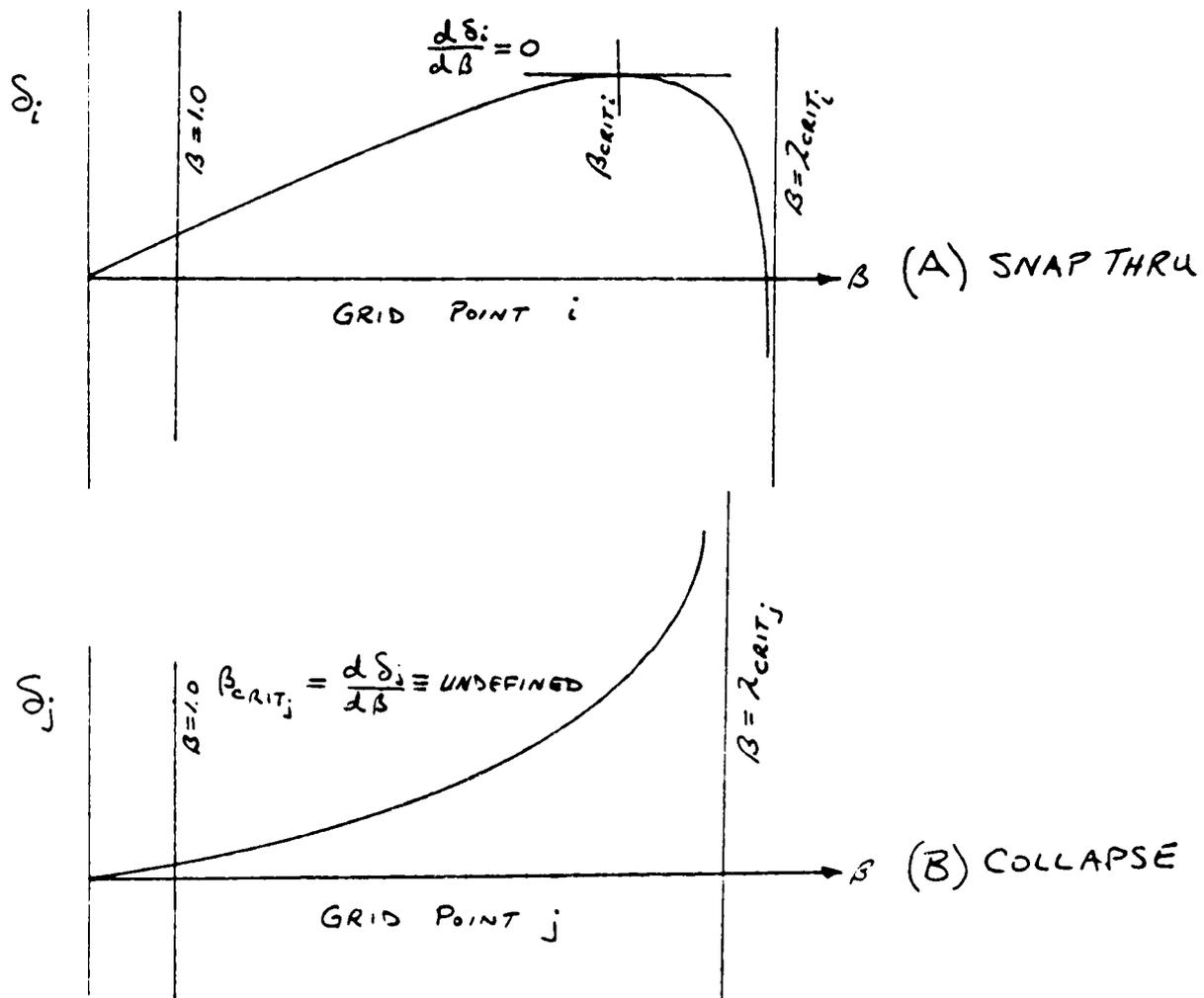
FIGURE 5-4 - TYPES OF STABILITY TRACKING
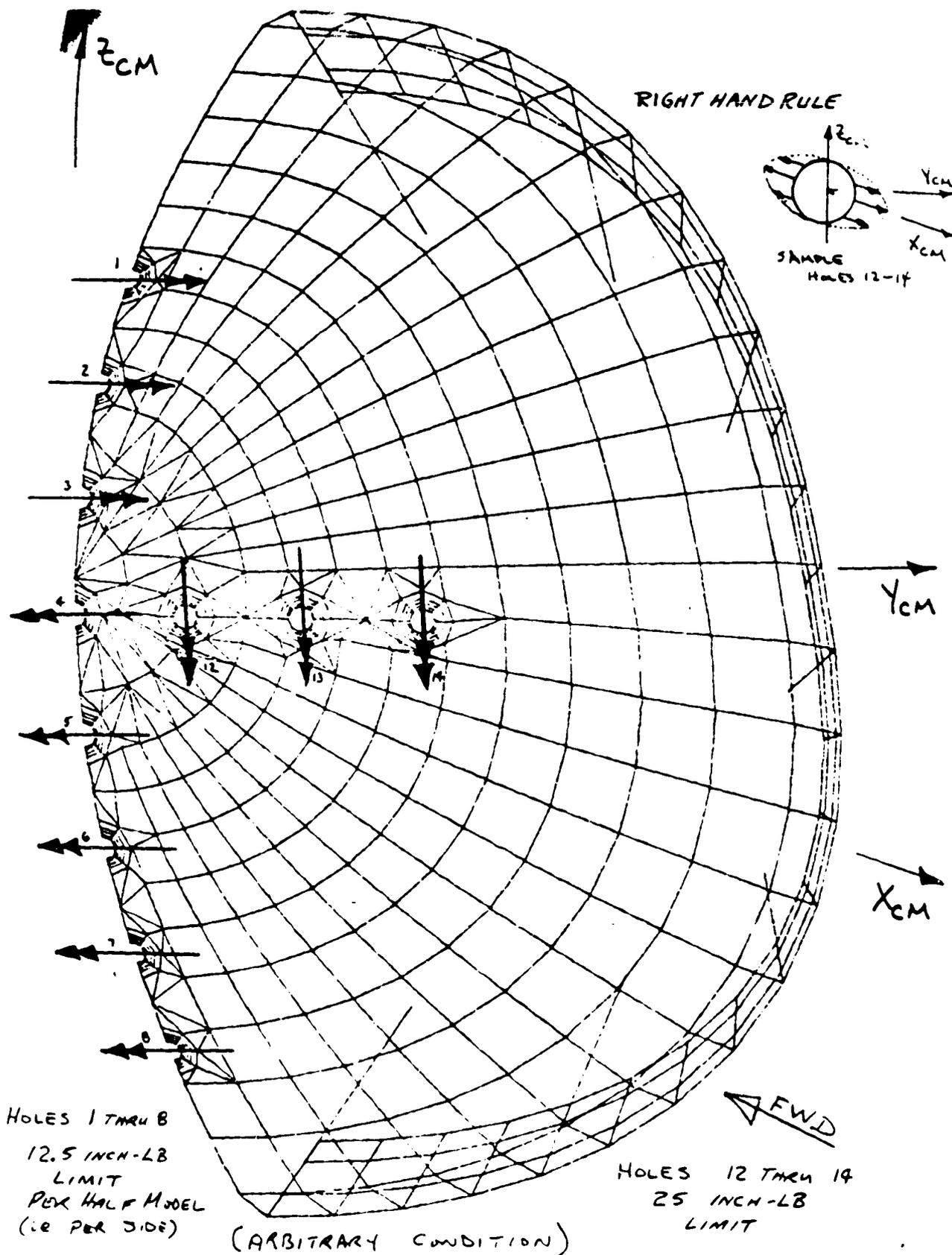
FIGURE 5-5 — ORIFICE TUBE INDUCED MOMENTS APPLIED TO SEADS NOSE CAP
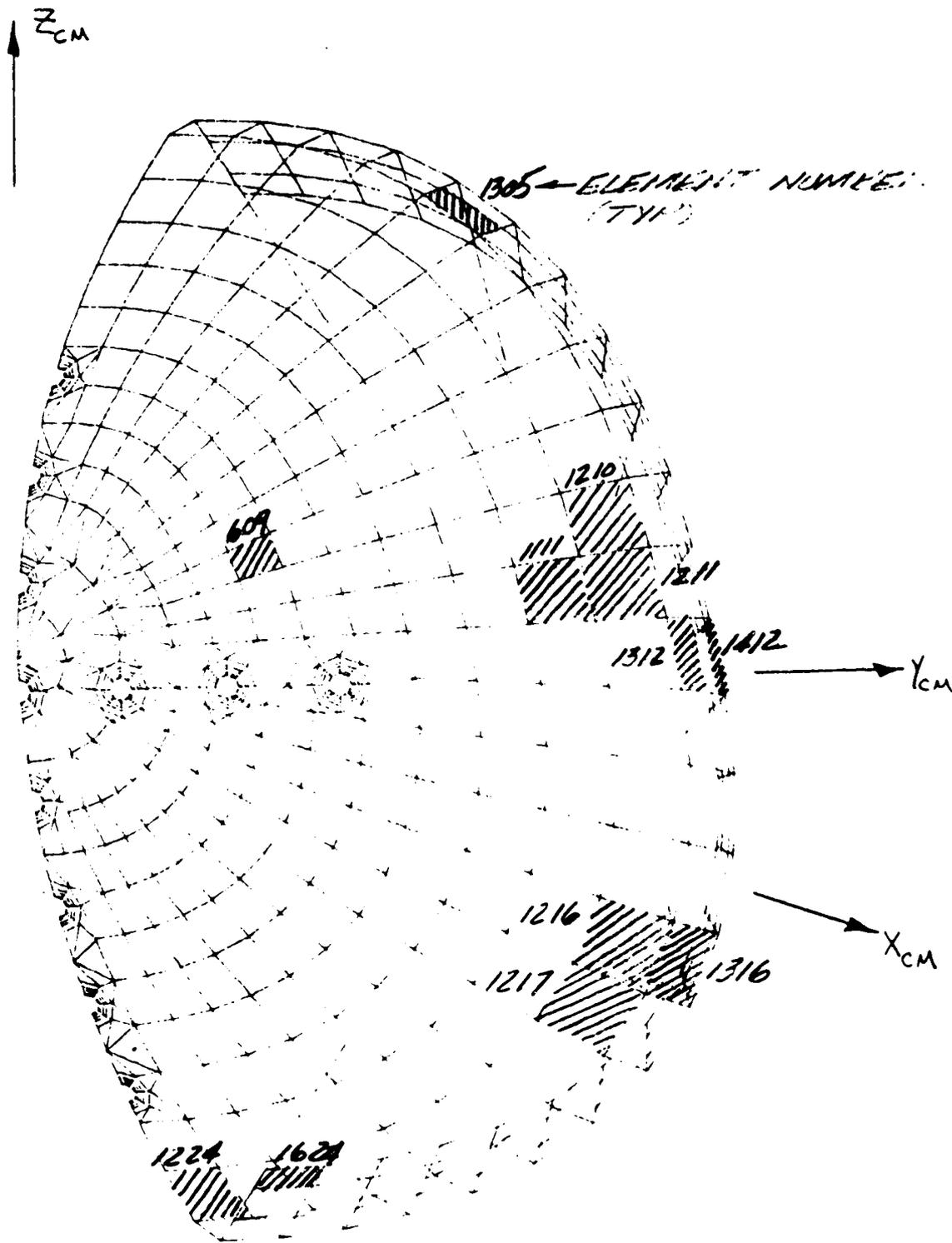
FIGURE 5-6 - LOCATION OF CRITICAL STRENGTH ELEMENTS
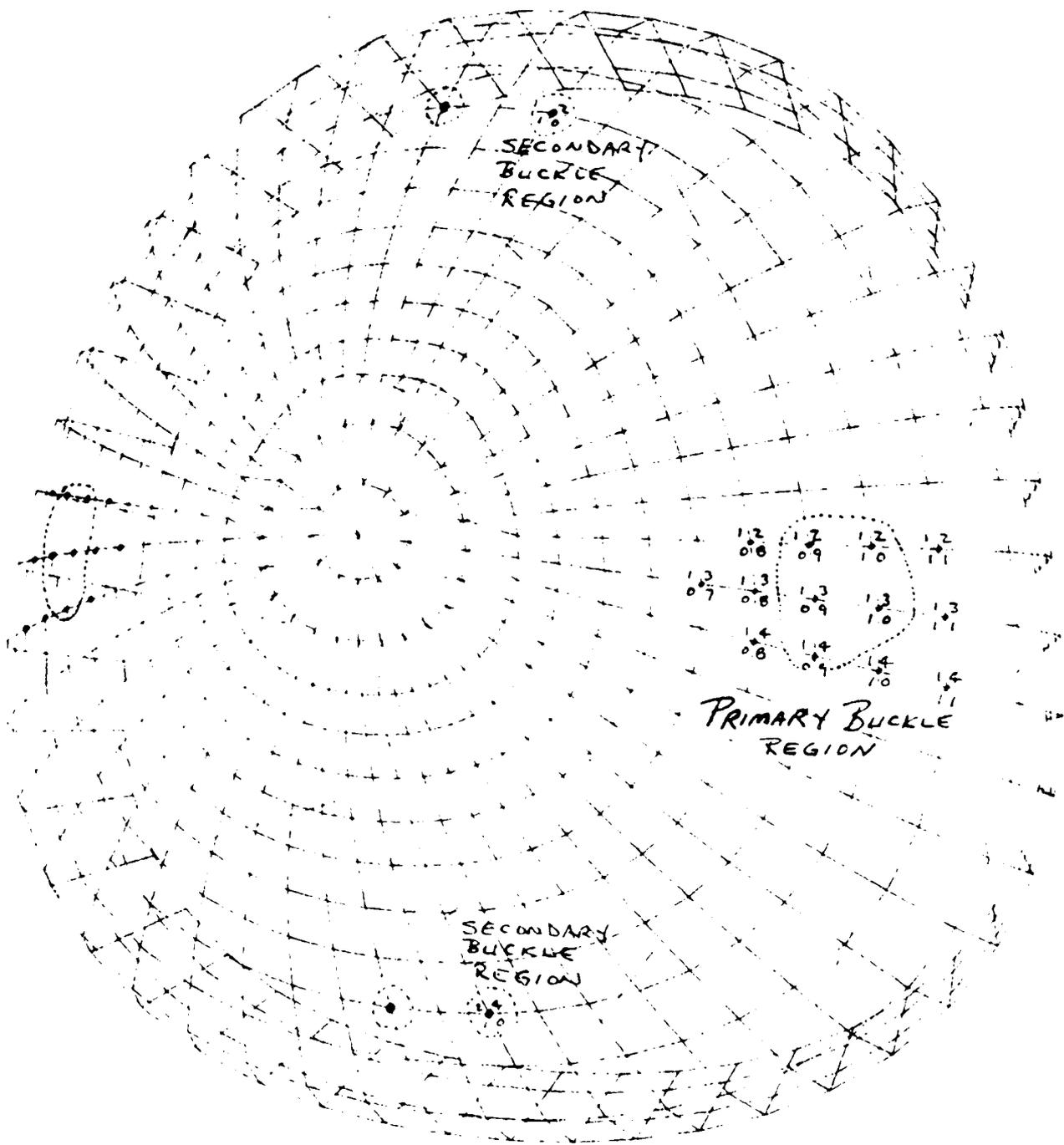
FIGURE 5-7 - PRODUCTION NOSE CAP, REGIONS OF INSTABILITY
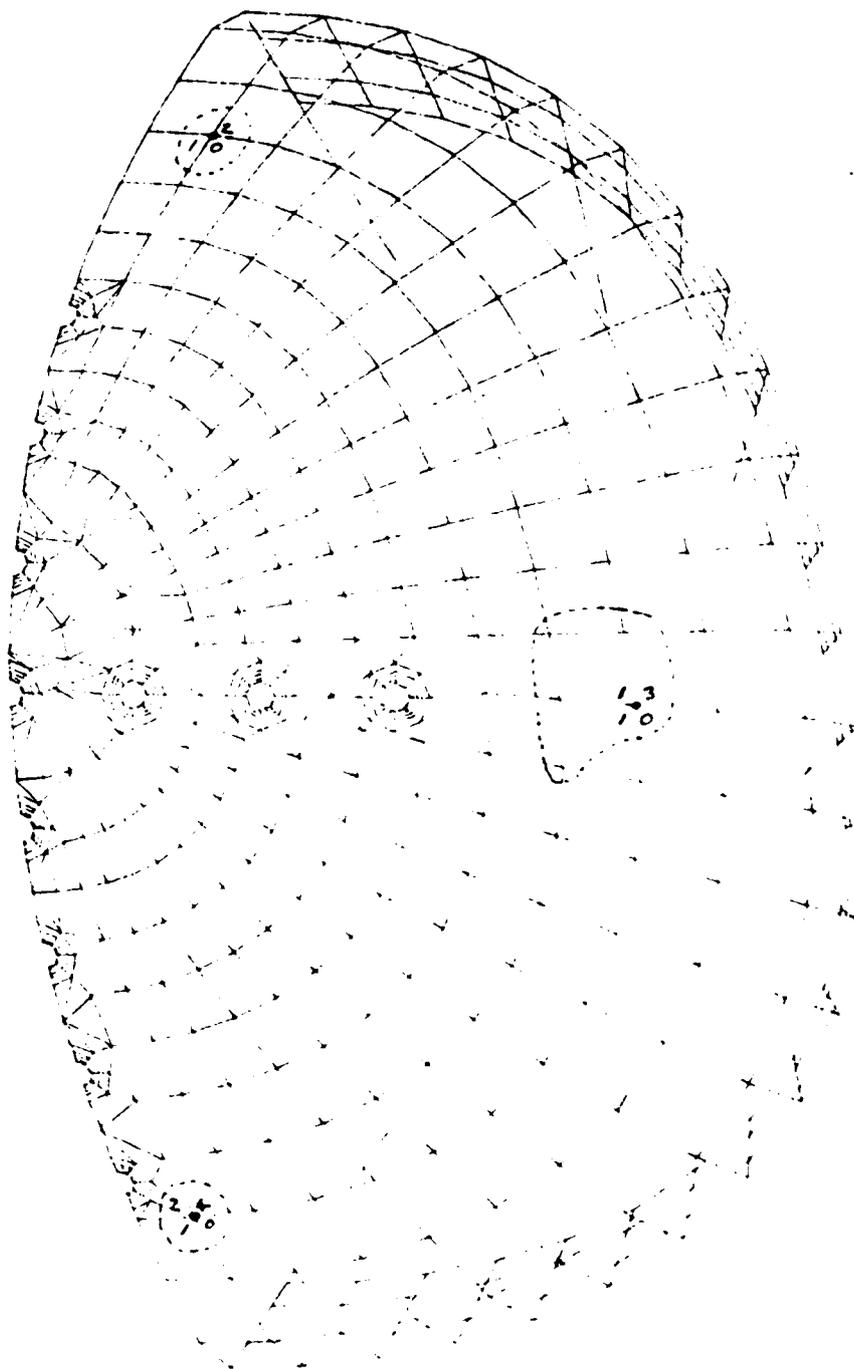
FIGURE 5-8 - SEADS NOSE CAP, REGIONS OF INSTABILITY

FIGURE 5-9 - SEADS FLAT SIDED HOLE
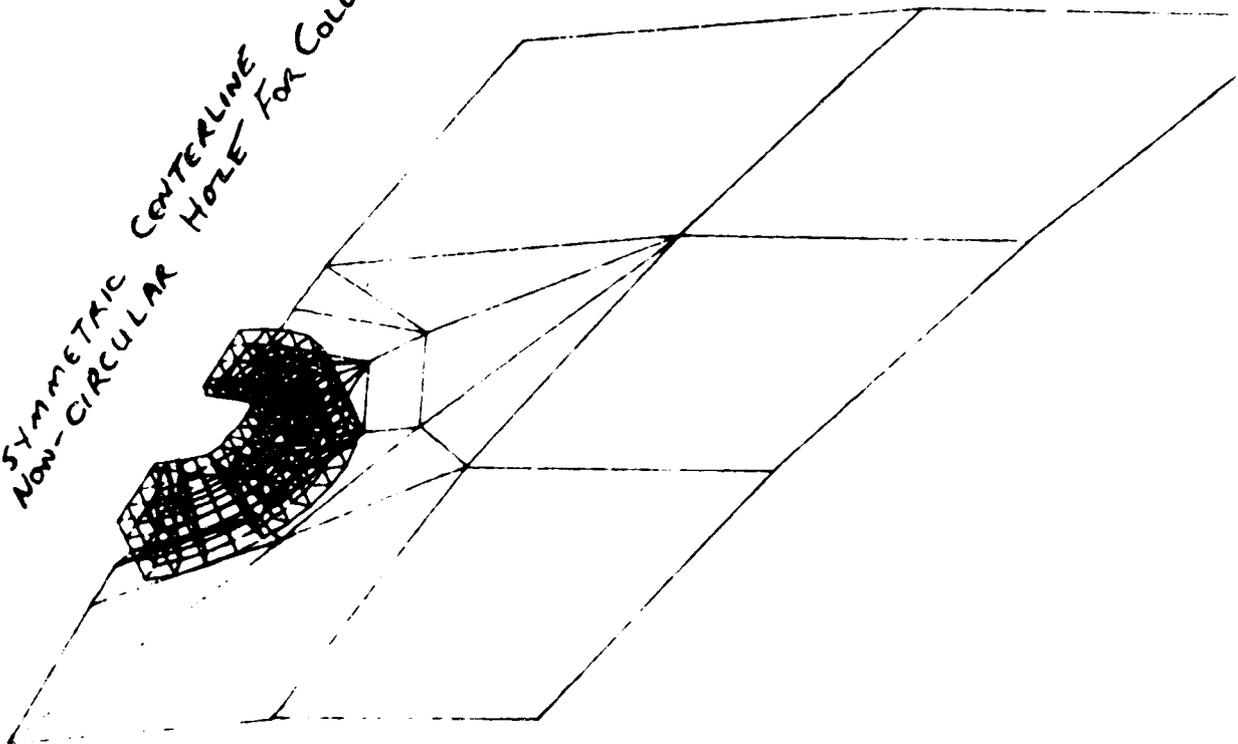
FIGURE 5-10 - DETAIL SEADS NO. 1 NASTRAN MODEL, 2D & 3D
ELEMENTS
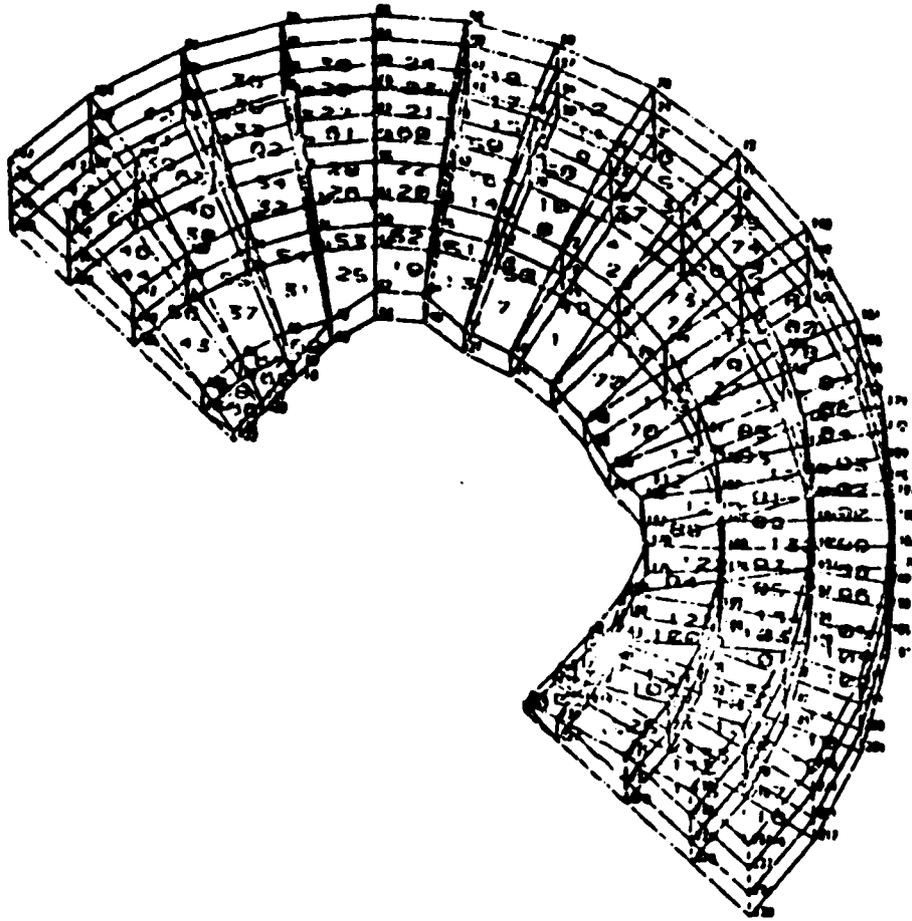
FIGURE 5-11 - DETAIL SEADS NO. 1 HOLE NASTRAN MODEL,
3D ELEMENT LOOKING AFT

REF. DWG. 2216T4071

SECTION A-A

QUADRANT 1

QUADRANT 2

QUADRANT 3

NOSE CAP

SPACER
T/C MOUNT
UNION
NUT

NODE NUMBERS FOR
QUADRANT NO. 2

PRESSURE TUBE
(PLATINUM 20% RHODIUM)

NUT (COLUMBIUM)

UNION (COLUMBIUM)

T/C MOUNT (IRIDIUM)

WASHER (COLUMBIUM)

SPACER (RCC)

PLUG (COLUMBIUM)

RCC NOSE CAP

Labels	ZONE 2 NODE NO.	ZONE 1 NODE NO. (TEMP.)	ZONE 3 NODE NO. (TEMP.)
UNION	6	37 (2594)°F	45 (2593)°F
TE MOUNT	16	36 (2579)	44 (2598)
TE MOUNT	17	38 (2599)	46 (2599)
SPACER	19	39 (2607)	47 (2606)
SPACER	21	40 (2618)	48 (2617)
NOSECAP	23	41 (2636)	49 (2636)
BHD INSUL	51	50 (2567)	52 (2551)

NODE 54 NOSE CAP INSIDE SURFACE 2551°F

NODE 53 BULKHEAD INSULATION 2528°F

NODE NO.

ZONE 2 TEMPERATURES
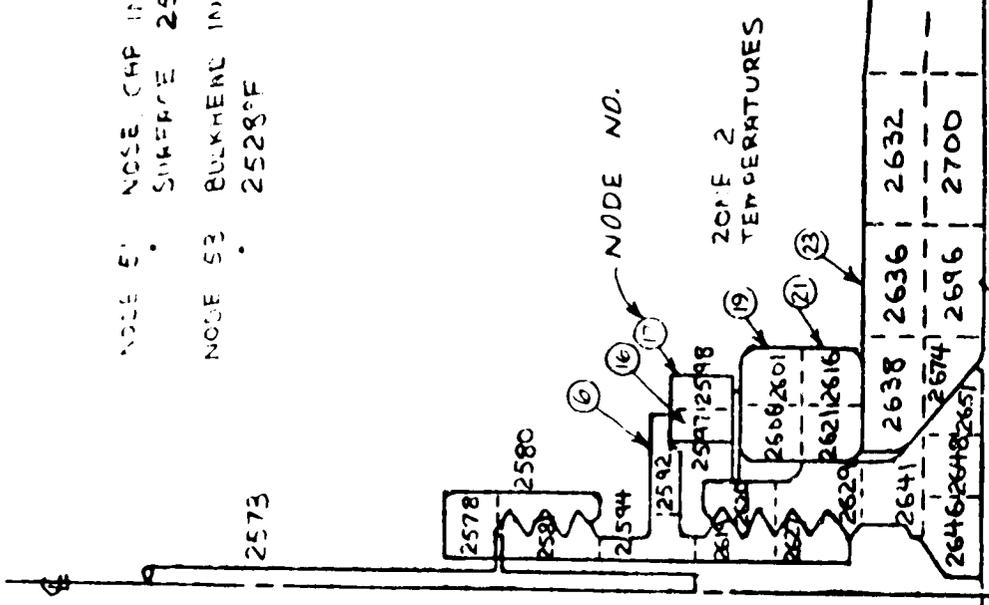
FIGURE 5-13 — TEMPERATURE DISTRIBUTION (°F) AT 700 SECONDS PENETRATION PLUG LOCATION NO. 7 WINDWARD SIDE

167

ZONE 2 NODE NO.	ZONE 1 NODE NO. (TEMP.)	ZONE 3 NODE NO. (TEMP.)	ΔT
6	37 (2270)°F	45 (2299)°F	29
16	36 (2269)	44 (2287)	18
17	38 (2268)	46 (2287)	19
19	39 (2257)	47 (2293)	36
21	40 (2247)	48 (2274)	27
23	41 (2244)	49 (2246)	2
51	50 (2119)	52 (2567)	N.A.

NODE 51 · NOSE CAP INSIDE SURFACE 2344°F

NODE 52 · BULKHEAD INSULATION 2346°F

NODE NO.

ZONE 2 TEMPERATURES
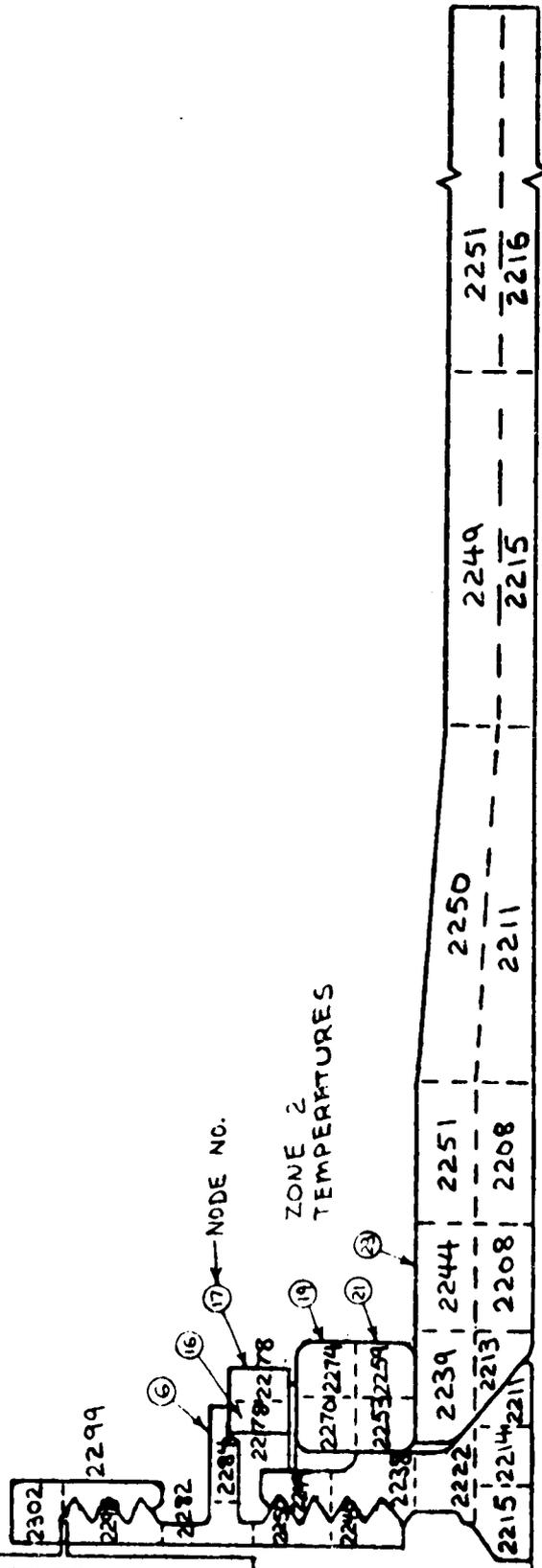
FIGURE 5-14 – TEMPERATURE DISTRIBUTION (°F) AT 700 SECONDS
PENETRATION PLUG LOCATION NO. 1 LEEWARD SIDE

168
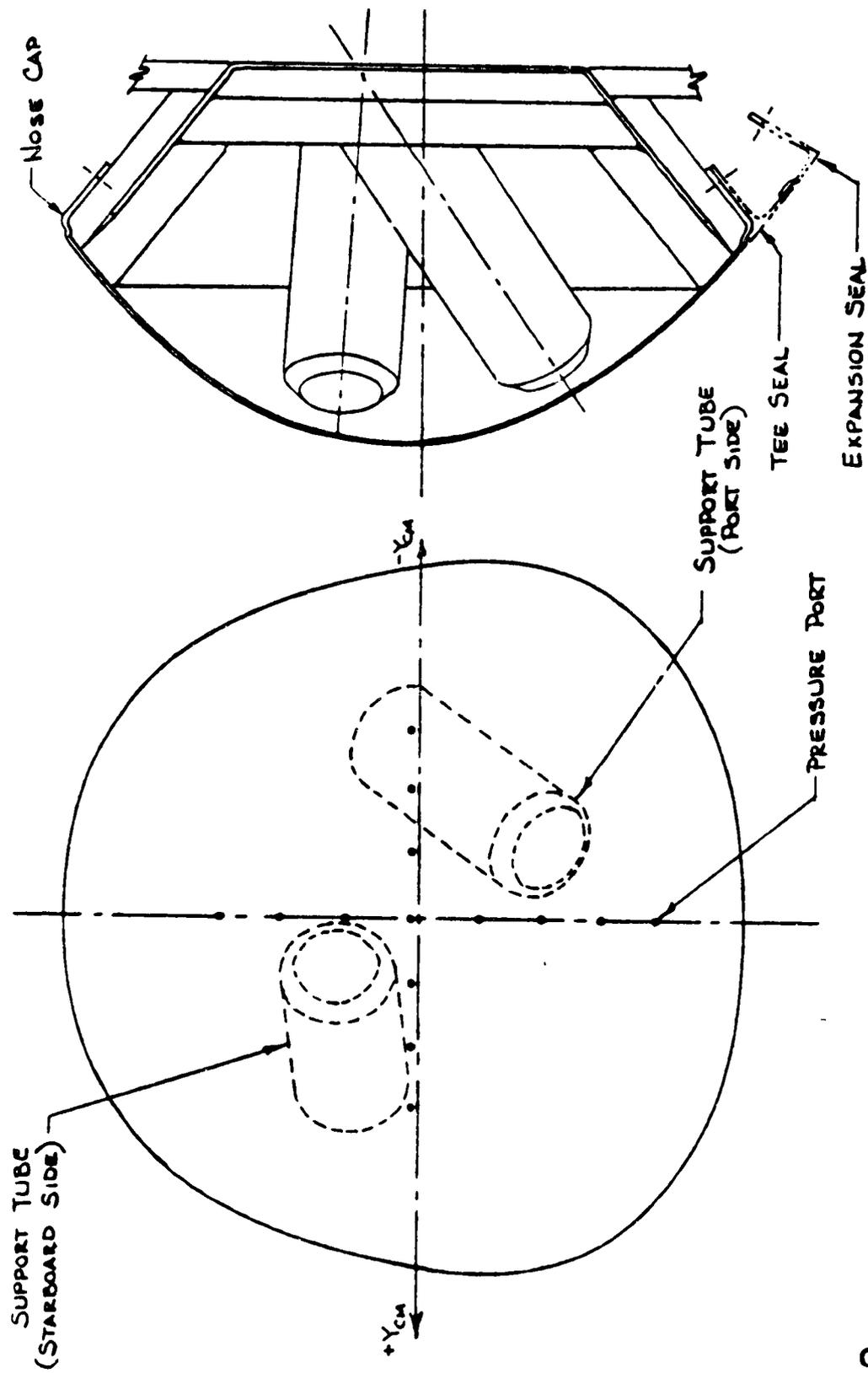
FIGURE 5-15 - SEADS SUPPORT TUBE ARRANGEMENT

NOSE CAP

SUPPORT TUBE
(PORT SIDE)

TEE SEAL

EXPANSION SEAL

PRESSURE PORT

SUPPORT TUBE
(STARBOARD SIDE)

$-Y_{CM}$

$+Y_{CM}$

(a.) EXTERNAL SURFACE NODES

(b) INTERNAL SURFACE NODES

FIGURE 5-16 - CHANGE IN PEAK TEMPERATURES CAUSED BY SUPPORT TUBES
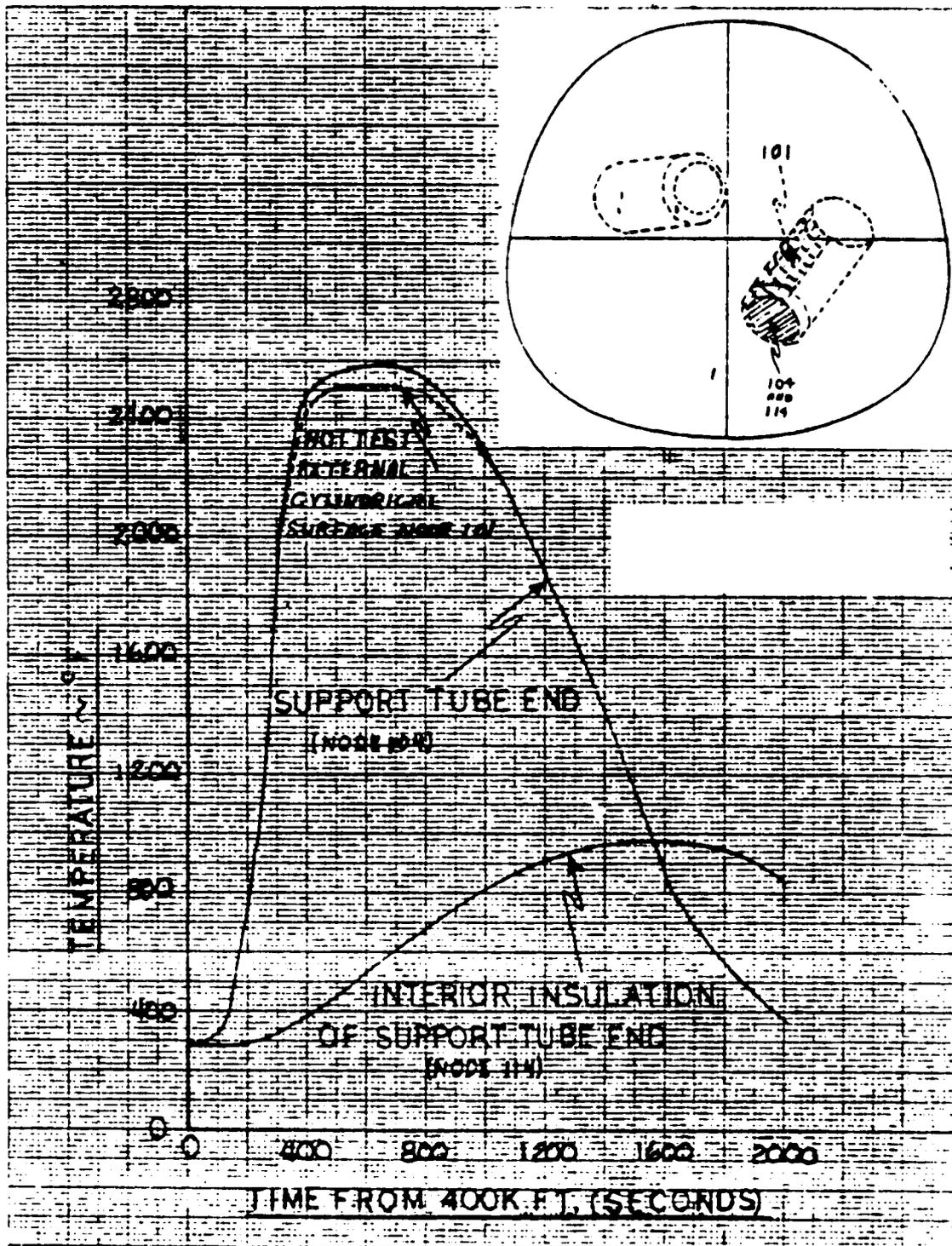
FIGURE 5-17 - SUPPORT TUBE TEMPERATURES - PORT SIDE
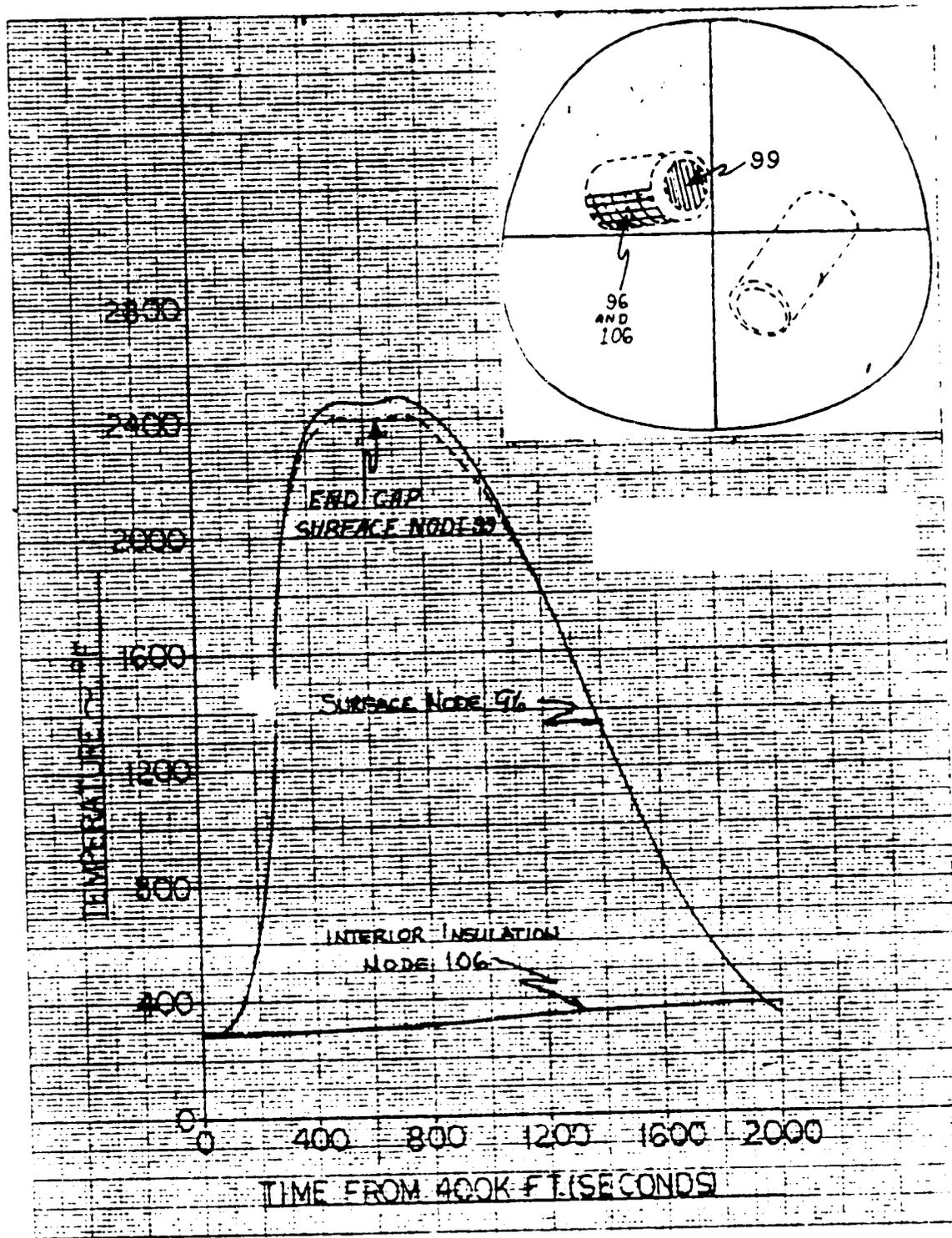
FIGURE 5-18 - SUPPORT TUBE TEMPERATURE - STARBOARD SIDE
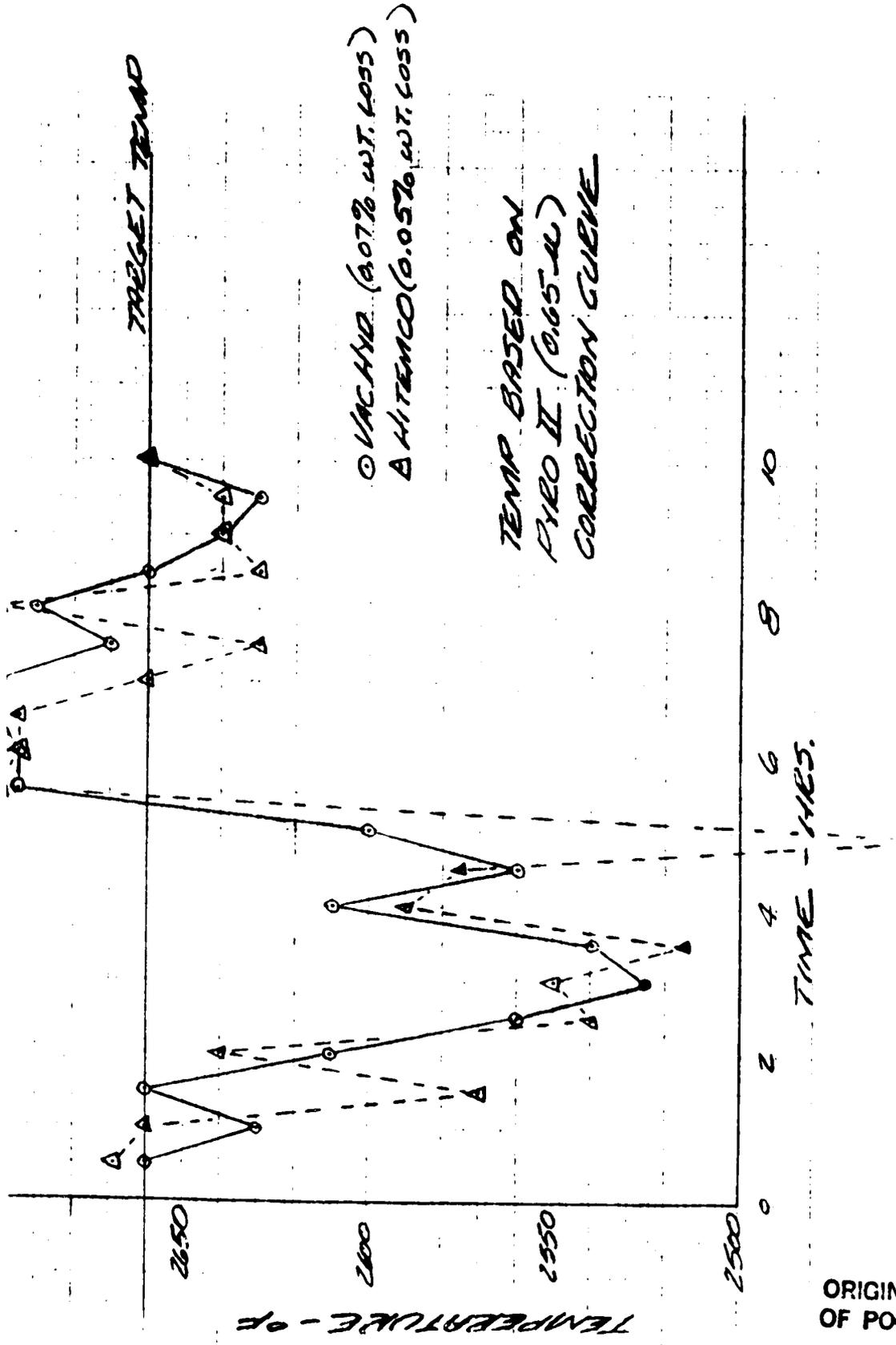
FIGURE 6-1 - COATED COLUMBIUM DISCS, 180 KW PLASMA ARC TEST

173

LOAD & DEFLECTION

4.00"

~ 1.6"

PRESS. TUBE OR STEEL ROD

FERRULES (SERIES I TESTS C

NUT

UNION

PORT

SPACER TUBE

2.8" D. R

CLAMP
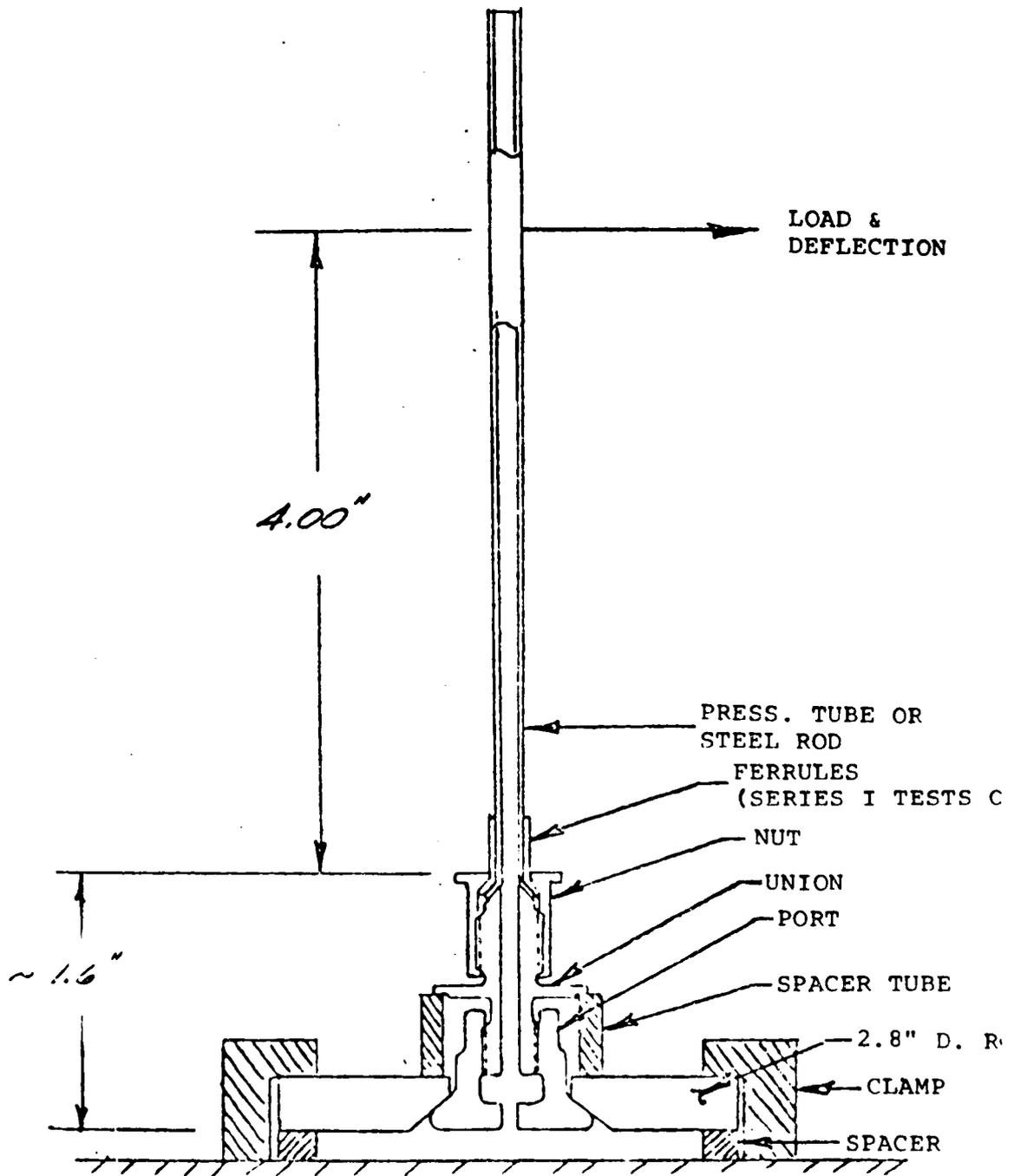
SPACER

FIGURE 6-2 - BENDING TEST SETUP
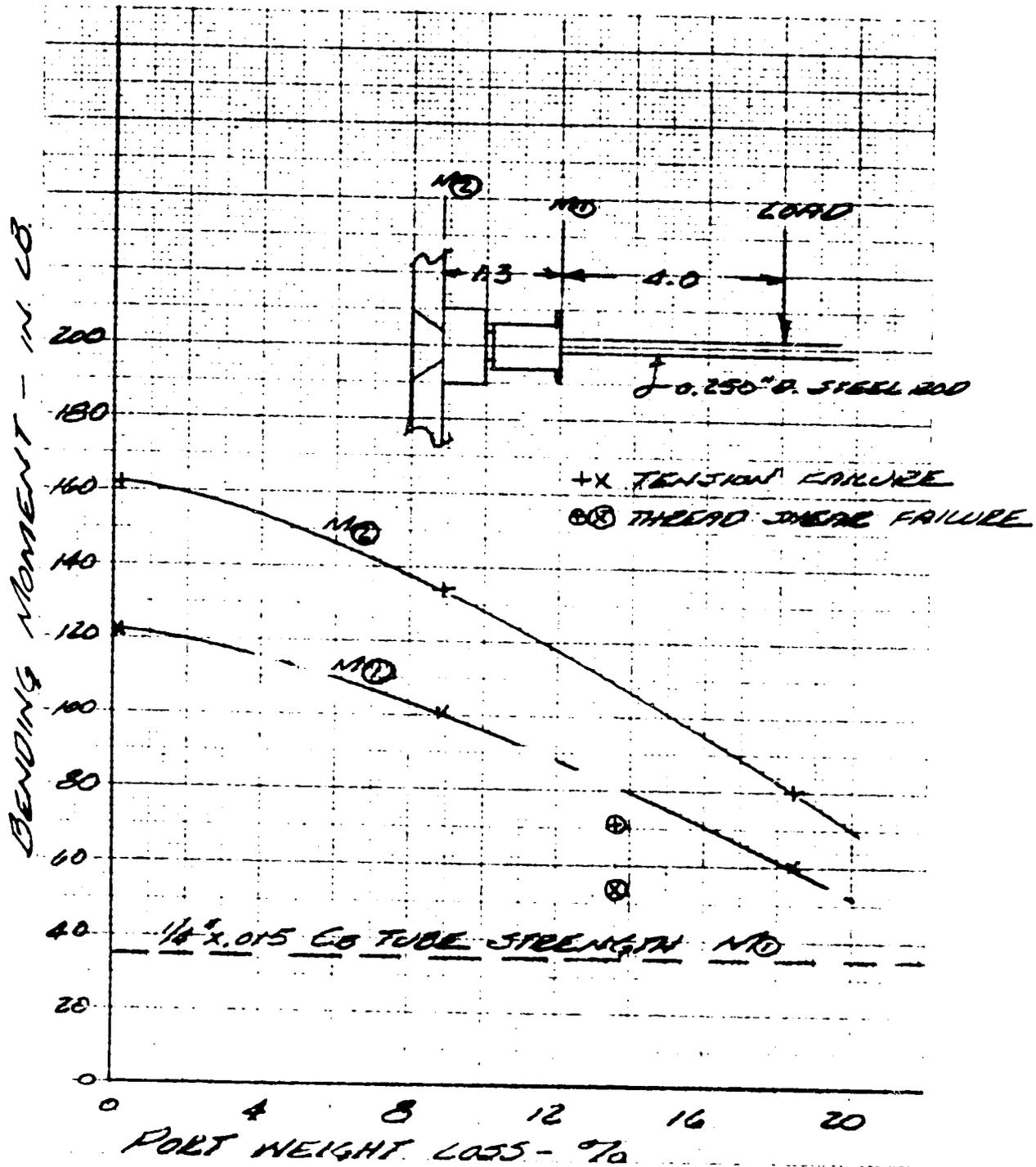
FIGURE 6-3 - GRAPHITE PORT BENDING FAILING LOAD TEST, SERIES 2
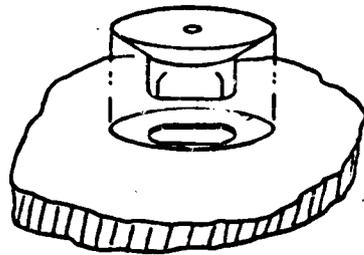
CONCEPT 1 — FLATS ON PORT MATCH ROU' FLATS IN NOSE CAP (FLAT SIDED HOLE)
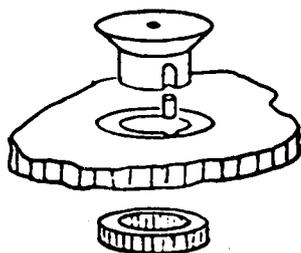
CONCEPT 2 — PORT KEYED TO NOSE CAP BY PIN / SPACER TRAPS PIN
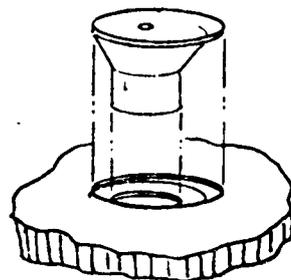
CONCEPT 3 — ECCENTRIC COUNTERBORE
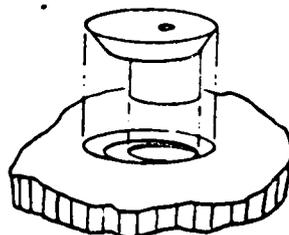
CONCEPT 4 — ECCENTRIC COUNTERSINK

FIGURE 6-4 – SEADS SYSTEM ANTI-ROTATION CONCEPTS

CONCEPT 5
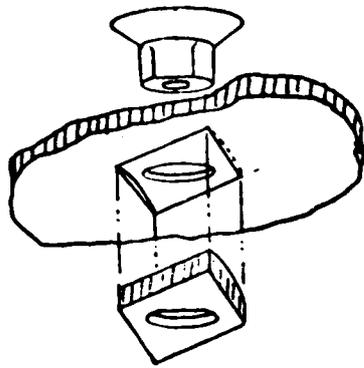
FLATS ON PORT MATCH FLATS
ON SPACER

SPACER KEYED TO NOSE CAP BY
SHALLOW ROUNDED IMPRESSION

CONCEPT 6
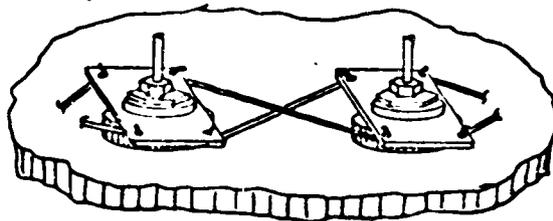
CROSS WIRING BETWEEN
ASSEMBLIES PROVIDES MUTUAL
SUPPORT

CONCEPT 7
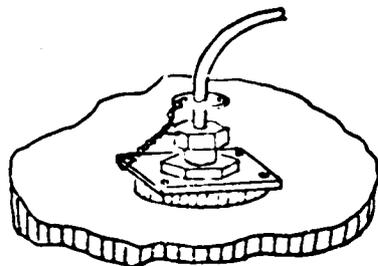
PRESSURE TUBE LOCKWIRED TO
PENETRATION ASSEMBLY TO
LIMIT ROTATION

CONCEPT 8
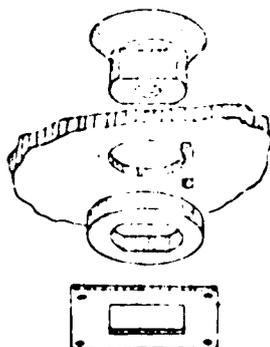
FLATS ON PORT MATCH FLATS ON
SPACER

SPACER KEYED TO NOSE CAP BY
TRAPPED BALL

(BALL LOCK)

FIGURE 6-4 (CON'T.) - SEADS SYSTEM ANTI-ROTATION CONCEPTS
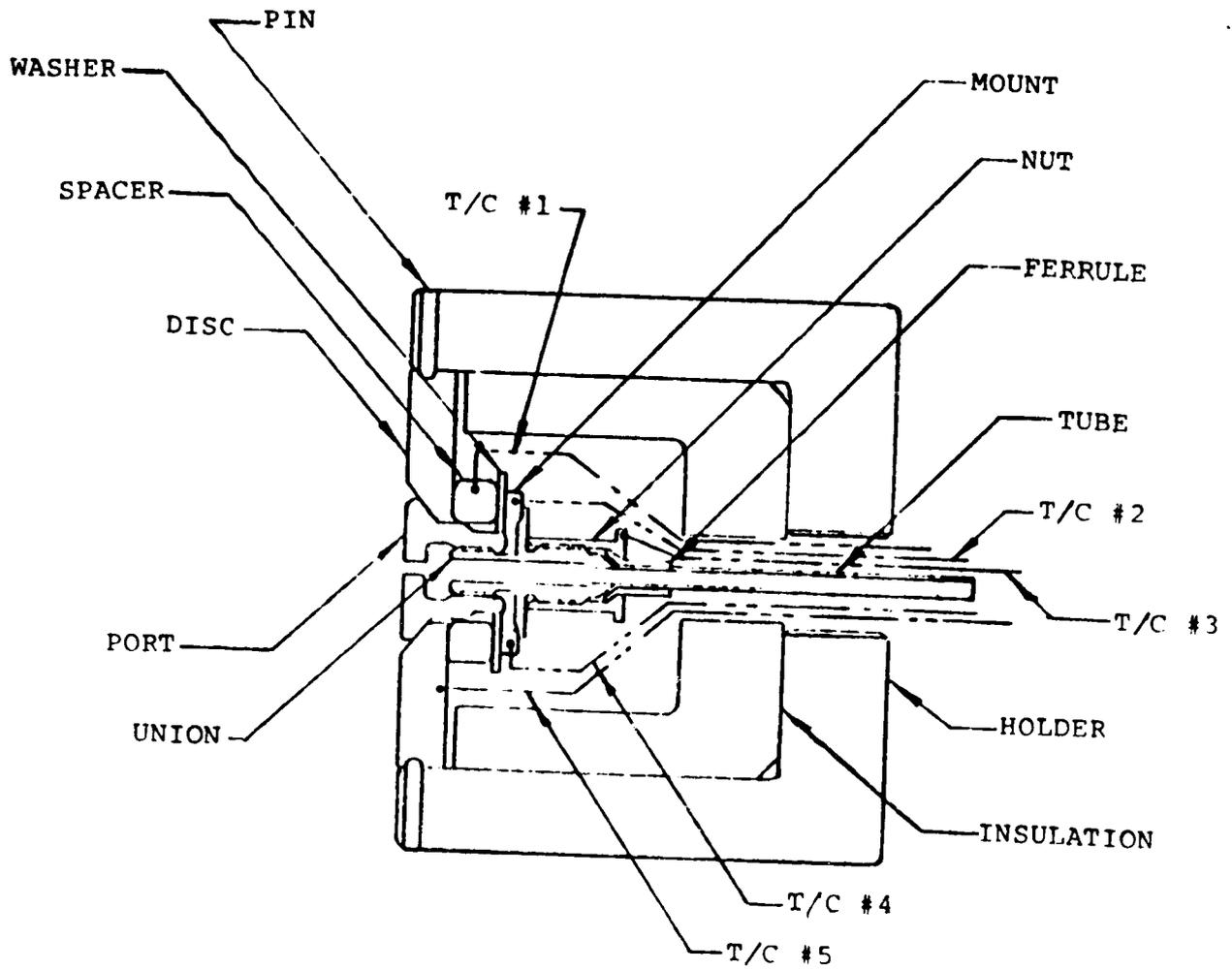
FIGURE 7-1 - TEST MODEL CONFIGURATION

T/C TUNGSTEN 5% RHENIUM/TUNGSTEN 26% RHENIUM 3 REQD

2219L4005-10 HOLDER

2219L4005-11 INSULATION

2219T4031-103 PIN 4 REQD

2219T4071-12 DISC
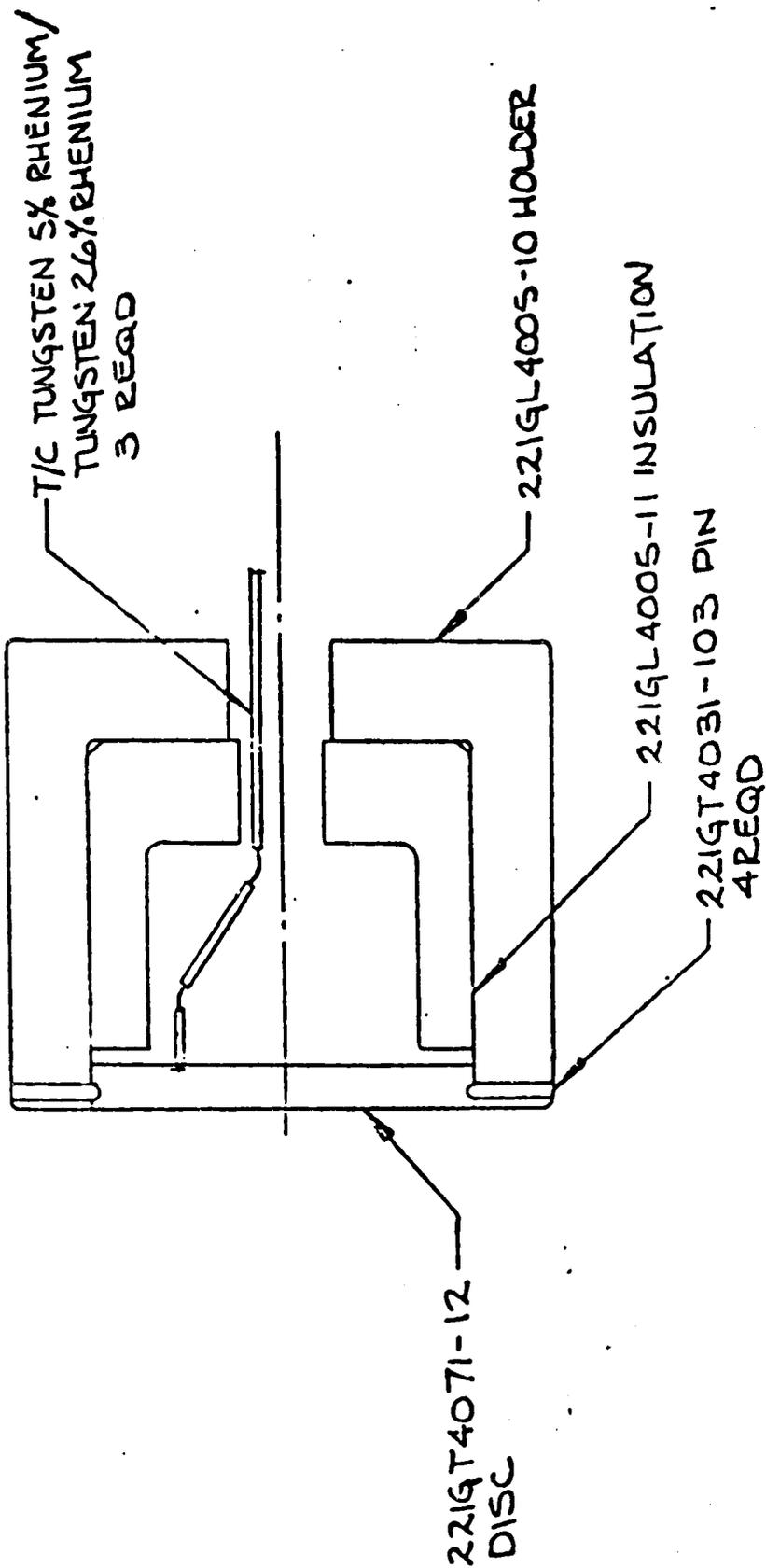
FIGURE 7-2 - CALIBRATOR CONFIGURATION

179

FERRULES

PORT

NUT

T/C MOUNT

FIGURE 5-2 - S-GLASS COMPOSITE, 5 HOURS EXPOSURE

FIGURE 7-4 - -2 MODEL PRESSURE TUBE, 5 HOURS EXPOSURE

FIGURE 7-6 - -2 MODEL PORT FRONT FACE, 5 HOURS EXPOSURE

FIGURE 7-7 - -2 MODEL LOCKWASHER, 5 HOURS EXPOSURE

FIGURE 7-8 – PYROMETER INDICATED TEMPERATURE CORRECTION TO RCC TRUE TEMPERATURE
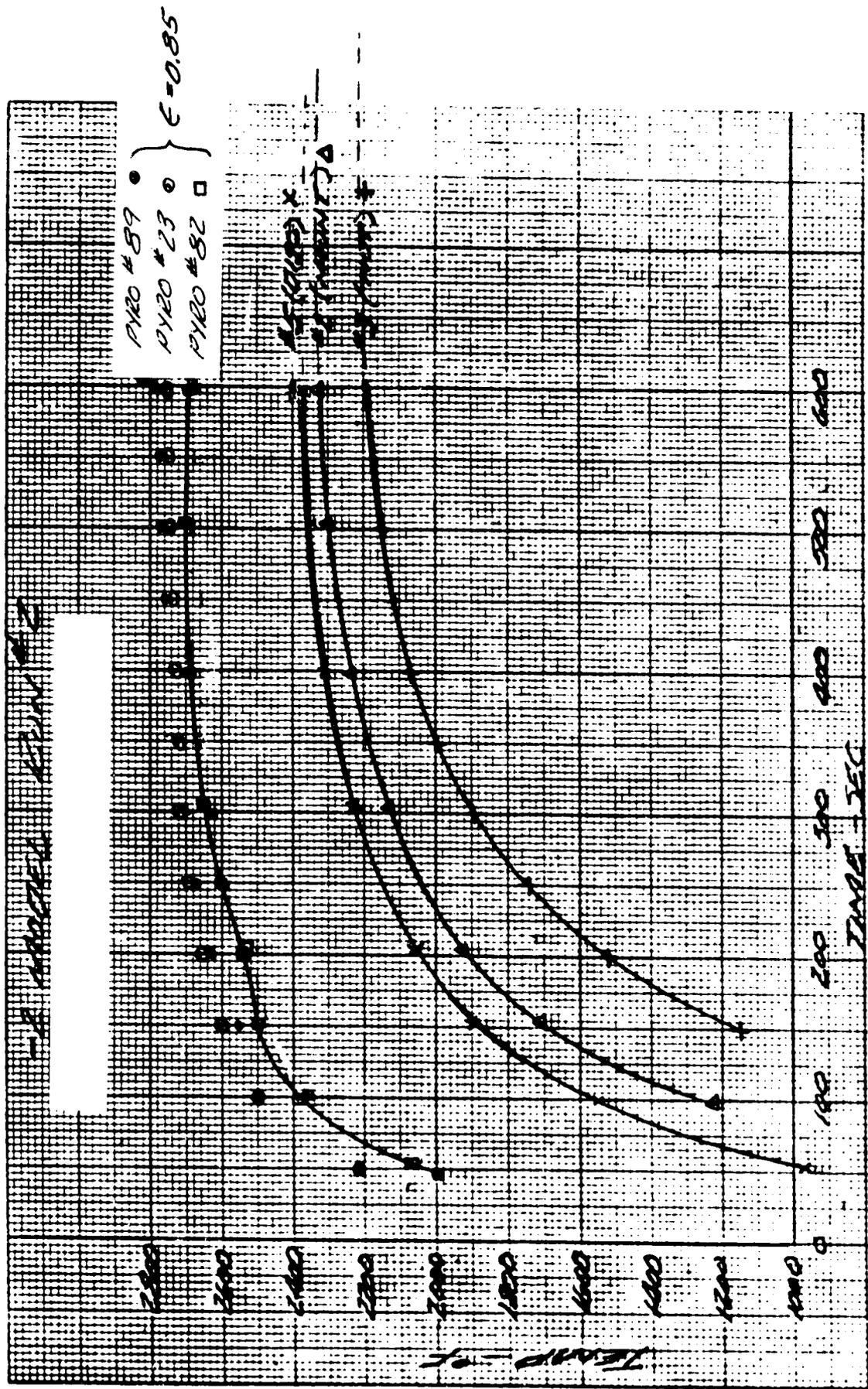
FIGURE 7-9 - TEMPERATURE HISTORY
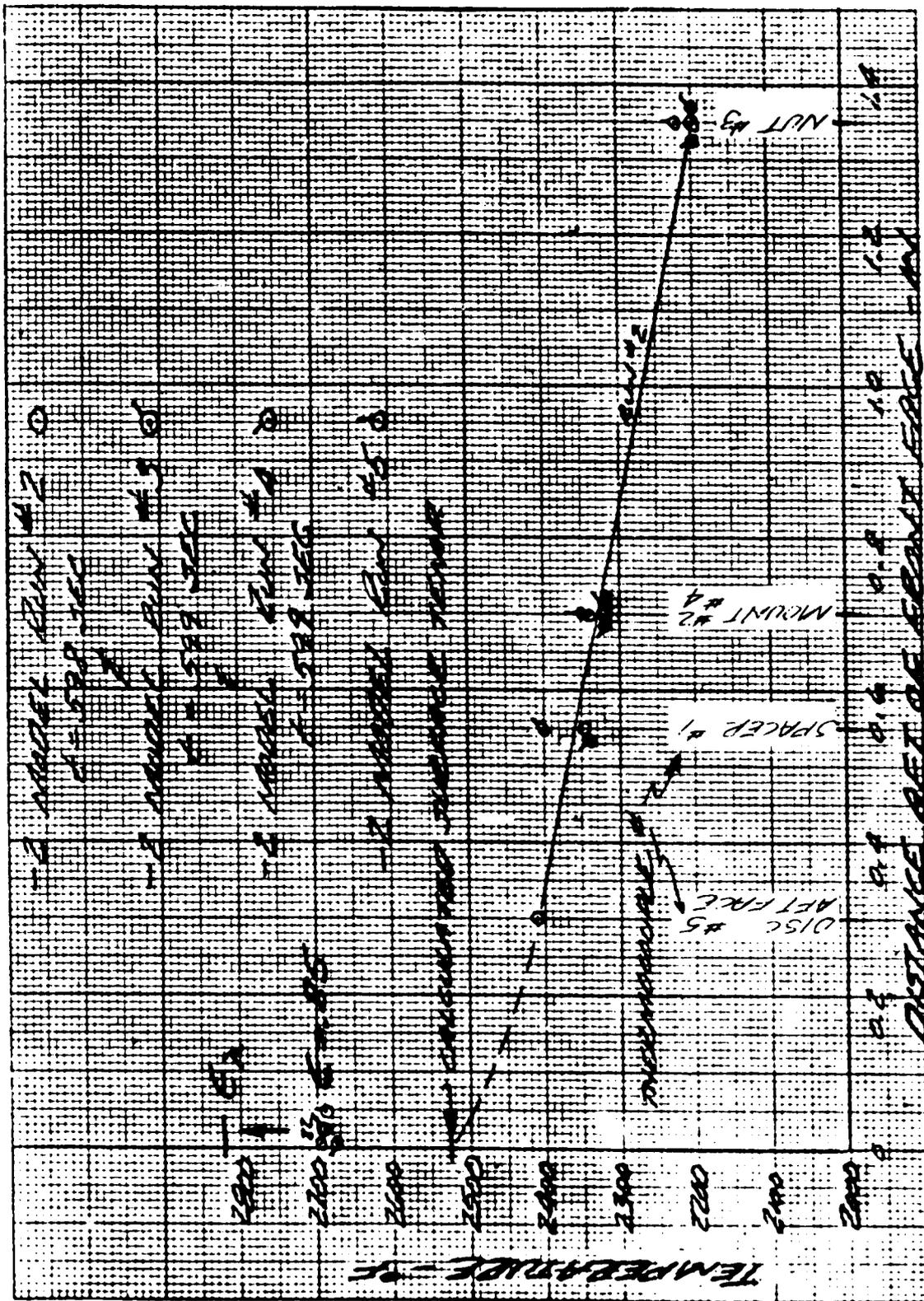
FIGURE 7-10 - END OF RUN TEMPERATURE DISTRIBUTION

187
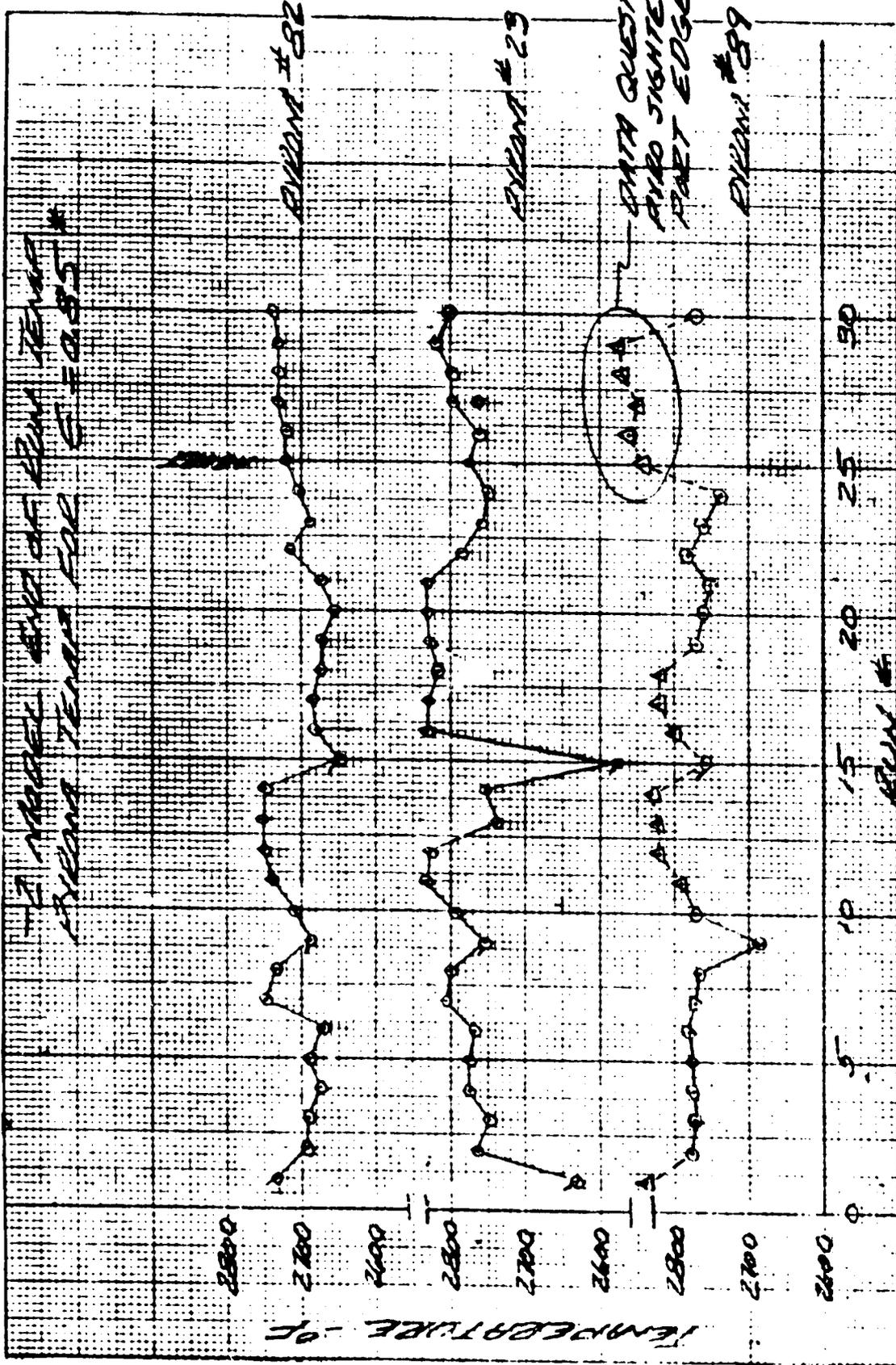
NOTE: DOES NOT INCLUDE 2.3 μ CORRECTION

188

FIGURE 7-12 - -1 MODEL FRONT FACE, 5 HOURS EXPOSURE

ORIGINAL PAGE
BLACK AND WHITE PHOTOGRAPH
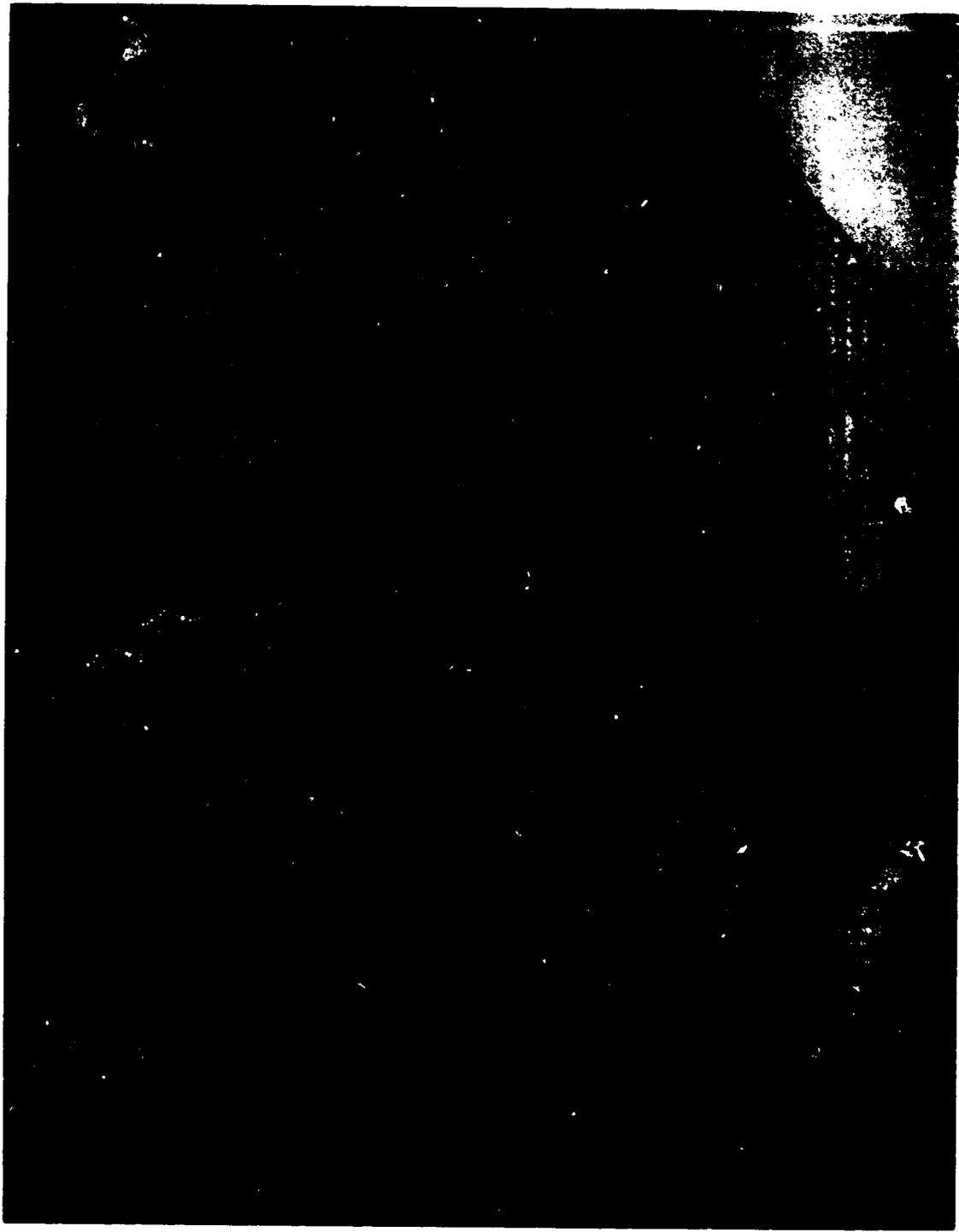
FIGURE 7-14 - -1 MODEL PCC DISC, 5 HOURS EXPOSURE
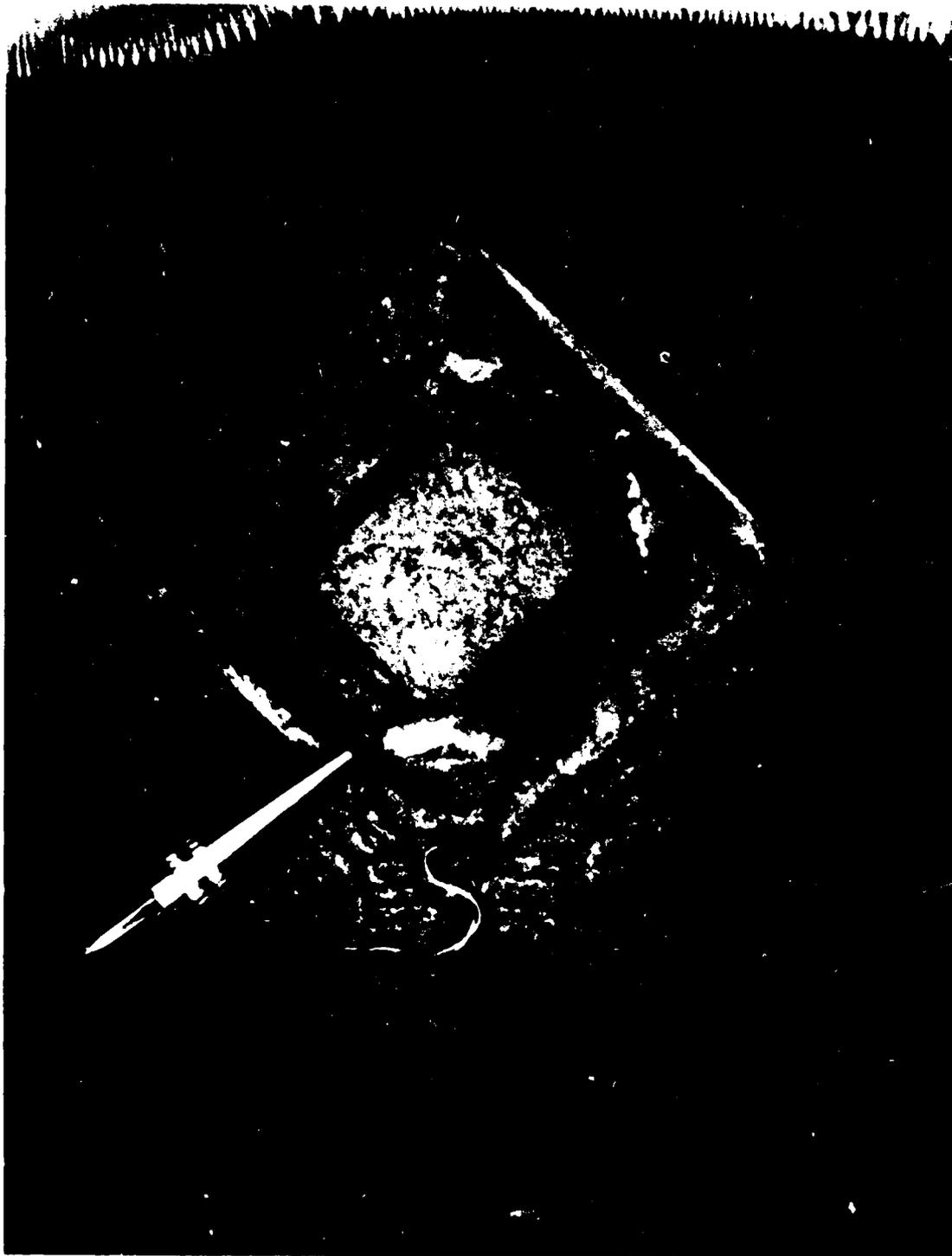
FIGURE 7-15 - -1 MODEL LOCKWASHER, 5 HOURS EXPOSURE
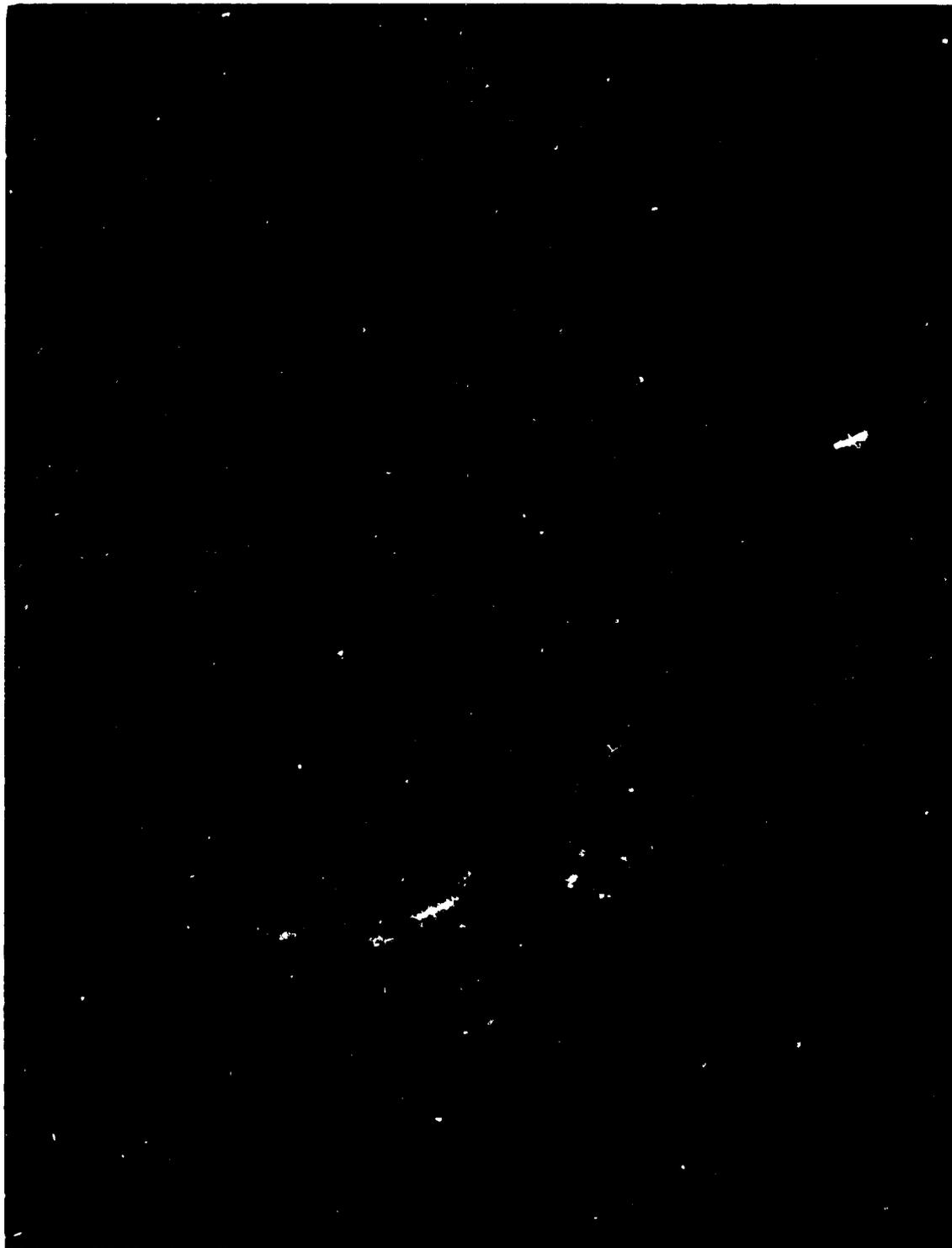
FIGURE 7-16 - -1 MODEL GRAPHITE PORT SHOWING CHIPPED THREADS, 5 HOURS EXPOSURE
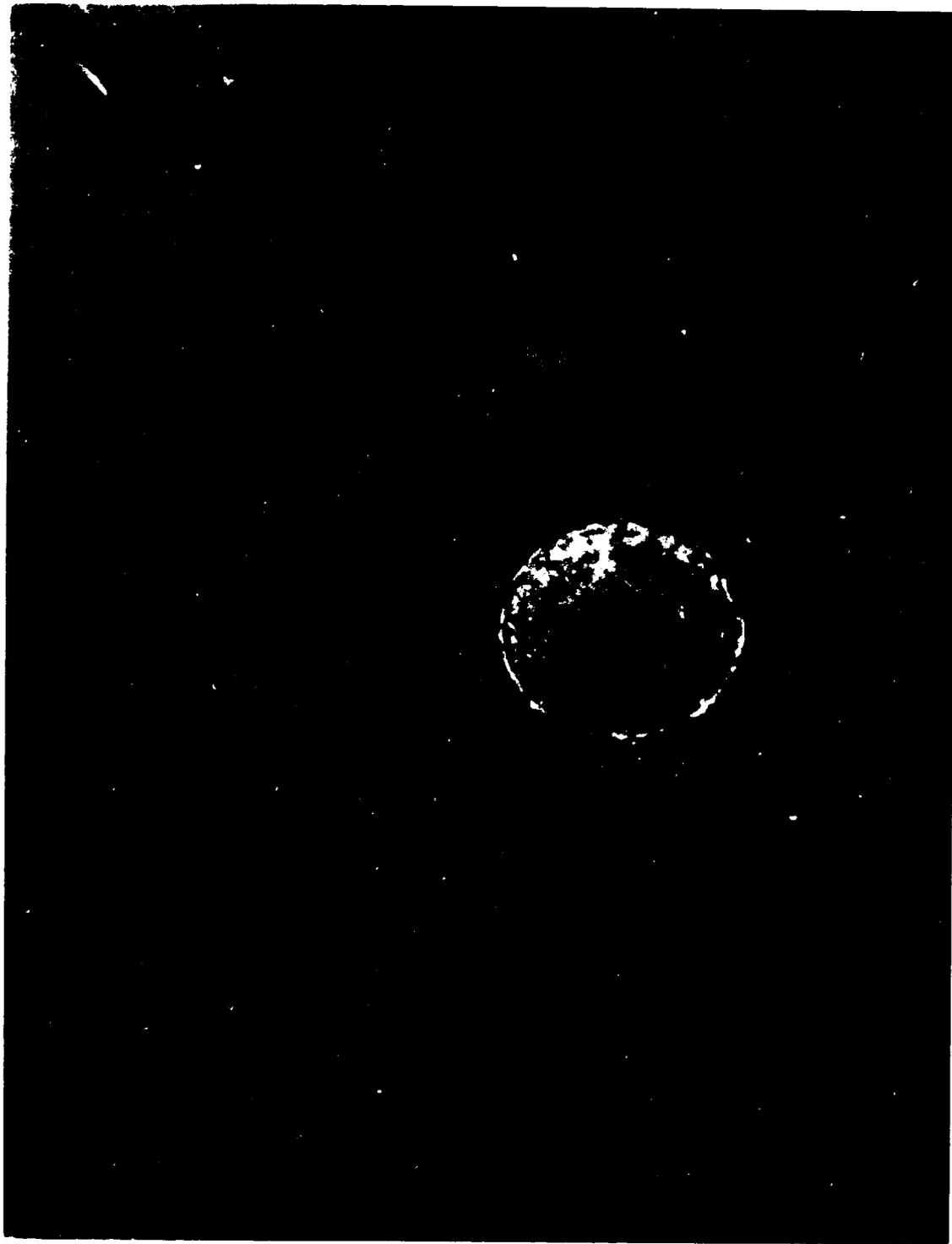
FIGURE 7-17 - -1 MODEL PRESSURE TUBE SHOWING LOCAL SCALLOPING
DUE TO OXIDATION, 5 HOURS EXPOSURE

FIGURE 7-18 - -1 MODEL UNION, 5 HOURS EXPOSURE

FIGURE 7-19 -- -1 MODEL NUT FLANGE SHOWING OXIDATION, 5 HOURS EXPOSURE
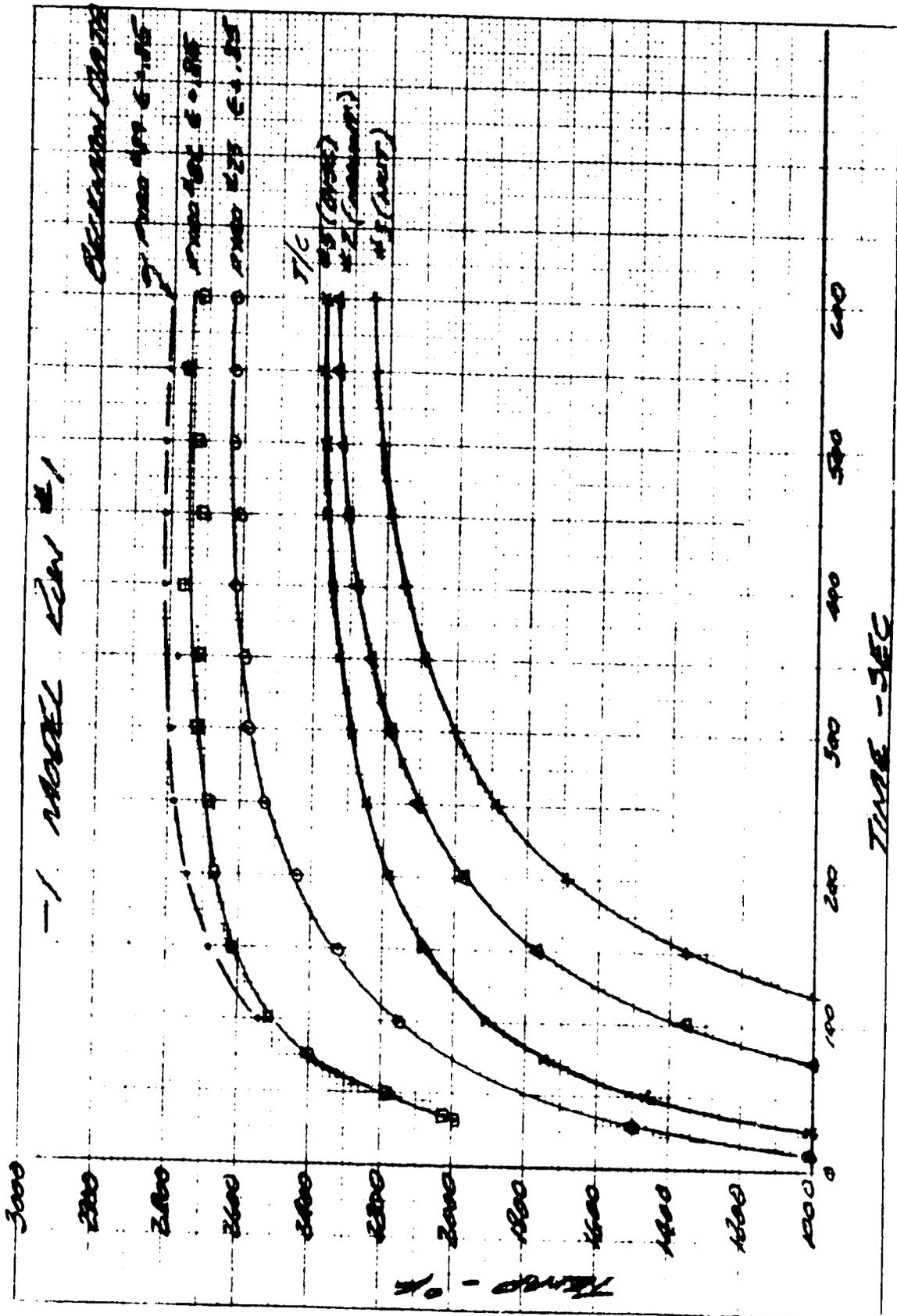
FIGURE 7-20 - TEMPERATURE HISTORY
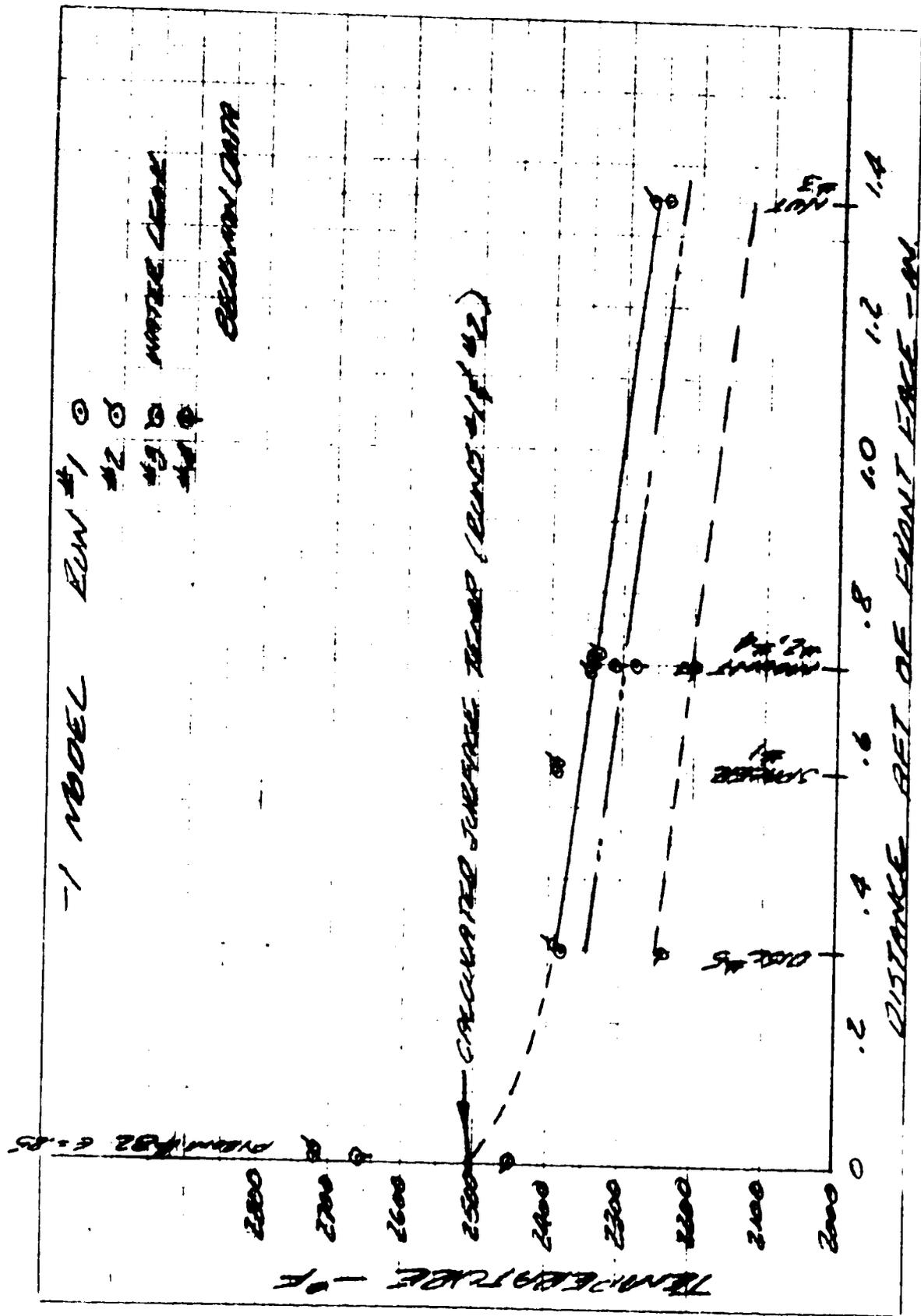
FIGURE 7-21 - END OF RUN TEMPERATURE DISTRIBUTION
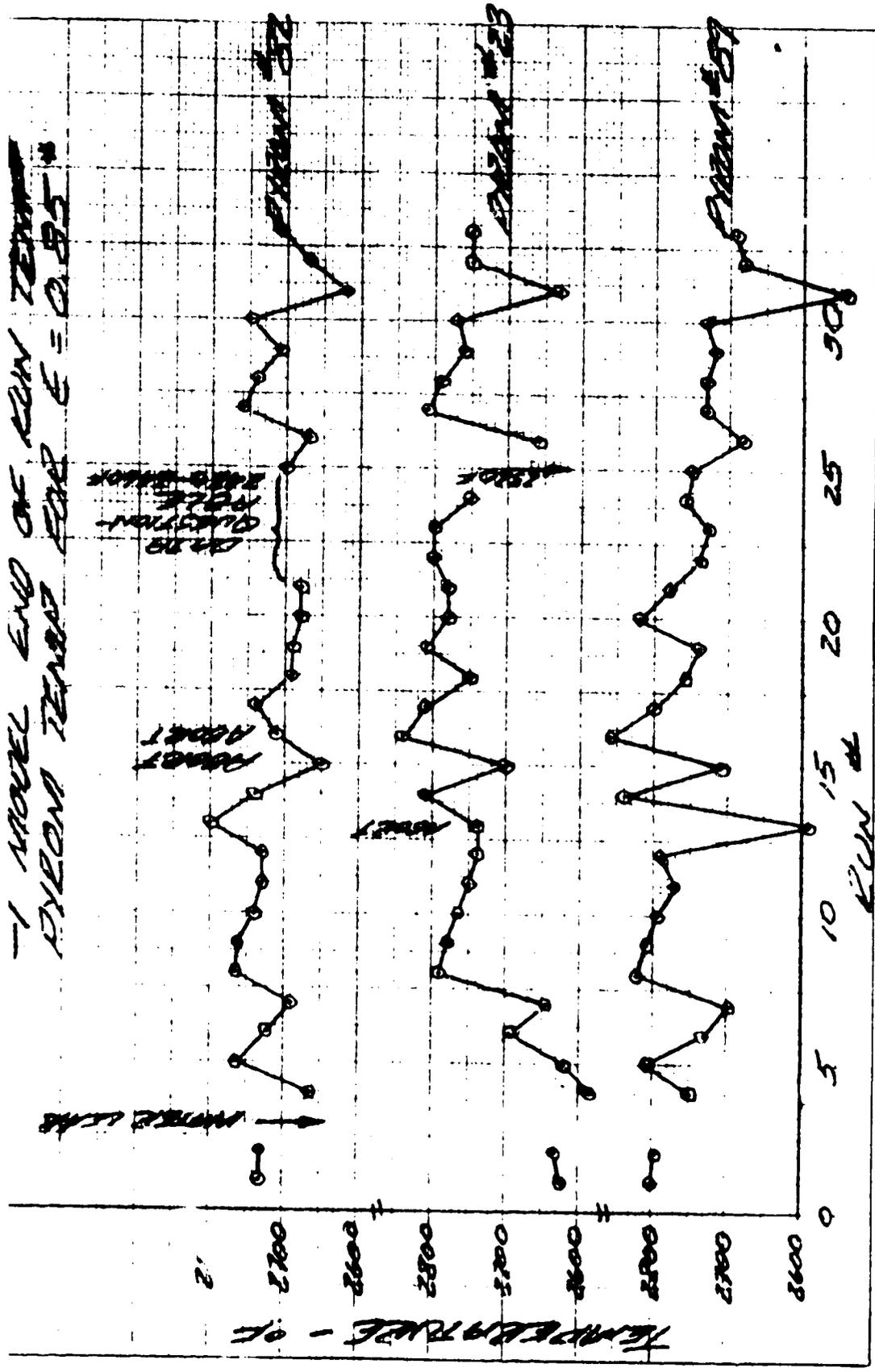
FIGURE 7-22 -- -1 MODEL END OF RUN TEMPERATURE
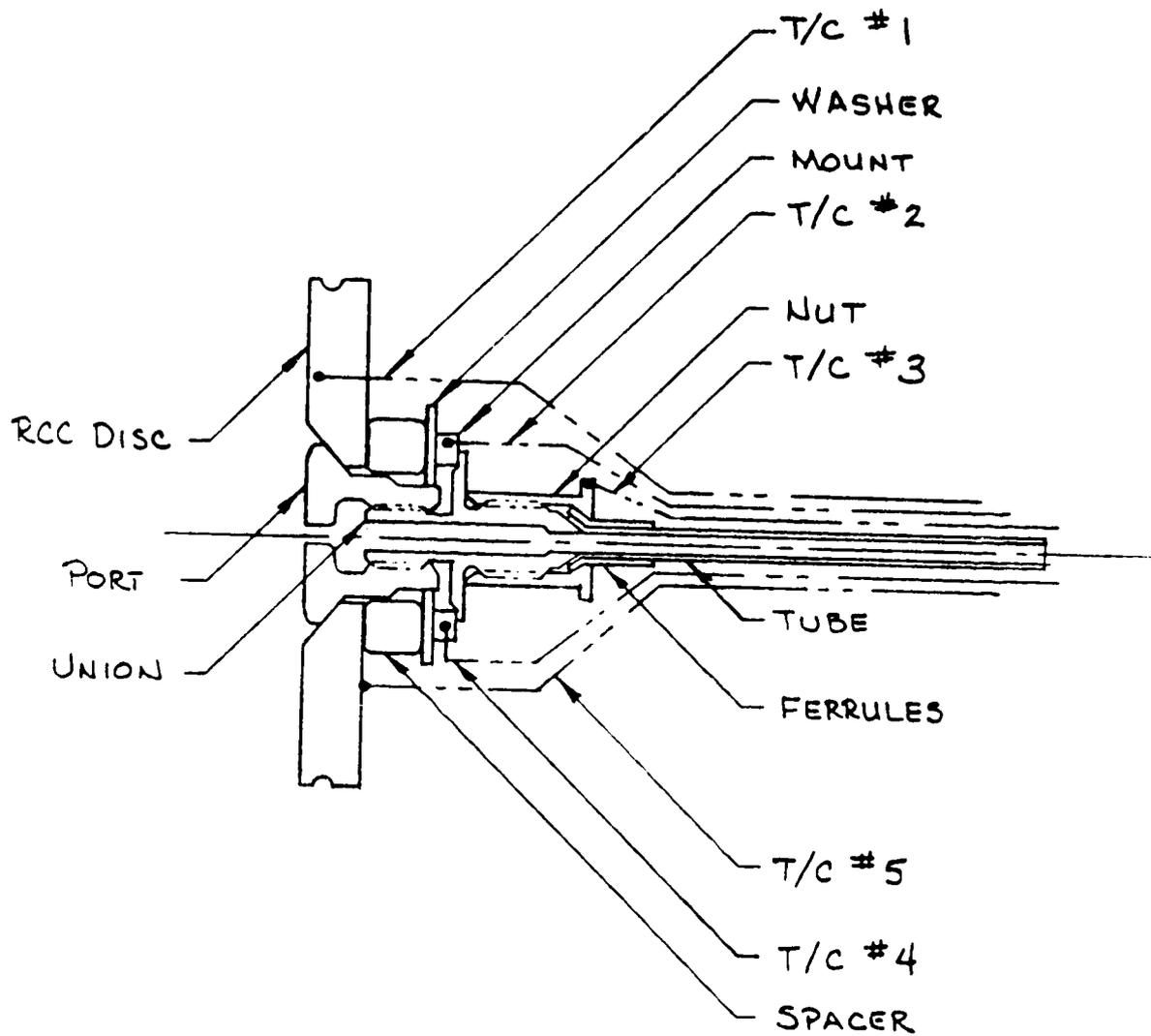
FIGURE 7-23 - SEADS PENETRATION TEST ASSEMBLY
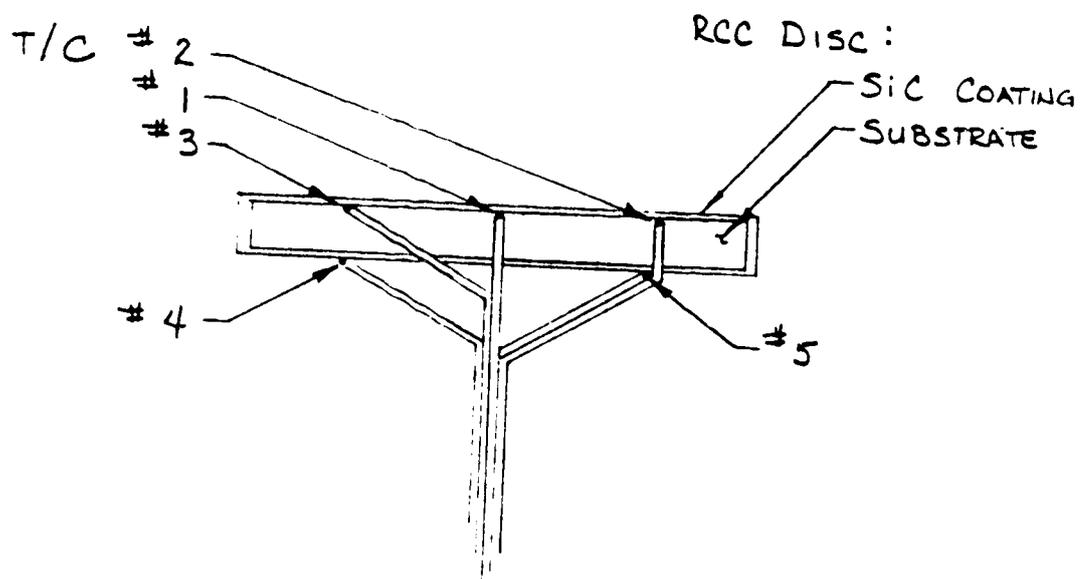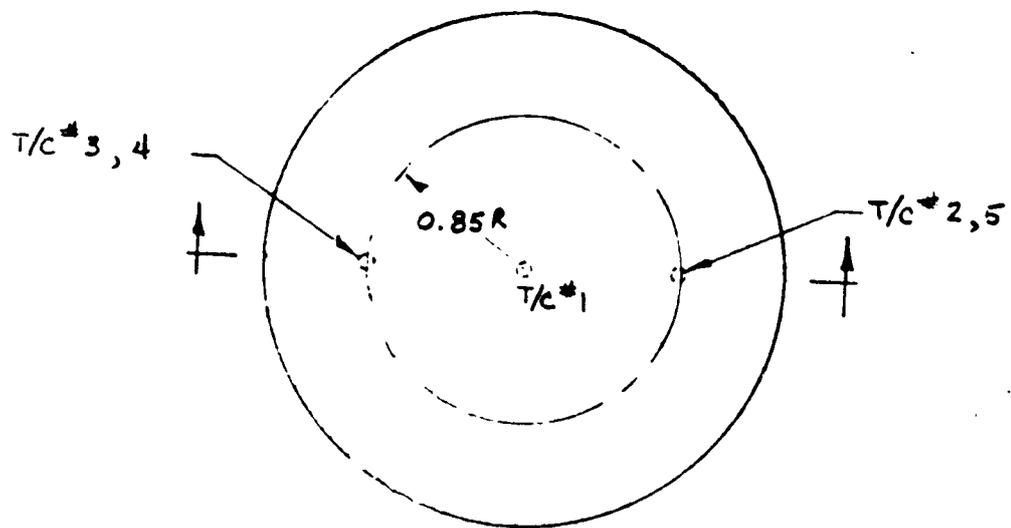
FIGURE 7-24 - SEADS CALIBRATION SPECIMEN
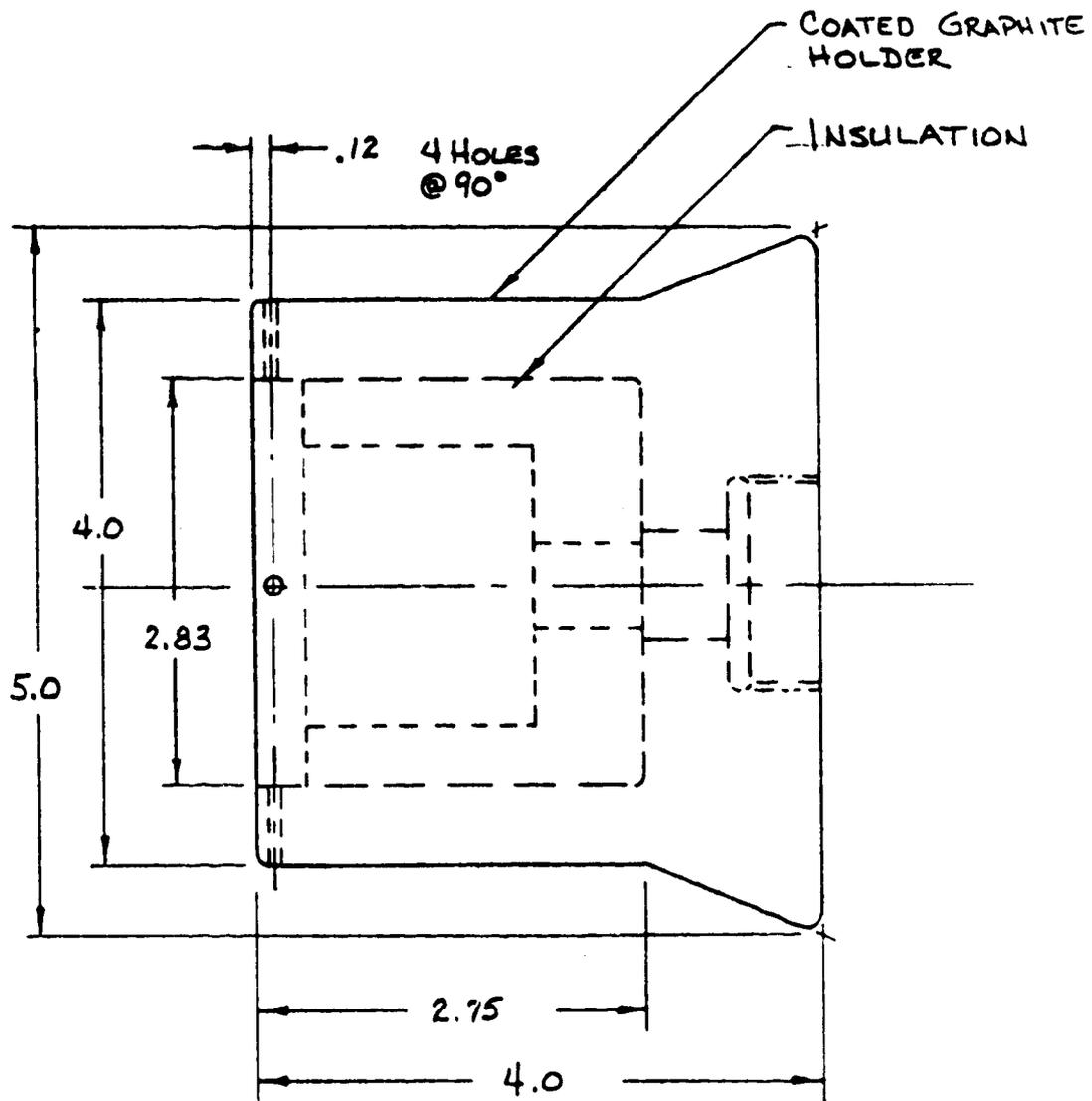
FIGURE 7-25 – SEADS MODEL HOLDER FOR NASA/ARC PLASMA ARC TEST
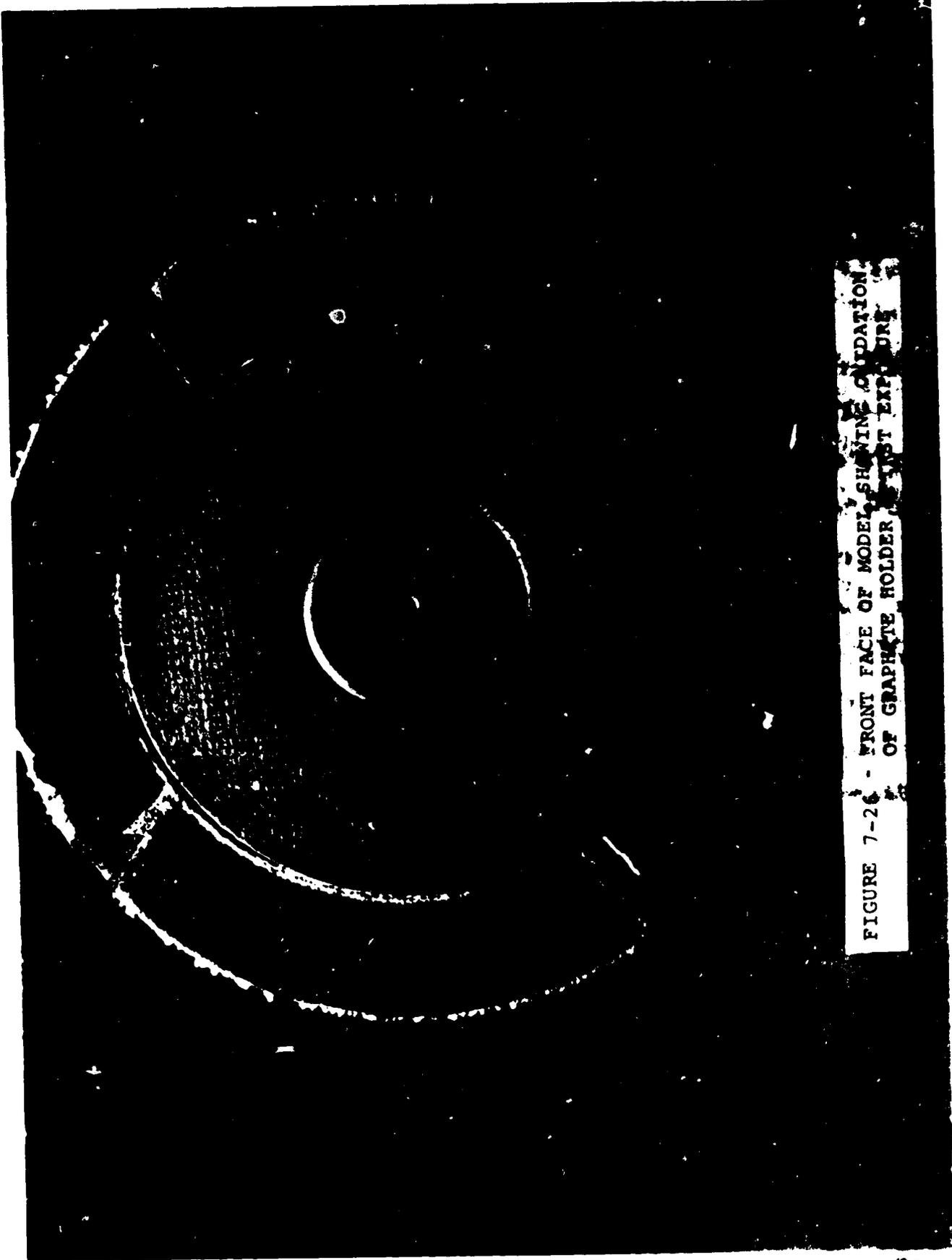
FIGURE 7-26 - FRONT FACE OF MODEL SHOWING OXIDATION OF GRAPHITE HOLDER FIRST EXPOSURE

FIGURE 7-27 - PENETRATION ASSEMBLY AFTER FIRST EXPOSURE

ORIGINAL PAGE
BLACK AND WHITE PHOTOGRAPH
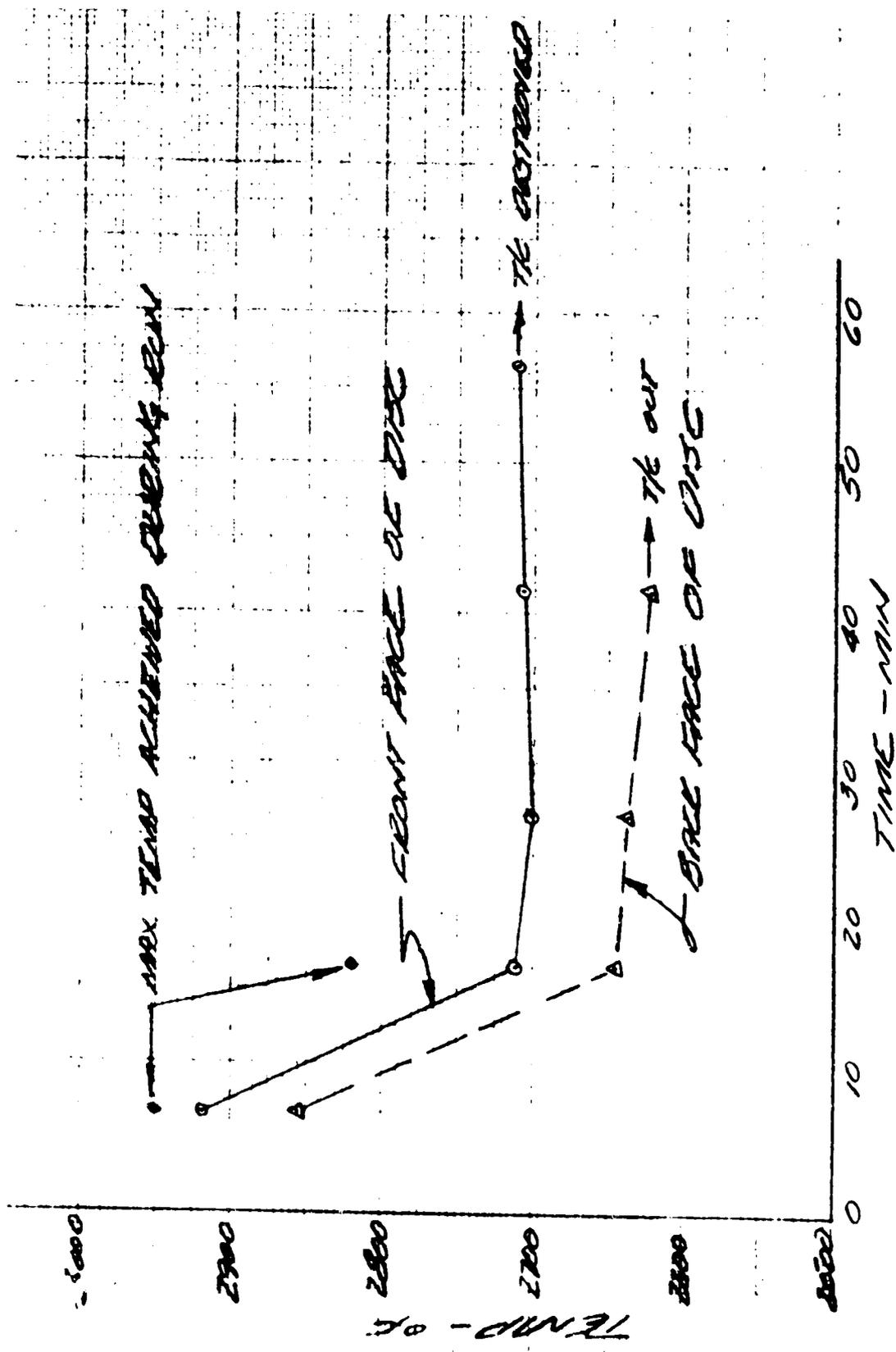
FIGURE 7-28 - END OF RUN THERMOCOUPLE TEMPERATURE

205

TIME - SEC

TEMP - °C
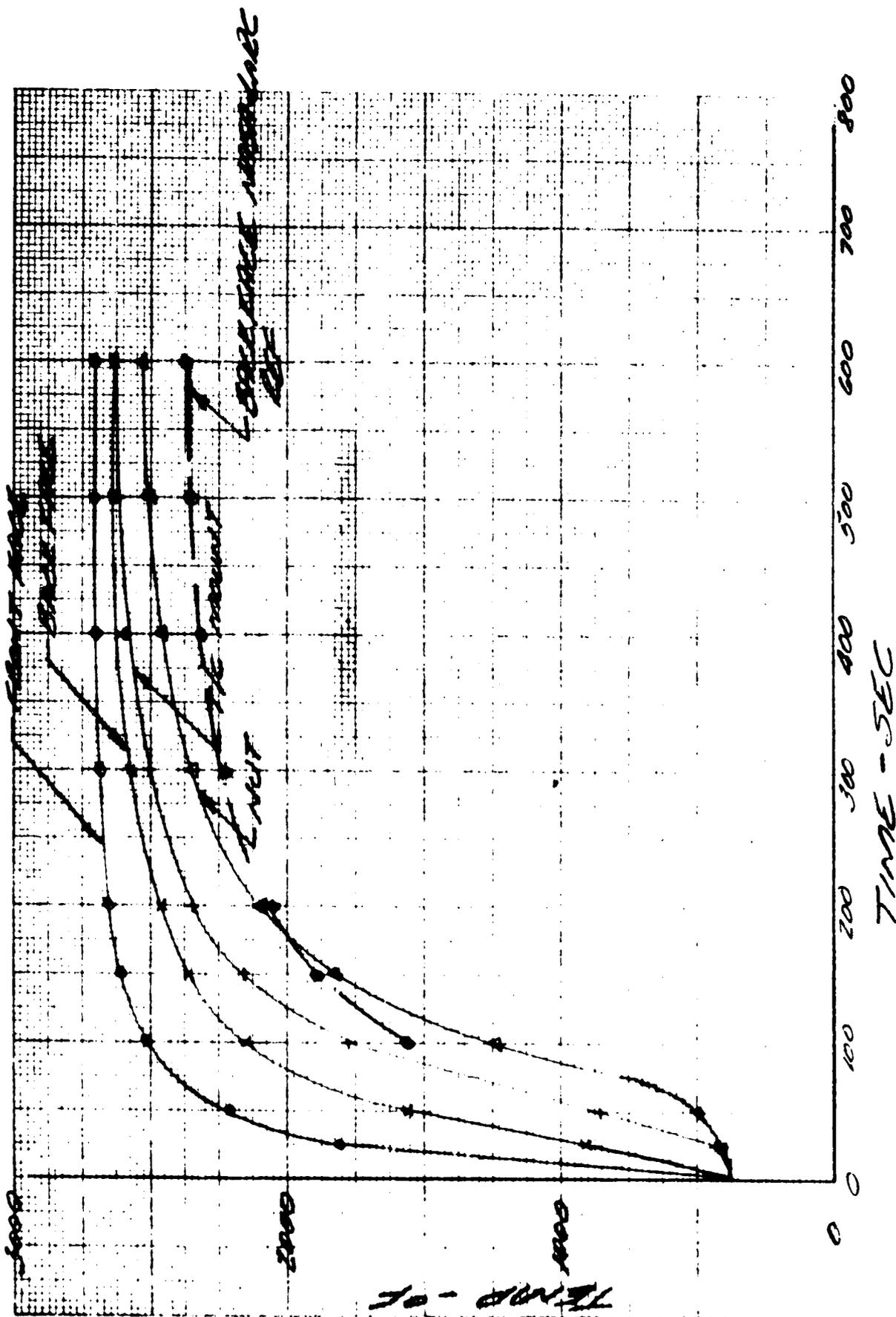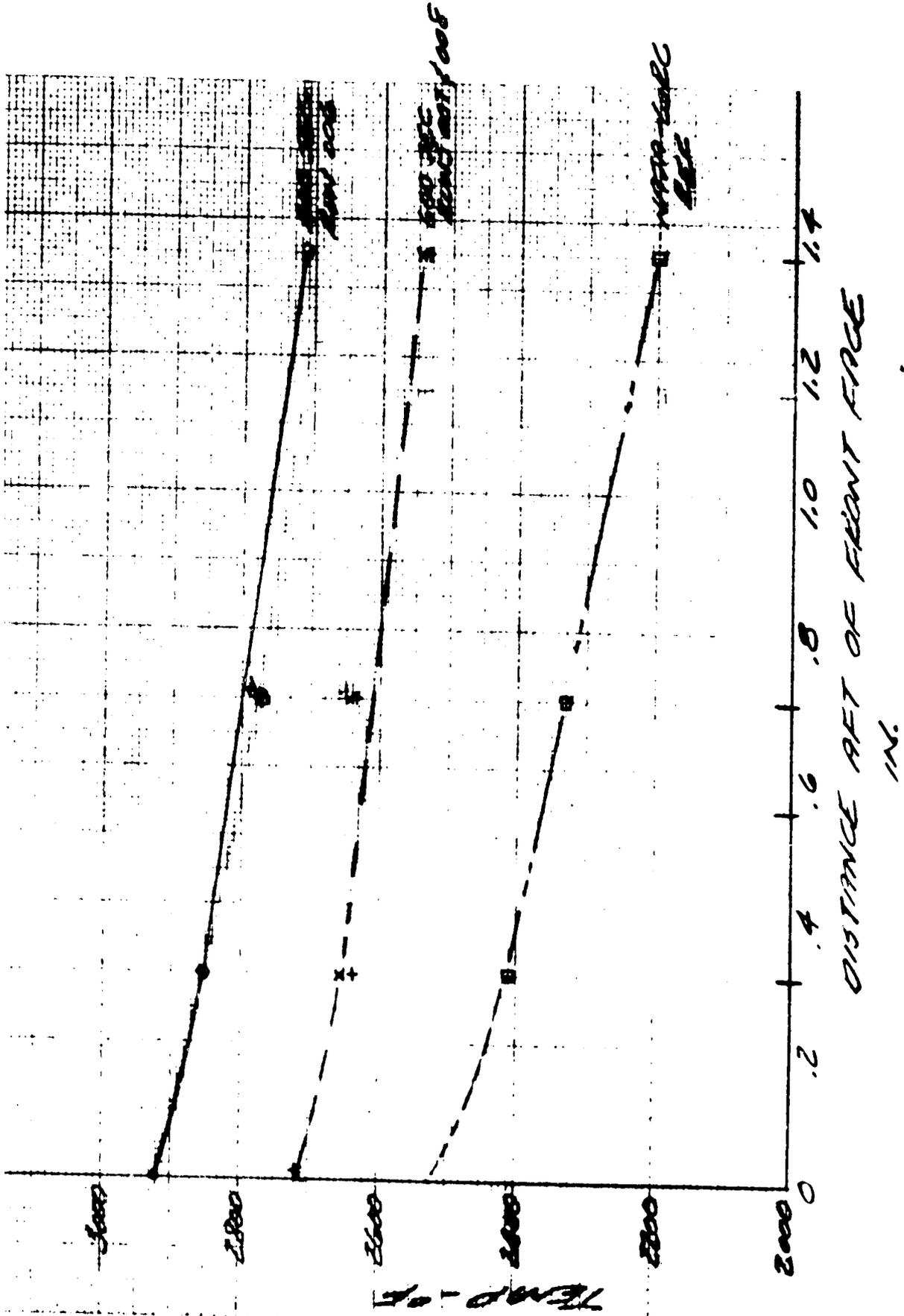
FIGURE 7-30 - END OF RUN TEMPERATURE DISTRIBUTION
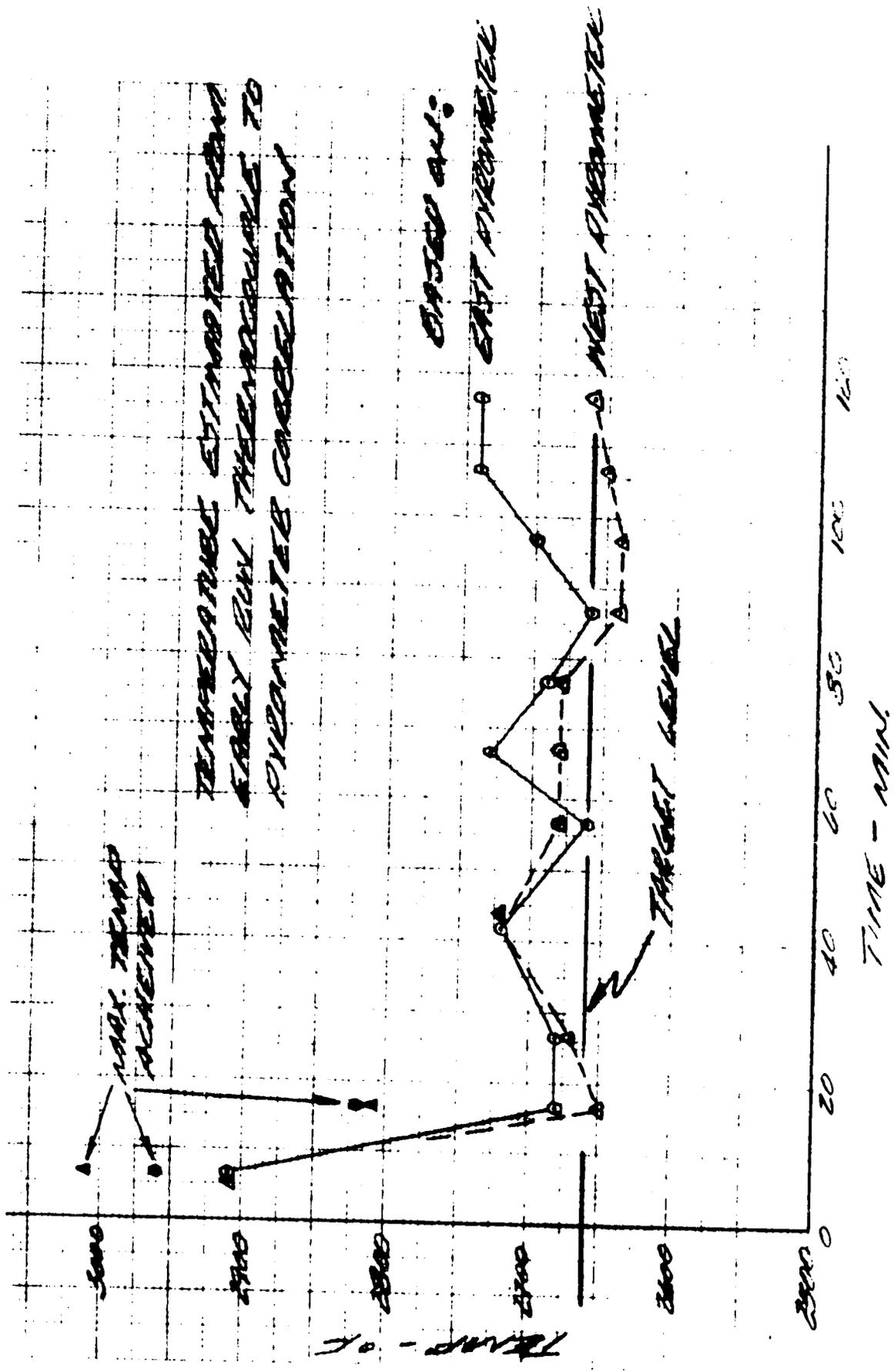
FIGURE 7-31 - FOOTMARKER END-OF-RUN TEMPERATURE
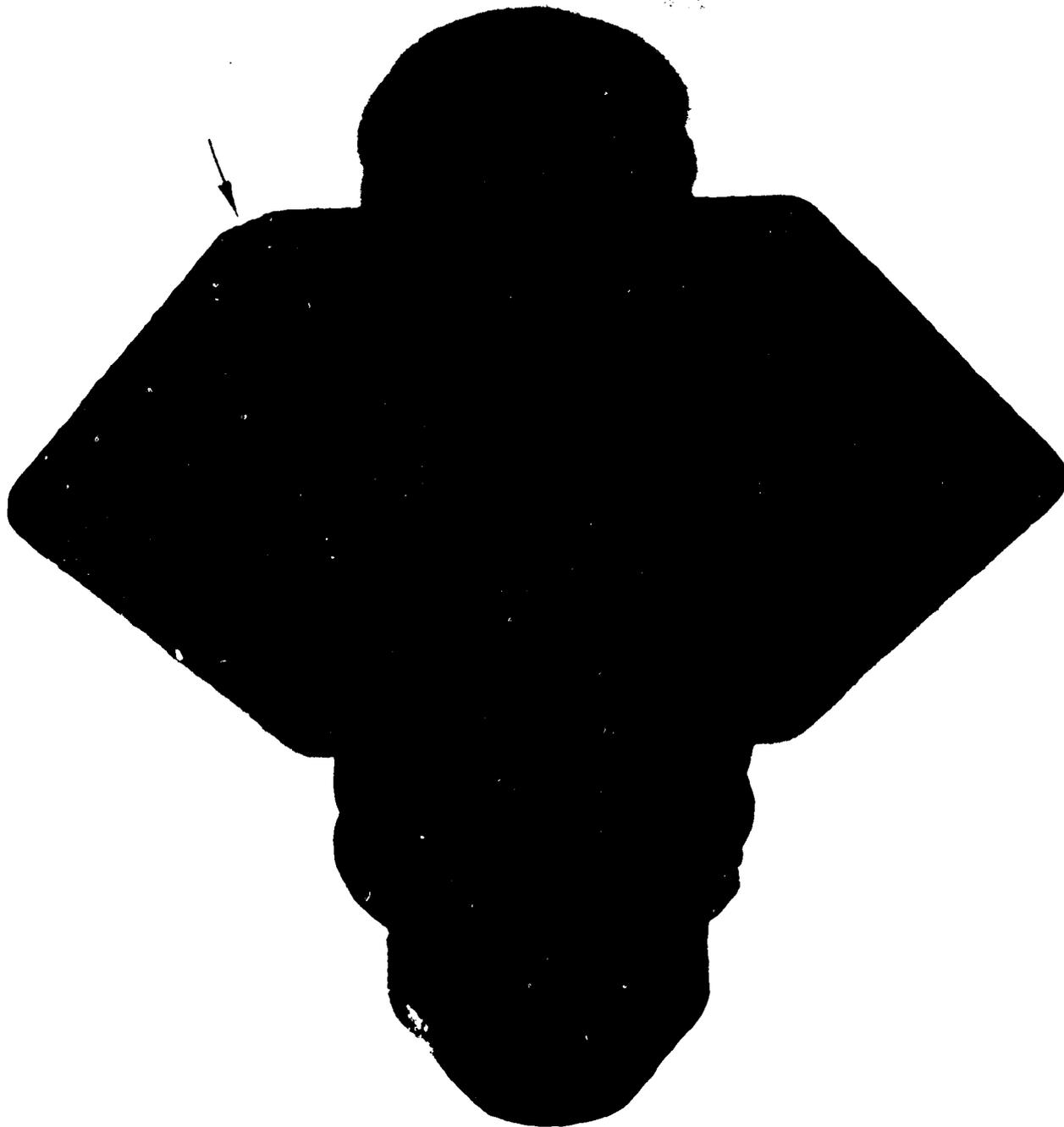
FIGURE 7-32 - UNION AT CONCLUSION OF TEST SHOWING DAMAGED AREA
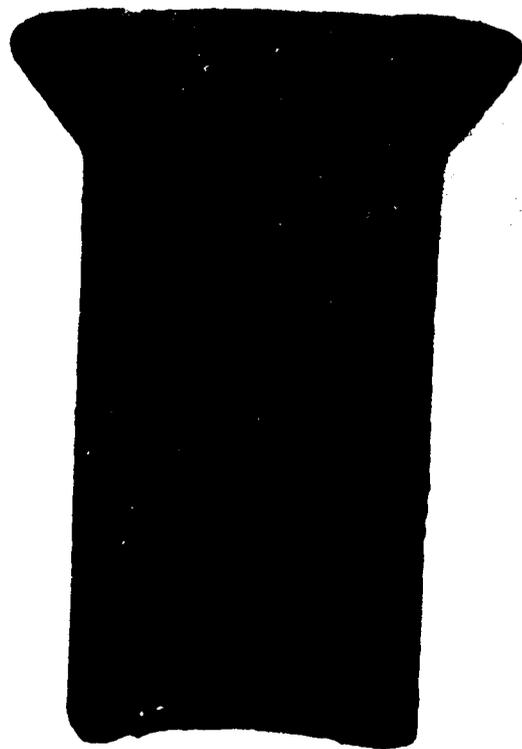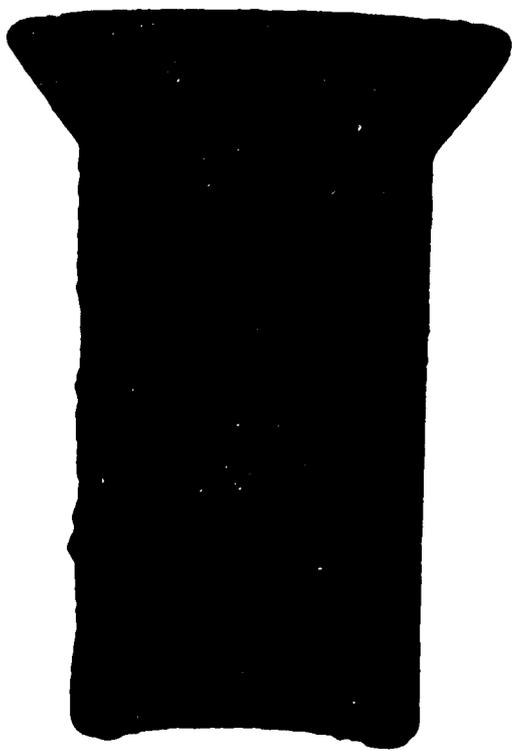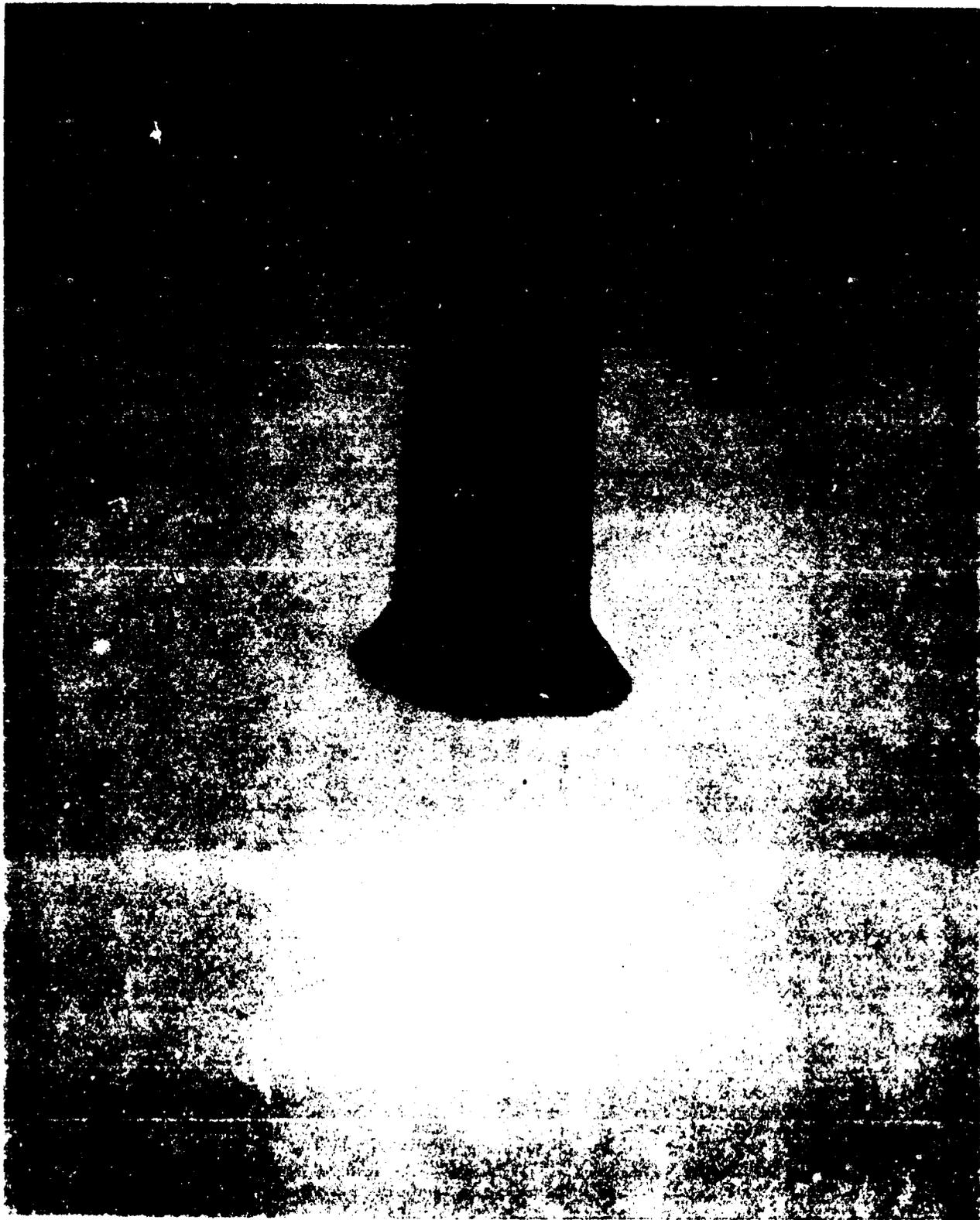
FIGURE 7-34 - PRESSURE TUBE AT CONCLUSION OF TEST
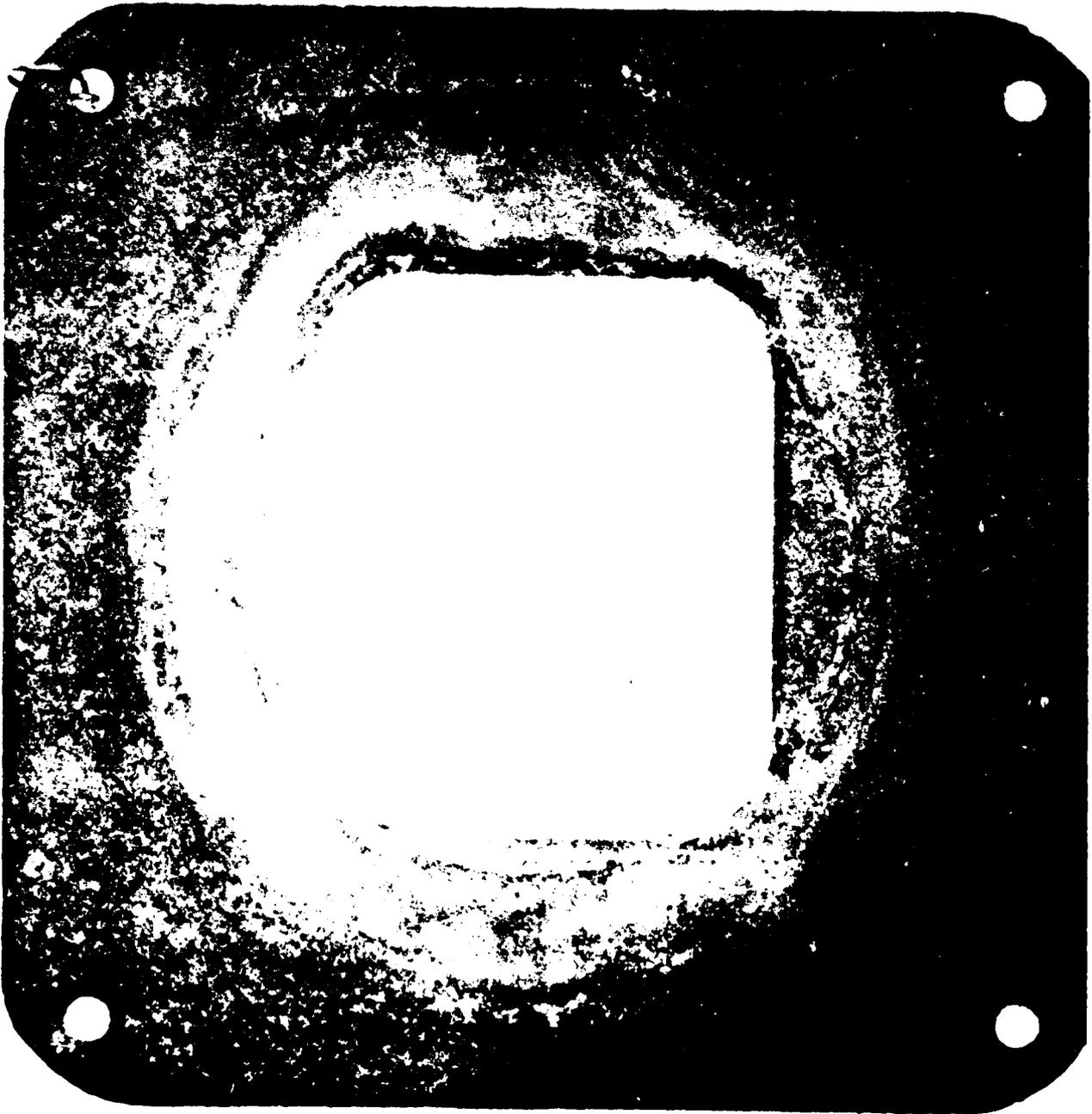
FIGURE ... TRANSMITTER AT COMPLETION OF TEST
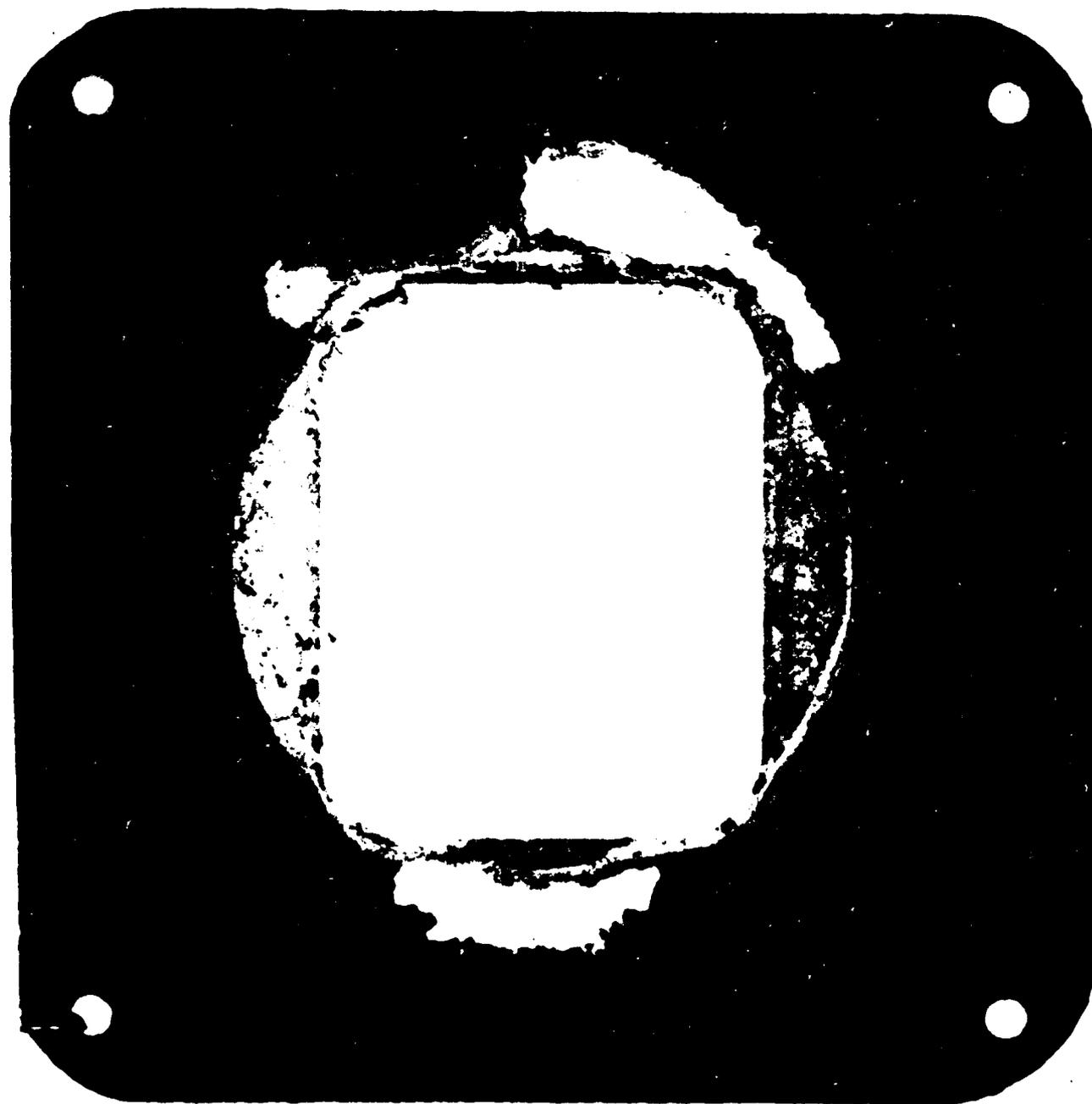
FIGURE 7-36 - LOCKWASHER AT CONCLUSION OF TEST SHOWING AREAS
WHERE T/C MOUNT REACTED WITH SILICIDE COATING

ORIGINAL PAGE
BLACK AND WHITE PHOTOGRAPH

FIGURE 7-27 - UNIT AT CONCLUSION OF TEST
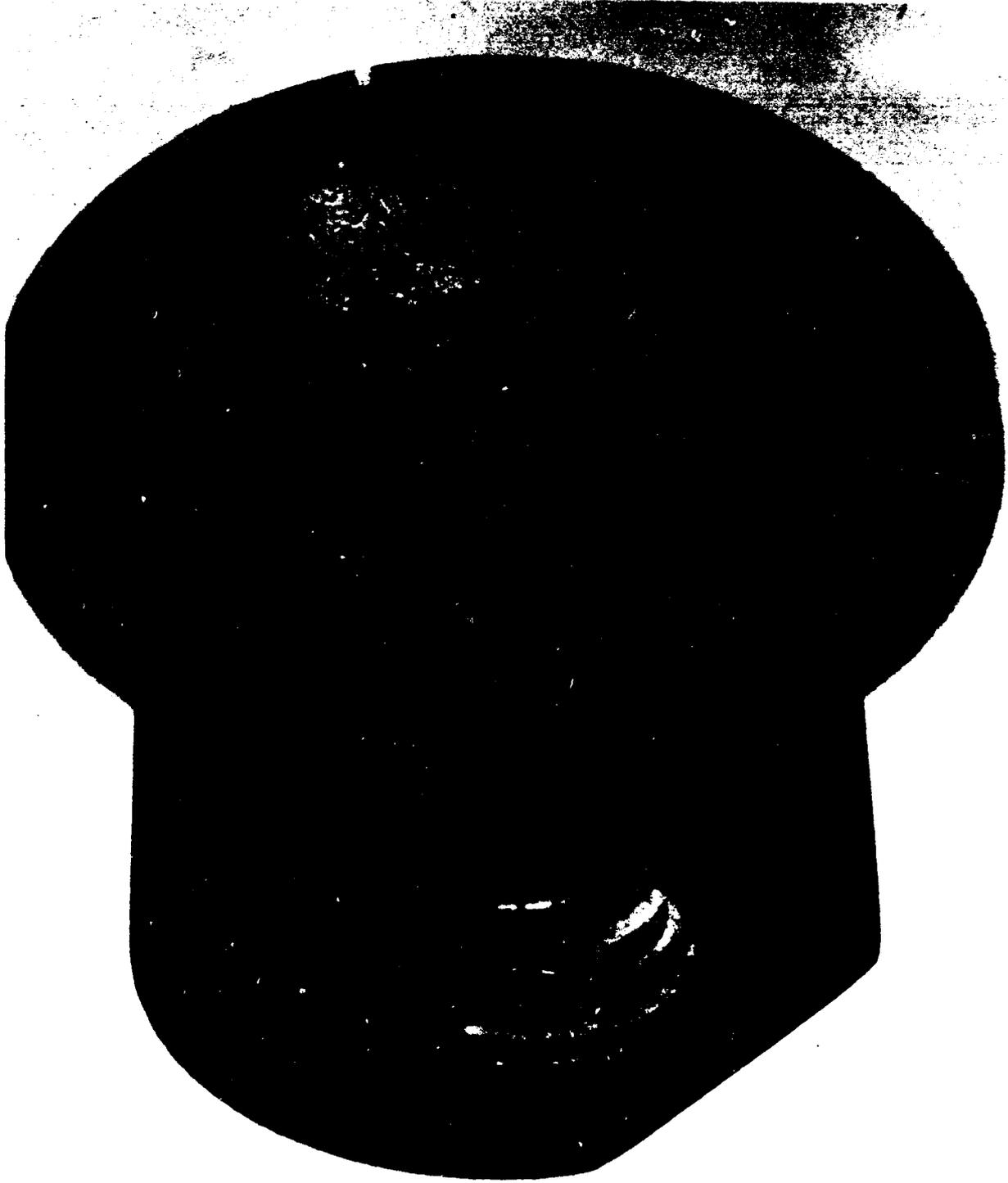
FIGURE 7-38 - POPT AT CONCLUSION OF TEST
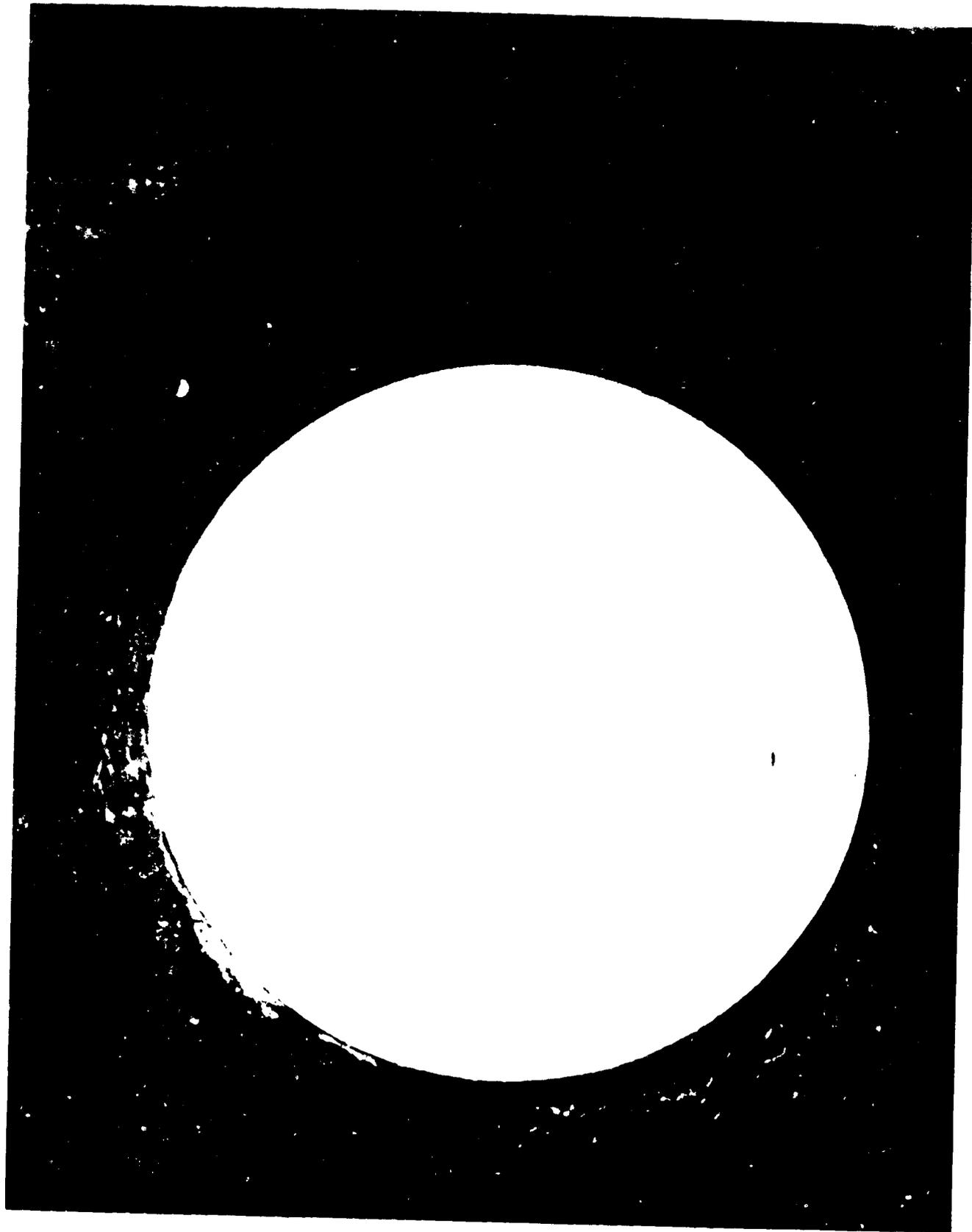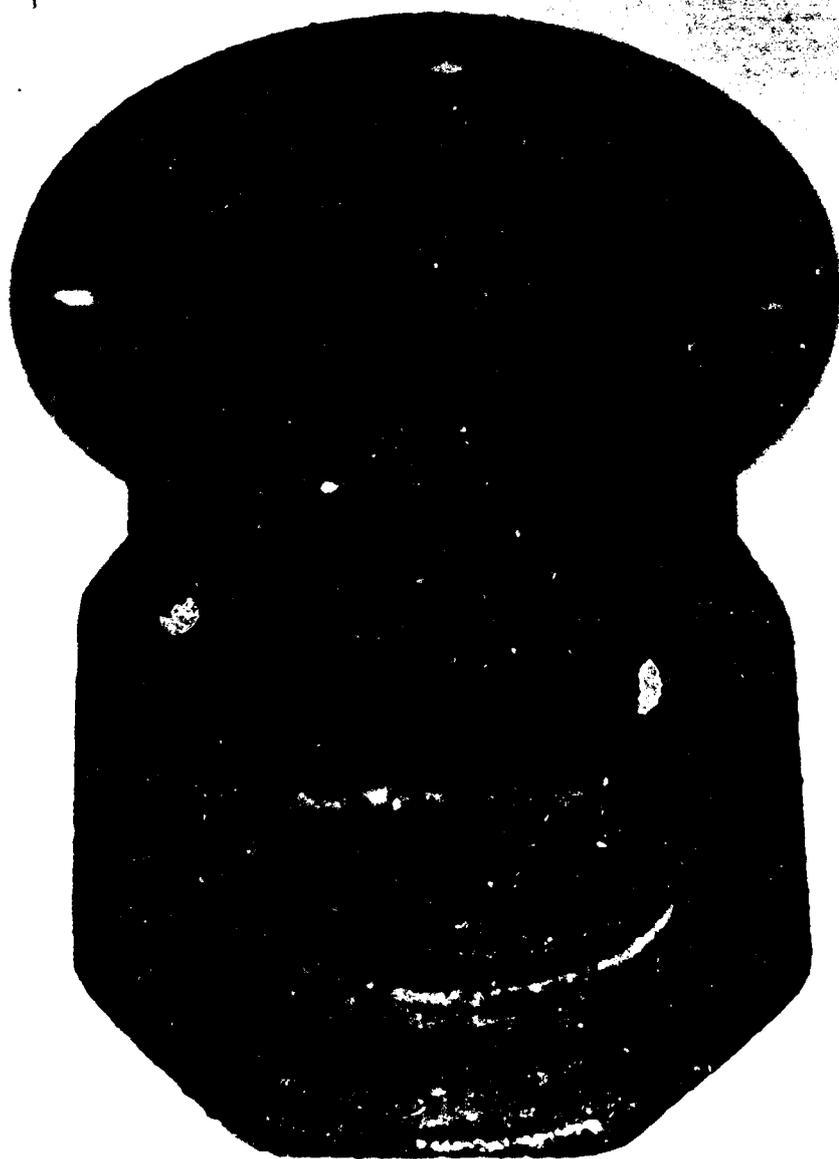
FIGURE 7-40 - NUT AT CONCLUSION OF TEST

FIGURE 7-42 - RCC SPACER FACE ADJACENT TO LOCKWASHER AT CONCLUSION
OF TEST
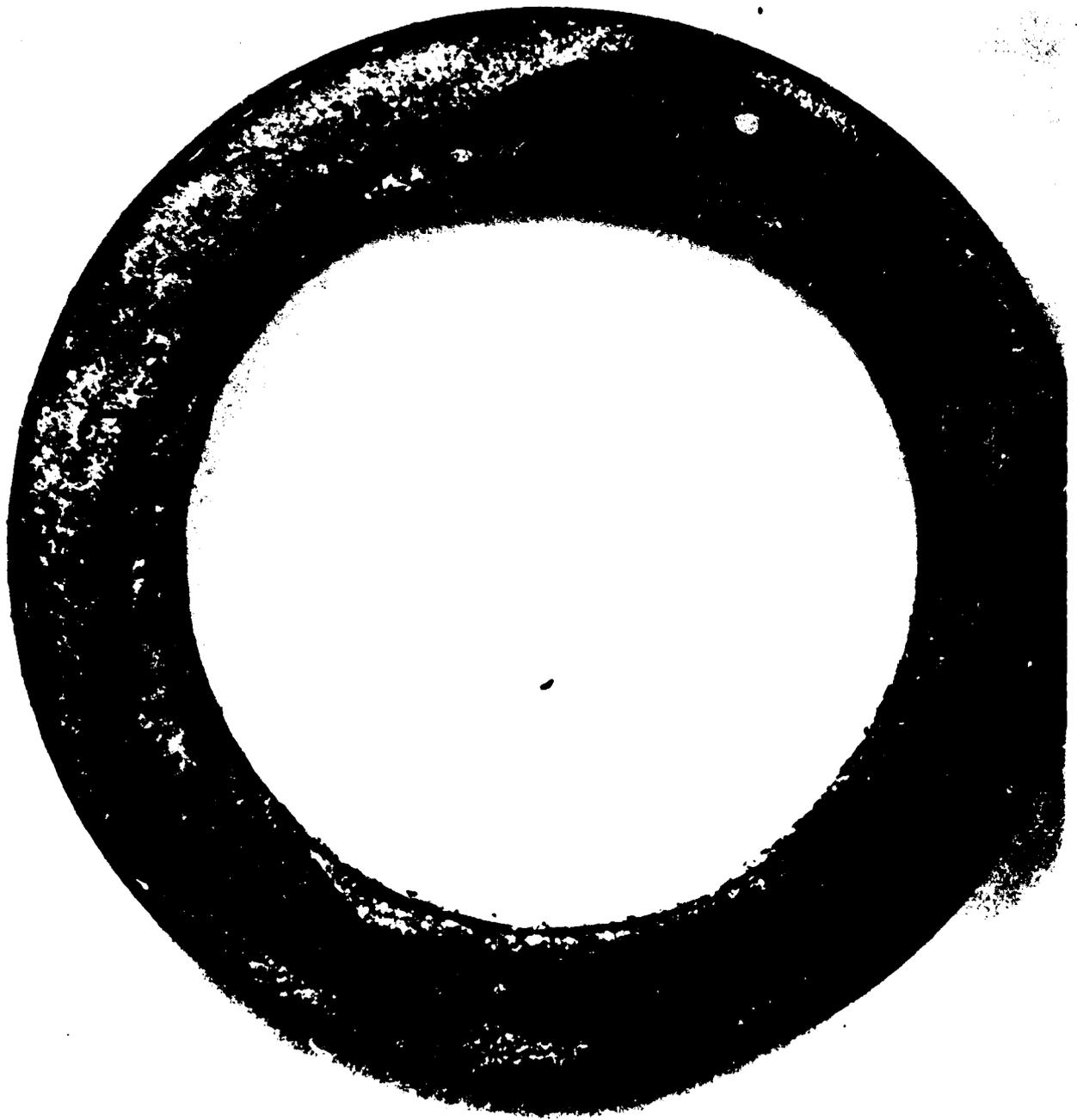
FIGURE 7-43 — [illegible caption text]

FIGURE 7-44 — THERMAL MODEL NODE IDENTIFICATION

TOTAL NUMBER OF NODES = 51

NODE NUMBERS
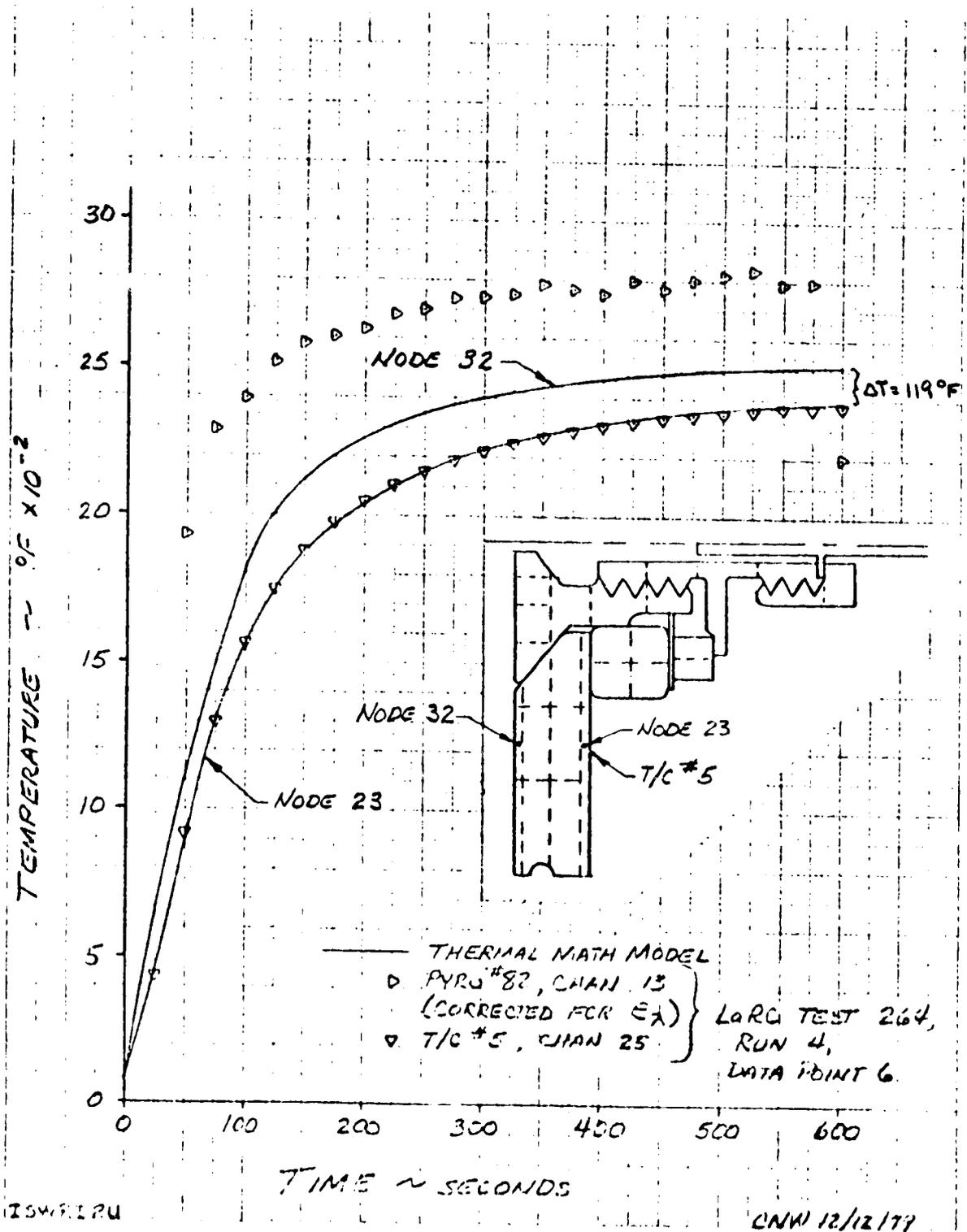
FIGURE 7-45 - NODE 23 CONTROLLED TO T/C #5
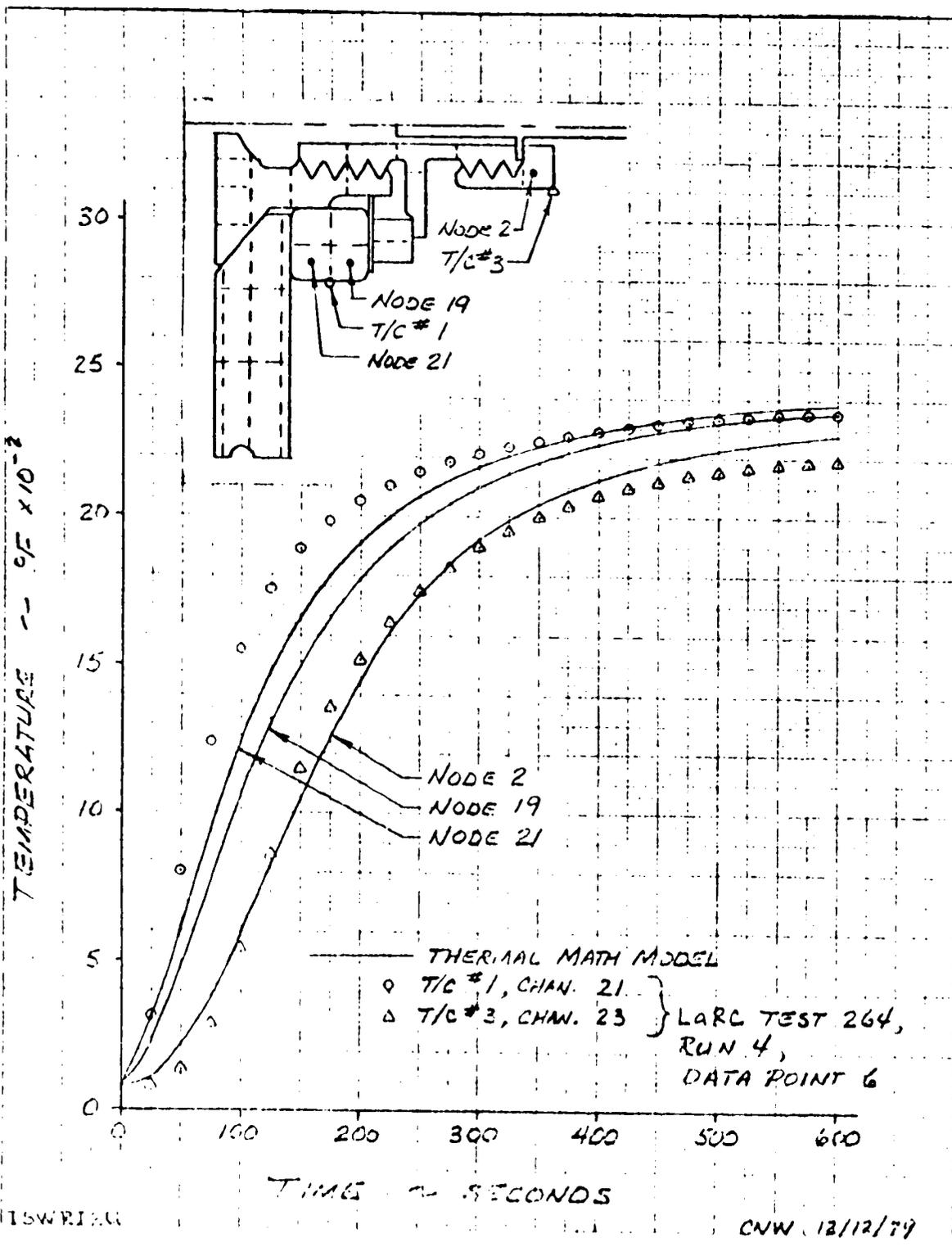
FIGURE 7-46 - NODE 23 CONTROLLED TO T/C #5

223
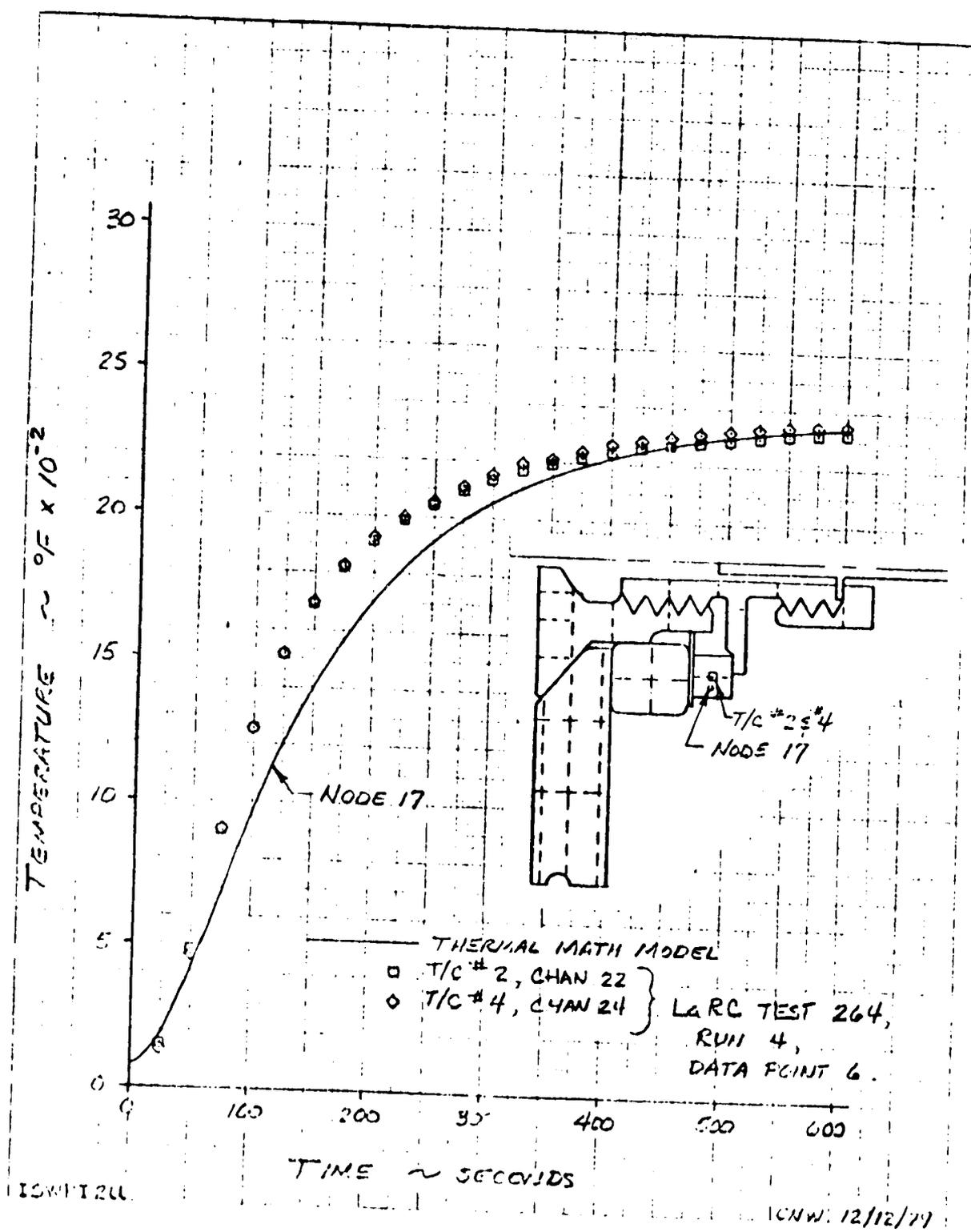
FIGURE 7-47 - NODE 23 CONTROLLED TO T/C #5
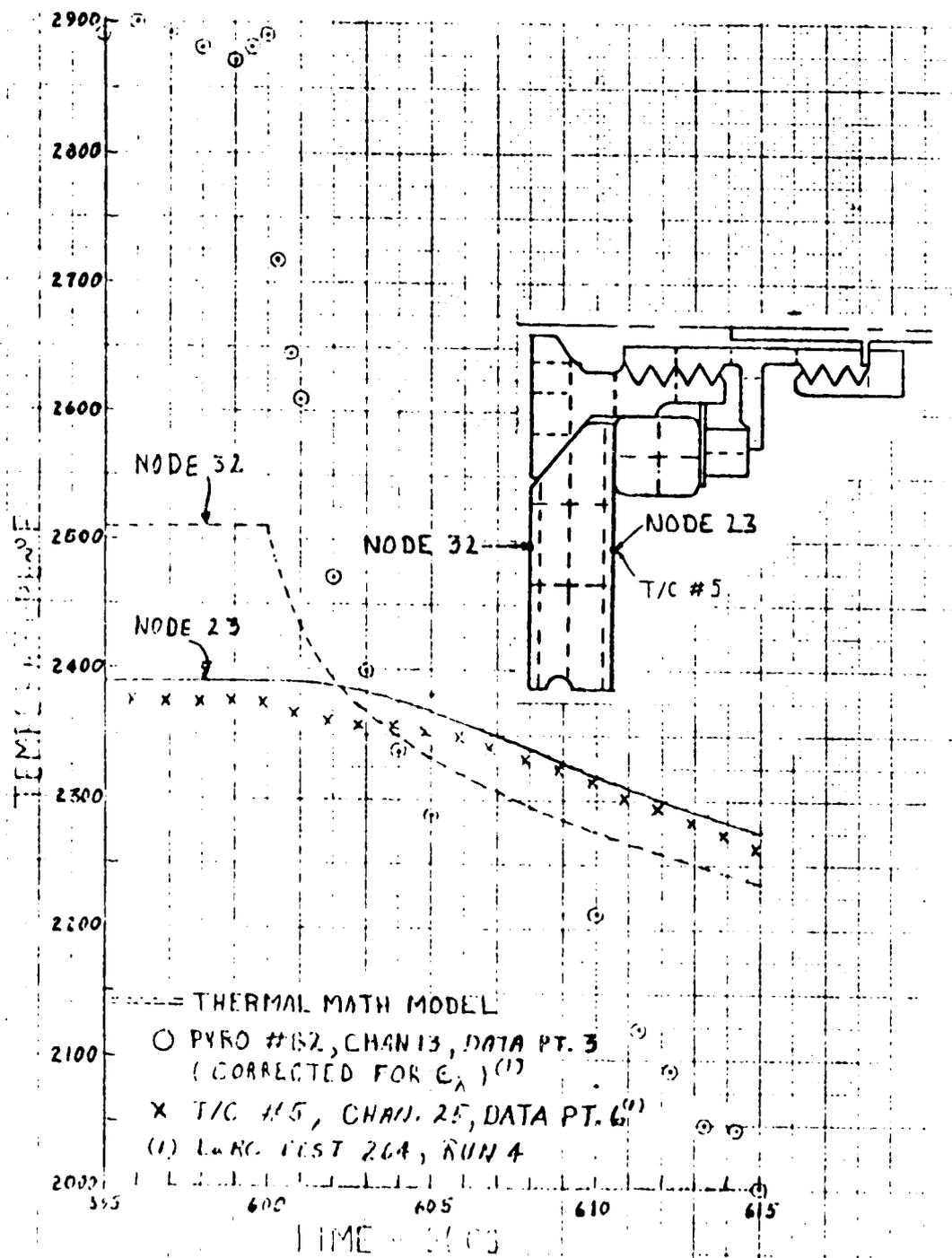
FIGURE 7-48 - NODE 23 CONTROLLED TO T/C #5 (COOLDOWN)

225
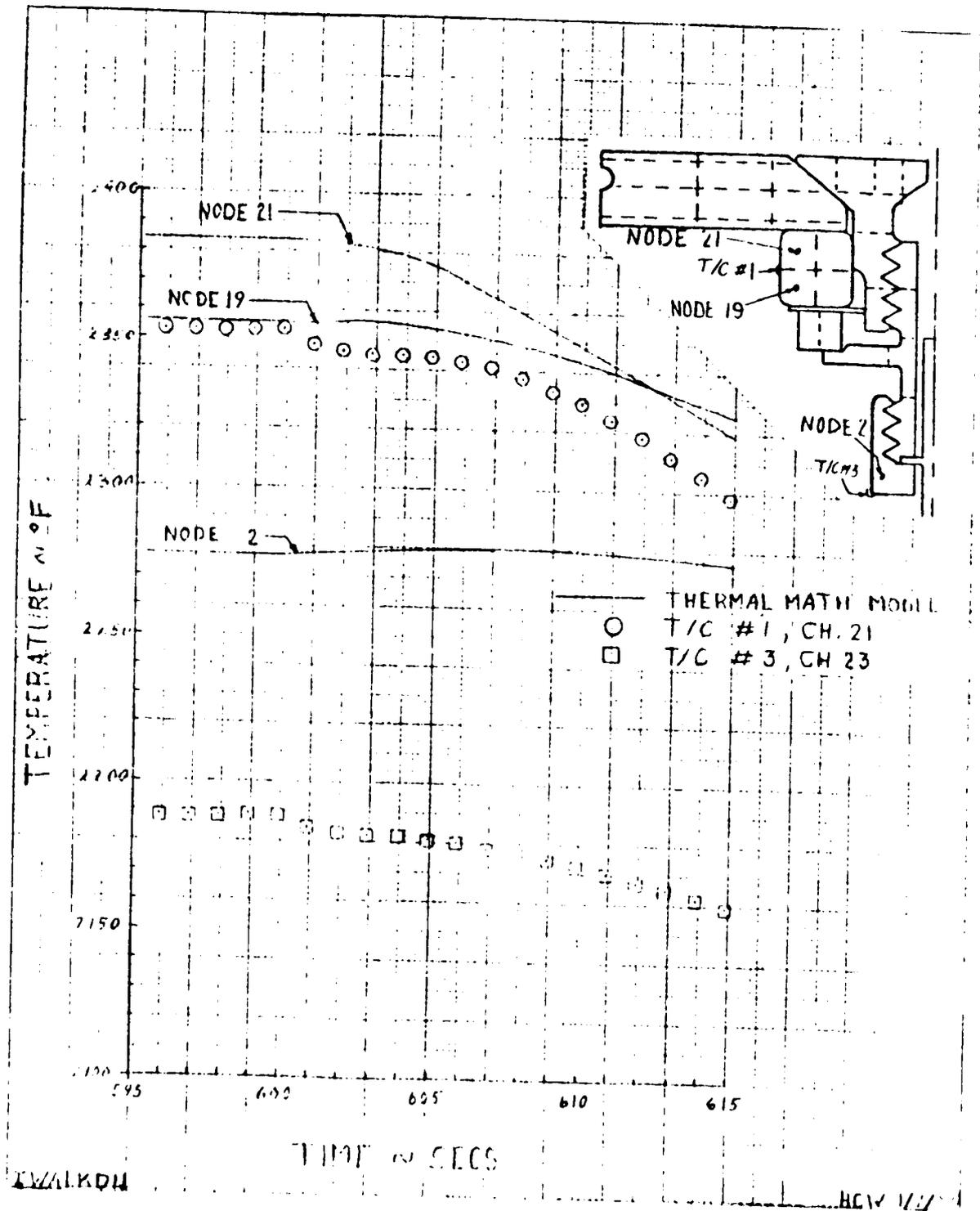
FIGURE 7-49 - NODE 23 CONTROLLED TO T/C #5 (COOLDOWN)
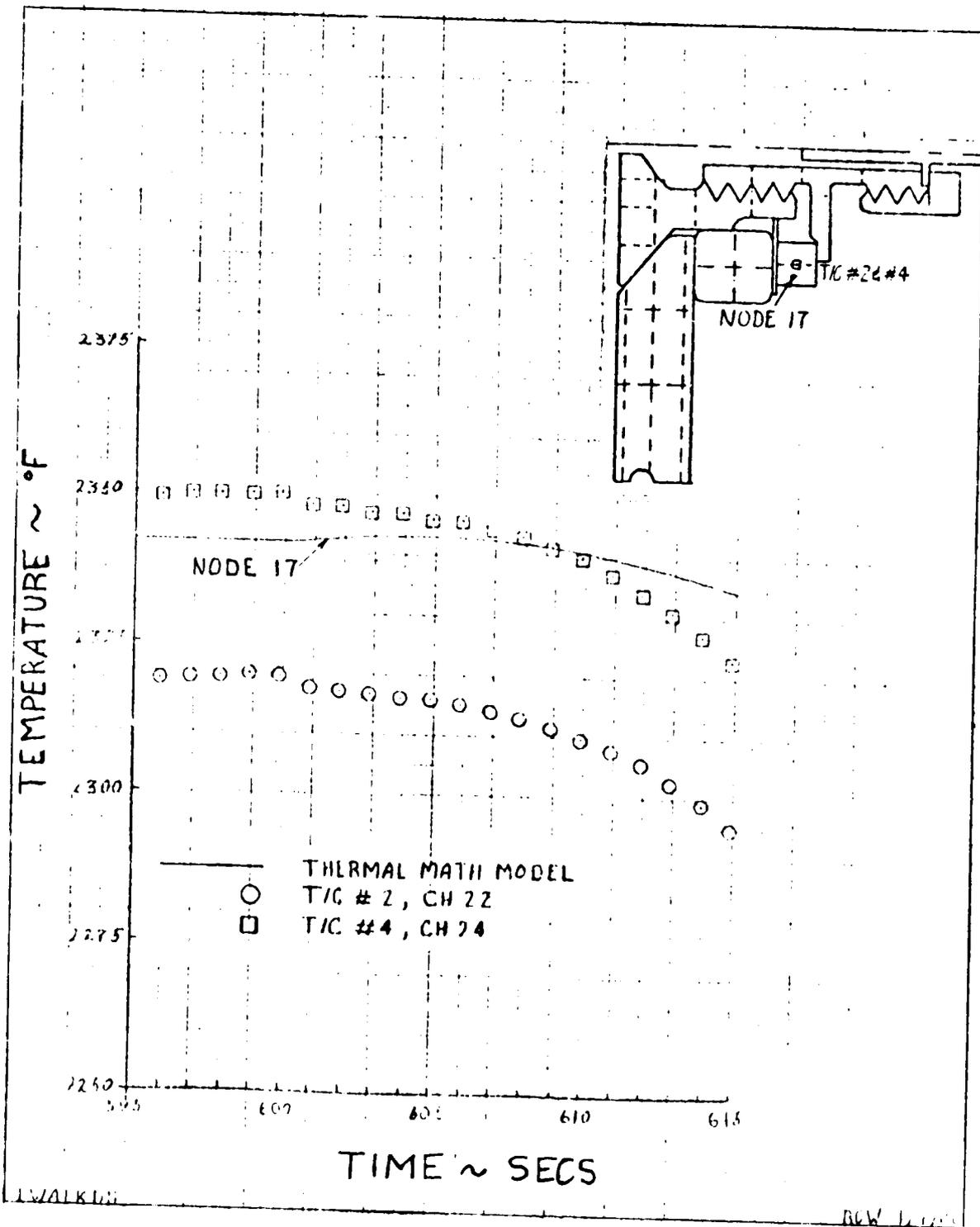
FIGURE 7-50 - NODE 23 CONTROLLED TO T/C #5 (COOLDOWN)
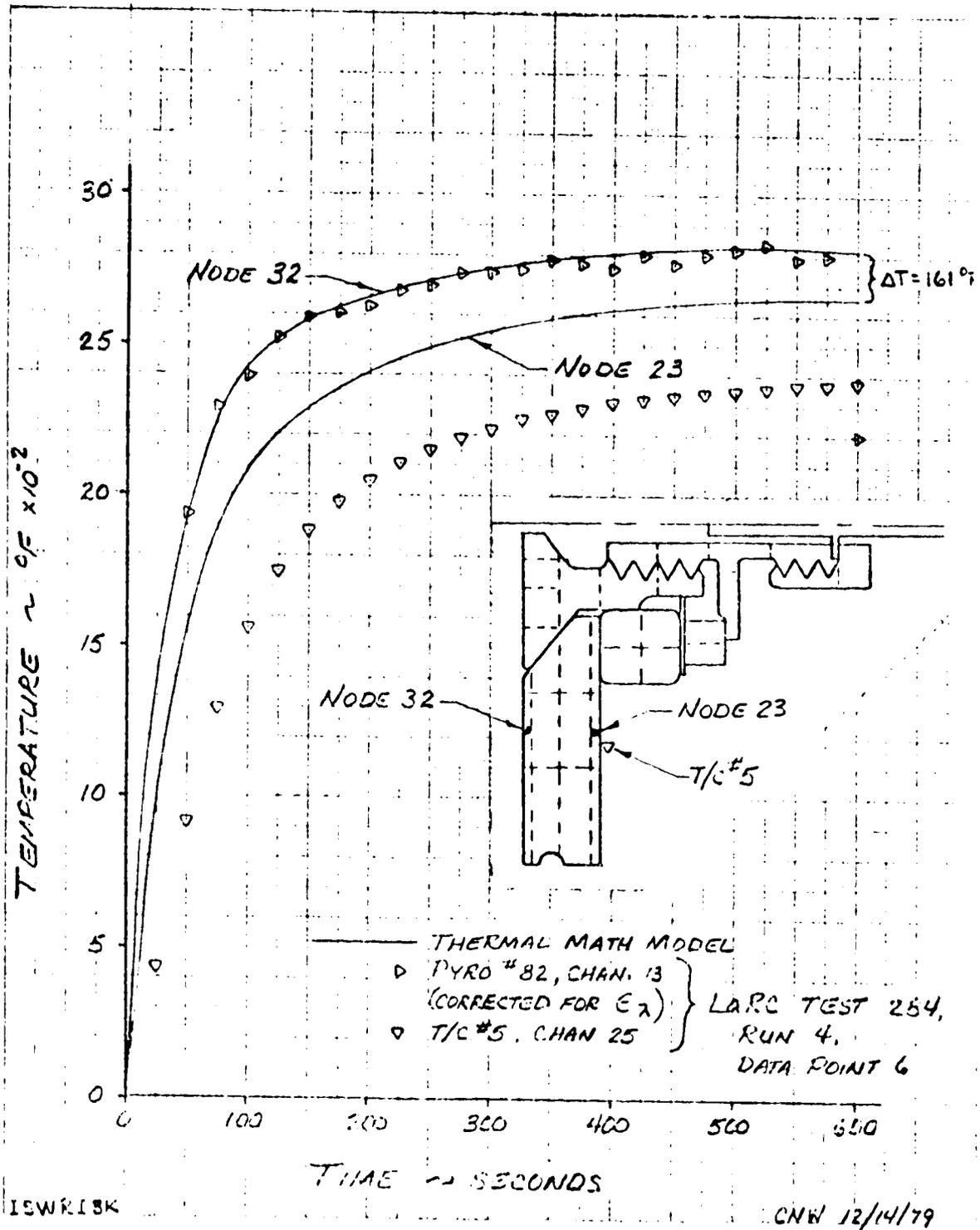
FIGURE 7-51 - NODE 32 CONTROLLED TO PYROMETER #82
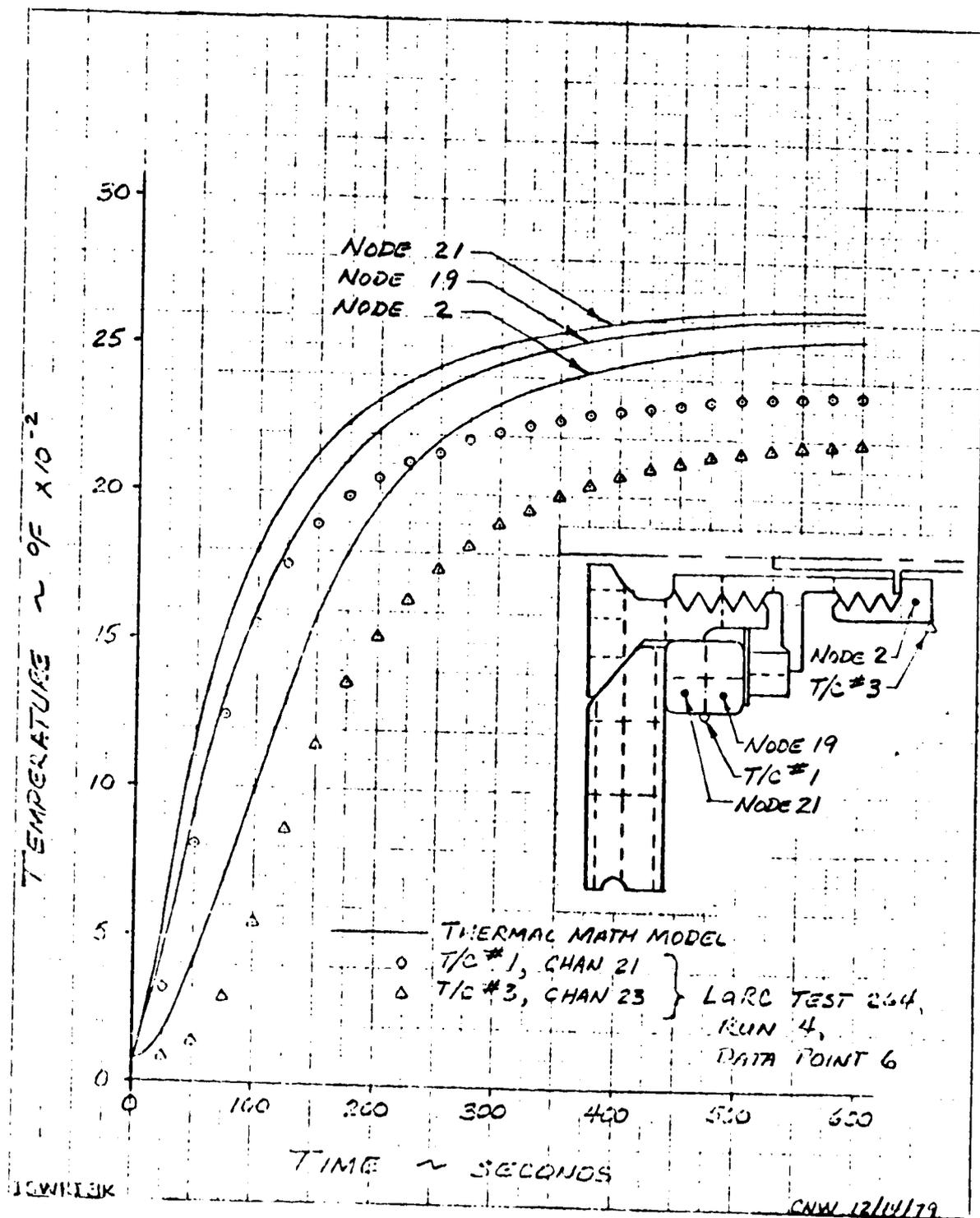
FIGURE 7-52 - NODE 32 CONTROLLED TO PYROMETER #82
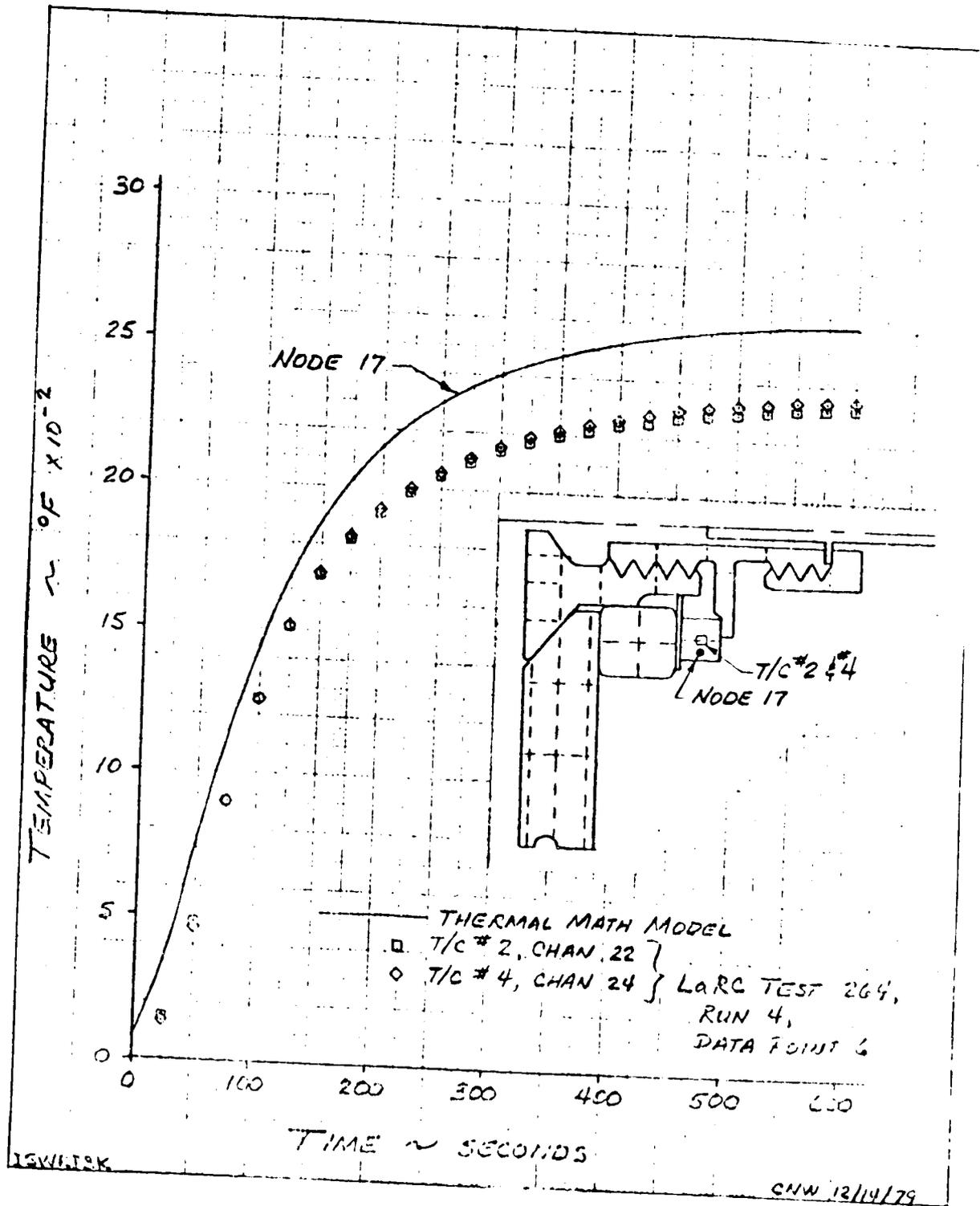
FIGURE 7-53 - NODE 32 CONTROLLED TO PYROMETER #82
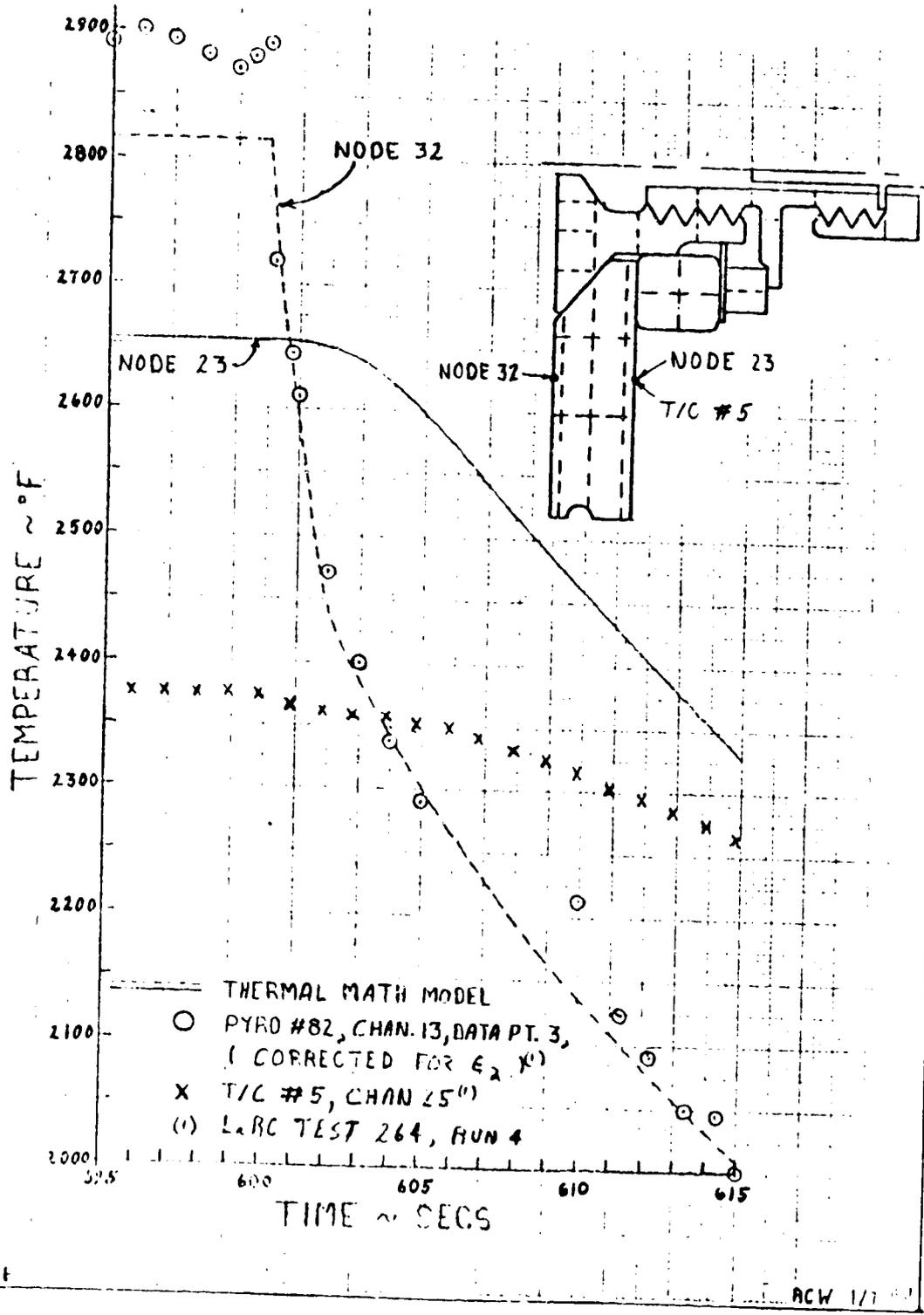
FIGURE 7-54 - NODE 32 CONTROLLED TO PYROMETER #82 (COOLDOWN)

231
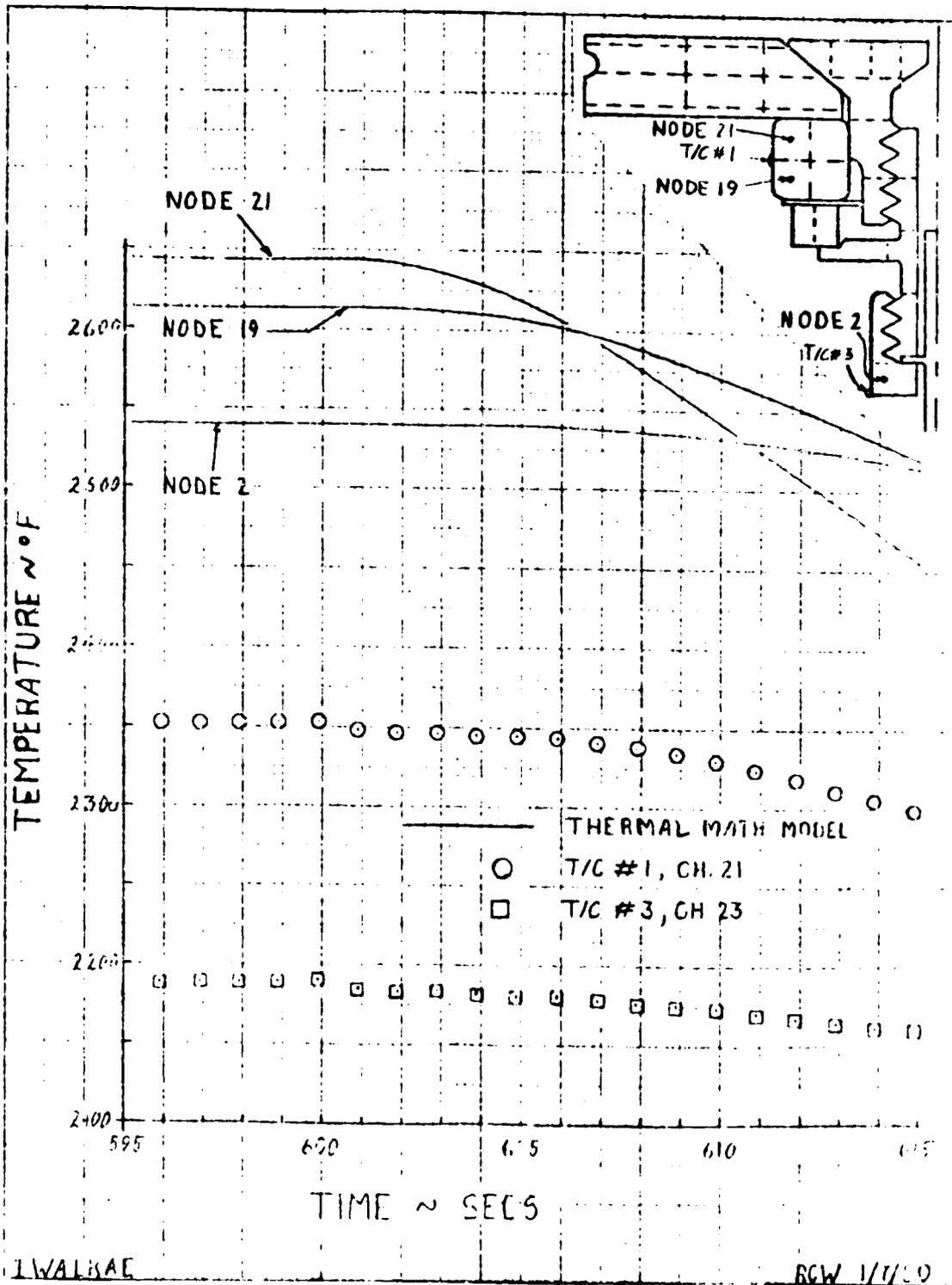
FIGURE 7-55 - NODE 32 CONTROLLED TO PYROMETER #82 (COOLDOWN)
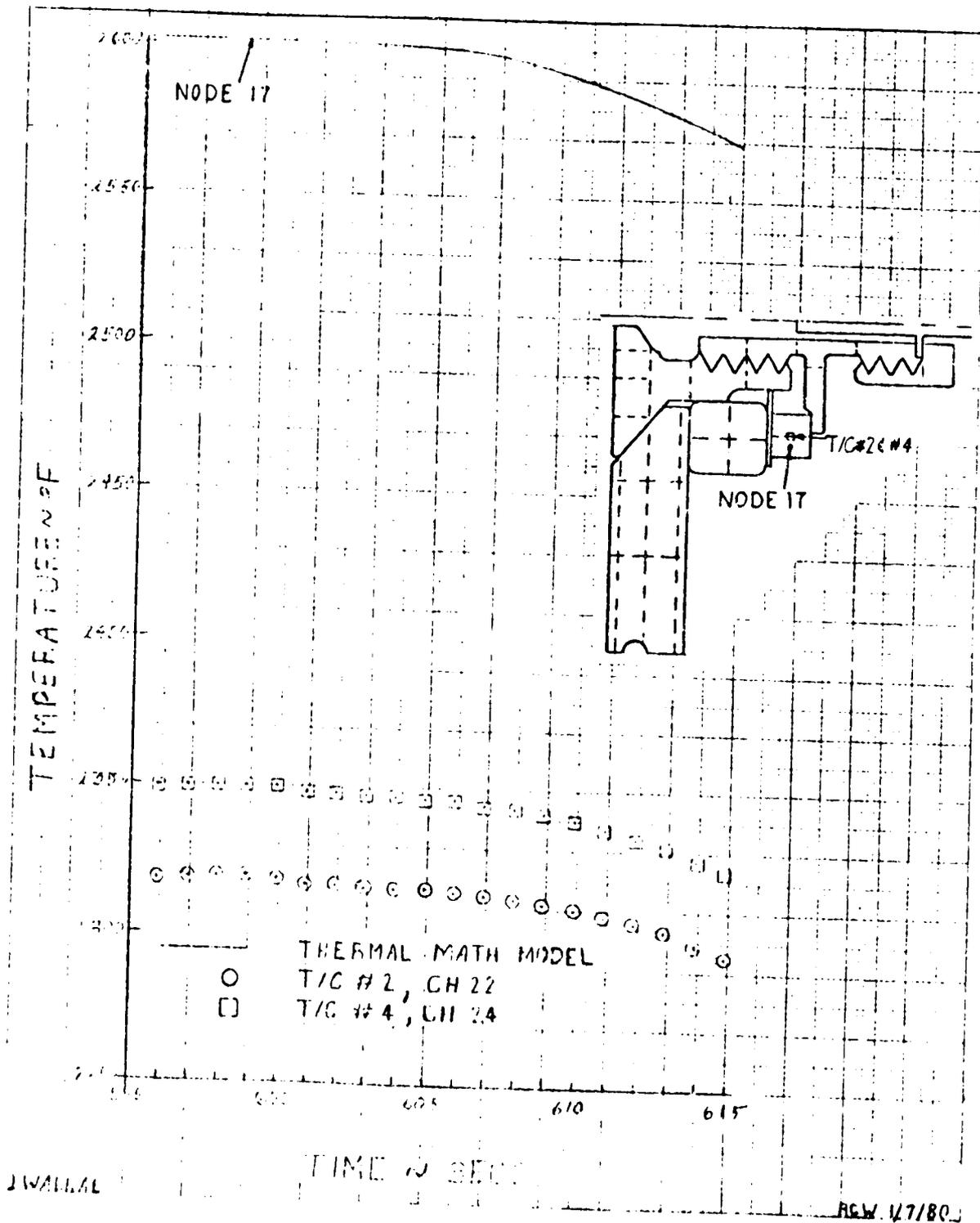
FIGURE 7-56 - NODE 32 CONTROLLED TO PYROMETER #82 (COOLDOWN)
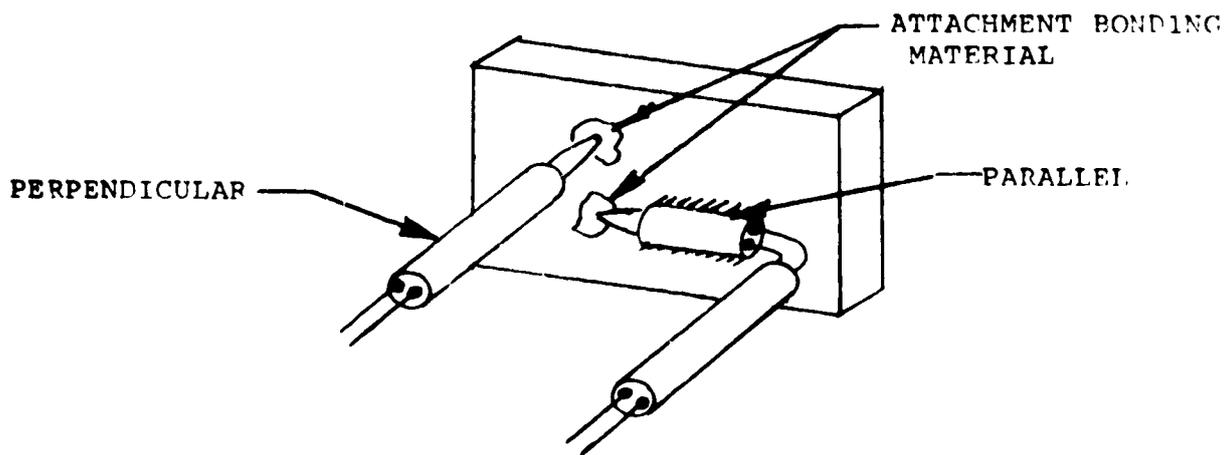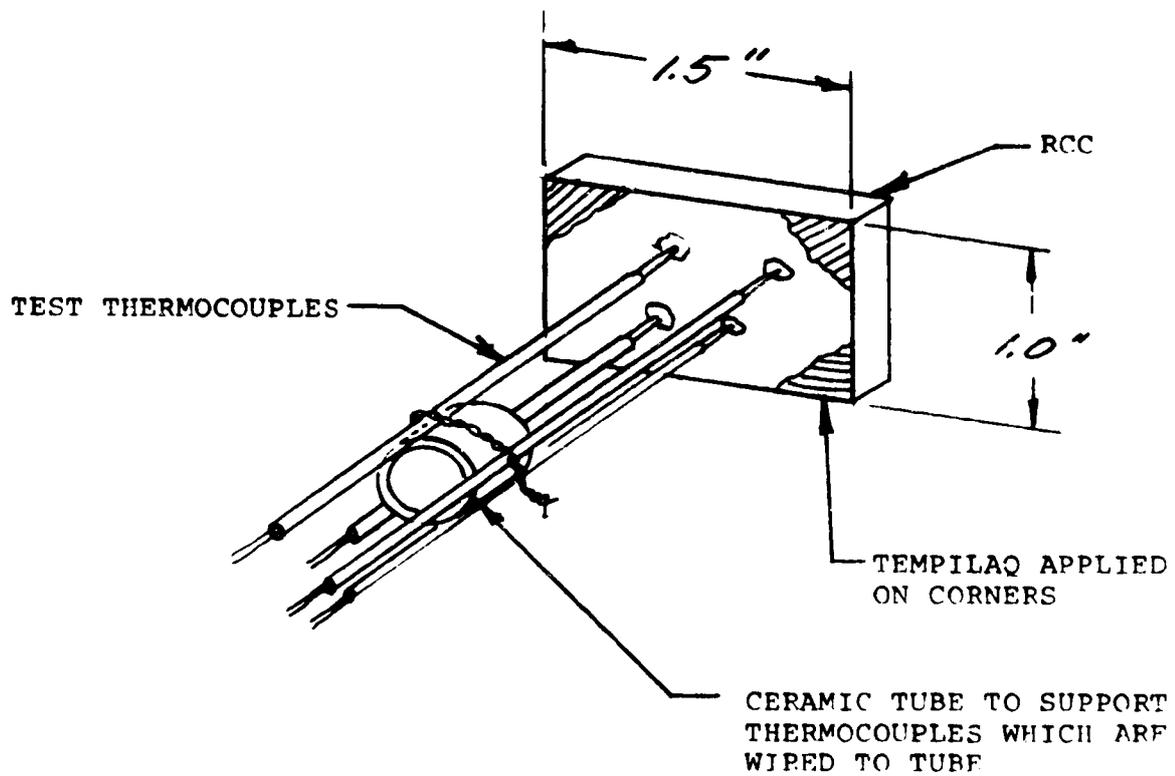
FIGURE 7-57 - TYPICAL TEST SPECIMEN & ATTACHMENT TYPES

238

IRCON 300 PYROM.

TUBE FURNACE

TEST SPECIMEN

PLATINUM RHODIUM
THERMOCOUPLE

INSULATION BLANKET COVERING
THERMOCOUPLE LEADS
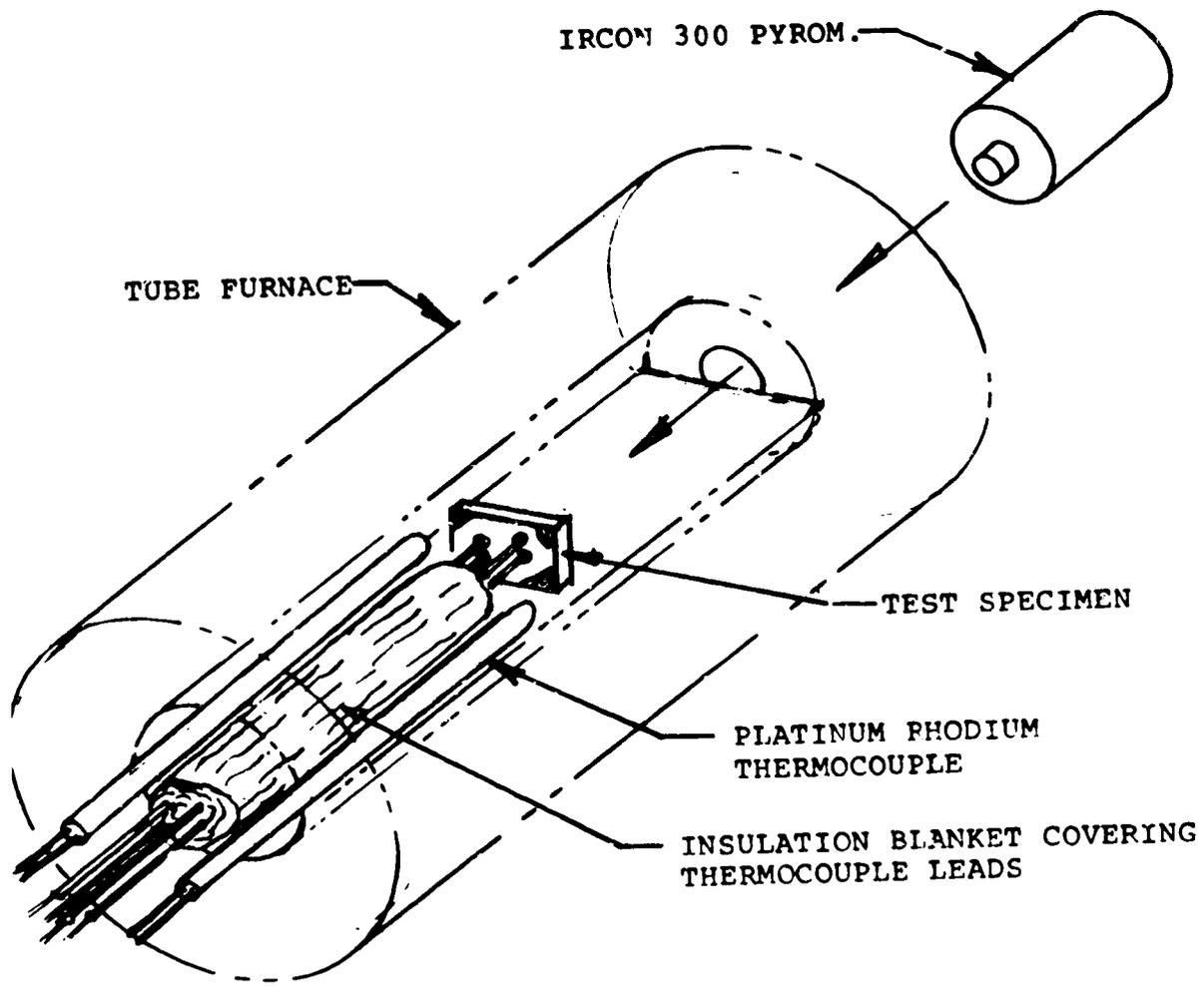
FIGURE 7-58 – TESTING APPROACH

FIGURE 7-60 - THERMOCOUPLE MOUNTING FOR
PERPENDICULAR CONFIGURATION

FIGURE 7-59 - TUBE FURNACE SETUP
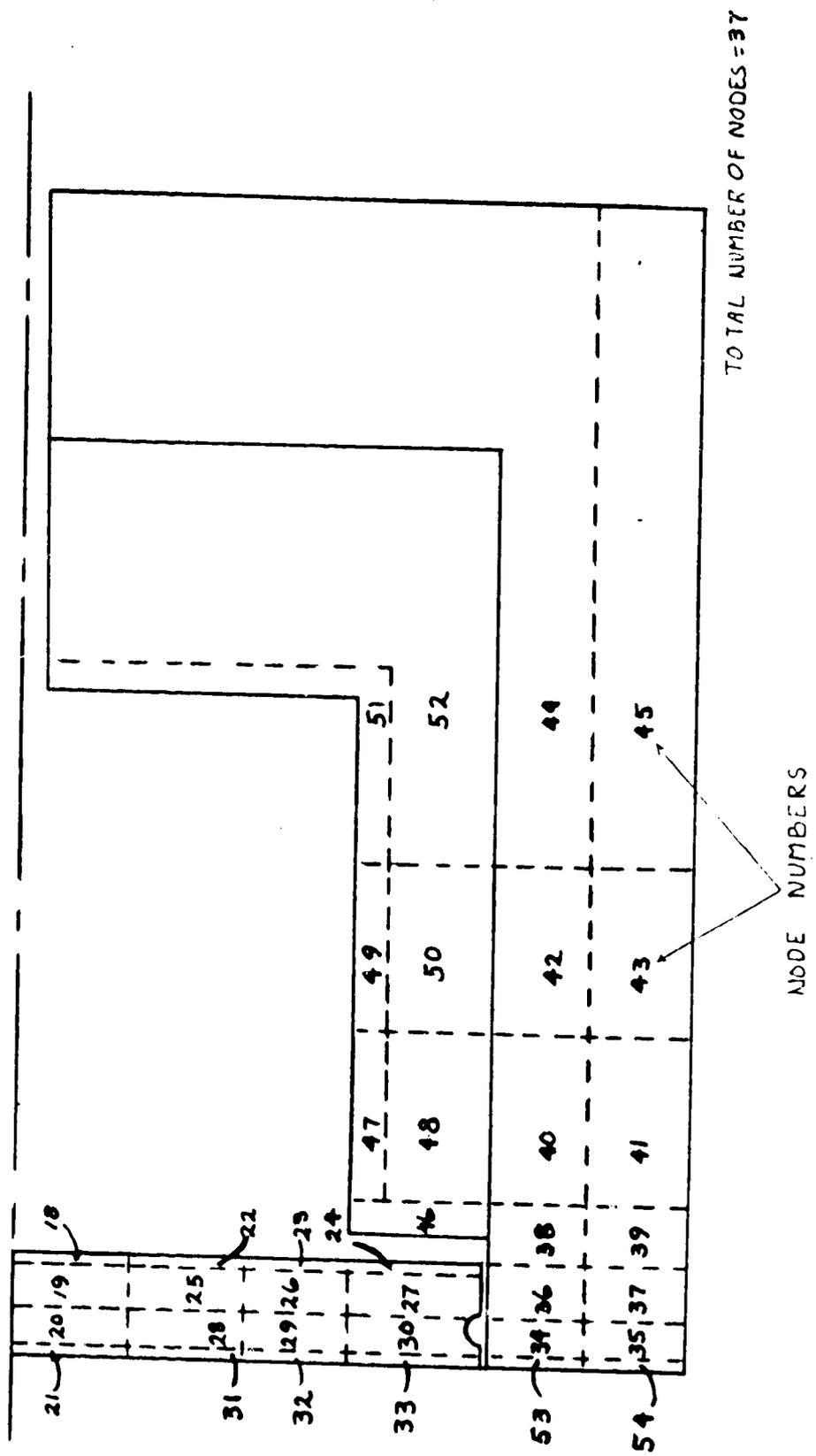
FIGURE 7-63 - CALIBRATION SPECIMEN THERMAL MODEL
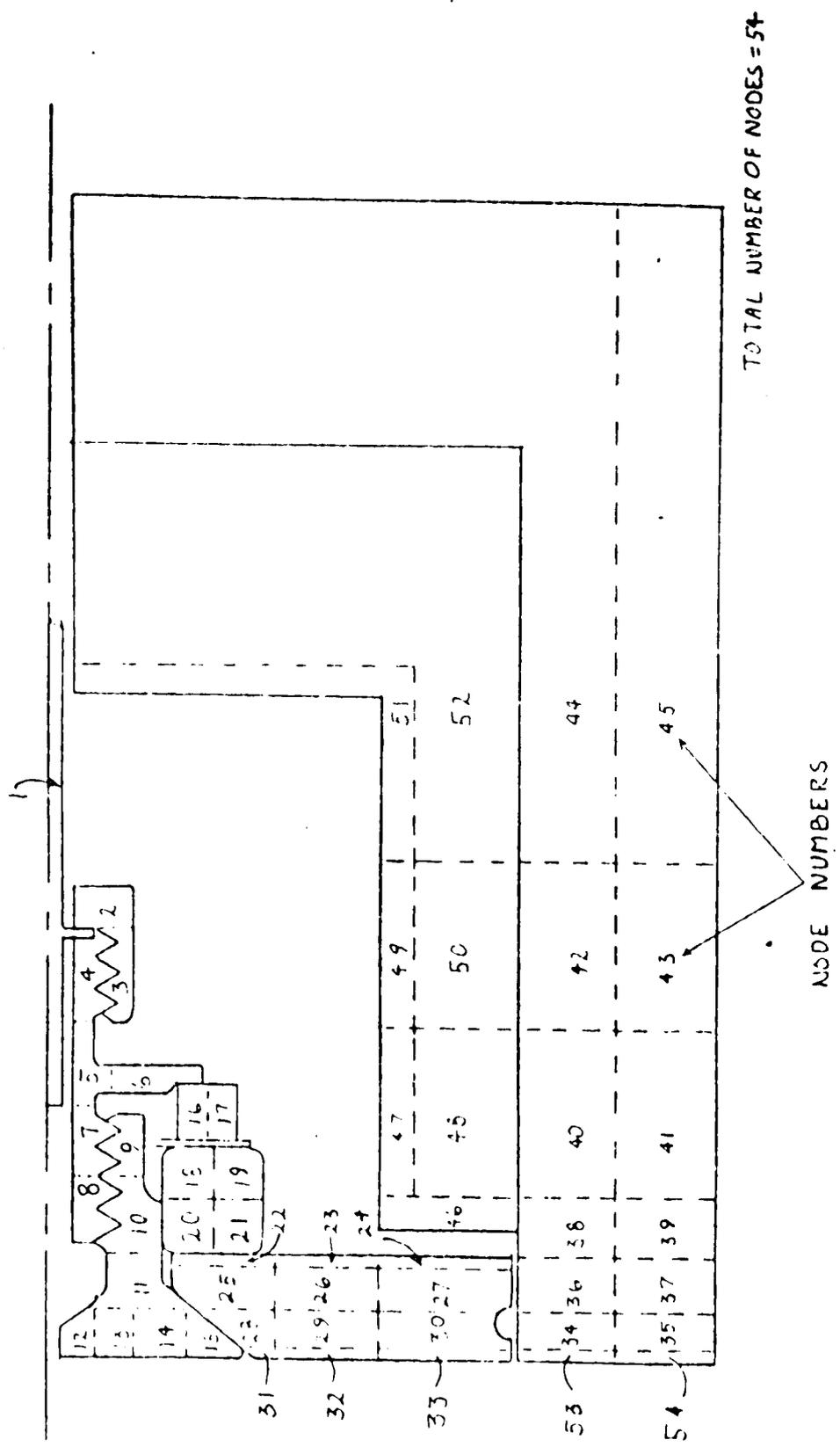
FIGURE 7-64 - SEADS TEST SPECIMEN THERMAL MODEL
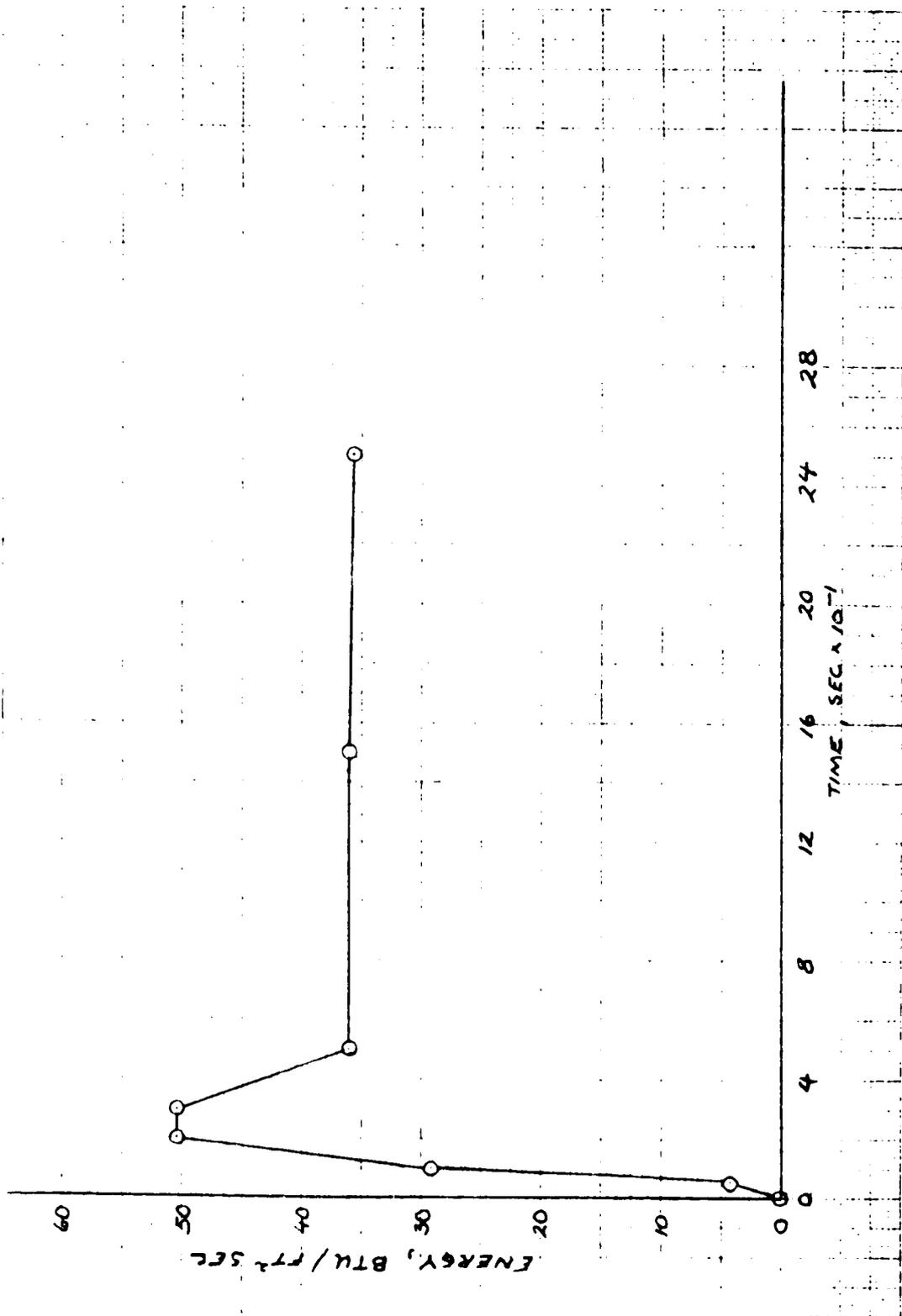
FIGURE 7-65 - PREDICTED STAGNATION ENERGY FOR TEST RUN NO. 5, CALIBRATION SPECIMEN
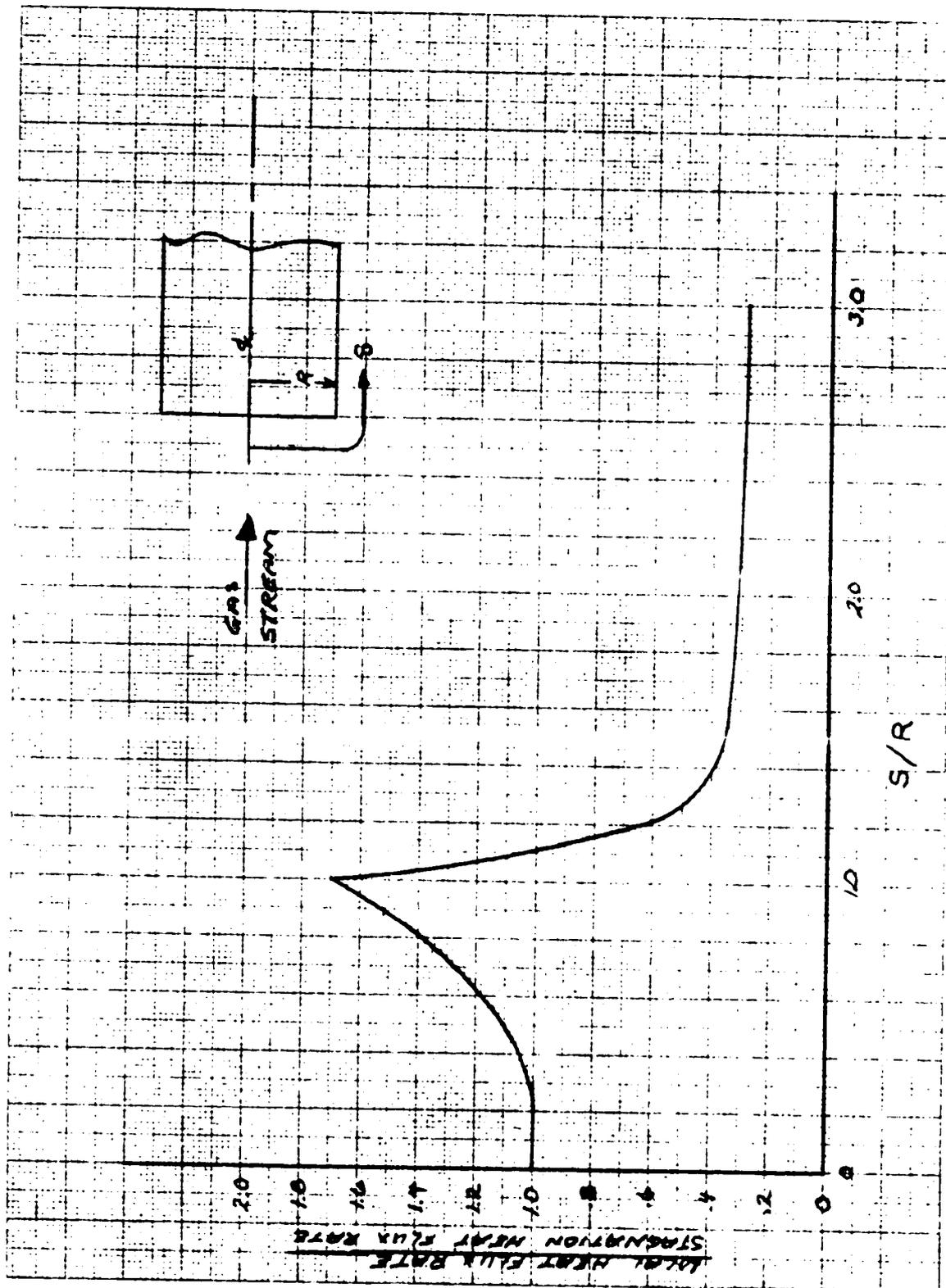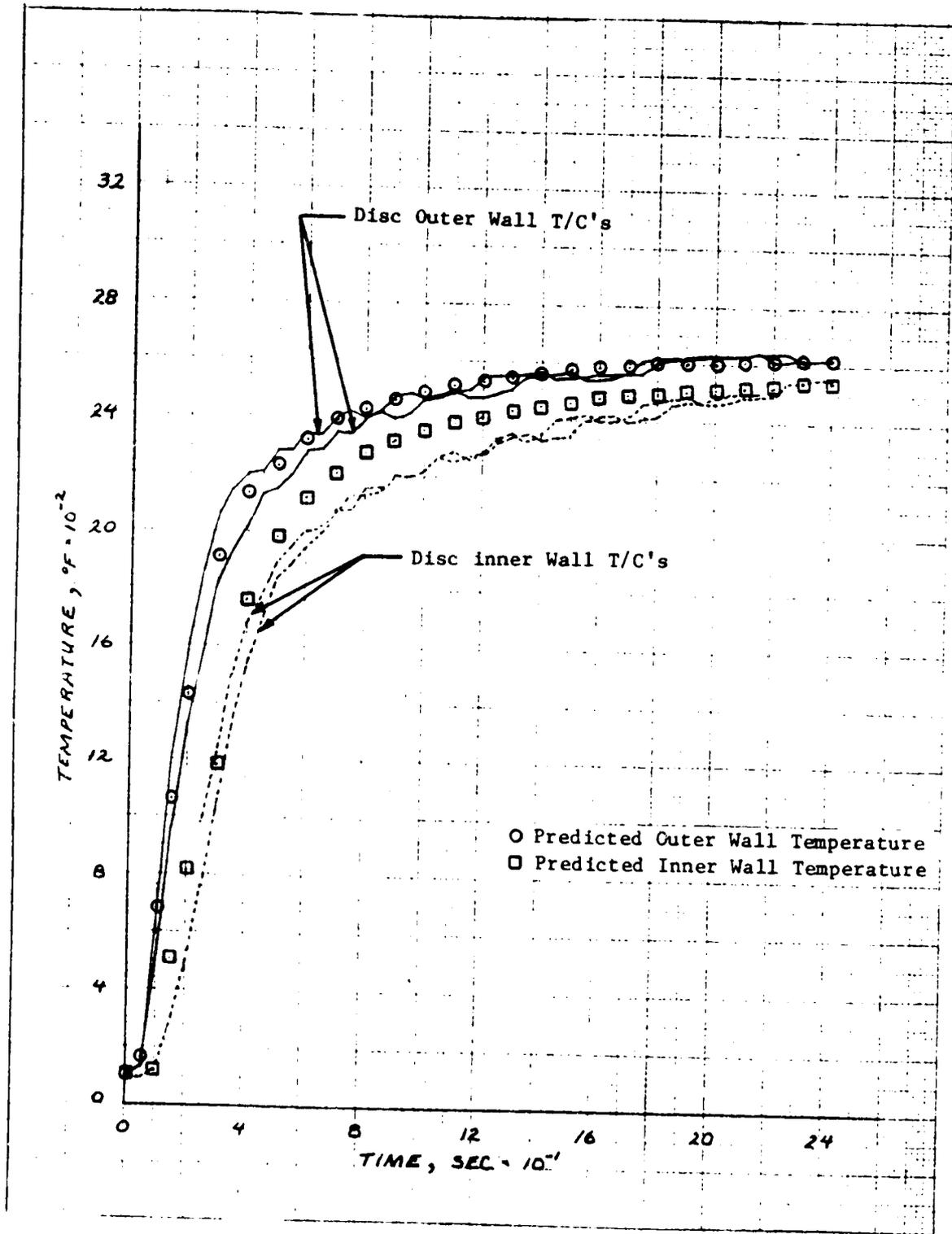
FIGURE 7-67 - COMPARISON OF PREDICTED TEMPERATURES WITH TEST RUN NO. 5, CALIBRATION SPECIMEN
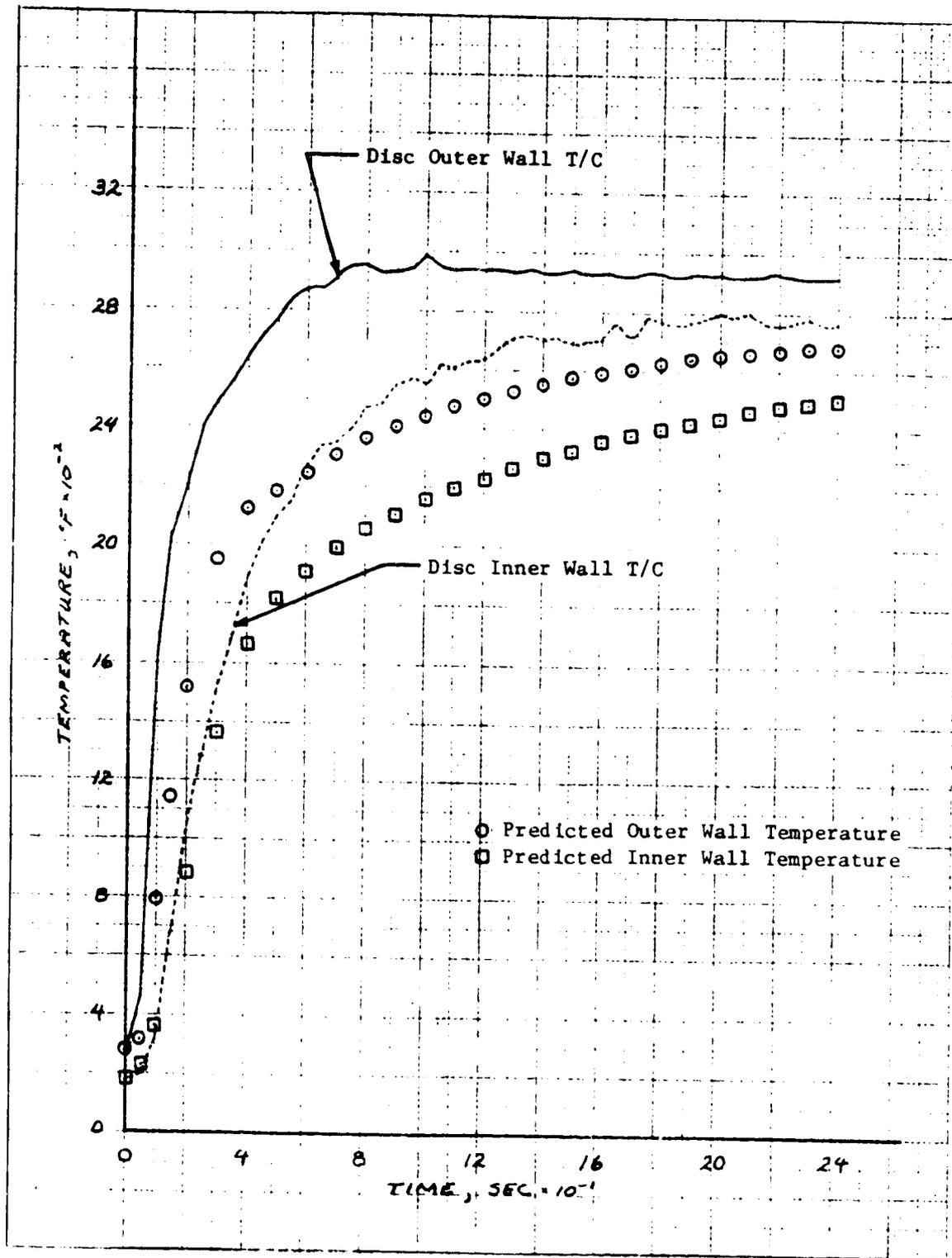
FIGURE 7-68 - COMPARISON OF PREDICTED TEMPERATURES WITH TEST RUN Nᶜ
SEADS TEST SPECIMEN WITH NO CATALYTIC HEATING
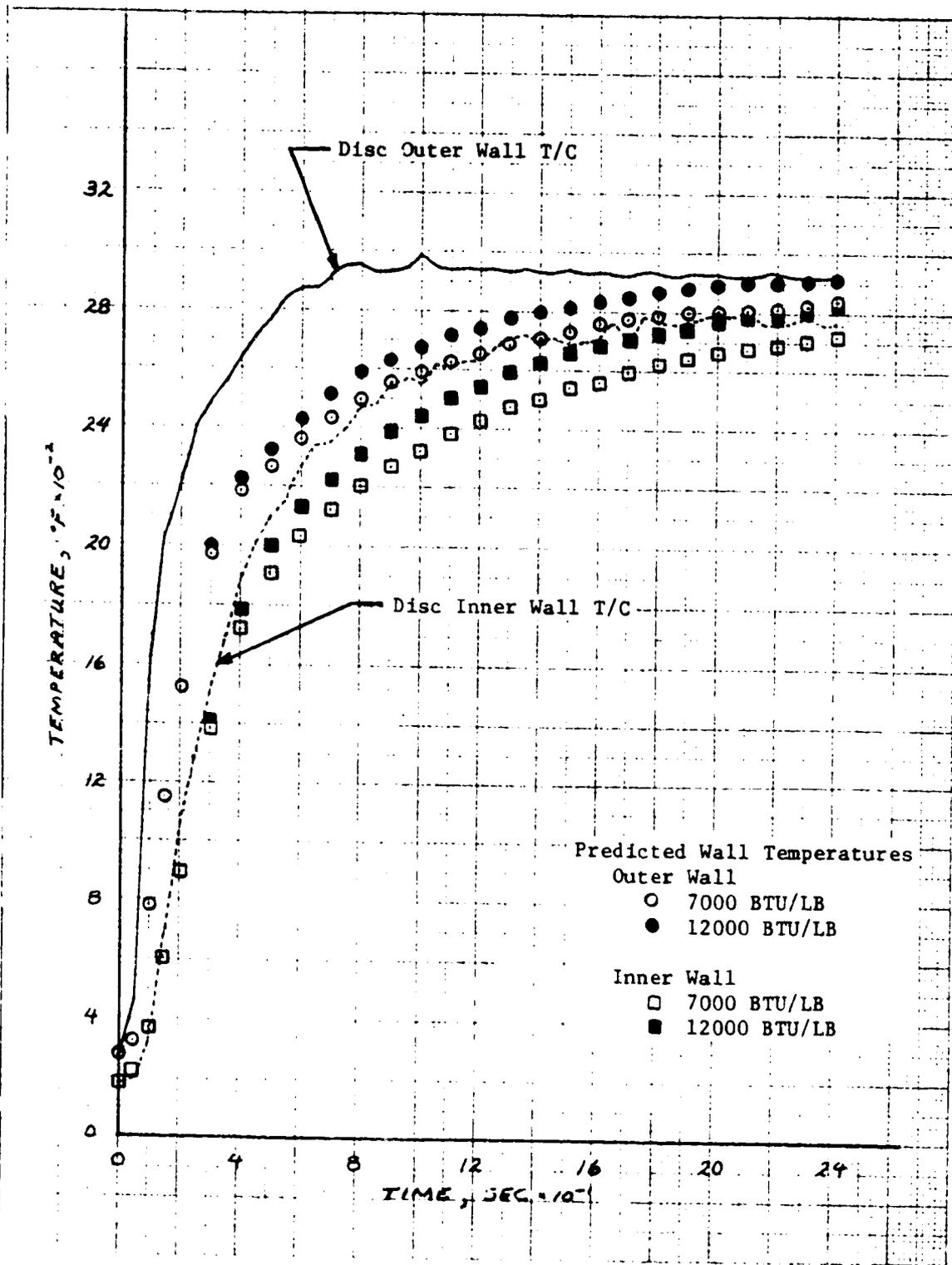
FIGURE 7-69 COMPARISON OF PREDICTED TEMPERATURES WITH TEST RUN NO. 6,
SEADS TEST SPECIMEN WITH HOLDER FACE FULLY CATALYTIC
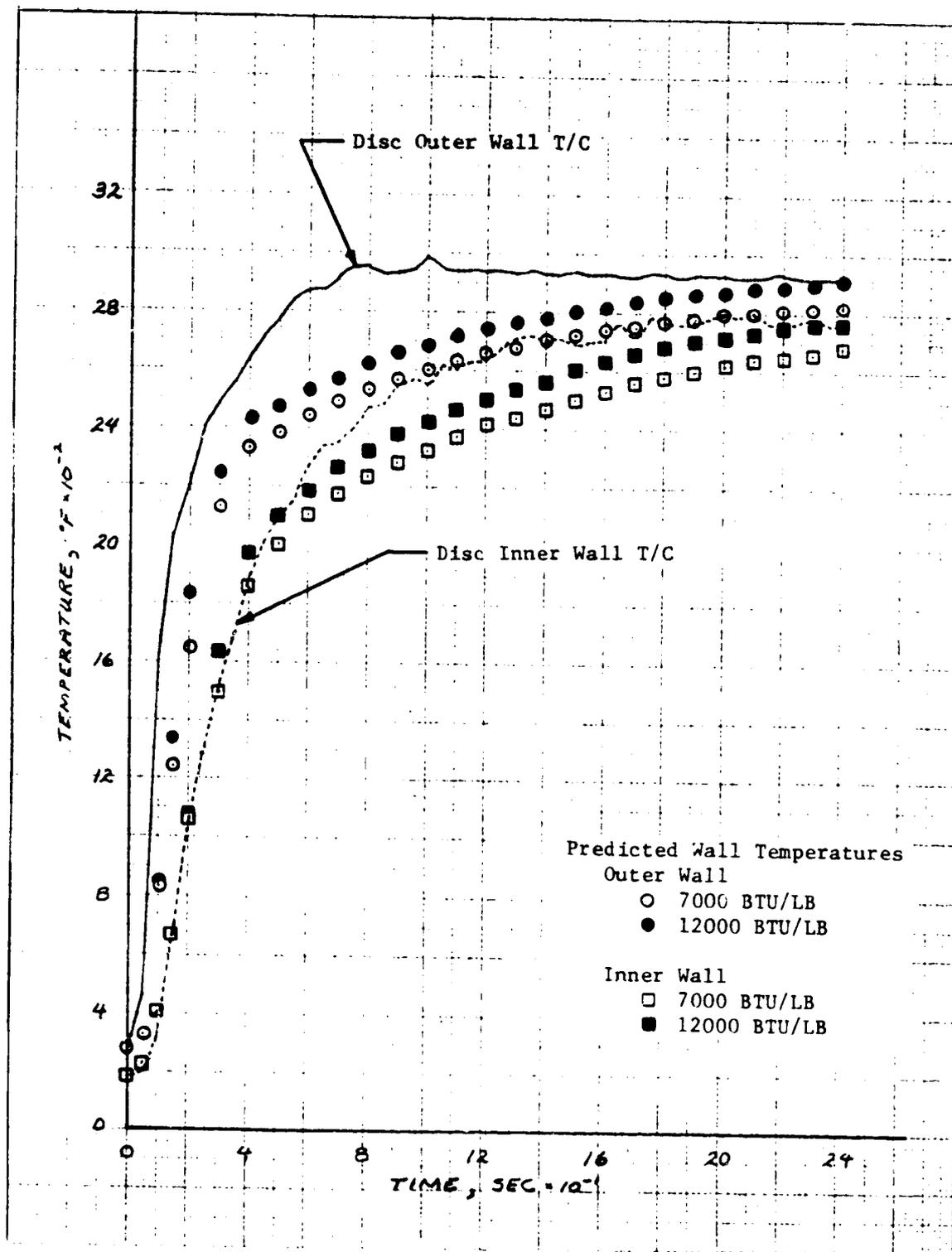
FIGURE 7-70 · COMPARISON OF PREDICTED TEMPERATURES WITH TEST RUN NO. 6,
SEADS TEST SPECIMEN WITH PENETRATION PORT FULLY CATALYTIC
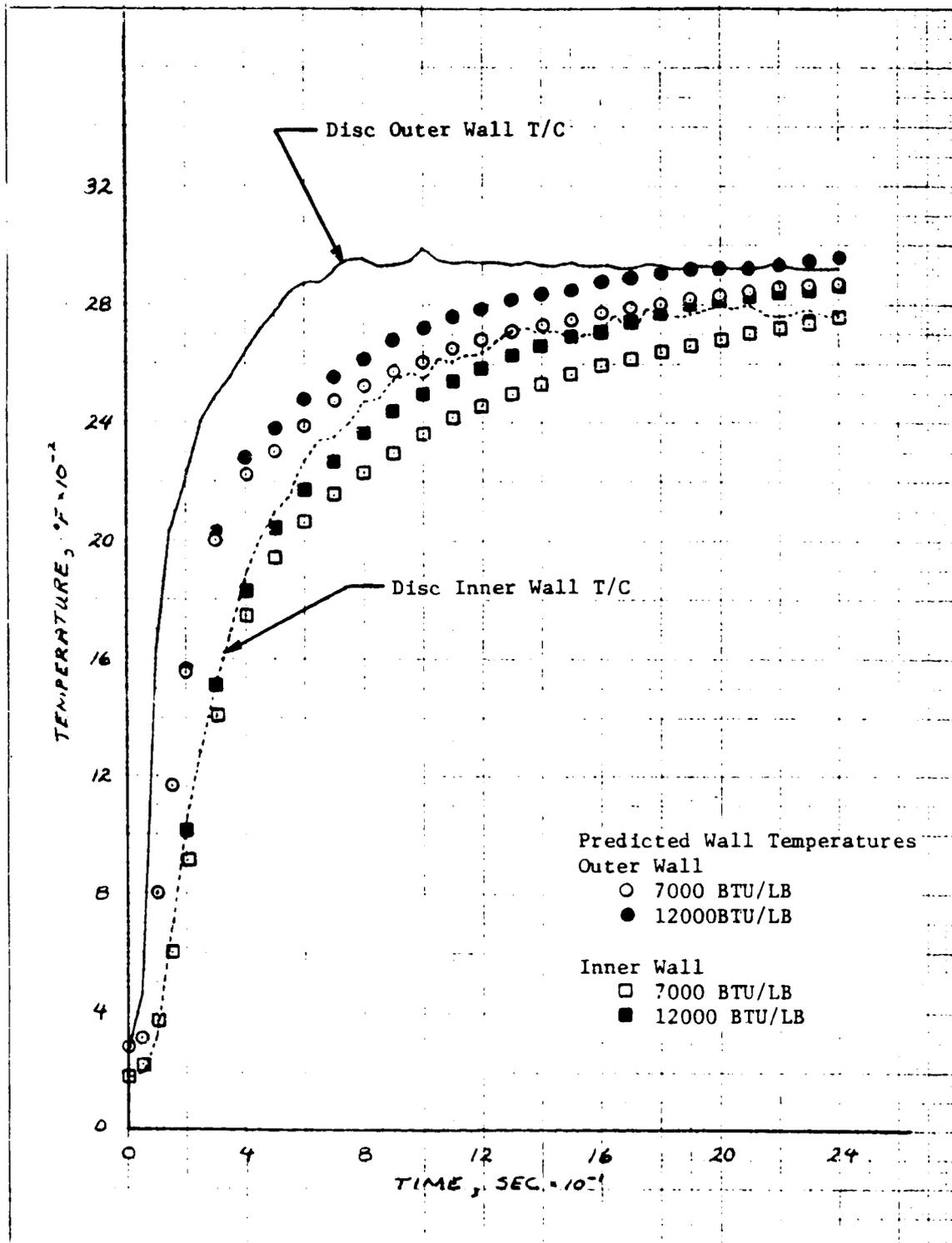
FIGURE 7-71 - COMPARISON PREDICTED TEMPERATURES WITH TEST RUN NO. 6,
SEADS TEST SPECIMEN WITH HOLDER FACE FULLY CATALYTIC AND
PENETRATION PORT PARTIALLY CATALYTIC

"NOSE CAP" END

221GT4074-2
PENETRATION ASSEM.

221GT4099
HOLDER
GRAPHITE

GRAPHITE
BOLT & CLAMP

PRESSURE
TUBE

"MANIFOLD END"

BASE PLANE FOR
MEASURING TUBE HEIGHT

GRAPHITE BOLT & CLAMP
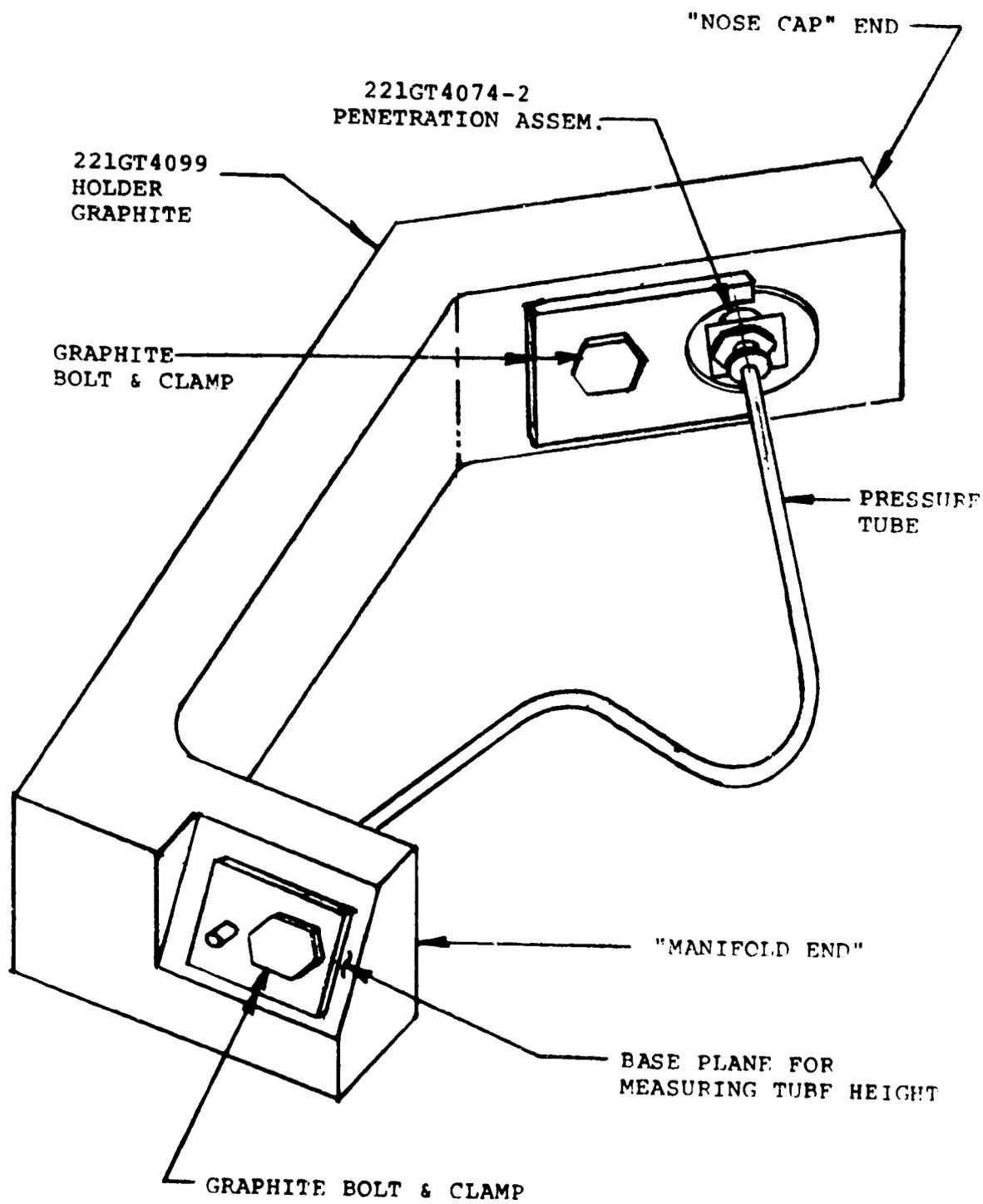
FIGURE 8-1 - TEST CONFIGURATION

246
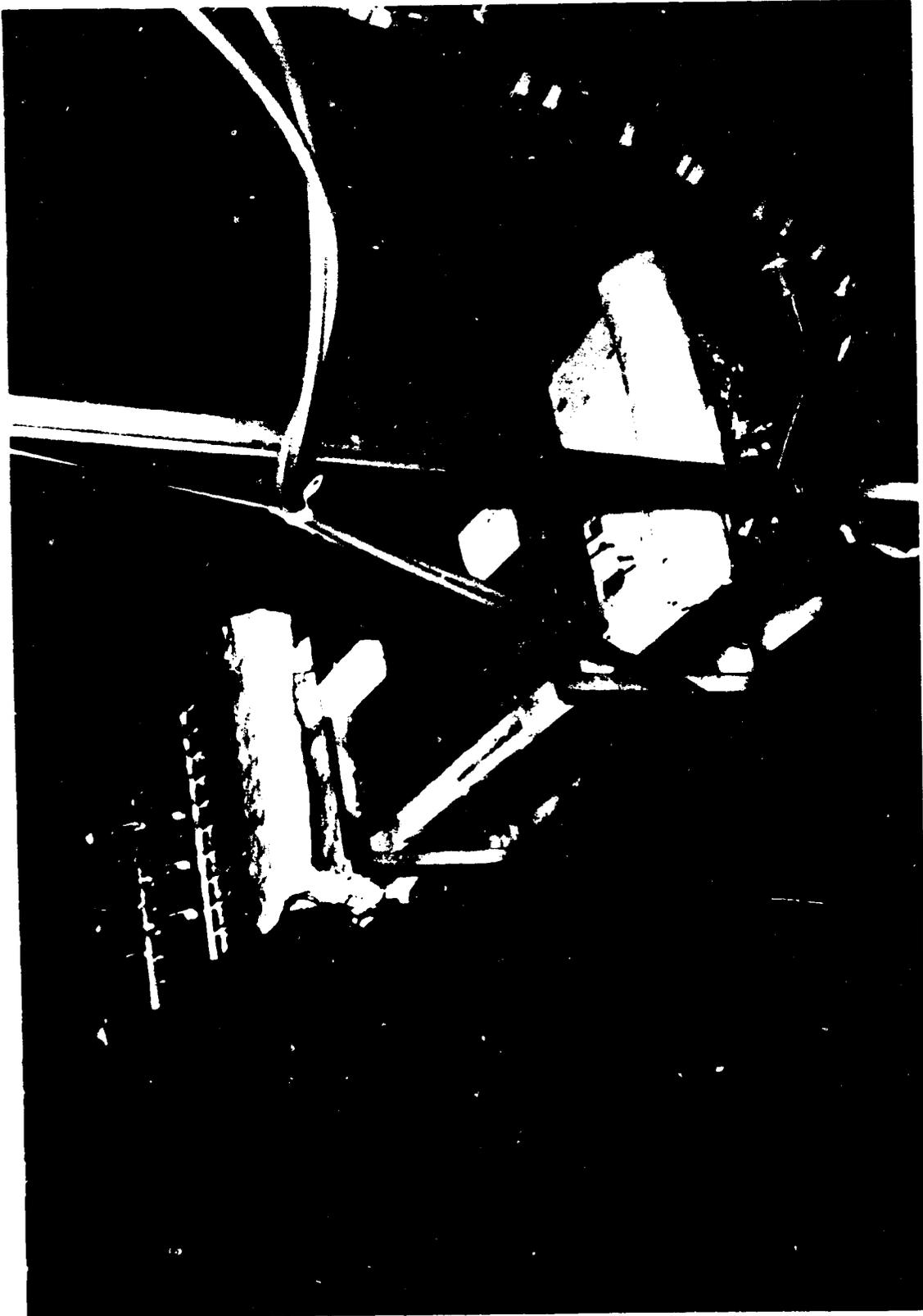
FIGURE 8-2 - SEADS PRESSURE TUBES THERMAL TEST - SET-UP IN NERVA CHAMBER

FIGURE 8-3 - SEADS PRESSURE TUBES THERMAL TEST - HEATER BARS AND TEST ZONE WITH

FIGURE 8-4 – SEADS PRESSURE TUBES THERMAL TEST – COOLDOWN ZONE
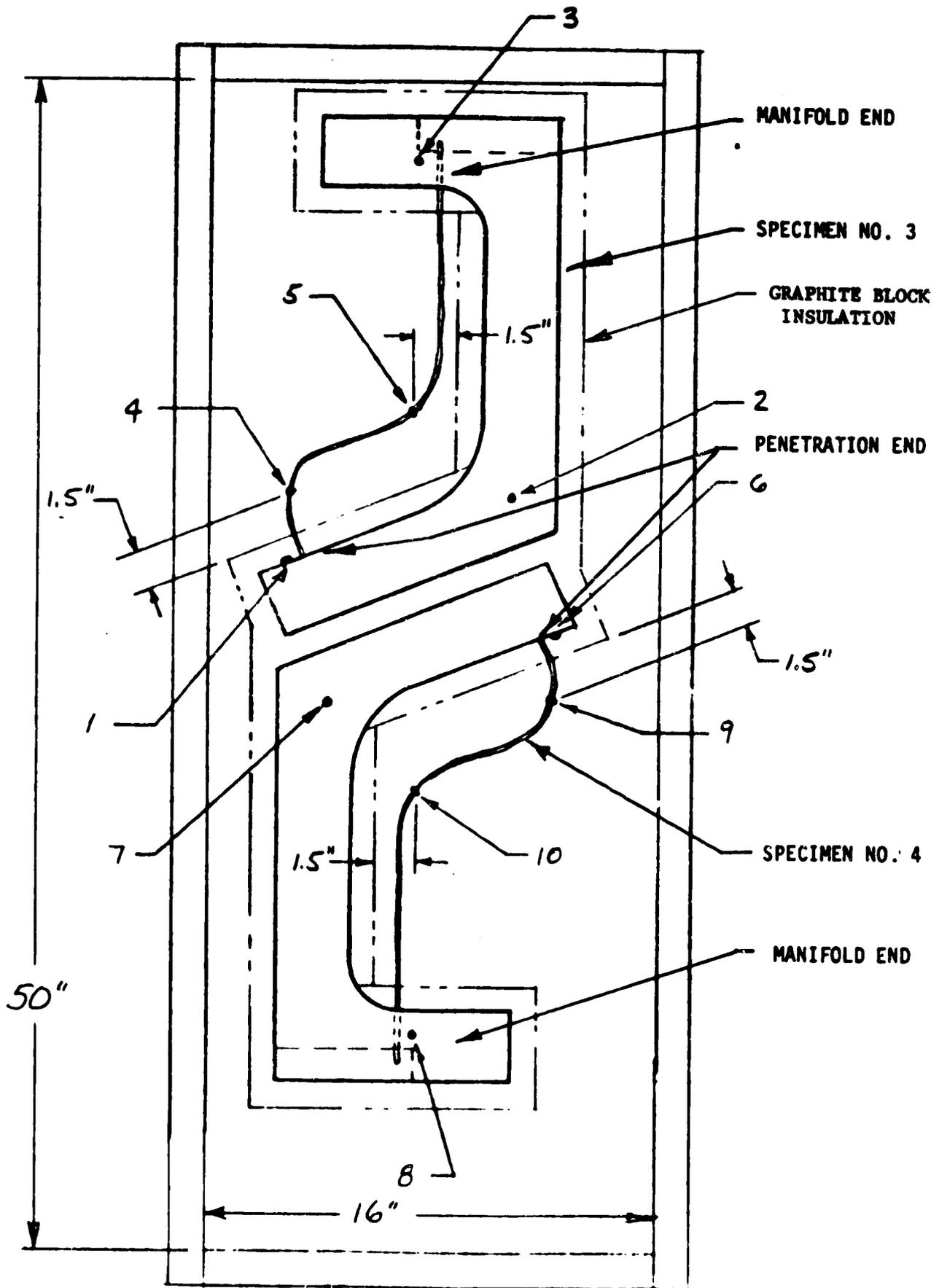
FIGURE 8-5 – THERMAL DEFLECTION TEST OF SEADS PRESSURE TUBES,
SPECIMENS NO. 3 & NO. 4 THERMOCOUPLE LOCATIONS
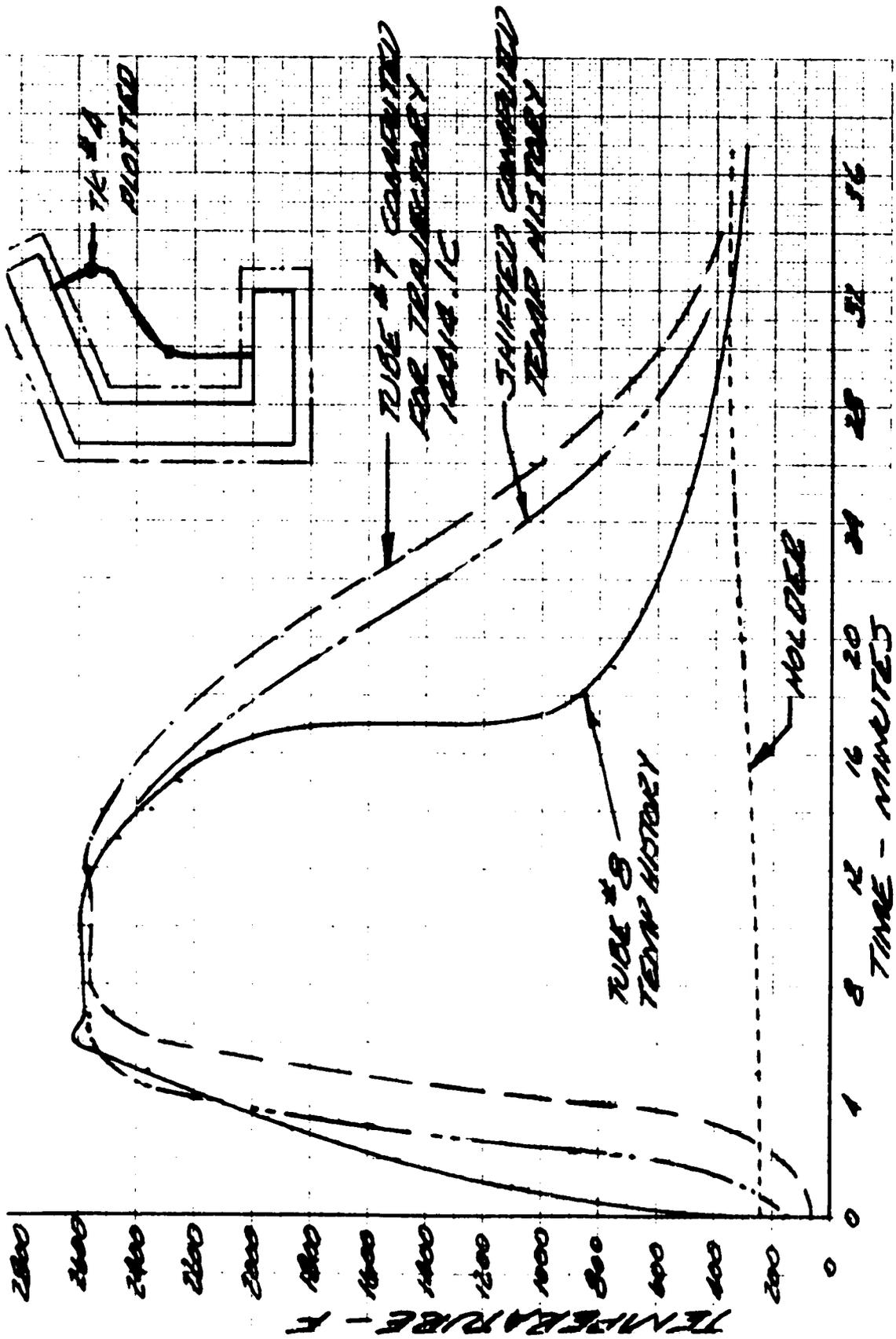
FIGURE 8-6 - TYPICAL THERMAL TEST TEMPERATURE HISTORY

251

68 CYCLES
SPEC. NO. 3
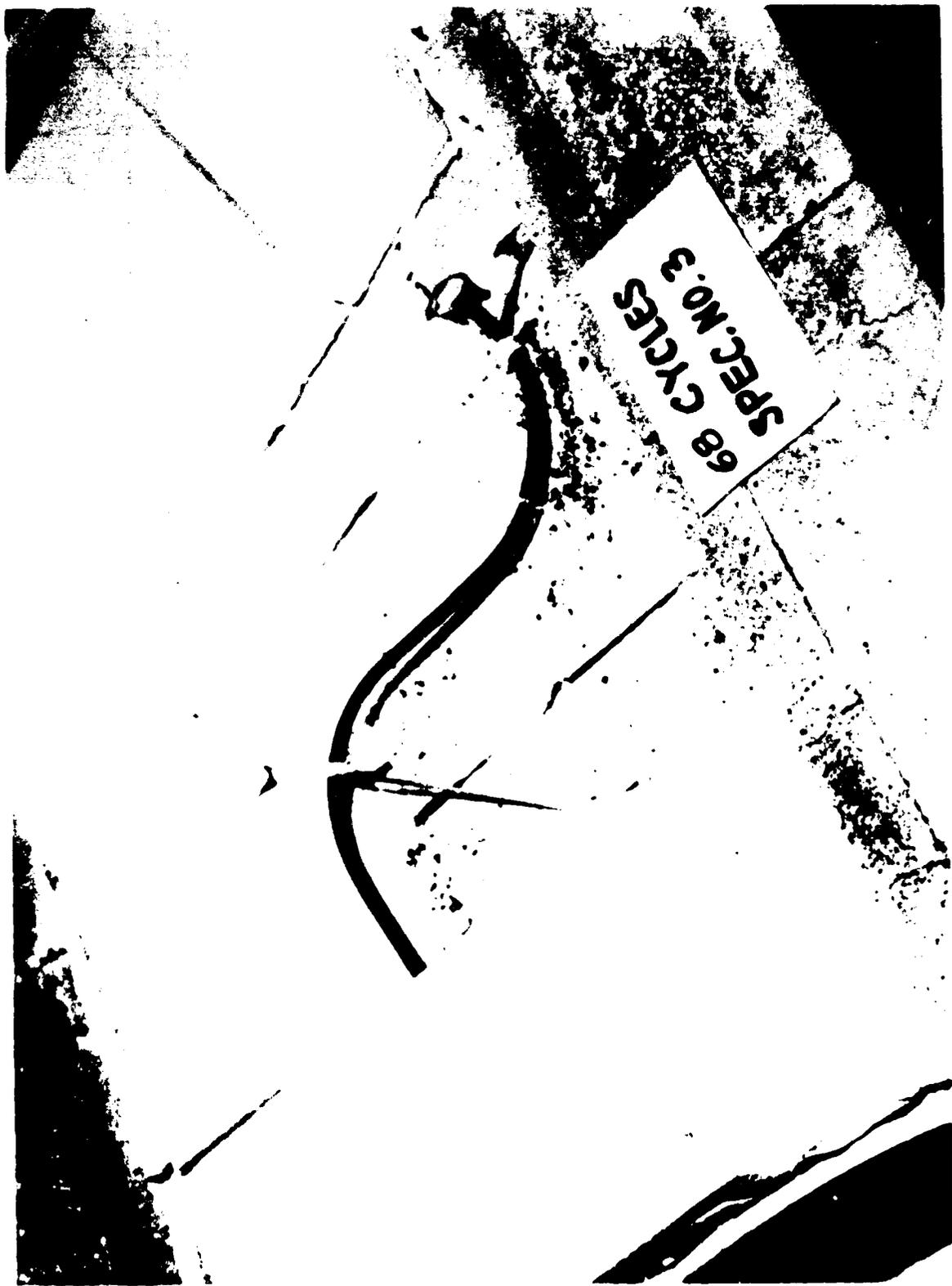
ORIGINAL PAGE
BLACK AND WHITE PHOTOGRAPH
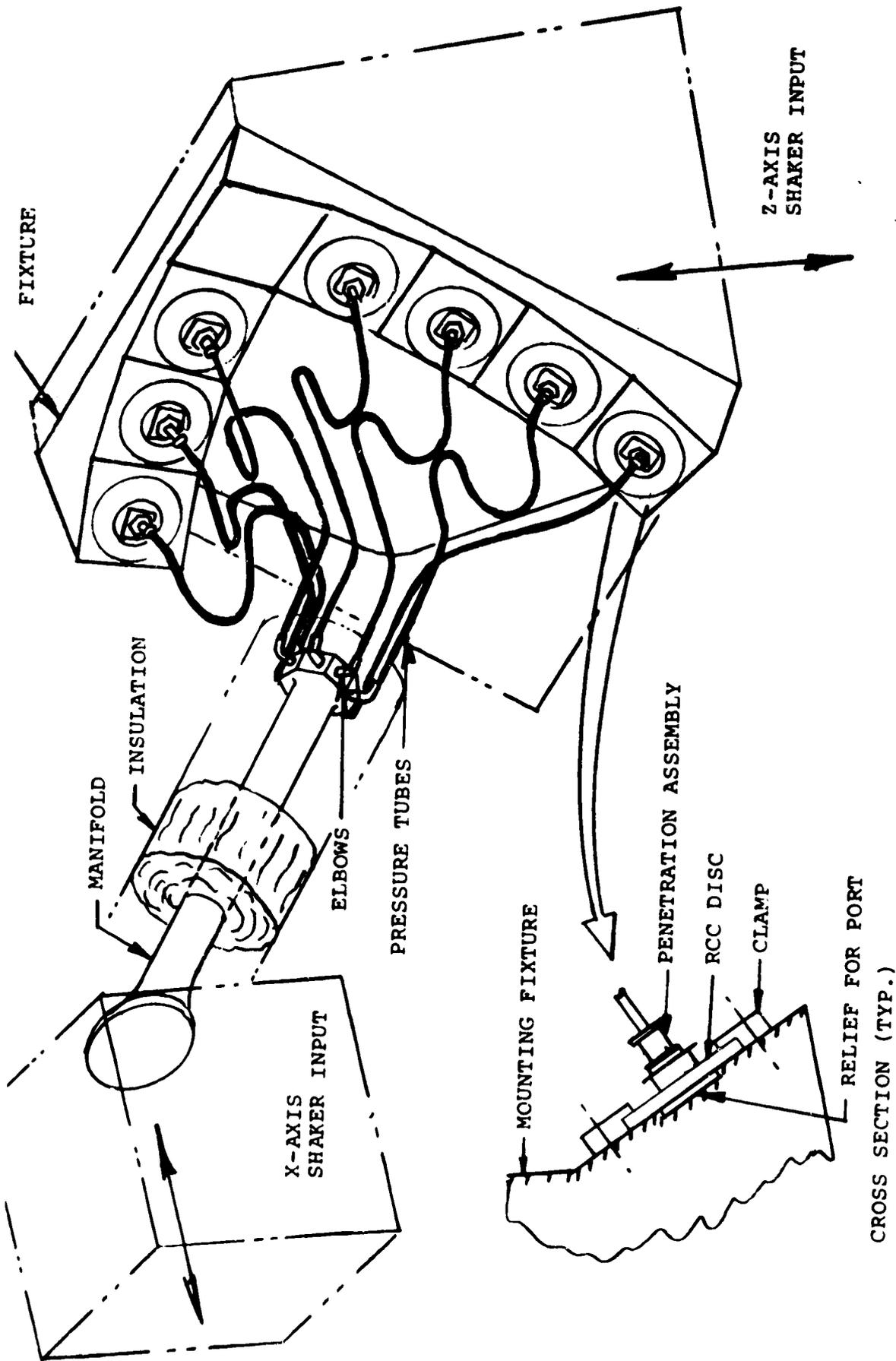
FIGURE 9-1 - VIBRATION TEST CONCEPT

FIXTURE

Z-AXIS SHAKER INPUT

MANIFOLD

INSULATION

ELBOWS

PRESSURE TUBES

X-AXIS SHAKER INPUT

MOUNTING FIXTURE

PENETRATION ASSEMBLY

RCC DISC

CLAMP

RELIEF FOR PORT

CROSS SECTION (TYP.)

253
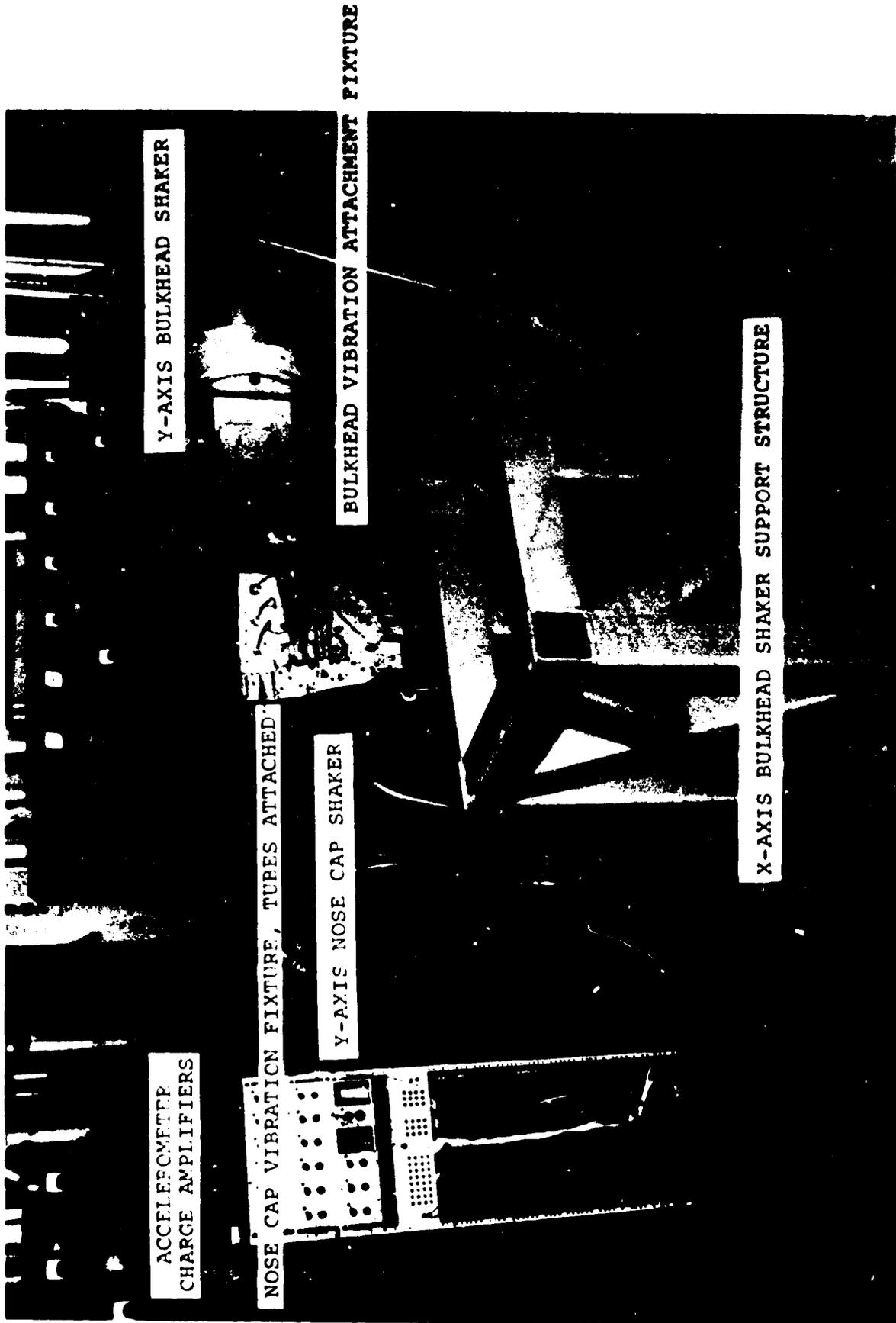
Y-AXIS BULKHEAD SHAKER

BULKHEAD VIBRATION ATTACHMENT FIXTURE

X-AXIS BULKHEAD SHAKER SUPPORT STRUCTURE

ACCELEROMETER CHARGE AMPLIFIERS

NOSE CAP VIBRATION FIXTURE, TUBES ATTACHED

Y-AXIS NOSE CAP SHAKER

FOLDOUT FRAME 1,

VIEW B-B
SCALE: FULL SIZE

Xcm = 180.00

221 GT 4084 FITTING REF
AL ALY CASTING '356 T6

VIEW LOOKING
DOWN

Xcm = 66.684

ADAPTOR PROVIDED BY
ENVIRONMENTAL TEST LAB
SEE NOTE 5

Zcm
280.00
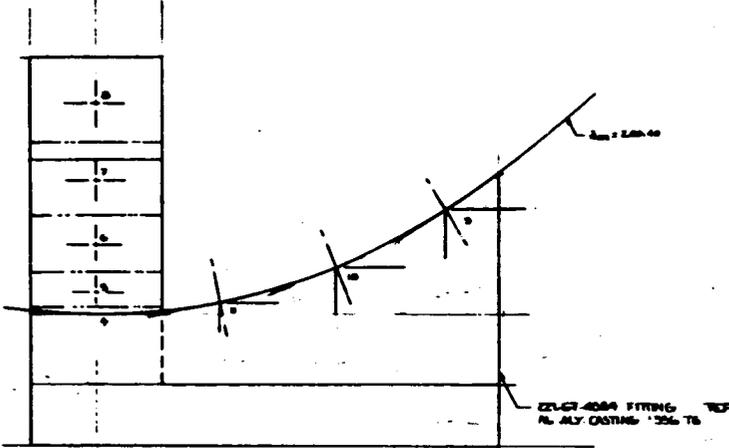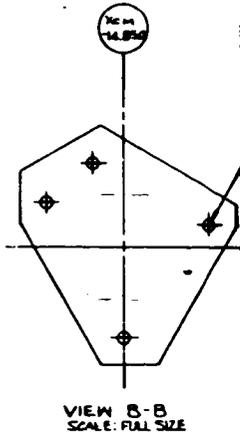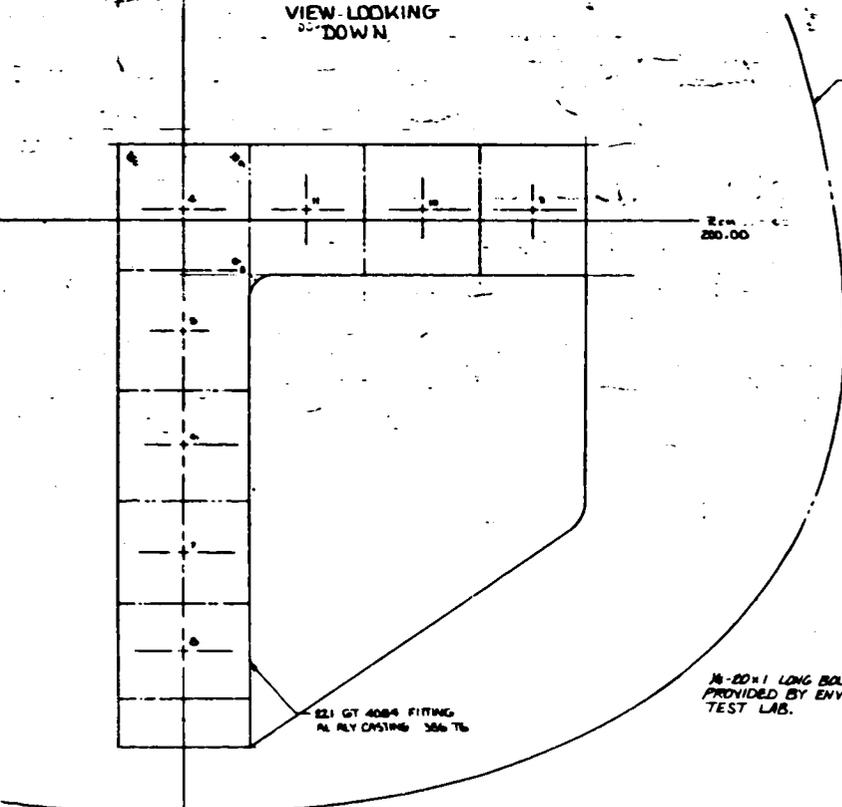
LOCATION OF AXIAL STRAIN GAGES
(TYPICAL FOR EACH TUBE) 3 AT EACH
END, AND AT A CENTER LOCATION.
STRAIN GAGES TO BE SPACED
120° APART. SPECIFIC LOCATIONS
WILL BE DEFINED BY T.R.

PORT ASSY
SEE TAB

1/4-20 × 1 LONG BOLT TO BE
PROVIDED BY ENVIRONMENTAL
TEST LAB.

SEE NOTE 4

221 GT 4084 FITTING
AL ALY CASTING '356 T6
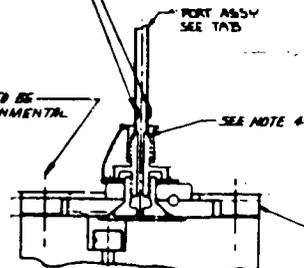
221 GT 4095
INSTALL THE RETAINER RING.
MEASURE THE GAP AND SHIM
AS REQD WITH 221 GT 4096 TO
REDUCE THE GAP TO .010.
TORQUE BOLTS 80 TO 95 IN LB.

SECT A-A
TYPICAL PORT ASSY
7 PLACES

SEE TABLE A FOR EXACT
SPECIMEN CONFIGURATION

VIEW LOOKING
AFT

X
SHAKER AXIS

A

BOLTS TO BE PROVIDED BY
ENVIRONMENTAL TEST LAB

LOCATION 9

LOCATION 10

LOCATION H

76 DIA BOLTS TO BE PROVIDED BY
ENVIRONMENTAL TEST LAB

ADAPTOR PROVIDED BY
ENVIRONMENTAL TEST
LAB

FITTING

TRIAXIAL
ACCELEROMETER

LOCATION OF THREE REMOTE
STRAIN GAGES ON MANIFOLD
SPACED 120° APART

GT 4084 FITTING
AL ALY CASTING 356 T6

TRIAXIAL
ACCELEROMETER
(CONTROL)

5579-00267

5579-00256

TRIAXIAL
ACCELEROMETER

25°

TRIAXIAL
ACCELEROMETER

TRIAXIAL
ACCELEROMETER
(CONTROL)

MANIFOLD AT
BHD PLANE

TRIAXIAL
ACCELEROMETER
(CONTROL)

HOLES IN FITTING ARE TO
MATCH HOLES IN ADAPTOR

LOCATION 5

LOCATION 6

LOCATION 2

LOCATION 8

TRIAXIAL
ACCELEROMETER

SHAKER
SHAKE AXIS AT
BULKHEAD END

REF 221 GT 4084 FITTING
AL ALY CASTING 356 T6

NOTES:

1. MANIFOLD ASSEMBLY INSULATION AND PRESSURE TUBES
   ARE ROCKWELL SUPPLIED

2. PRESSURE TUBES TO BE FITTED TO SS 79-00256 MANIFOLD
   ON ASSEMBLY. TUBE ENDS WILL BE CUT AND FLARED ON
   ASSEMBLY TO PRODUCE ESSENTIALLY NO PRELOAD INTO TUBES.

3. ADAPTER SHALL BE SIZED TO PERMIT EXCITATION IN
   EITHER X, Y OR Z AXIS FINAL SHAKE AXIS IS TBD.

4. 221 GT 4088-1 UNION SHALL HAVE APPLICATION OF SILICON
   CARBIDE AND METHOCEL APPLIED BEFORE ASSEMBLY BY
   ENGINEERING MATERIALS LAB. ASSEMBLY OF COMPONENTS
   SHALL BE FINGER TIGHT. LOCKWIRE WITH 10 MIL PURE
   IRIDIUM WIRE, NUT TO WASHER, TWO PLACES.
   INSTALL THE WIRE SO THAT TENSION IN THE WIRE TENDS TO
   TIGHTEN THE NUT.

TABLE A

LOCATION	PORT ASSY
8	221 GT 4094 - 3
2	221 GT 4094 - 5
6	221 GT 4094 - 1
5	221 GT 4094 - 3
11	221 GT 4094 - 4
10	221 GT 4094 - 2
9	221 GT 4094 - 1

FIGURE 9-3   VIBRATION
TEST DRAWING

VOUGHT
CORPORATION

COMPONENT VIBRATION TEST
SHUTTLE ENTRY AIR DATA SYSTEM

80378   221 GT 4090

255

FIGURE 9-5 - INSULATION COMPONENTS
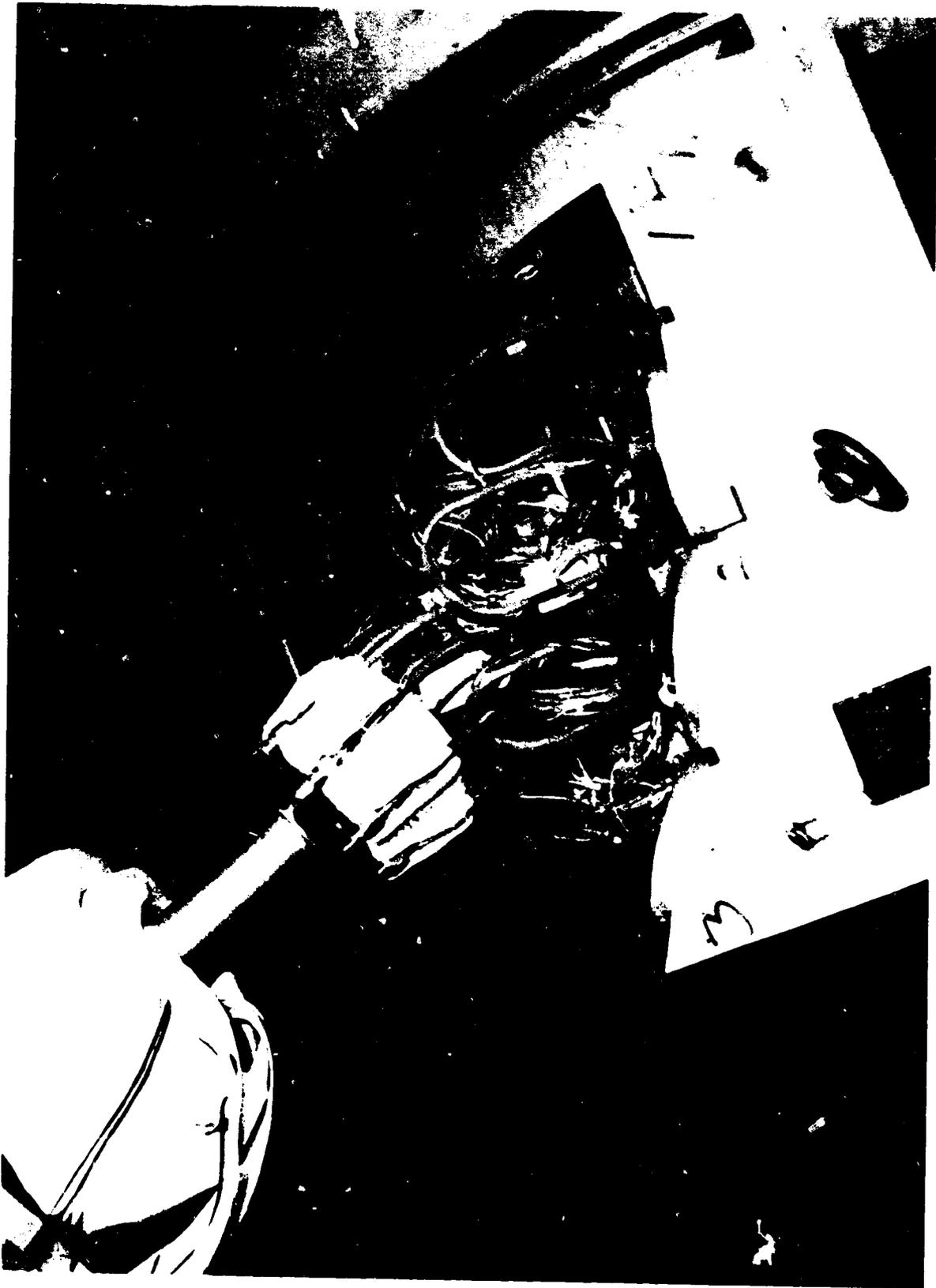
ORIGINAL PAGE
BLACK AND WHITE PHOTOGRAPH
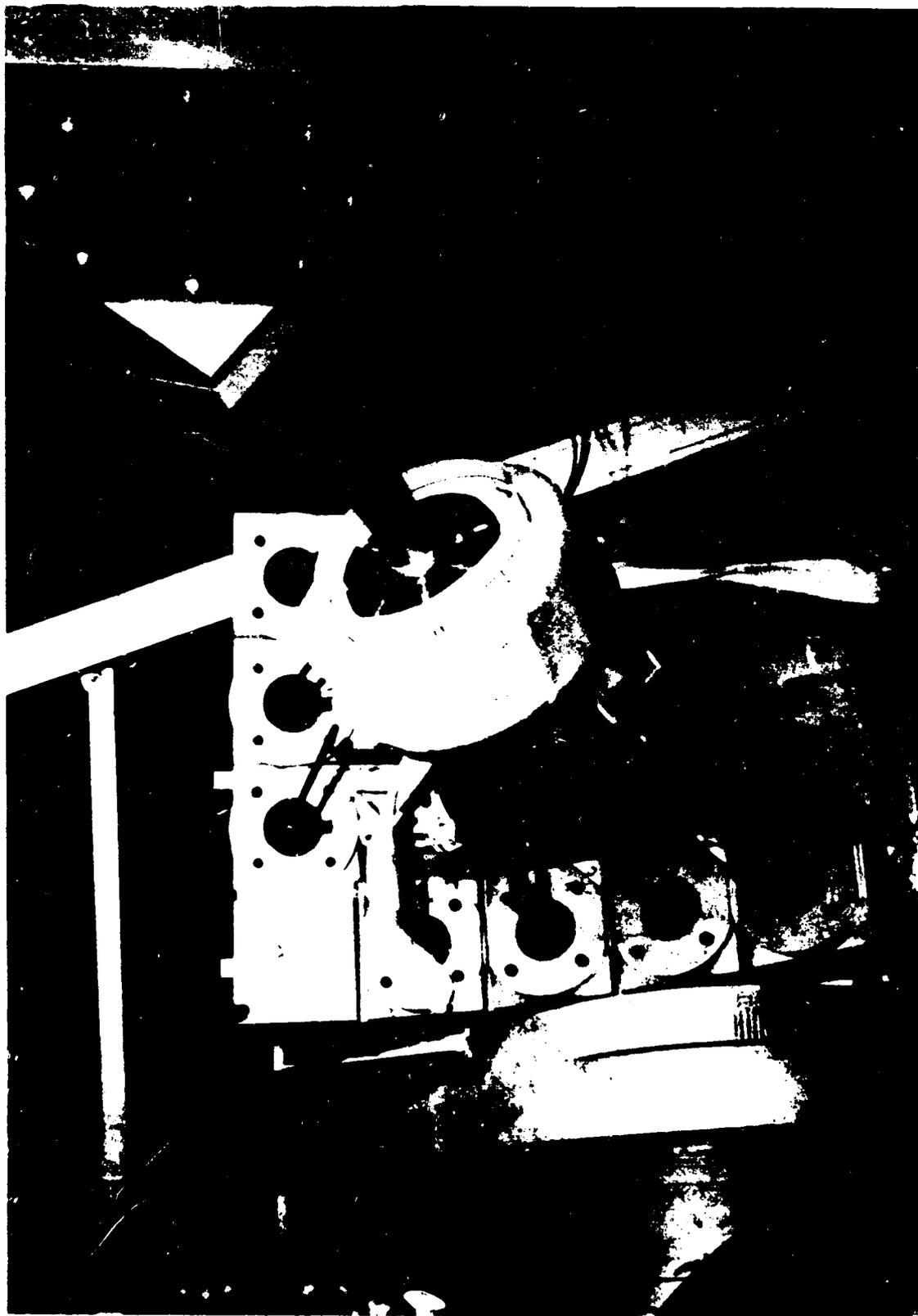
FIGURE 9-7 – INSULATION INSTALLATION
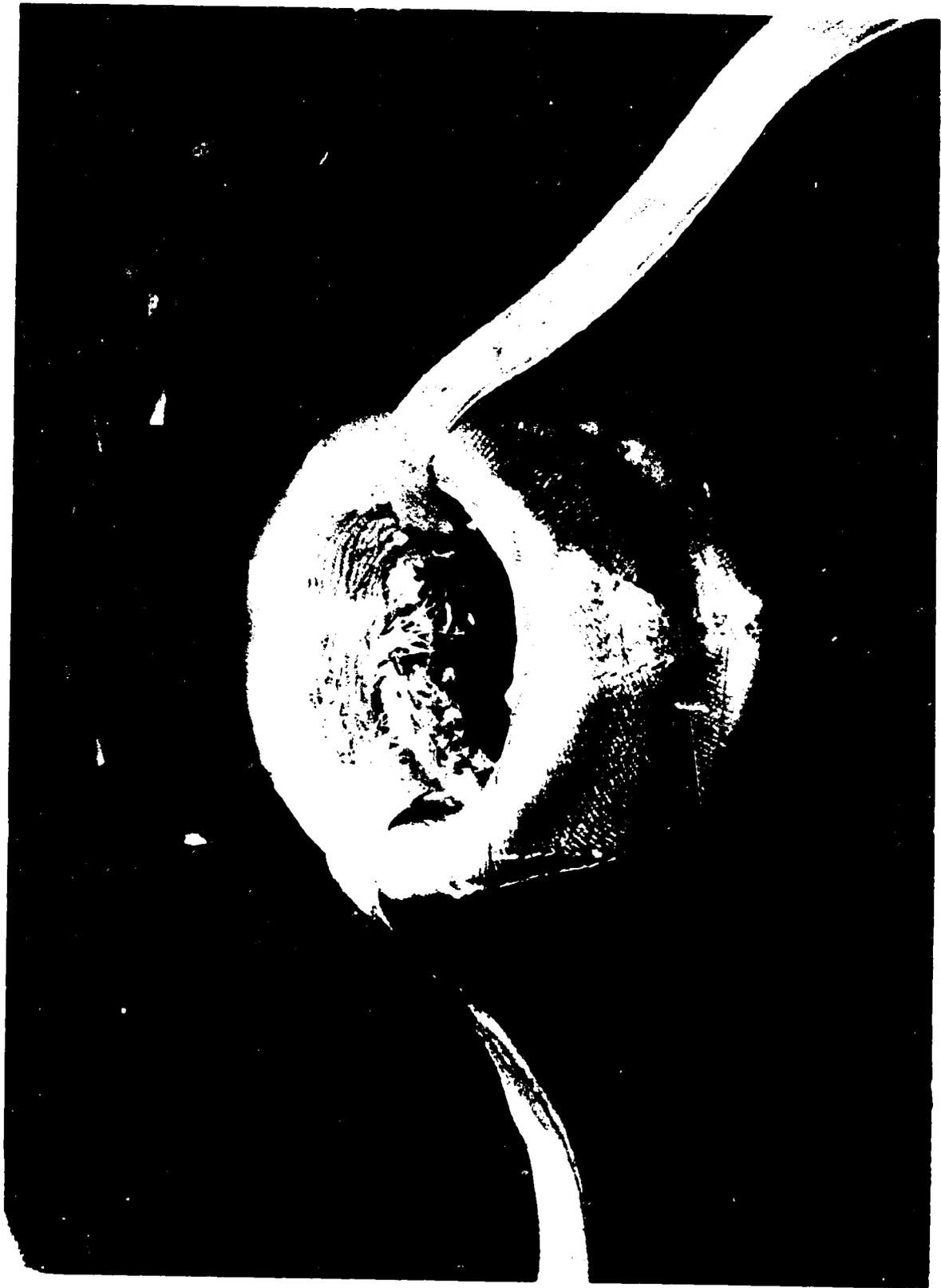
ORIGINAL PAGE
BLACK AND WHITE PHOTOGRAPH
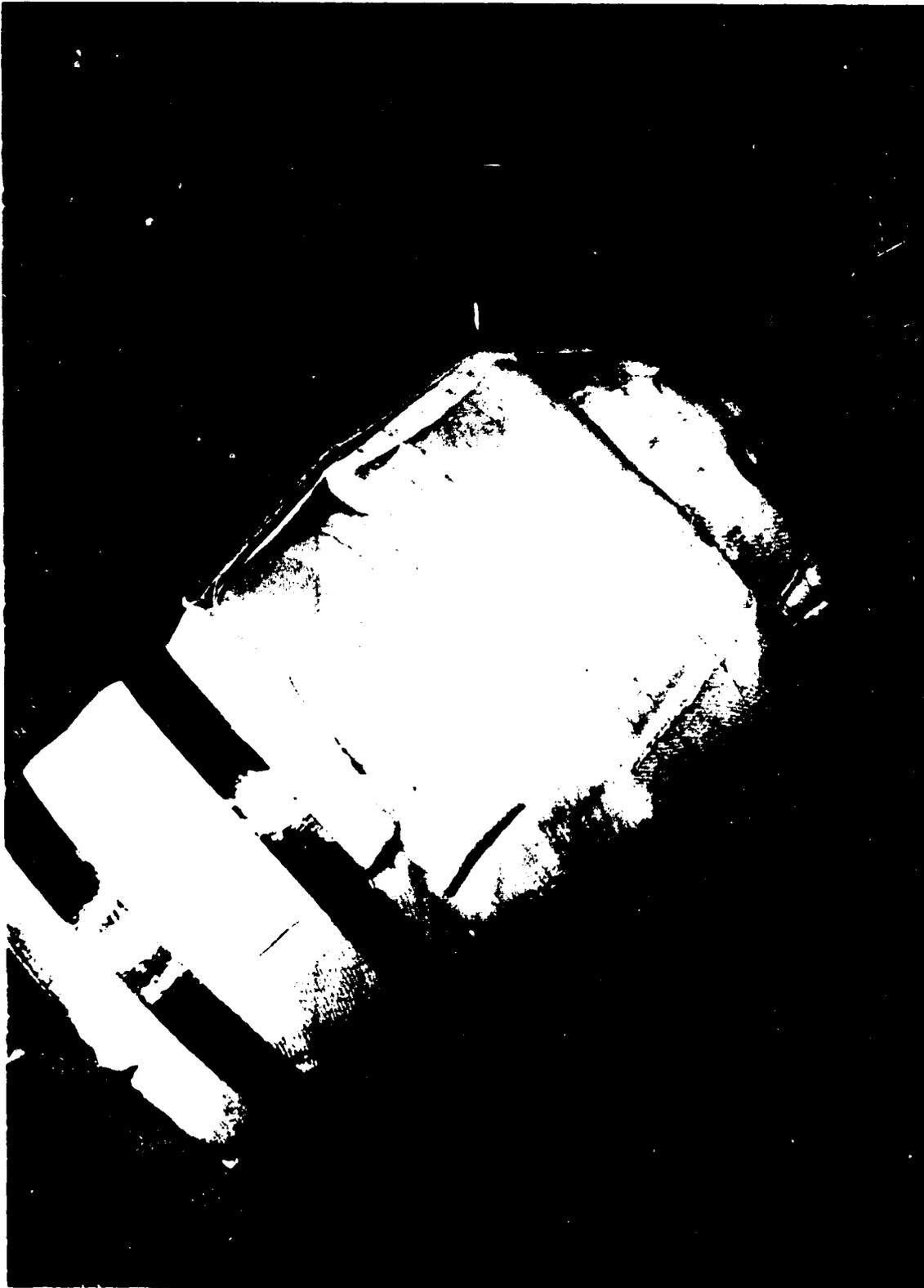
FIGURE 9-9 - INSTALLED INSULATION

SEADS RANDOM VIB.Y-Y

1980/09/29
15:04:24.35

NOSE CAP Y   FREQUENCY - HZ 2000 HZ BANDWIDTH 250 LINES
TOTAL GRMS 10.12   199 D.O.F

262

FIGURE 9-11 - CONTROL ACCELEROMETERS Y-Y AXIS, ACCELEROMETER 6 (YBC) BULKHEAD Y-AXIS

SEADS RANDOM VIBRATION X-Z AXIS

NOSE CAP-Z

TOTAL GRMS   9.12

1980/10/03
09:29:56.03

2000 HZ BANDWIDTH   250 LINES
199 D.O.F

FREQUENCY - HZ

G2/HZ
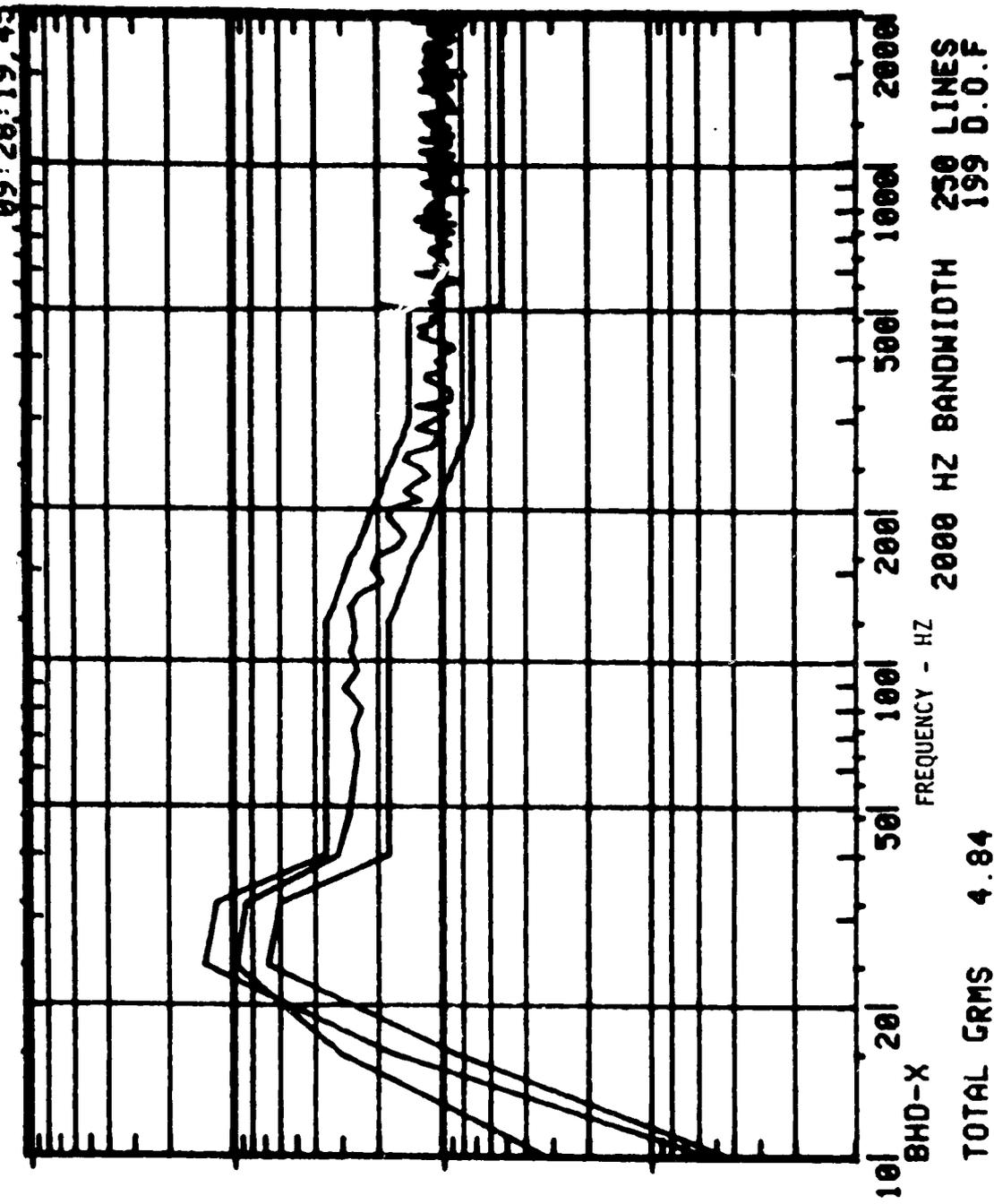
FIGURE 9-13 - CONTROL ACCELEROMETERS X-Z AXIS, ACCELEROMETER 6 (XBC)
BULKHEAD X-AXIS
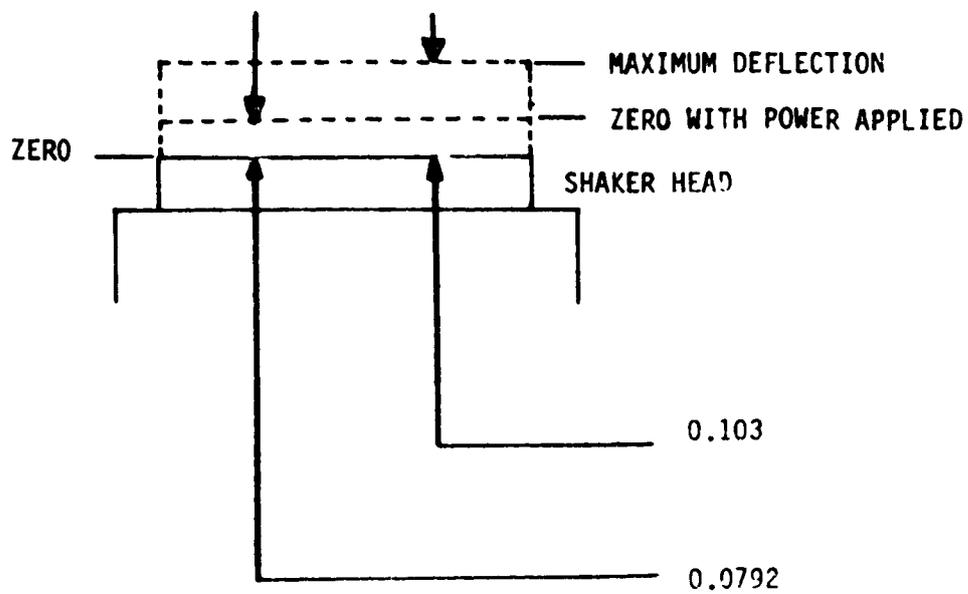
BULKHEAD SHAKER X AXIS AND Y AXIS
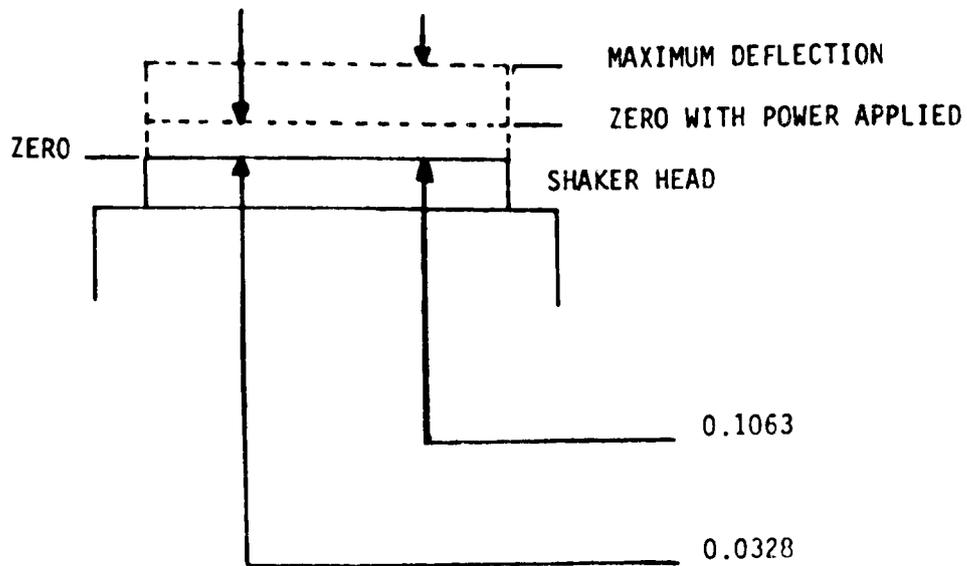
NOSECAP SHAKER Z AXIS AND Y AXIS

FIGURE 9-14 - STATIC SHAKER DEFLECTION WHEN POWER APPLIED TO SYS'
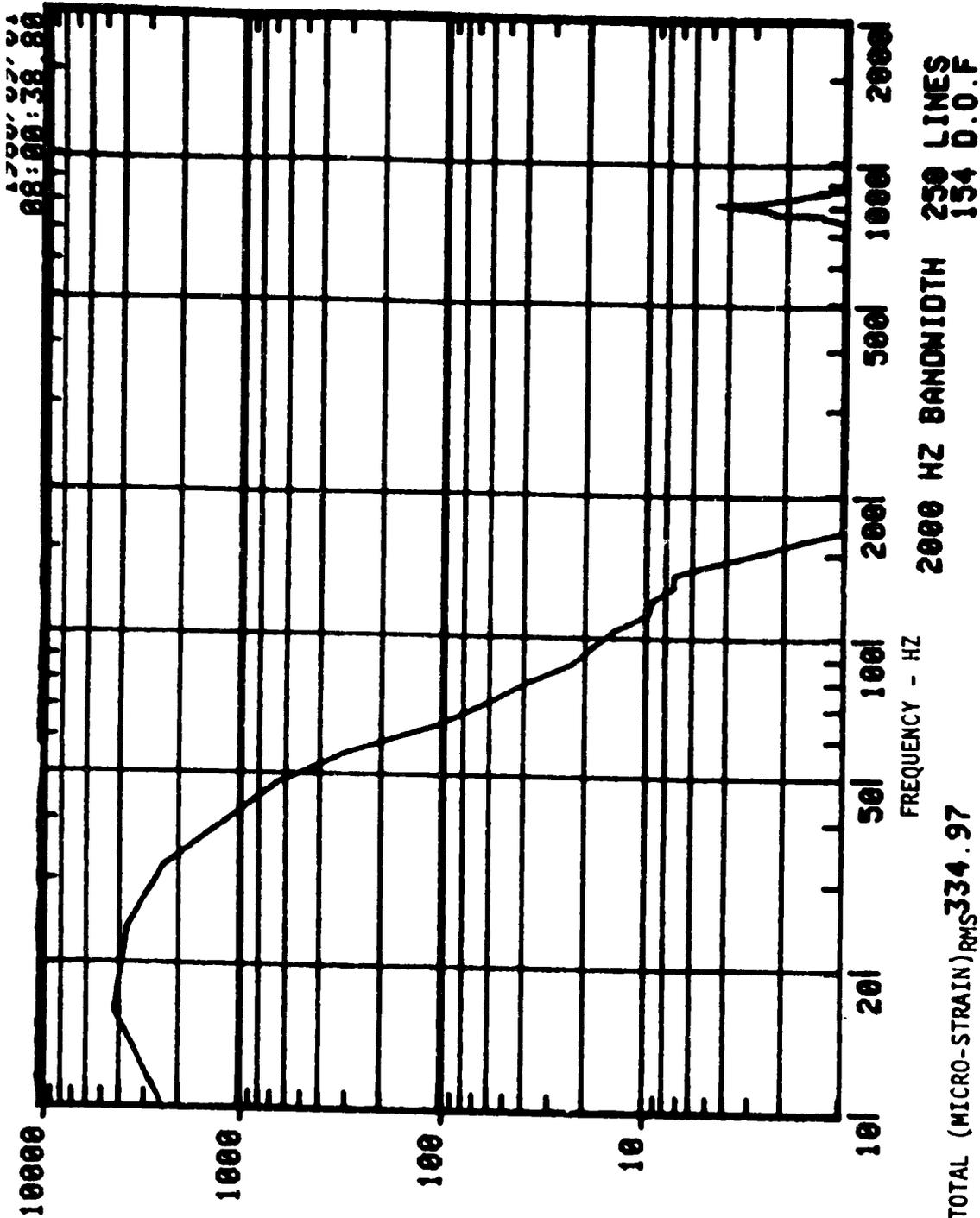
FIGURE 9-15 - STRAIN RESPONSE PLOT Y-Y AXIS, STRAIN GAGE 800M

SEADS RANDOM VIB.

FIGURE 9-16. - STRAIN RESPONSE PLOT X-X AXIS, STRAIN GAGE GAGE

TOTAL (MICRO-STRAIN)_{RMS} 93.33

FREQUENCY - HZ

2000 HZ BANDWIDTH   250 LINES
                    154 D.O.F

STRAIN - (MICRO-STRAIN)^2/HZ

FREQUENCY - HZ
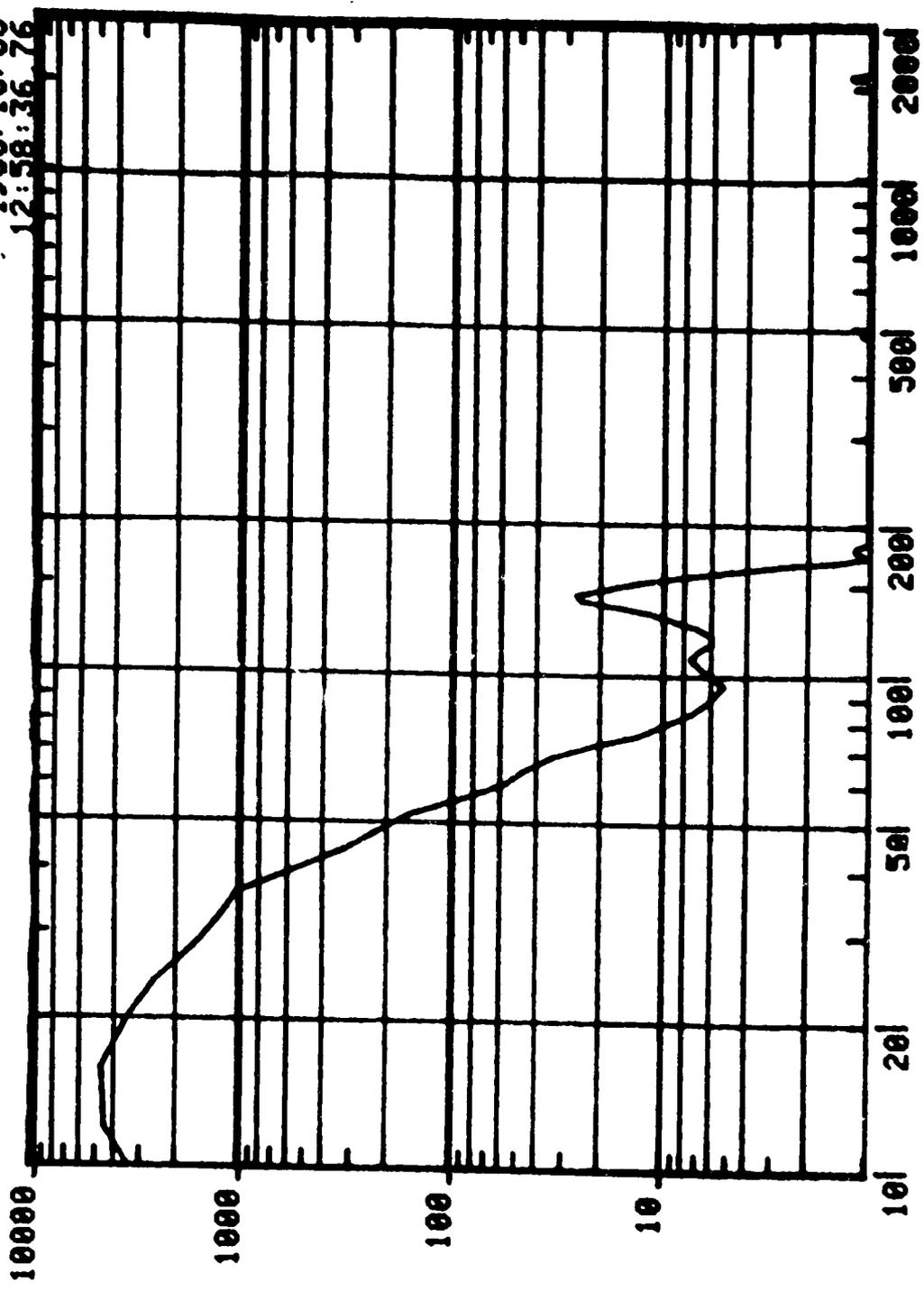
TOTAL (MICRO-STRAIN)$_{RMS}$ 782.00

2000 HZ BANDWIDTH 500 LINES
154 D.O.F

12:58:36.76

FIGURE 9-17 - STRAIN RESPONSE PLOT X-Z AXIS, STRAIN GAGE 800M

STRAIN - (MICRO-STRAIN)²/HZ

FIGURE 9-18 - STRAIN RESPONSE PLOT X-Z AXIS SPREADY GAGE 0002
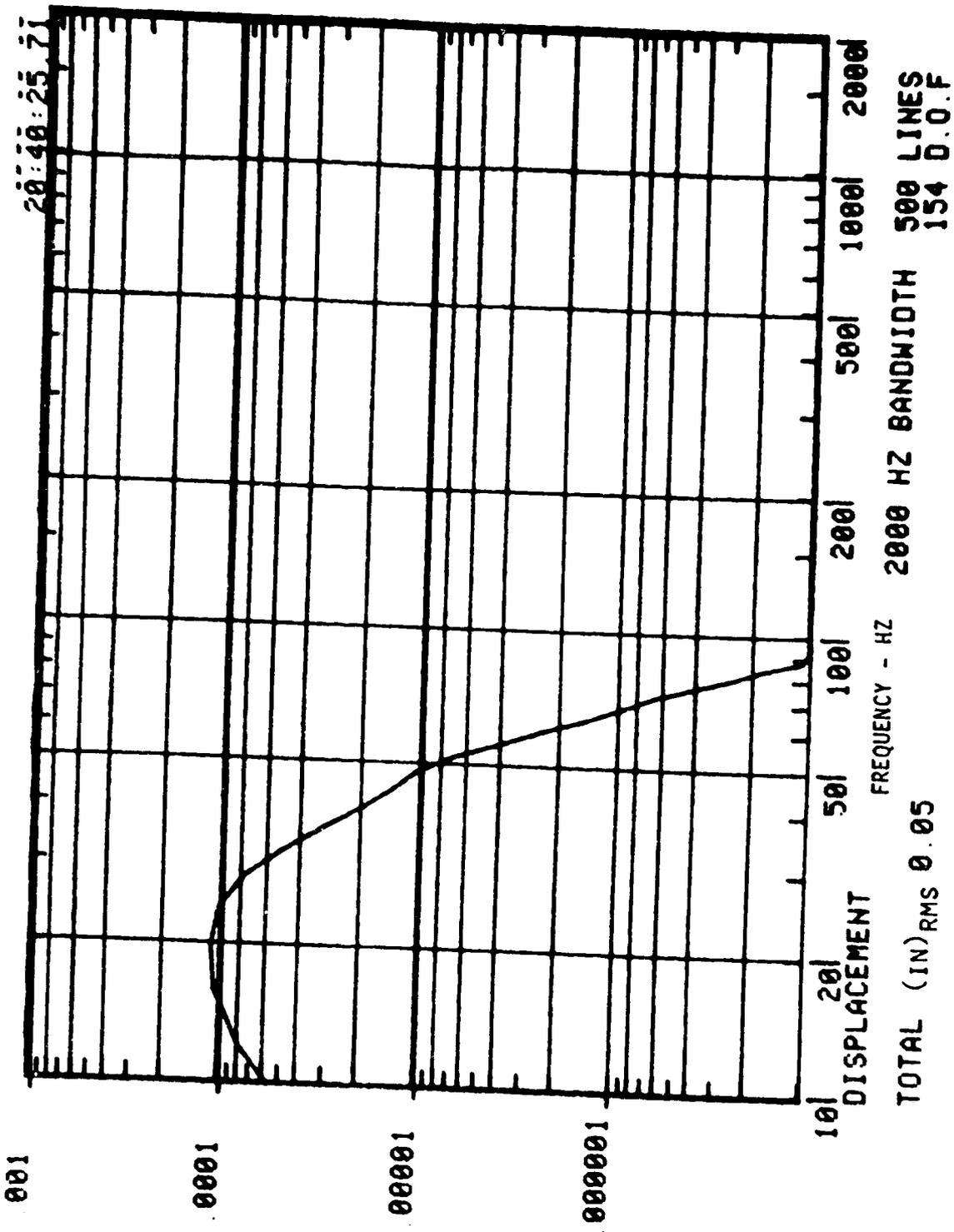
FIGURE 9-19 - DISPLACEMENT PLOT OF NOSE CAP INPUT SPECTRUM Y-AXIS

271

BH-Y, NC-Y AXES INPUTS
—— TEST
----- ANALYSIS

FREQUENCY, HZ

SSD, (μ IN./IN.)²/HZ
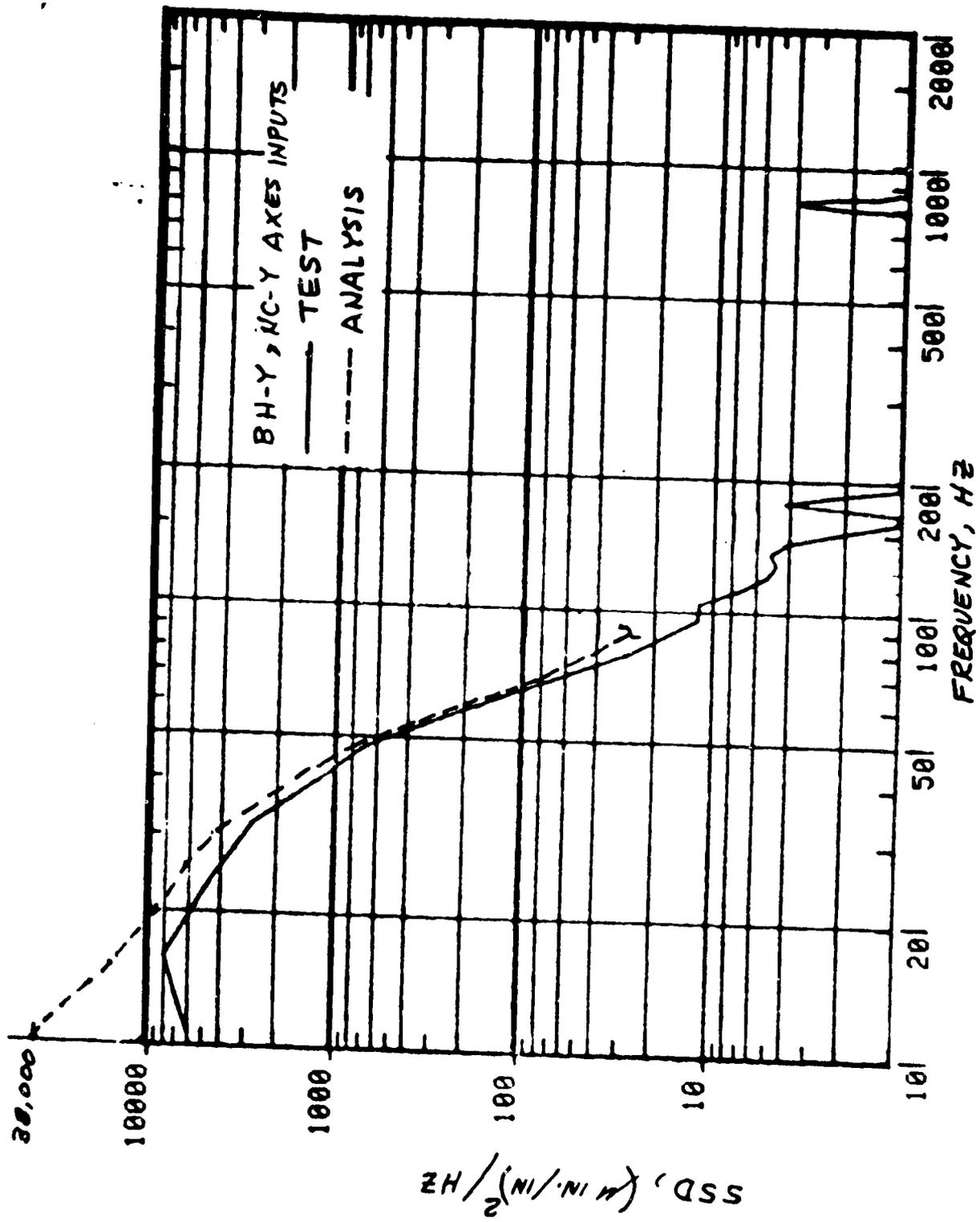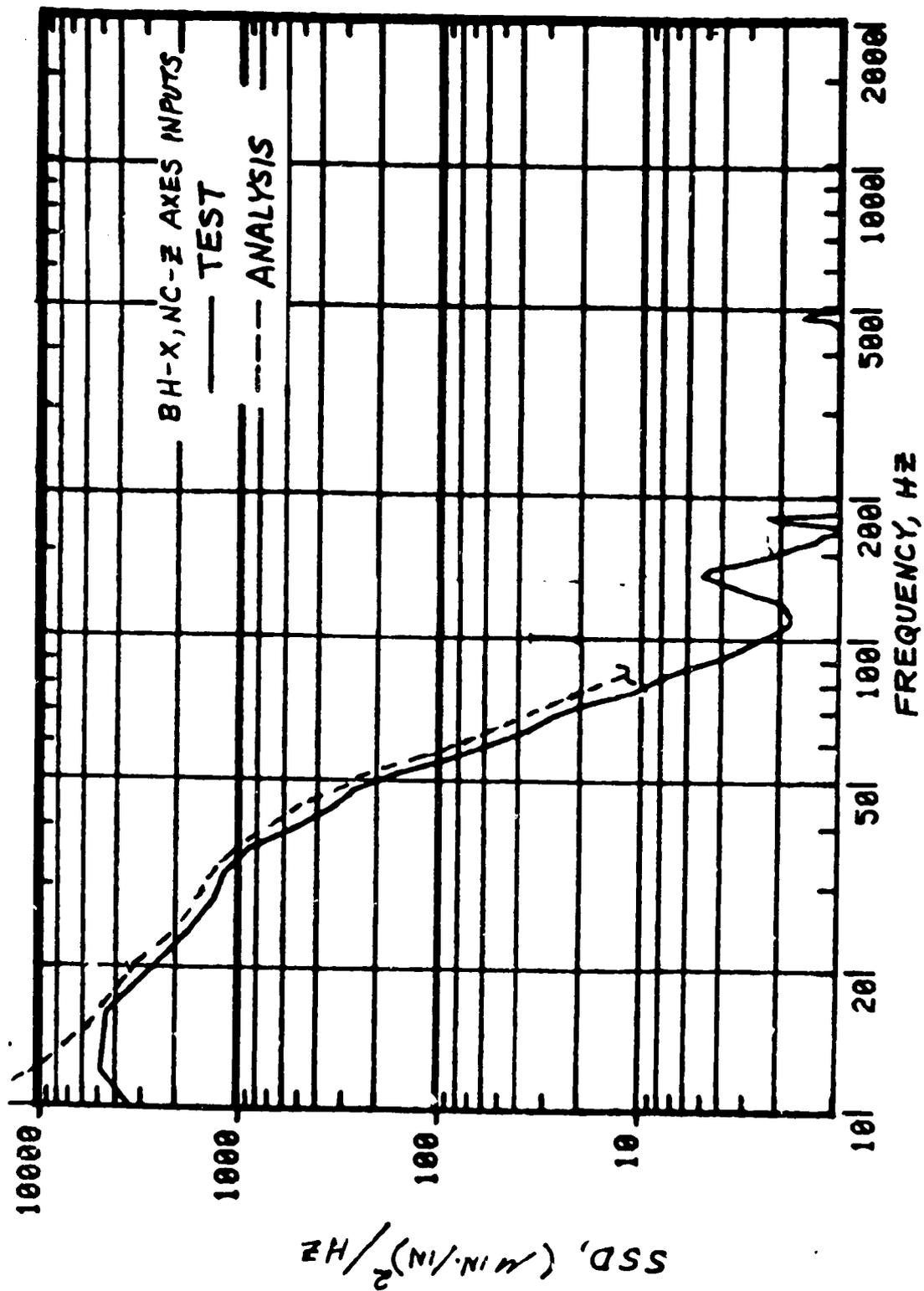
FIGURE 9-21 - STRAIN SPECTRAL DENSITY COMPARISONS - TUBE 8/MANIFOLD END

TUBE #11

TUBE #5

TUBE #8

TUBE #6

FIGURE 9-22 - TUBE ENDS AFTER VIBRATION TEST

274

APPENDIX A

INITIAL CONCEPTS

CONCEPT 1 & 1A

RCC NOSE CAP

PORT NUT
(CERAMIC)(RCC)
(CTD GR)

TUBE (METAL)

BOND MATL ON
THD FOR LOCK

SPACER

PLUG
(CERAMIC)
(CTD GRAPHITE)

ALTERNATE 1A
COUNTERSINK
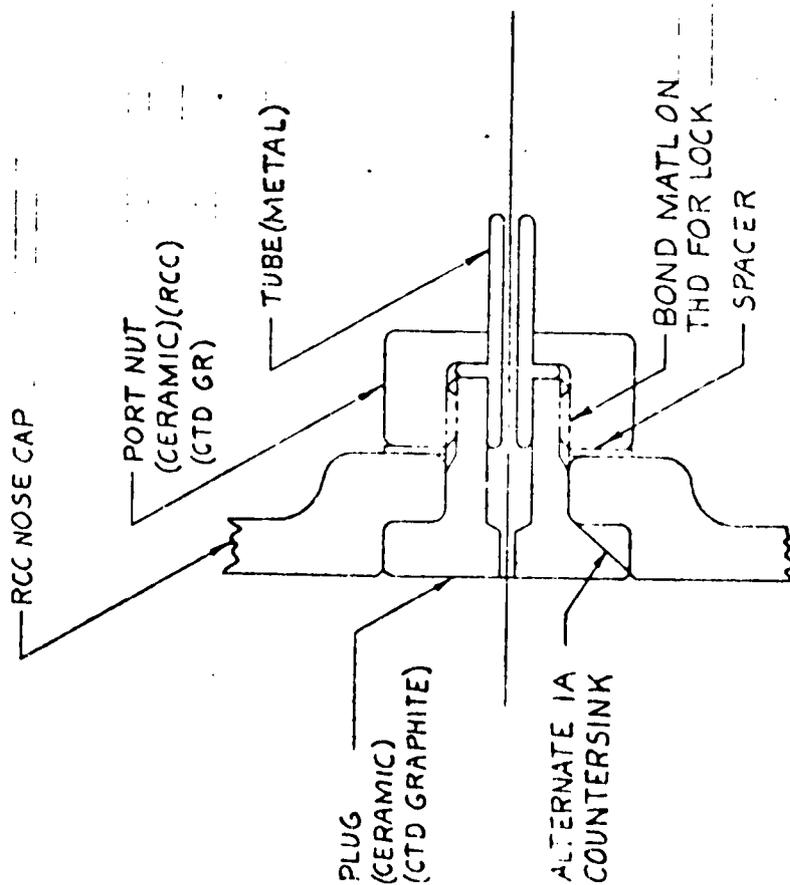
ADVANTAGES

1. VERY LITTLE OVERHANG KEEPS VIBRATION LOADS DOWN
2. SHORT PLUG EASILY COATED
3. THREADS PROVIDE POSITIVE RETENTION
4. ONLY 2 MACHINED PARTS
5. THREAD BOND LOCK BETWEEN COATED PARTS SHOULD BE SOUND
6. EASE OF ASSEMBLY

DISADVANTAGES

1. BOND FOR LOCK MAY DAMAGE PARTS DURING REPLACEMENT
2. SHIM FEATURE DIFFICULT TO ADJUST TO ACCOMMODATE RCC THICKNESS VARIATIONS
3. LOCKING DEPENDENT ON BOND
4. TUBE FLANGE COULD CAUSE THERMAL EXPANSION PROBLEM WITH COATED CARBON, CERAMIC, OR RCC NUT
5. NO REDUNDANCY EXCEPT THREAD FOR RETENTION
6. REQUIRES BUILD UP OF NOSE CAP THICKNESS LOCALLY FOR COUNTERBORED RCC; NO PROBLEM WITH COUNTERSINK
7. PROBABLY DIFFICULT DISASSEMBLY
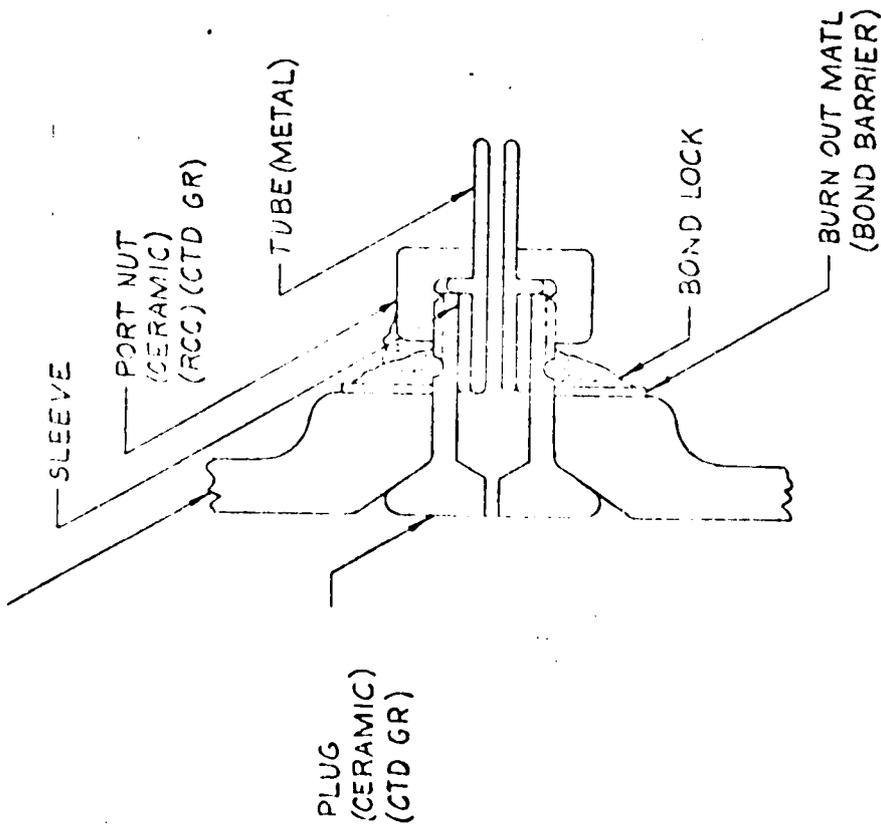
ADVANTAGES

1. BOND FOR RETENTION BUT THREADS PREVENT TOTAL LOSS

2. EASILY REPLACEABLE WITHOUT DAMAGE TO NOSE CAP

3. SHORT OVERHANG FOR VIBRATION LOADING

4. BOND MATERIAL LOCKED IN TO PLUG

5. ALLOWS FOR NOSE CAP THICKNESS VARIATIONS

DISADVANTAGES

1. DIFFICULT TO HOLD FOR BONDING

2. LOCKING DEPENDENT UPON BOND

3. LOOSENESS OF INSTALLATION AFTER FIRST MISSION BURNOUT

4. TUBE FLANGE COULD CAUSE THERMAL EXPANSION PROBLEM WITH COATED GRAPHITE, CERAMIC OR RCC NUT

5. PARTS PROBABLY DESTROYED DURING DISASSEMBLY

SLEEVE

PORT NUT
(CERAMIC)
(RCC)(CTD GR)

TUBE (METAL)

BOND LOCK

BURN OUT MATL
(BOND BARRIER)

PLUG
(CERAMIC)
(CTD GR)

VOUGHT SYSTEMS DIVISION
LTV AEROSPACE CORPORATION

277

CONCEPT 3 & 3A

RCC NOSE CAP

SPACER
(CERAMIC)
(RCC)(CTD GR)

THREADED PARTS
FOR BOND LOCK

ALTERNATE 3A
BOND ON THREADED

TUBE (METAL)

BREAK-OFF
REPLACEMENT

THERMOCOUPLE

BOND

PLUG
(CERAMIC)
(CTD GR)

SCALE 2/1
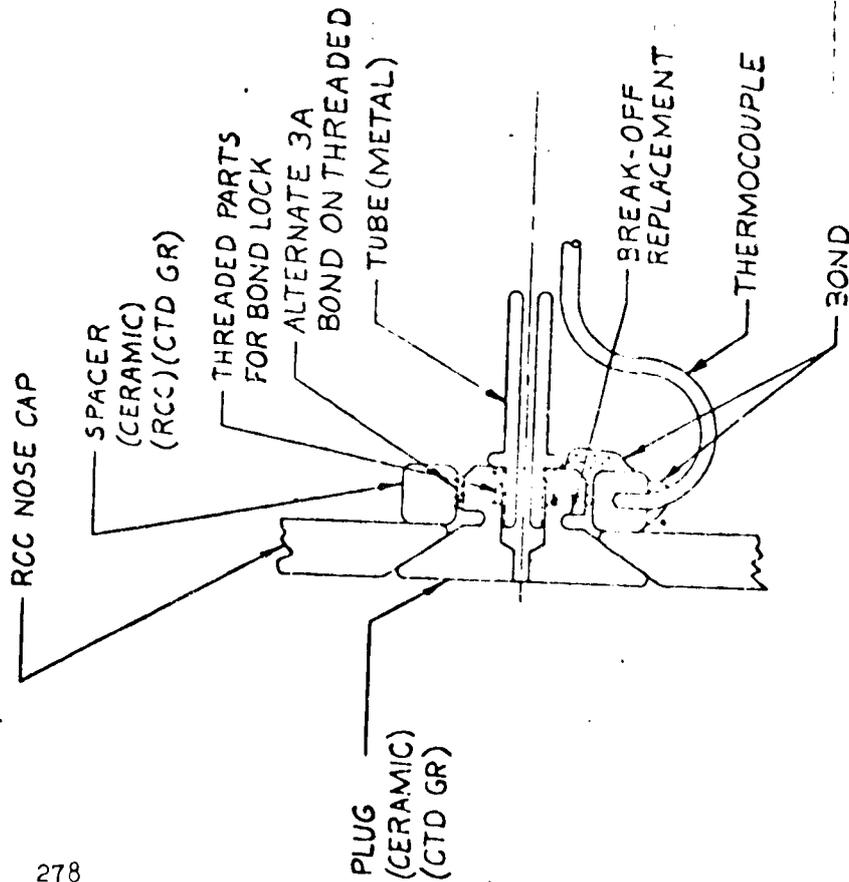
ADVANTAGES

1. BREAK OFF FEATURE FOR EASE OF REPLACEMENT

2. VERY SHORT FOR STRUCTURAL STRENGTH ESPECIALLY UNDER VIBRATION

3. ONLY 2 PARTS

4. READILY ACCOMMODATES THICKNESS VARIATIONS IN RCC

DISADVANTAGES

1. RELIES SOLELY ON BOND FOR STRUCTURAL INTEGRITY UNLESS THREADED PARTS ARE USED

2. FAILURE OF BOND OR PLUG GROOVE WOULD RESULT IN TOTAL LOSS OF PLUG - NO REDUNDANCY UNLESS THREADED PARTS ARE USED

3. ASSEMBLY MAY BE DIFFICULT

4. NO DISASSEMBLY FOR INSPECTION

5. DISASSEMBLY DESTROYS PLUG AND PLUG NUT

6. THERMAL EXPANSION POSSIBLE PROBLEM WITH METAL TUBE AND BOND

278

1. USE OF ONE LEFT HAND AND ONE RIGHT HAND THREAD PROVIDES POSITIVE LOCKING

2. FLEXIBLE SPACER ELIMINATES THERMAL EXPANSION PROBLEM AND DOES NOT REQUIRE LOOSENESS

3. NO BONDING REQUIRED

4. COMPLETELY REPLACEABLE AND INSPECTABLE

5. METAL AWAY FROM HIGHEST TEMPERATURE REGION

6. LOSS OF EITHER NUT OR THREADED CONNECTION DOES NOT RESULT IN COMPLETE LOSS OF PLUG

DISADVANTAGES

1. POSSIBLE THERMAL EXPANSION PROBLEM AT TUBE FLANGE

2. FOUR PARTS

3. INNER AND OUTER THREADS ON PLUG LEADS TO LARGE DIAMETER PLUG AND RCC HOLE
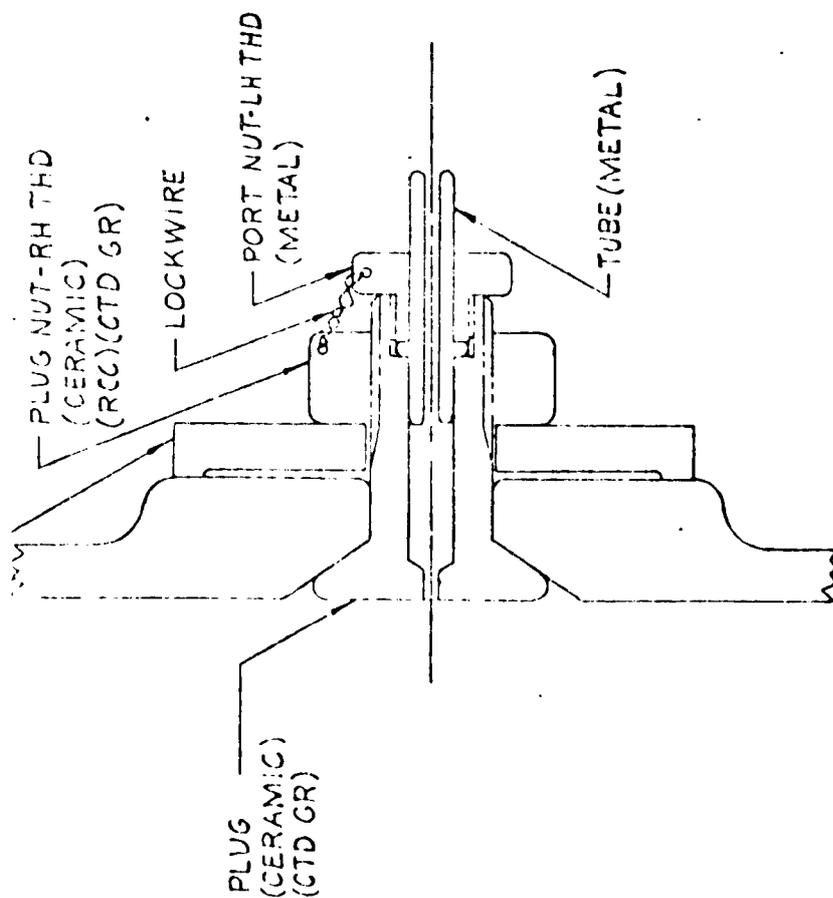
PLUG NUT-RH THD
(CERAMIC)
(RCC)(CTD GR)

LOCKWIRE

PORT NUT-LH THD
(METAL)

TUBE (METAL)

PLUG
(CERAMIC)
(CTD GR)

SCALE 2/1

VOUGHT SYSTEMS DIVISION
LTV AEROSPACE CORPORATION

CONCEPT 5

RCC NOSE CAP
FLEX SPACER (RCC)
LOCKWIRE
PLUG NUT (CERAMIC) (RCC)(CTD GR)
PLUG (CERAMIC) (CTD GR)
BOND
TUBE (METAL)
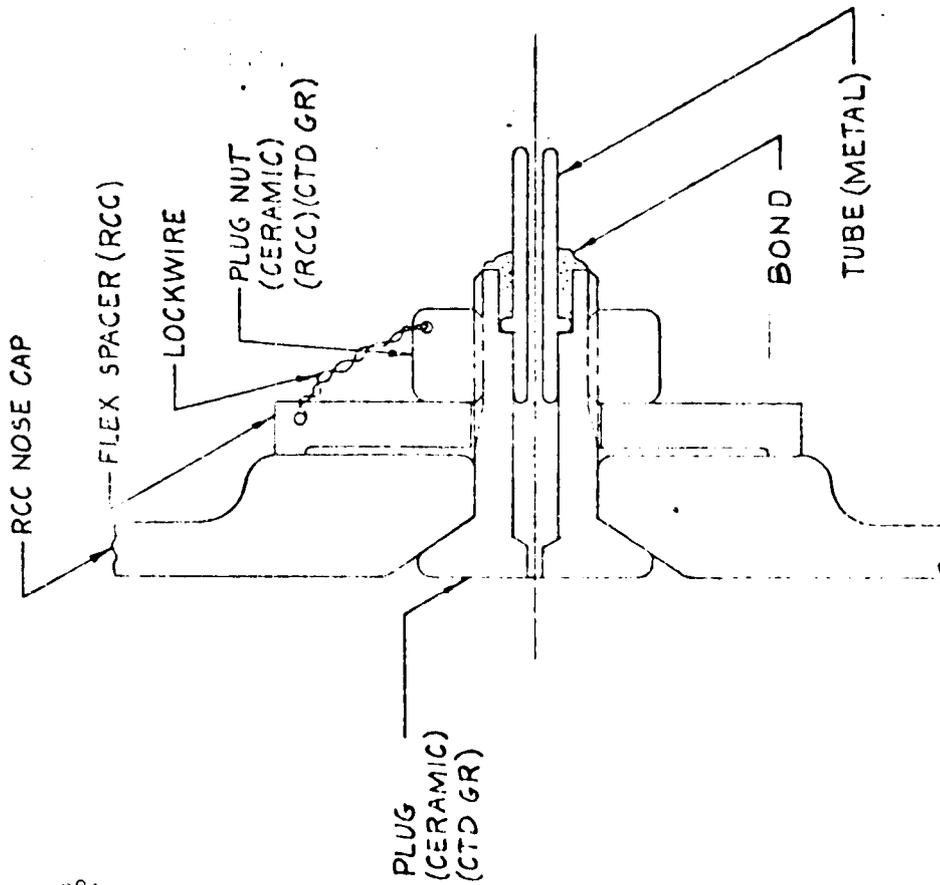
ADVANTAGES

1. ELIMINATES LOOSENESS REQUIRED IN OTHER CONCEPTS FOR THERMAL EXPANSION ACCOMMODATION

2. FLEX MEMBER DOUBLES AS INSULATOR

3. LARGE PLUG HOLE COATABLE

4. ACCOMMODATES RCC THICKNESS VARIATIONS

5. EASE OF ASSEMBLY

6. METAL PARTS IN LOWER TEMPERATURE REGION

7. FAIRLY POSITIVE LOCKING FEATURE

DISADVANTAGES

1. DISASSEMBLY PROBABLY DESTROYS PLUG

2. NO REDUNDANCY FOR CERAMIC BOND OR THREAD FAILURE

3. CANNOT BE DISASSEMBLED FOR INSPECTION WITHOUT DESTROYING PLUG

4. QUESTIONABLE POSITIVE PRESS PORT LOCK IN A VIBRATION ENVIRONMENT

5. PRELOAD ALSO FLEXES NOSE CAP WHICH COULD INCREASE SUBSURFACE ATTACK UNLESS NOSE CAP IS BEEFED UP LOCALLY

6. NUMBER OF PARTS - 3

7. THERMAL EXPANSION POSSIBLE PROBLEM WITH METAL TUBE AND BOND

280

2. GOOD ACCOMMODATION OF T/C POSSIBLE

3. NO BONDING TO RCC REQUIRED

4. POSITIVE ATTACHMENT OF PLUG AND PORT - NO BONDING

5. ACCOMMODATES RCC THICK VARIATIONS

6. EASE OF ASSEMBLY AND DISASSEMBLY UNLESS LOCK FEATURE INTERFERES

7. HOT GAS LEAKAGE AND SNEAK-THROUGH RESTRICTED

8. READILY DISASSEMBLED FOR INSPECTION/REPLACE

9. PRESSURE PORT CAN BE REPLACED WITHOUT REPLACING PLUG

10. T/C MAY BE READILY INSTALLED IN SPACER OR COUPLER

11. PROBABLY ONLY THE COUPLER NEEDS TO BE PLATINUM WITH PRESS PORT AND NUT OF LOWER COST METAL

DISADVANTAGES

1. INTERNAL PLUG THREADS MORE DIFFICULT TO MACHINE OR CLEAN UP AFTER COAT THAN EXTERNAL THREADS

2. METAL ADAPTER MAY RUN HOT DECREASING TEMPERATURE MARGIN WITH SHORT PLUG - BUT GOOD FOR PLATINUM

3. SLIGHT LOOSENESS MAY BE REQUIRED TO ACCOMMODATE THERMAL EXPANSION MISMATCH AT PLUG

4. NUMBER OF PARTS - 4

5. NO REDUNDANCY IF THREADS FAIL

6. DISASSEMBLY POSSIBLY DIFFICULT WITH PIN LOCK
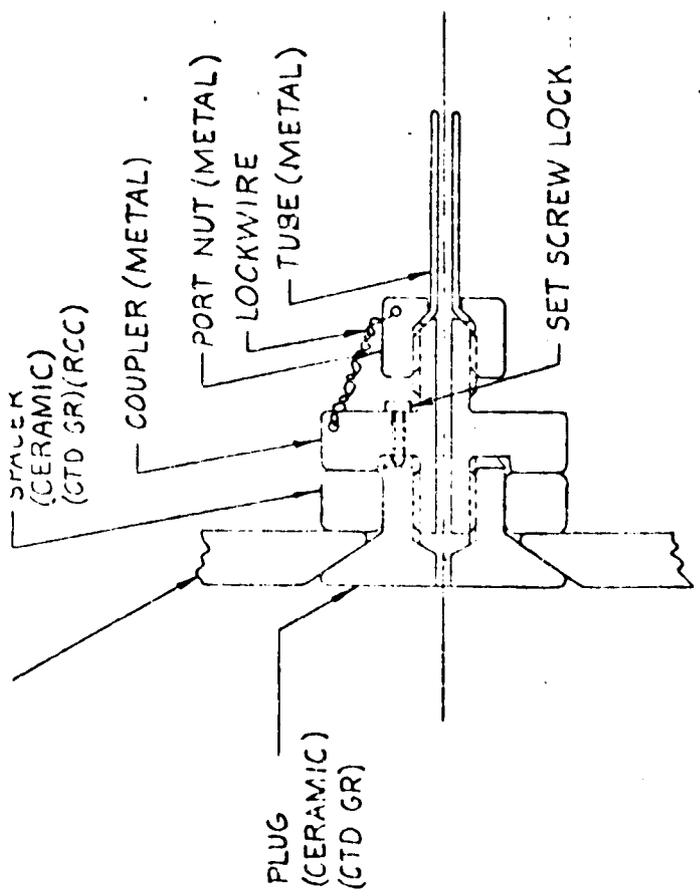
SPACER
(CERAMIC)
(CTD GR)(RCC)

COUPLER (METAL)

PORT NUT (METAL)

LOCKWIRE

TUBE (METAL)

SET SCREW LOCK

PLUG
(CERAMIC)
(CTD GR)

SCALE 2/1

VOUGHT SYSTEMS DIVISION
LTV AEROSPACE CORPORATION

281

CONCEPT 7

RCC NOSE CAP

SPACER
(CERAMIC)
(CTD GR)(RCC

PORT NUT
(METAL)

TUBE (METAL)

LOCK PIN-STAKED
IN PLACE

PLUG
(CERAMIC)
(CTD GR)

SCALE 2/1
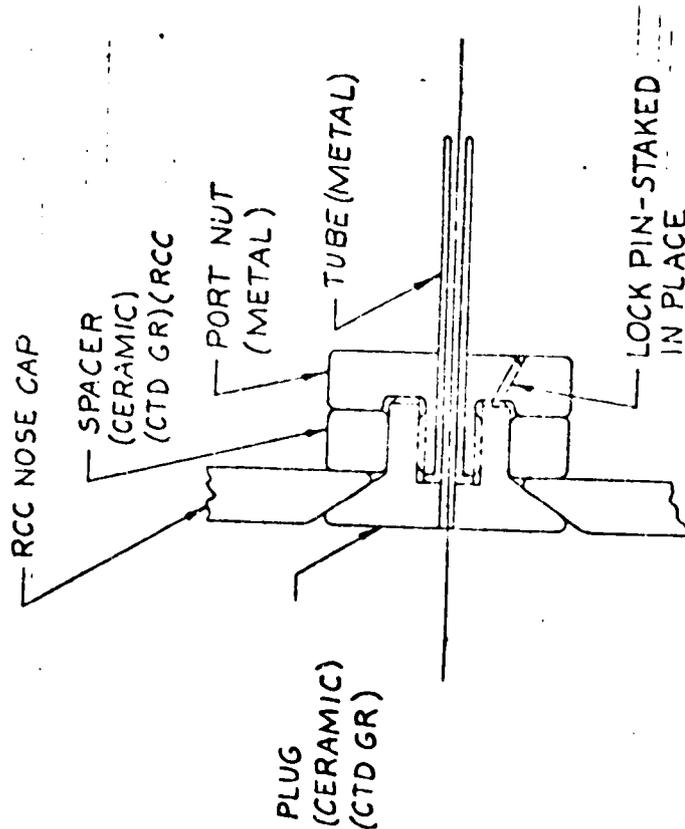
ADVANTAGES

1. EASILY INSTALLED AND REPLACED

2. INSPECTABLE

3. SHORT OVERHANG FOR VIBRATION LOADING

4. NO BOND TO RCC

5. GOOD CONFIGURATION FOR COATING OF PLUG

6. ELIMINATES ONE PART COMPARED TO CONCEPT 6

7. T/C MAY BE READILY INSTALLED IN SPACER OR WELDED TO NUT

DISADVANTAGES

1. NO APPARENT METHOD OF LOCKING EXCEPT BOND OR PIN

2. METAL NUT VERY CLOSE TO CONTOUR HEAT SOURCE - BUT GOOD FOR PLATINUM

3. NO REDUNDANCY, IF THREADS BREAK; PORT IS LOST

4. LOOSENESS OF INSTALLATION AFTER INSTALLATION FOR THERMAL EXPANSION

5. POSSIBLE TOLERANCE PROBLEM UNLESS SHIMS ARE USED BETWEEN NUT AND SPACER

6. BOTH PORT NUT AND PRESS PORT NEED TO BE PLATINUM WITH COUPLING TO LESS EXPENSIVE MATERIAL DOWNSTREAM

3. DISASSEMBLY FOR INSPECTION GOOD IF BOND BREAKS CLEAN

4. GOOD ACCOMMODATION FOR RCC THICK VARIATIONS

DISADVANTAGES

1. THE HOLE DIFFICULT TO COAT - MAY BE UNCOATABLE

2. SOME LOOSENESS MAY BE REQUIRED TO ACCOMMODATE THERMAL EXPANSION MISMATCH AT PLUG

3. NUMBER OF PARTS - 3

4. QUESTIONABLE INTEGRITY OF LOCKING FEATURE

(CERAMIC)
(CTD GR)(RCC)

LOCKWIRE

TUBE (METAL)

BOND LOCK

THERMOCOUPLE

PORT NUT
(METAL)

PLUG
(CERAMIC)
(CTD GR)

SCALE 2/1

VOUGHT SYSTEMS DIVISION
LTV AEROSPACE CORPORATION

CONCEPT 9

RCC NOSE CAP

RETAINING RING
(CERAMIC)
(RCC)(CTD GR)

LOCKWIRE

TUBE (METAL)

THREADED PARTS FOR BOND LOCK

BURN OUT MATL (BOND BARRIER)

PLUG (CERAMIC)(CTD GR)
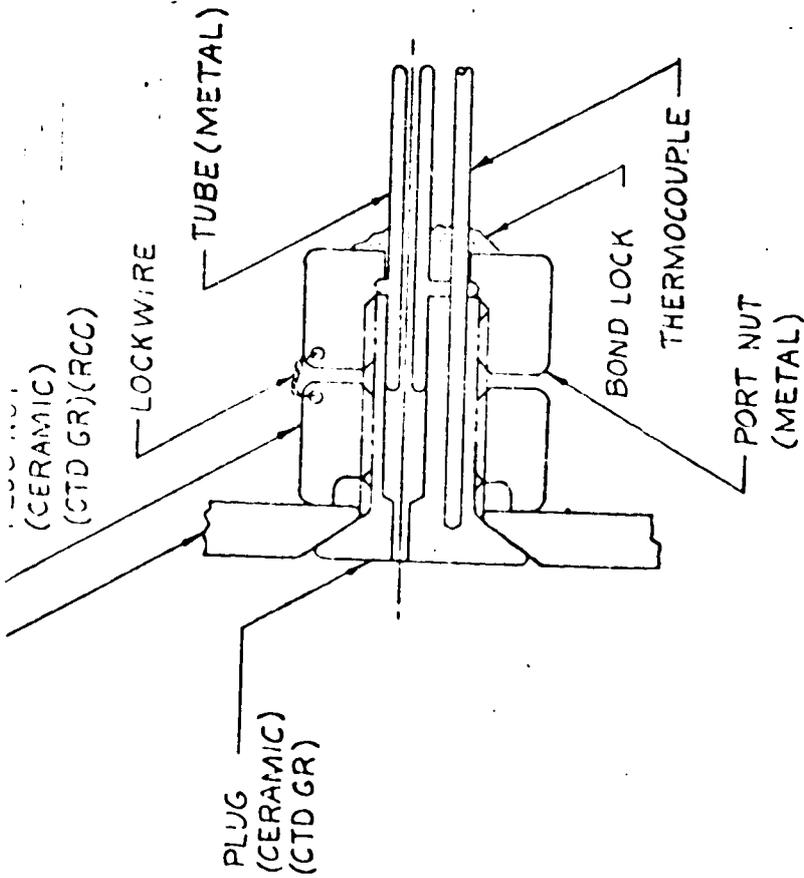
SCALE 2/1
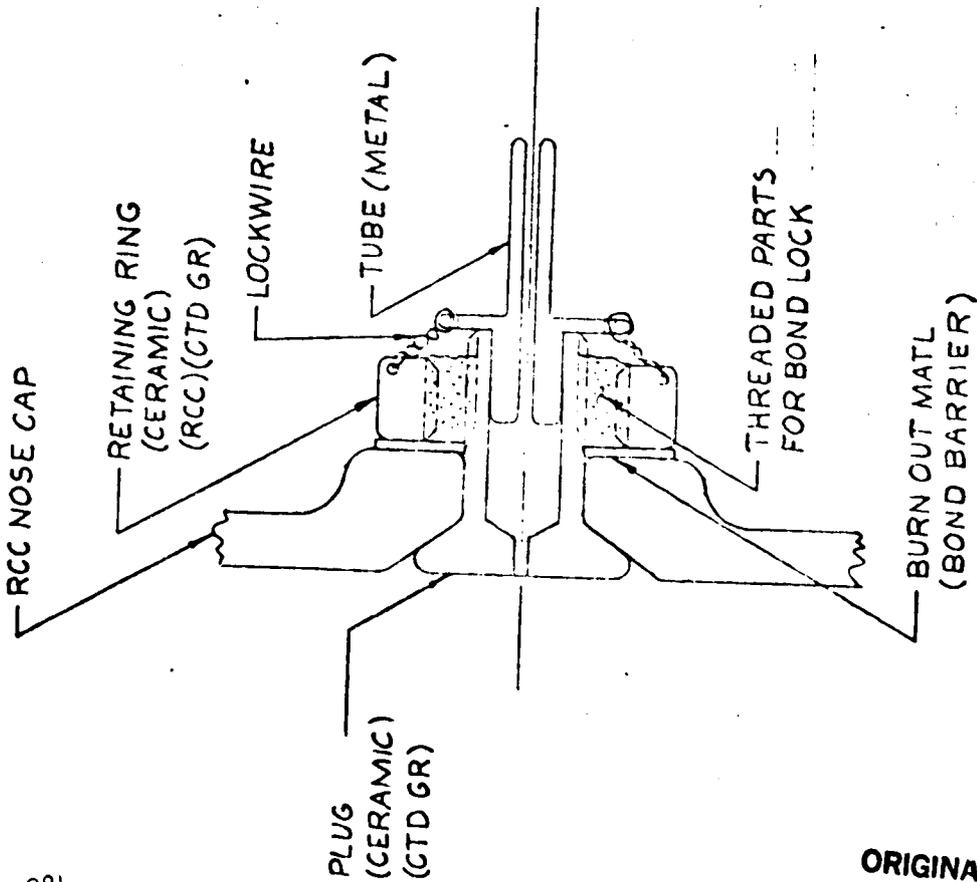
ADVANTAGES

1. PLUG READILY COATED
2. NUMBER OF PARTS - 2
3. ACCOMMODATES RCC THICKNESS VARIATIONS
4. BOND MATERIAL POSITIVELY LOCKED

DISADVANTAGES

1. RELIES SOLELY ON BOND FOR STRUCTURAL INTEGRITY BUT PLUG HAS LITTLE CHANCE OF BEING LOST COMPLETELY
2. RELIANCE UPON WIRE (OXIDATION, EMBRITTLING, VIBRATION) AS PRIMARY PRESS PORT RETENTION. HOWEVER, MULTIPLE WIRES ARE USED.
3. SLIGHT LOOSENESS REQUIRED FOR THERM EXPANSION AT PLUG
4. PLUG PROBABLY DESTROYED IN DISASSEMBLY
5. ASSEMBLY MAY BE DIFFICULT (HOLDING PLUG WHILE RETAINER IS BONDED)
6. PRESS PORT COULD BECOME LOOSE AT TEMP DUE TO WIRE EXPANSION AND STRESS RELAXATION

3. ONLY 1 MANUFACTURED PART
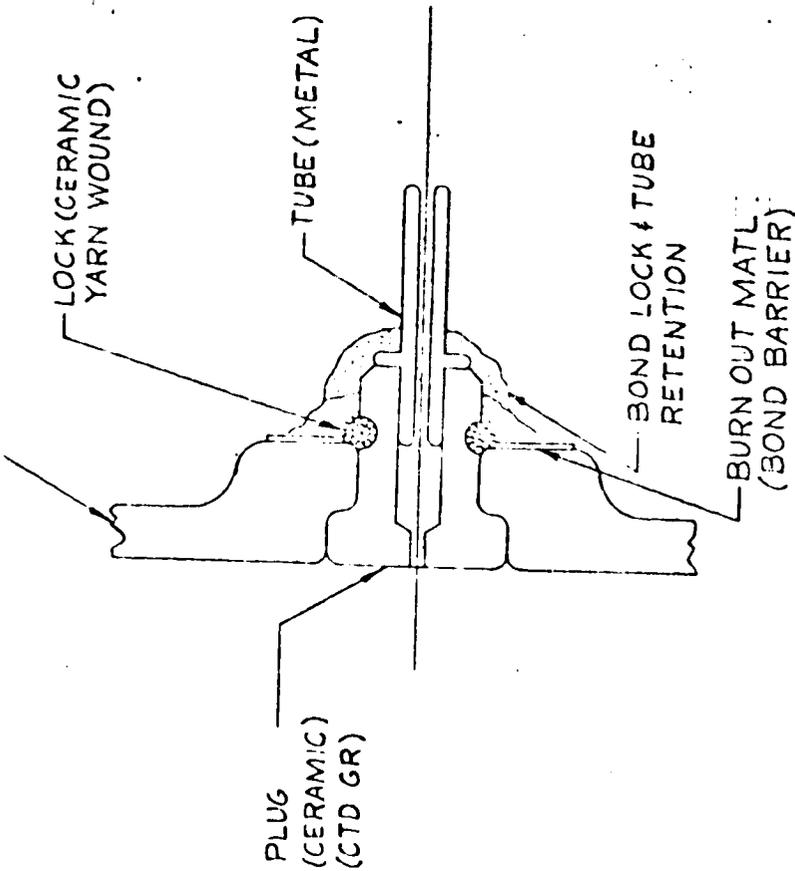
DISADVANTAGES

1. EXTRA TIME REQUIRED TO INSTALL

2. RELIES BASICALLY ON BONDING FOR RETENTION WITH QUESTIONABLE INTEGRITY AT PRESS PORT

3. THERMAL EXPANSION PROBLEM WITH METAL TUBE & BOND

4. NO DISASSEMBLY FOR INSPECTION

LOCK (CERAMIC YARN WOUND)

TUBE (METAL)

BOND LOCK & TUBE RETENTION

BURN OUT MATL (BOND BARRIER)

PLUG (CERAMIC) (CTD GR)

SCALE 2/1

VOUGHT SYSTEMS DIVISION
LTV AEROSPACE CORPORATION

CONCEPT II

RCC NOSE CAP
HORSESHOE RETAINER (RCC)(CTD GR)
TUBE(METAL)
PLUG (CERAMIC)(CTD GR)
BOND LOCK & TUBE RETENTION
BURN OUT MATL (BOND BARRIER)

SCALE 2/1

ADVANTAGES

1. IF BOND FAILS LOCALLY NOSE SHOE WASHER WILL RETAIN PARTS IN NOSE CAP

2. NO COATING PROBLEMS

DISADVANTAGES

1. THERMAL EXPANSION PROBLEM WITH METAL TUBE AND BOND

2. NO DISASSEMBLY FOR INSPECTION

3. NARROWED SECTION OF PIN PROMOTES LARGE DIA HOLE IN RCC

4. BOND IS SOLE RETENTION OF METAL PRESSURE PORT & HAS QUESTIONABLE INTEGRITY IN THERMAL/VIBRATION ENVIRONMENTS

5. PARTS PROBABLY DESTROYED UPON DISASSEMBLY
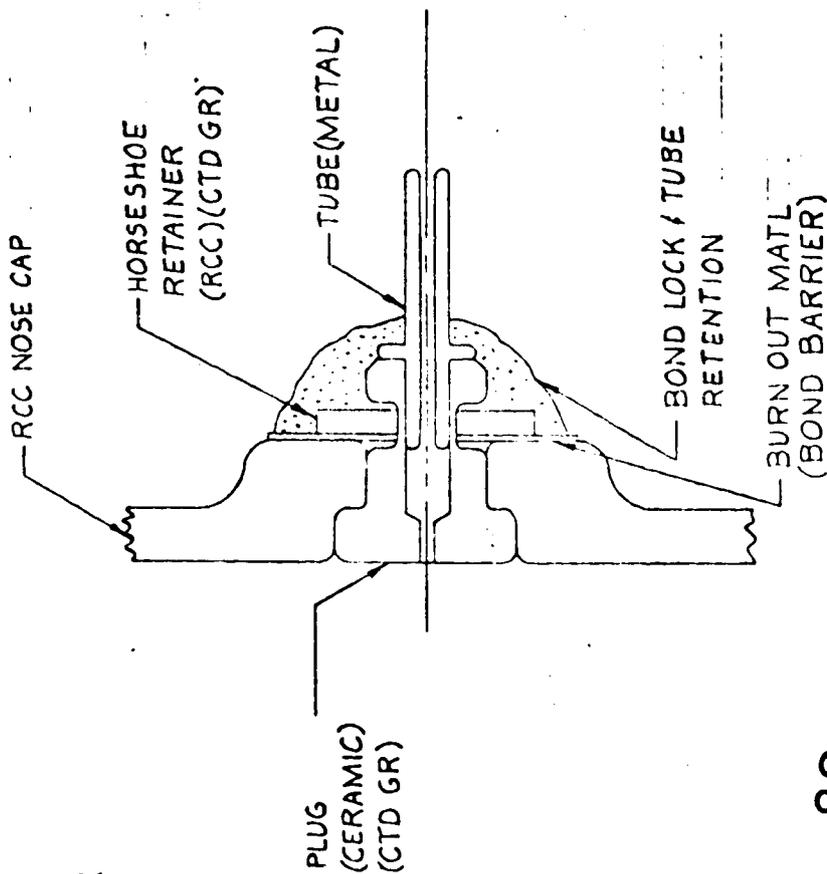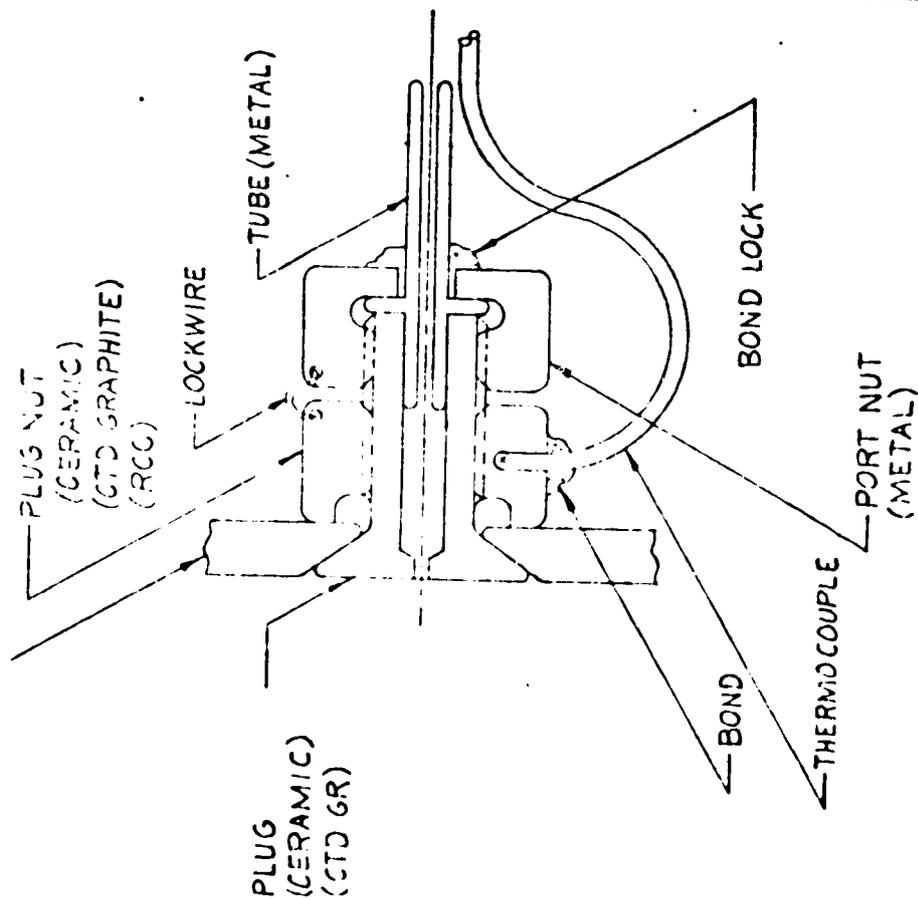
286

4. WITHIN RCC PLUG NUT, METAL PARTS ARE RESTRICTED TO COOLER REGIONS
5. LARGE INTERNAL HOLE IN PLUG IMPROVES COATABILITY FOR GRAPHITE PART
6. POSITIVE ATTACHMENT OF PLUG & PRESS PORT - NO BONDING
7. READILY DISASSEMBLED FOR INSPECTION/REPLACE
8. EXTERNAL PLUG THREADS COATABLE OR MACHINABLE
9. DUAL NUT REDUCES POSSIBILITY OF COMPLETE LOSS
10. PRESS PORT CAN BE REPLACED W/O REPLACING PLUG

DISADVANTAGES

1. NUMBER OF PARTS - 3
2. SLIGHT LOOSENESS MAY BE REQUIRED TO ACCOMMODATE THERMAL EXPANSION MISMATCH AT PLUG
3. THREADED CERAMICS OR GRAPHITE COULD BE EXPENSIVE OR LEAD TO HIGH SCRAPPAGE
4. BOND LOCK HAS QUESTIONABLE INTEGRITY

PLUG NUT
(CERAMIC)
(CTD GRAPHITE)
(RCC)

LOCKWIRE

TUBE (METAL)

PLUG
(CERAMIC)
(CTD GR)

BOND

THERMOCOUPLE

PORT NUT
(METAL)

BOND LOCK

SCALE 2/1

VOUGHT SYSTEMS DIVISION
LTV AEROSPACE CORPORATION

CONCEPT 13

RCC NOSE CAP
PLUG NUT- RH THD (CTD GR)(RCC)
LOCKWIRE
PORT NUT (METAL) LH THD
TUBE (METAL)
PLUG (CTD GR)
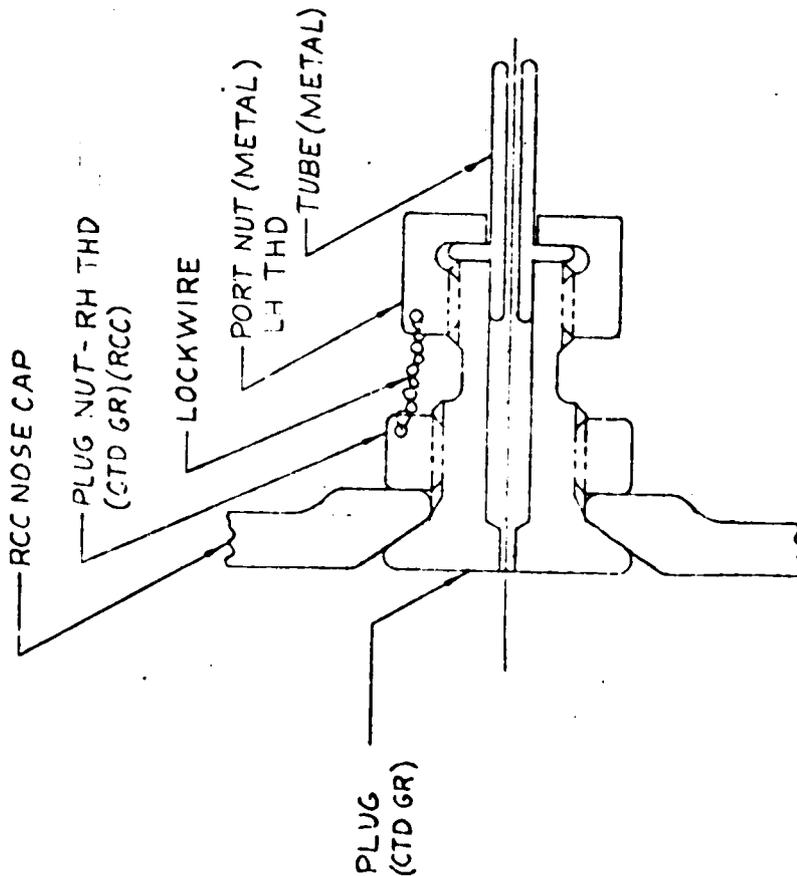
ADVANTAGES

1. POSITIVE LOCKING

2. NO THERMAL EXPANSION INCOMPATIBILITY

3. EASE OF INSTL AND REPLACEMENT

4. EASE OF INSPECTION

5. NO BONDING

6. RUGGED FOR VIBRATION LOADING

7. METAL MAX DISTANCE FROM HEAT SOURCE

8. ACCOMMODATES THICKNESS VARIATIONS IN RCC

9. CAN ACCOMMODATE T/C INSTALLATION LIKE 12

DISADVANTAGES

1. GRAPHITE PLUG LENGTH MAY BE DIFFICULT TO COAT

2. NUMBER OF PARTS - 3

3. SLIGHT LOOSENESS MAY BE REQUIRED FOR THERMAL EXPANSION ACCOMMODATION

4. DUAL THREAD LEADS TO LARGE DIA HOLE IN RCC

289

APPENDIX B

Drawings of the detail parts used in the second phase of the program are included in this appendix.

T/C # 5 TUNGSTEN 5% RHENIUM /
TUNGSTEN 26% RHENIUM

T/C #1 .040 PLATINUM 13% RHODIUM/
PLATINUM - PLATINUM 20% RHODIUM SHEATH

T/C # 4 TUNGSTEN 5% RHENIUM /
TUNGSTEN 26% RHENIUM

T/C # 2 .0625 PLATINUM 13% RHODIUM/
PLATINUM - PLATINUM 20% RHODIUM SHEATH

T/C # 5 TUNGSTEN 5% RHENIUM /
TUNGSTEN 26% RHENIUM

-9 ASSY (USED ON -1)
-10 ASSY (USED ON -2)
-11 ASSY (USED ON -3)
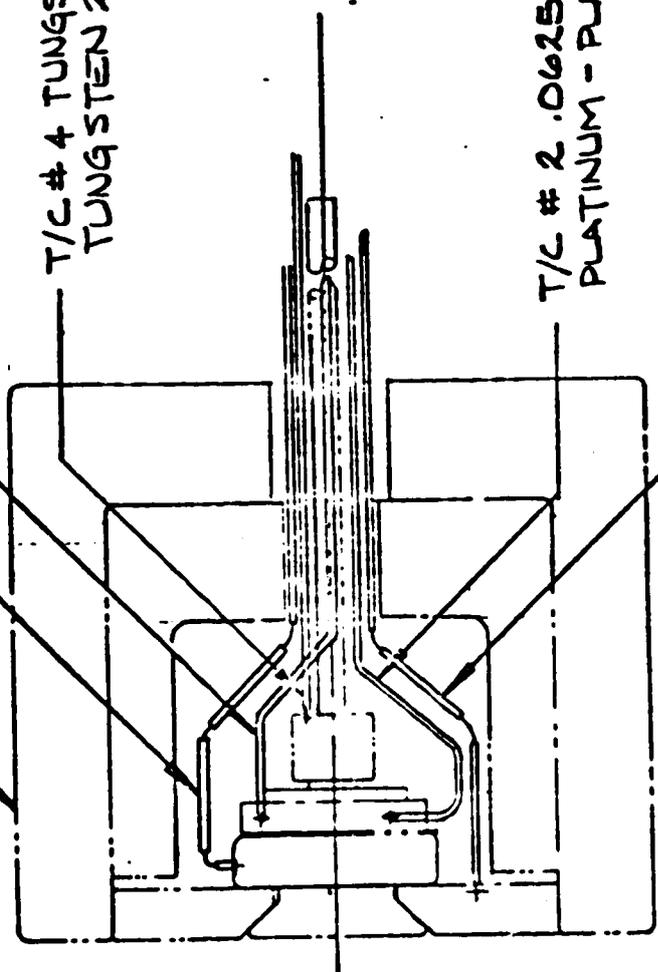
PLASMA MODEL -1

PLASMA MODEL -2

290

TUNGSTEN 26% RHENIUM
2 REQD

221GL4005-10 HOLDER

221GL4005-11 INSULATION

221GT4031-103 PIN
4 REQD

221GT4071-12
DISC

PLASMA CALIBRATION MODEL -7

VOUGHT CORPORATION

Post Office Box 5907
Dallas, Texas 75222

SIZE	CODE IDENT NO	DRAWING NO.
	80378	221GT4072
SCALE	REV LTR —	SHEET 7

PLASMA ASSY-9

221GL4005-10 HOLDER

221GL4005-11 INSULATION

LOCKWIRE WITH PLATINUM
THERMOCOUPLE WIRE

221GT4071-13 TUBE

221GT4071-10 NUT

221GT4071-8 UNION

221GT4031-103
PIN 4 REQD

221GT4071-3
SPACER

221GT4071-2
PLUG

221GT4071-11
DISC

221GT4071-4
WASHER

221GT4071-6
T/C MOUNT

VOUGHT CORPORATION

292

PLASMA ASSY I-10

PIN 4 REQD

221GL4005-11 INSULATION

LOCKWIRE WITH IRIDIUM (.010 DIA)
THERMOCOUPLE WIRE

221GT4071-13 TUBE

221GT4071-3 SPACER

221GT4071-2 PLUG   -16

221GT4071-11 DISC

221GT4071-5 WASHER   -17

221GT4071-7 T/C MOUNT

221GT4071-10 NUT

221GT4071-9 UNION   -18

VOUGHT CORPORATION   Post Office Box 5907
Dallas, Texas 75222

SIZE | CODE IDENT NO | DRAWING NO.

80378   221GT4072

SCALE | REV LTR | SHEET   10

293

PLASMA ASSY-11

221GL4005-10 HOLDER

221GL4005-11 INSULATION

LOCKWIRE WITH PLATINUM
THERMOCOUPLE WIRE

221GT4071-13 TUBE

221GT4071-10 NUT

221GT4071-8 UNION

221GT4031-103
PIN 4 REQD

221GT4071-3
SPACER

221GT4071-1
PLUG

221GT4071-11
DISC

221GT4071-4
WASHER

221GT4071-6
T/C MOUNT

VOUGHT CORPORATION

Post Office Box 59.
Dallas Texas 7522.

SIZE CODE IDENT NO DRAWING NO

.294

	PART OR IDENTIFYING NO	NOMENCLATURE OR DESCRIPTION	MATERIAL OR NOTE		
SH12	-14	WASHER	⑪ X.4X.4	⑮	③
SH12	-13	TUBE ASSY			⑱
SH11	-12	DISC	25PLYX2.9X2.9	⑨	⑰ ⑥⑧/14
SH10	-11	DISC	25PLYX2.9X2.9	⑨	⑰ ⑥⑥/14
SH9	-10	NUT	.5X.6X.6 ⑮	M3 ⑱	⑮ 2⑶
SH8	-9	UNION	1.2X1.2X1	M2 ⑮ ⑱	⑥/6
SH8	-8	UNION	1.2X1.2 ⑮	M1 ⑱	⑷/3
SH7	-7	T/C MOUNT	.170X1.25 X1.25	M4 ⑱	②⑶
SH7	-6	T/C MOUNT	.170X1.25 X1.25 ⑮	M3 ⑩	②⑶
SH6	-5	WASHER	.020X1.25X1.25	M2 ⑮ ⑱	②⑶/6
SH6	-4	WASHER	.020X1.25 X1.25 ⑮	M3 ⑱	②⑶
SH5	-3	SPACER	25PLY1.5X1.5	⑨⑸ ⑸/14	
SH4	-2	PLUG	1.75DIA X.8	M2 ⑮	⑶
SH4	-1	PLUG	1.75DIA X.8	M1 ⑩	⑷⑹

ZONE	CODE IDENT	PART OR IDENTIFYING NO	NOMENCLATURE OR DESCRIPTION	MATERIAL OR NOTE
			LIST OF MATERIAL	

	MATERIAL	SPECIFICATION	PROTECTIVE FINISH
M5	NICKONEL 7C2	AMS5350	
M4	IRIDIUM		
M3	NICKEL-CHROME	YONICRA	
M2	MCLYP IRIDIUM ALLOY(MTNG4(TZM)		
M1	CARBIT TUBULET	STACKPOLE 2020	

CONTRACT NUMBER

VOUGHT CORPORATION

CODE IDENT NO. 80378 SIZE B 221GT4571

SCALE NONE REV SYM SHEET 2

295

SECT A-A
SCALE 10/1

-1 AND -2
(SAME EXCEPT MATL)

.5070 -.0000 TO .510 DEPTH
+.0140
(PRIOR TO THD RELIEF)
CSK 110° ±10° X .400
3/8 -16UNJC-3B
MIL-S-8879
MODIFIED AS SHOWN
IN SECT A-A

VOUGHT
CORPORATION

SIZE	CODE IDENT NO	DRAWING NO		
	80378	221GT4071		
SCALE 2/1	NOT	REV LTR		SHEET 4

.526

.060 4 PLCS

.750

1.500

-3

.020±.002

.06R 4PLCS

DR 1/16 (.0625)
2 HOLES

.12R 4PLCS

.09 4PLCS

.94

.600

.13

.730

.90

-4 AND -5
(SAME EXCEPT MAT'L)

VOUGHT
CORPORATION

SIZE | CODE IDENT NO | DRAWING NO
| 80378 | 221T4071

SCALE 2/1 | REV LTR | SHEET 6

221
Pag

298

VOUGHT
CORPORATION

SIZE	CODE IDENT NO	DRAWING NO.	
	80378	221GT4071	
		REV LTR	SHEET
SCALE 2/1			

.085

.170±.002

DR 60(.040)

DR 1/16 (.0625)

1.15

.440
4 PLCS

.455
4 PLCS

.790

-6 AND -7
(SAME EXCEPT FOR MAT'L)

DR 1/16 (.0625)

DR 60 (.040)

299

DETAIL A

.3617 +.0000 -.0054

3/8-16UNJC-3?
MIL-S-8879
MODIFIED AS SHOWN
IN DETAIL A
2PLCS

.030R 2PLCS

CHAM 45°±5'×.050 3PLCS

.030R 5PLCS

.450
.180
.140
.480
.060
.030

.790 DIA 2PLCS

45±5° 2PLCS

.770 DIA

1.08 REF

-8 AND -9
(SAME EXCEPT FOR MAT'L)

.015 .009 R

DETAIL A
SCALE 10/1

.171 .177

.940 3PLCS
.923

VOUGHT CORPORATION

SIZE	CODE IDENT NO	DRAWING NO
	80378	221GT4C71
	REV LTR	SHEET
SCALE 2/1		

300

.171
.177

.3070 -.0000 +.0040

CSK 110°±10° x .400
3/8-16UNC-2B
HDBK 2B

45°±5°

.502
.492
4PLCS

.110

.044 DIA
.039

45°±5°

.050R
2PLCS

.050R

.050R

.410

.150
.075

.060

.160

.575 DIA
.319 DIA
THD RELIEF

-10

SIZE	CODE IDENT NO	DRAWING NO	
	80378	221GT4071	
		REV LTR	SHEET 9
SCALE			

VOUGHT CORPORATION

301

.065R 4PLCS

.050R

DR 1/16(.0625)
.06 DEEP
3 HOLES

.060 4PLCS

STOCK (.526)

.050R

.120 4PLCS

2.800

.852

.750 +.050 -.000 DIA

CSK 100° ±1° X .1246 DIA
IN -11 ONLY

302

.063 2 4 PLACES

.060 4 PLCS

.120 4 PLCS

STOCK (.326)

2.800

.85R

-12

D℟ 1/16 (.0625)
.06 DEEP
3 HOLES

303

FILLET WELD PER
CVA 17-13 CLASS C

12.00 ±.10

.50

-15

-13

-14

.290

APPENDIX C

COMPONENT DESIGNS USED IN THE THIRD PLASMA ARC TEST SERIES

DETAIL A SCALE NONE
4 PL

CLEAN UP MISMATCH
WITH .187 DIA CUTTER

.097 ±.005 SPHERICAL RADIUS

.720 DIA

.590

.460 R

.340 R

1.620

632

.030 R

.080 R 4 PLCS

.097 REF

// A .005
MACHINE IF REQD

.000

DAM THICK

-A-

6. FABRICATE PER SME 208-7-40
   USING CROSS-PLY LAYUP, EXCEPT
   NO COATING SPECIFIED REQUIRED

5. THICKNESS EQUIVALENT TO 25-PLY LAYUP
   IF THICKER RAW STOCK USED, MACHINE
   RAG SIZE SURFACE TO OBTAIN CORRECT THICKNESS

4. _____ APPLY AFTER _____

3. MACHINED SURFACES 125/ MAX

2. _____ PER SPEC _____

SEE SEPARATE PARTS LIST

VOUGHT CORPORATION

SPACER - TEST , SE-DS

NOTES (UNLESS OTHERWISE SPECIFIED)
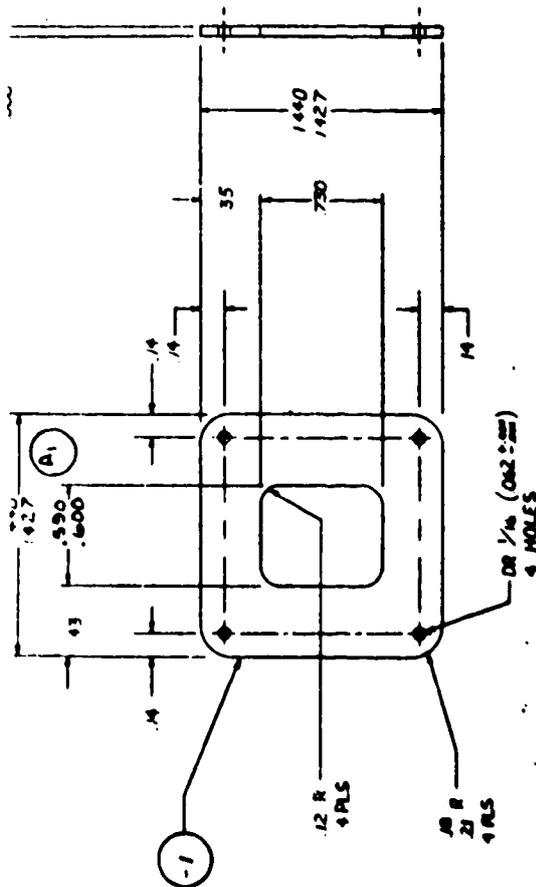
8. PART SHALL BE PRE-OXIDIZE COATED TO 2000°F FOR 1/2 HOUR IN AIR
7. COATED PARTS SHALL BE CAPABLE OF WITHSTANDING TEMPERATURE OF 2500°F AT 1 ATM FOR 10 HOURS
6. TOTAL COATING THICKNESS .003 - .005
5. ALL DIMS APPLY AFTER COATING
4. SURFACE FINISH 125/ MAX
3. EDGE RADII .010 - .020 INCLUDING HOLES
2. SILICIDE COATING VH-100 (VAC-HYD)
1. MTL: COLUMBIUM ALLOY C-103

DR 1/16 (.062 ±.005) 4 HOLES

.12 R 4 PLS

1.440 / 1.427

.35

.730

UNLESS OTHERWISE SPECIFIED
DIMENSIONS ARE IN INCHES

VOUGHT CORPORATION

WASHER . LOCK - TEST
SEADS   DSI - 250

SIZE C   CODE IDENT NO 80378   DRAWING NO 221GT4087   REV LTR A

AIRFRAME

SEE SEPARATE PARTS LIST

DET A

DET A
SCALE NONE

DR 1/64 (.266 ± ...) THRU
DR 3/8 (.375 ± ...) TO .192 DIA ⑩
7/16-14 UNJC-3BG
MAJOR DIA .4199 MIN (SEE DETAIL A)
MIL-S-8879 MODIFIED
CSK 100° ± 10° X .46 ± .01

FULL THDS

.048
4 PLS

DR 3/64 (.047 ± ...)
4 HOLES

.012 R
.009

.4199 MIN DIA (REF)

.012 R
.009

NOTES: (UNLESS OTHERWISE SPECIFIED)

⑩ HOLE DIA AFTER COATING SHALL BE .363 MIN.

9. PART SHALL BE PRE-OXIDIZE COATED TO 2000°F
   FOR 1/2 HOUR IN AIR.

8. COATED PARTS SHALL BE CAPABLE OF WITHSTANDING A
   TEMPERATURE OF 2500°F AT 1 ATM FOR 10 HOURS.

7. ALL DIMS APPLY AFTER COATING

6. TOTAL COATING THICKNESS .003 - .008

5. SURFACE FINISH 125/ MAX

4. EDGE RADII .012 - .050 INCLUDING HOLES

3. FILLET RADII .025 - .015

2. SILICIDE COATING VH-109 (VAC HYD)

1. MATL COLUMBIUM ALLOY C-103

VOUGHT CORPORATION

NUT - TEST SEADS
DSI - 250

SIZE C | CODE IDENT NO 80378 | DRAWING NO 221GT4089

AIRFRAME

310

SEE SEPARATE PARTS LIST

VOUGHT CORPORATION

DISC - TEST . SEADS

DSI - 250

VIEW A-
4/1 SCALE 4 PL

CLEAN UP MISMATCH
WITH .187 DIA CUTTER

.326 ± .028

.030 R

.030 R

BAG SIDE

2.600

.590

.720 DIA

MACHINE IF REQD

UNLESS OTHERWISE SPECIFIED
DIMENSIONS ARE IN INCHES
TOLERANCES FOR
DIMENSIONED FEATURES ARE
LINEAR   ANGULAR
.XXX = ±.010
.XX = ±.03
.X = ±.

7. MEASURE COATING THICKNESS 4 PLACES EACH SIDE
   AT APPROXIMATELY THE CENTER OF EACH
   QUADRANT

6. THICKNESS EQUIVALENT TO 25 PLY LAYUP
   IF THICKER RAW STOCK IS USED, MACHINE
   BAG SIDE SURFACE TO OBTAIN CORRECT THICKNESS

5. ALL DIMS APPLY AFTER COATING

4. MACHINED SURFACES 125 MAX

3. COAT PARTS PER SPEC 208-7-41, 208-7-42, 208-9-76

2. FABRICATE PER SPEC 208-7-40 USING CROSSPLY LAYUP
   EXCEPT NO CONTROL SPECIMENS REQD

DISC - TEST . SEADS
DSI - 250

C | 80378 | 221GT4091
REV LTR A

SEE SEPARATE PARTS LIST

VOUGHT CORPORATION

CONTR NO
PREPARED | OLFMAN | 10/6/7
CHECKED
GROUP
STRESS
PROJ ENGR

AIRFRAME

ORIGINAL PAGE IS
OF POOR QUALITY

NOTES

8 CSK TO MATCH 221GT4074-1 OR 221GT4086-1
   POST SO THAT THREAD .010 .000 POSITIVE STEP
   TO -.010 NEGATIVE STEP. POSITIVE STEP
   IS PORT PROTRUSION.

7 MEASURE COATING THICKNESS 4 PLACES EACH SIDE
   AT APPROXIMATELY THE CENTER OF EACH
   QUADRANT.

4 THICKNESS EQUIVALENT TO 25 PLY LAYUP
   IF THICKER RAW STOCK IS USED, MACHINE
   BAG SIDE SURFACE TO OBTAIN CORRECT THICKNESS

3 ALL DIMS APPLY AFTER COATING

1 MACHINED SURFACES 125/ MAX

3 COAT PARTS PER SPEC 208-7-41, 208-7-42 & 208-9-76
   USING ITP 24 PER SPEC 209-21-001 EXCEPT NO
   CONTROL SPECIMENS REQD

2 LAMINATE IN 1-PLY AT 0 & N3 CROSSPLY LAYUP
   EXCEPT NO CONTROL SPEC MENS REQD
   MATL GRAPHITE PER CLOTH, PHEN IMPG PER SPEC 207-7-450

MACHINE IF REQD
.526 ± .025
BAG SIDE
.080 R
.090 R
2.800
.057 ± .005 SPHERICAL RAD.
.15 ± .3 DIA HOLE
CSK 100° ± 1° × 1.264 DIA

SPACER - TEST - SEADS

DSI - 250

VOUGHT CORPORATION

SEE SEPARATE PARTS LIST

REVISIONS

BAG SIDE

.060 R
+ PL

.226

1.300 - .750

//A/.005
MACHINE IF REQD

-A-

NOTES:

6. FABRICATE PER SPEC 208-7-40 USING CROSSPLY LAYUP. EXCEPT NO CONTROL SPECIMEN REQD.

5. THICKNESS EQUIVALENT TO 25-PLY LAYUP. IF THICKER RAW STOCK IS USED, MACHINE BAG SIDE SURFACE TO OBTAIN CORRECT THICKNESS.

4. ALL DIMS APPLY AFTER COATING

3. MACHINED SURFACES 125/ MAX

2. COAT PARTS PER SPEC 208-7-41 AND 208-7-42 USING TTP 14-1 PER SPEC 209-21-C01 AND SPEC 208-9-76. EXCEPT NO CONTROL SPECIMEN REQD

UNLESS OTHERWISE SPECIFIED
DIMENSIONS ARE IN INCHES
TOLERANCES FOR
DIMENSIONED FEATURES ARE
LINEAR   ANGULAR
.XXX = ± .010
.XX = ± .03

NONSTANDARD SYMBOLS
INDICATES REFERENCE
CALLOUT OF DASH
NO. OF THIS DRAWING
INDICATES GENERAL
NOTE ON SEPARATE

CONTR NO
PREPARED J L HEAD
CHECKED
GROUP
STRESS
PROJ ENGR

.1875 ± .0001 DIA SPHERE.

NOTES

1. MATL: INDUSTRIAL GRADE RUBY/SAPHIRE
GRADE 25

SEE SEPARATE PARTS LIST

VOUGHT CORPORATION

BALL - TEST, SEADS
DSI - 250

SIZE	CODE IDENT NO	DRAWING NO
C	80378	221GT4093

SCALE

AIRFRAME

OFFICIAL ENGINEERING RELEASE

UNLESS OTHERWISE SPECIFIED
DIMENSIONS ARE IN INCHES
TOLERANCES FOR DIMENSIONED FEATURES ARE
LINEAR   ANGULAR

NONSTANDARD SYMBOLS

TEST MODEL - SEADS
DSI - 250

REVISIONS

LTR	DESCRIPTION	DATE	APPROVED
A	1. ADDED -4 AND -5		

PARTS LIST

221GT4097-1	PORT
221GT4093-1	BALL
221GT4092-1	SPACER
221ST4091-1	DISC
221GT4090-1	DISC
221ST4089-1	NUT
221GT4088-1	UNION
221GT4087-1	WASHER
221GT4066-1	SPACER
221GT4065-1	PORT

VOUGHT CORPORATION

NOTES:

221GT4089-1 NUT

221GT4093-1 BALL
USED ON -2,4,-5

P.I. SUPPLIED TUBE REF

221ST4087-1
WASHER

221GT4066-1 SPACER
USED ON -2,4,-5

221GT4092-1 SPACER
USED ON -1,-3,-4

221GT4090-1 DISC
USED ON -1

221GT4091-1 DISC
USED ON -2,-3,-4,-5

221GT4065-1 PORT
USED ON -1,-2,4,-5

221GT4097-1 PORT
USED ON -4,-5

221GT4088-1 UNION

-1 ASSY
-2 ASSY
-3 ASSY
-4 ASSY
-5 ASSY

1. ALL THREADED JOINTS TO HAVE A MIXTURE OF
   METHOCEL AND SILICON-CARBIDE BAKED ON
   BEFORE ASSEMBLY - ENG MATLS LAB

.010 STOCK

3.00

4.85

.020

1.31

1.33

2.66

NOTES:

1. MATERIAL: 2024 T3 CLAD   QQA 250/5

2. BREAK SHARP EDGES.

AIRFRAME

CONTR NO.		
PREPARED	MORESI	
CHECKED		
GROUP		
STRESS		
PROJ ENGR		
MFG		

SHIM HALF

SIZE	CODE IDENT NO	DRAWING NO
C	80378	221 GT 4096

SEE SEPARATE PARTS LIST

VOUGHT CORPORATION

SECT A-A
SCALE 10/1

DR 5/16 (.313 ± .005) TO .58 DEPTH
CSK 100° ± .5° × .400 DIA
3/8-14 UNJS-3BG
MAJOR DIA .3574 MIN
PITCH DIA .3316 - .3364
MINOR DIA .3084 - .3204
MIL-S-8879 MODIFIED

.700

.580
.570

.060 R (REF)

.060 R REF

C SYM

.050 R REF

.060 R

.030 R REF

.3574 MIN DIA REF

.012 R
.048

.012 R
.009

.780

.61

.549

.13

.400 DIA

.185 DIA
.188

.1250 DIA

.1000 DIA
.1040

r = 1.00°

NOTES:

7. PRIOR TO USE, PARTS SHALL BE PRE-
   OXIDIZED AT 2000° FOR 1/2 HOUR
   BY VOUGHT MATLS LAB

6. EDGE RADII .030±.05; INCLUDING
   PORT HOLE, EXCEPT AS NOTED

5. ALL DIMS. APPLY AFTER COATING

4. SURFACE FINISHES 125/ MAX

3. FILLET RADII .062R

2. SiC COATING AND TEOS (VOUGHT MATLS
   LAB, MSE)

UNLESS OTHERWISE SPECIFIED
DIMENSIONS ARE IN INCHES
TOLERANCES FOR
DIMENSIONED FEATURES ARE
LINEAR   ANGULAR
XXX = ±.010   ± 0° 30'
XX = ±.03
X = ±.1

NONSTANDARD SYMBOLS
INDICATES REFERENCE
CALLOUT OF DASH
NO OF THIS DRAWING

INDICATES GENERAL
NOT ON SEPARATE

PITCH DIA .3316 - .3314
MINOR DIA .3084 - .320~
MIL-S-8879 MODIFIED

SECT A-A
SCALE 10/1

.699
.15

1250 DIA

.400 DIA

DIAS
.100

.320 DIA
.310

100° ± 1°

.030 R
.060 R REF
.060 R
.030 R REF

.042 R
.009 R

.3574 MIN DIA
REF.

.012 R
.018 R

SYM

.880
.870

.700

A

-1

NOTES:

9. PART SHALL BE CAPABLE OF EXPOSURE TO 2600°F FOR 1/2 MIN. IN AIR.

8. COATED PARTS SHALL BE CAPABLE OF WITHSTANDING TEMPERATURE OF 2500°F AT 1 ATM FOR 10 MOLPS

7. TOTAL COATING THICKNESS .003-.005

6. ALL DIMS. APPLY AFTER COATING

5. SURFACE FINISH 125/ MAX

4. EDGE RADII .03±.015 EXCEPT AS NOTED

3. FILLET RAD .060 R

2. SILICIDE COATING VH-109 (VAC HYD)

1. MAT'L COATING JR ALLOY C-103

1. Report No. NASA CR-166044 (Vol. II)	2. Government Accession No.	3. Recipient's Catalog No.
4. Title and Subtitle Shuttle Entry Air Data System (SEADS) Hardware Development Volume II, History		5. Report Date January 1983
		6. Performing Organization Code
7. Author(s)		8. Performing Organization Repc
9. Performing Organization Name and Address Vought Corporation P. O. Box 22590, Dallas, Texas 75265		10. Work Unit No.
		11. Contract or Grant No. NAS 1-16000
12. Sponsoring Agency Name and Address NASA Langley Research Center Hampton, Virginia 23665		13. Type of Report and Period C Summary, 11-75 to
		14. Sponsoring Agency Code

16. Abstract

   Hardware development of the Shuttle Entry Air Data System (SEADS) is descril The system consists of an array of fourteen pressure ports, installed in an Orbi nose cap, which, when coupled with existing fuselage mounted static pressure por permits computation of entry flight parameters. Elements of the system describe herein include: penetration assemblies to place pressure port openings at the s of the nose cap; pressure tubes to transmit the surface pressure to transducers; support posts or manifolds to provide support for, and reduce the length of, the individual pressure tubes; insulation for the manifolds; and a SEADS nose cap. Design, analyses, and tests to develop and certify design for flight are descril Specific tests include plasma arc exposure, radiant thermal, vibration, and stru

   The successful accomplishment of these tasks led to the fabrication of SEADS for early installation on Orbiter OV-102.

   Volume I summarizes   highlights of the program, particularly as they relate to the final design of SEADS. Volume II summarizes all of the Vought responsibl activities in essentially a chronological order.

17. Key Words (Suggested by Author(s)) Space Shuttle Air Data System Carbon-Carbon Columbium	18. Distribution Statement Distribution made by NASA

19. Security Classif. (of this report) Unclassified	20. Security Classif. (of this page) Unclassified	21. No. of Pages	22. Price